Geomagnetic field archaeointensities from Britain and the application of the microwave palaeointensity method to materials of differing dielectric properties

Thesis submitted in accordance with the requirements of the University of Liverpool for the degree of Doctor in Philosophy by Neil Anthony Suttie

September 2010

Geomagnetic field archaeointensities from Britain and the application of the microwave palaeointensity method to materials of differing dielectric properties

Neil Anthony Suttie

Abstract

The strength of the geomagnetic field is a subject of both scientific and public interest, with the decay over the past 160 years leading to speculation as to whether we are entering a geomagnetic reversal. Prior to 1840, there was no capability for direct measurements of geomagnetic field strength; to investigate the field strength at this time, palaeomagnetic and archaeomagnetic determinations must be made. Here we investigate the strength of the field in Britain over the past 1500 years as recorded by archaeological artefacts including ceramics, brick and burnt sandstone. Results are derived using both microwave and thermal demagnetisation. The theory of microwave demagnetisation is fully explained and equations governing the absorption of energy by an archaeomagnetic sample in a microwave cavity are derived. As a result, the possibility of demagnetising a palaeomagnetic sample using microwaves without significant heating is demonstrated for the first time. Geomagnetic field archaeointensities from seven British sites are reported.

A meta-analysis of global archaeointensity and palaeointensity data from 1590 to 1990 reveals that significant bias has been introduced to field models through inconsistent error estimation. It is shown that the principle source of uncertainty in archaeointensity should be considered as systematic, rather than experimental and that data of arbitrarily high precision can only marginally increase our knowledge of the field. Correspondingly, it is argued that while large data sets are informative enough to constrain the evolution of the geomagnetic field, archaeointensity can only have a limited application as an archaeomagnetic dating tool. It is demonstrated that when the uncertainties are properly quantified, the global data implies that the recent decay of the dipole, evident in magnetic observatory data from 1840 until the present day, is part of a longer term trend, starting as early as 1600.

Acknowledgements

This study was funded by the Natural Environment Research Council with the support of our CASE partners English Heritage (NERC award NER/S/J/2006/14310). I would like to express my gratitude to Paul Linford of English Heritage for supplying archaeological material for analysis, and would like to further acknowledge the great assistance afforded me by my supervisors, Professor John Shaw, Dr. Mimi Hill and Dr. Richard Holme. I am greatly indebted to those in the archaeological community who helped me in the collection of samples. In particular I would like to thank Dr. Cathy Batt of the University of Bradford, Matt Town of North Pennines Archaeology, Will Walker and Leigh Dodd of Earthworks Archaeology and Dr. John Meadows of the Scientific Dating Team at English Heritage. The considerable technical problems faced could not have been overcome without the electronics skills of Dr. John Share and the the practical advice of John Hakes of the Geomagnetism Laboratory, University of Liverpool. I would further like to thank all the staff and students at the Geomagnetism Laboratory for fostering a supportive research environment, especially Dr. Andrew Biggin for helpful discussions of an epistemological bent and Dr. Ceri Davies, not only for his insights into mineral physics, but also for many fruitful dialogues concerning the nature of scientific enquiry.

Table of contents

Chapter 1

Introduction

The firing of clay to produce pottery or building materials has been commonplace throughout antiquity and such materials form an important part of the archaeological record. During firing, iron often forms magnetic minerals, which become permanently magnetised on cooling in the Earth's magnetic field, a phenomenon known as thermoremanence. Pottery, bricks and burnt clay structures can then record information about changes in the geomagnetic field over archaeological timescales. In the early 1960s, the then editor of *Archaeometry* ,M.J. Aitken, realised that this could be exploited as an archaeological dating tool if enough information about past changes in the Earth's field could be accumulated and set about constructing a record of the variation in the direction of the geomagnetic field by measuring the direction of remanent magnetism of fired structures that had been excavated *in situ* with their orientation preserved (Aitken and Weaver 1962) . The best estimate for the date of firing was plotted against the two components of direction to give a secular variation curve that could be used to date other similar structures. It became clear that these records had important geophysical implications and it was realised that records from distant regions could be used to study non-dipole components of the geomagnetic field (Aitken 1964).

The motivation for this project was to produce a British archaeointensity record with which to constrain a geomagnetic field model for archaeomagnetic dating of British archaeological sites. It was further envisaged that if a high quality archaeointensity record could be created and that there were periods of rapid variation in field strength (e.g. Genevey et al. 2009), archaeointensity could itself be used to constrain archaeomagnetic dates. This aim presents two main challenges: obtaining enough well dated archaeological material for analysis and extracting reliable estimates of the ancient field strength. Material was obtained through a number of different sources: the CASE partner English Heritage made some samples available that had been collected for archaeomagnetic directional dating, some pottery was supplied by museums and some material was excavated by ourselves.

The determination of direction of remanence can be achieved fairly simply as long as the samples can be transferred from the field to the laboratory with their orientation preserved .Orientation errors are generally of the order of a few degrees so if enough

individual samples are taken, the mean direction can often be found to within 2-3°. Typically, the geomagnetic field at a given location will vary by this amount in 10-20 years, so if an accurate field model exists and the remanence is genuinely parallel to the field at the time of cooling, then it would be possible to achieve a dating uncertainty of +/-20 years. In some cases the direction of the remanent magnetisation may differ considerably from that of the ambient geomagnetic field either because of anisotropy of remanence or because of magnetic refraction. Archaeological materials, especially ceramics and bricks, can exhibit magnetic anisotropy, as the easy axes of magnetisation of magnetic minerals within the fabric tend to become aligned during the elaboration of the artefact. The anisotropy can be determined, and hence corrected for, by laboratory experiment although such experiments are difficult to execute. Magnetic refraction, the deflection of magnetic lines of flux as they pass between materials of different permeability, has never been fully explained in archaeological materials. There is empirical evidence for the inclination of the magnetic remanence to be shallower than that of the ambient field in flat structures of even moderate susceptibilty, but all existing models, while qualitatively reproducing the effect, only predict a noticeable effect for extremely high magnetic susceptibilities.

Theoretically, burnt materials should also record the strength of the ambient field at the time of firing but the determination of this is technically more demanding and often fails, principally because as the sample is reheated to impart a laboratory remanence, with which the ancient remanence can be compared, the minerals are prone to alteration (Walton 1980). Despite this, efforts were made to study the ancient field intensity using pottery, which, having been fired to high temperatures during its manufacture may be somewhat resistant to alteration, although such studies were rarely used to constrain archaeomagnetic dates (Sternberg 2008). As well as the problem of detecting alteration, the domain state of the magnetic remanence carriers may affect the resulting archaeointensity, as will anisotropy if not corrected for. Furthermore the strength of magnetisation of the material is a weak function of the rate at which it cooled as well as the strength of the field during cooling, so this must be taken into account. Intensity results may also be affected by magnetic refraction if the models used in archaeomagnetic directional studies are to be believed, but this does not seem to have ever been considered.

In an attempt to reduce thermo-chemical alteration of samples, microwave demagnetisation (Walton *et al.*1996) was principally used to demagnetise and remagnetise

the samples in this study to obtain archaeointensities. Explained simply, applying a small high frequency alternating magnetic field to a magnetically ordered crystal will cause the electronic magnetic moments to precess around the axis of the crystal's internal magnetic field. If an appropriate frequency is chosen the precession of the electrons will become coupled to the microwave field and the spin system will absorb energy. The magnetic vector of the grain can then re-orientate in much the same way as if it had absorbed thermal energy but without heating of the bulk matrix of the sample. The method also substantially reduces the time required to do a single archaeointensity determination as the sample takes only a couple of seconds to absorb the energy, compared to repeatedly heating and cooling it in an oven. Another important advantage for the purposes of this project is that the microwave system at the University of Liverpool uses small samples 5mm in diameter. This minimises the amount of destructive sampling that is necessary and so reduces the impact on culturally important assemblages, although the small sample size precludes the measurement of samples with a magnetisation of less than about 0.1 A/m. The method had been used successfully on British post-medieval brick (Casas et al. 2005), as well as Mexican pottery (Boehnel et al.2003) and recently Lapita ceramics from the south Pacific (Stark et al.2010) as well as volcanic rocks.

Despite its increasing acceptance as a palaeointensity technique, microwave demagnetisation has never been placed on a sound theoretical footing. The optimum frequency to use has never been established and the reasons why some samples are more resistant to demagnetisation than others have never been fully understood. In some cases in this study it was found not to be possible to demagnetise samples either because the samples themselves did not absorb microwave energy or because their presence in the microwave cavity prevented the coupling of the cavity to the power source. In an attempt to overcome these problems the theory of microwave demagnetisation was re-examined and it was shown that the main factor determining the propensity of a sample to absorb microwaves is its dielectric function. A major problem faced was how to adapt the microwave palaeointensity technique to British ceramics that generally have very different dielectric properties to previously studied materials. Through addressing this issue, it was shown that certain tenets of the existing theory of microwave demagnetisation lacked substance and the need for a thorough re-examination of both the theory and practice of the use of microwaves in archaeointensity became increasingly clear. The results of this work are given in chapters 2 to 4. A critique of the theory as formulated by Walton et al. (2004a) is given in chapter 2 and the various processes by which matter can absorb

microwaves are outlined with particular emphasis being laid on the difference between dielectric and magnetic absorption mechanisms. In chapter 3 methods for describing the fields in a microwave cavity are developed and it is shown that damping of the fields is primarily controlled by the dielectric function of the sample. This important point is then used to explain many previously reported experimental observations. Chapter 4, a reproduction of Suttie et al. (2010), uses the theories developed in chapters 2 and 3 to design an experiment that demonstrates the possibility of demagnetising a natural rock sample without excessive heating. By carefully choosing the geometry of both the cavity and the sample, it is shown that the dielectric and magnetic absorption can be distinguished from one another by employing the mathematical formalism of perturbation theory.

Before considering the data acquired throughout this project, we review the existing archaeomagnetic data set and consider how it has been used, and how informative it has proven to be. As the Earth's magnetic field varies over space, the archaeomagnetic reference curves, whether of field direction or magnitude, are only valid over limited regions and have tended to be constructed by a join-the-dots principle, the curve being hand-drawn through the data points. Later curves employed more advanced data modelling but still treated the three different components of the field as independent, although knowledge of one could be used to constrain the others. A different approach was proposed by Lodge and Holme (2008); by expanding the potential in spherical harmonics a global field model could be produced for the purpose of archaeomagnetic dating. Such a model ensures that the modelled field vectors are physically plausible because the potential is forced to be harmonic. While such a modelling strategy can be applied to purely directional data (e.g Jackson et al. 2000), the magnitudes of the field vectors provide powerful additional constraints as they contain different information about the field at the core mantle boundary from the directional data (Johnson and Constable 1997).Hence the acquisition of archaeointensity data has a two-fold purpose; the creation of a local British intensity variation curve which could complement the directional secular variation curves for archaeomagnetic dating and to provide important geophysical constraints to global geomagnetic field models which will help elucidate processes occurring within the Earth's core.

It is important to keep the distinction between these two objectives in mind when analysing archaeointensity data. For instance, data that exhibits a wide dispersion will be of

little use for archaeomagnetic dating, but as long as it is accurate (i.e. dispersed about the true value), then the data will still provide a useful constraint for geomagnetic field models if it is numerous enough. The overall quality of existing archaeointensity data, and indeed the assignment of uncertainties, is a matter of some debate. Quality is often assessed by various *ad hoc* quality factors, and data are often preferentially weighted according to experimental protocol when they are used for field modelling, yet there is little evidence to justify this approach. An alternative to building either local intensity variation curves or using weighted archaeointensity data to constrain field models is to use the existing global archaeointensity data set to scale a directional global field model, but such an approach is only justified if the data can be shown to be consistent and is numerous enough for uncertainties and small local variations, both in the model and in the actual field, to be averaged out. Previously this approach has been tried by Gubbins et al. (2006), but here we show the assignment of uncertainty to the data introduced a bias that made the conclusions unreliable. Genevey at al. (2009) focussed on a small data set of very precise archaeointensity measurements from France and argued that these could be used to scale a global field model. Here it is argued that a greater number of less precise data is more informative than a small number of data of arbitrarily high precision, because of the influence of systematic errors, although the associated uncertainties in the data must be rigorously assessed for meaningful conclusions to be drawn. Chapter 5 introduces the methodology of archaeointensity and describes some of the commonly used schemes for reporting results and assessing their reliability. These conventional schemes and statistics are used throughout the thesis in the reporting of results, but it is argued throughout that their largely *ad hoc* nature mean that there is no single set of criteria that can guarantee the reliability of results. Chapter 6, currently under revision for *Earth and Planetary Science Letters*, extends this theme by examining the effect of inconsistent error estimation and spurious weighting on geomagnetic field models. A meta-analysis of global archaeointensity results for the past 400 years is presented in order to test the validity of various archaeointensity methods. Importantly, it is shown that when justifiable estimates of uncertainty are assigned to the data they imply a rapidly decreasing dipole for the entire period, a result with far reaching implications. This work also allows a benchmark to be set, against which results obtained herein can be tested.

Archaeointensities from various materials are given in chapters 7 to14 with each chapter focussing on a particular site or assemblage. A short background to each site or assemblage is given followed by magnetic mineralogical investigations, archaeointensity analysis and a

discussion of any issues particular to the material being studied. Microwave and thermal archaeointensity results from Anglo-Saxon burned clay, previously analysed for archaeomagnetic directional dating, are presented in chapter 7. The results obtained by the two methods are shown to be consistent, but, it is argued, the resulting estimate of field strength may be in error due to diagenesis of the clay. Chapter 8 reports archaeointensity from tobacco pipes with the focus being on obtaining results from the strongly anisotropic stems. Post-medieval tobacco pipes are often well-dated and attempts to utilise them to measure field intensity have been tried before but the high degree of anisotropy made it difficult to obtain results from the commonly available stems (Games and Baker 1981). Chapter 9 gives microwave results from bricks from a post-Medieval kiln, previously dated by archaeomagnetic directions. The discussion focuses on the effect of cooling rate on archaeointensity and the problem of empirically deriving an estimate for its magnitude. An assemblage of pottery from the Brookhill pottery in North Wales is analysed in chapter 10. The number of pieces from a well-dated context allows for an analysis of the observed variance and it is shown in this case to be principally explained by the variance between the individual sherds. Chapter 11 discusses microwave results from late 16th/ early 17th C tiles taken from a kiln that had been dated using archaeomagnetic directions. The intensity data from these specimens are very high and, given the low dispersion of the data, the discussion dwells on what may be causing the apparently anomalous high result. For completeness, chapter 12 reports a single result from a Norman furnace, previously dated using archaeomagnetic directions. A number of objections are raised to the validity of this result, however, principally based on considerations of domain state and diagenesis.

The remainder of the archaeointensity results were obtained using conventional heating rather than by microwaves. Chapter 13 looks at the possibility of determining archaeointensity from burnt sandstone where the low remanent magnetisation means that the small samples used in microwave archaeointensity carry too low a magnetic moment for measurement. Two sets of samples, archaeomagnetically dated to the early 18th and mid 19th C, were analysed and the results, while imprecise, were found to be consistent with the field model proposed in chapter 6. The archaeomagnetism of a late 18th C Delftware kiln is analysed in depth in chapter 14. A description of the kiln, its excavation and sampling is given along with the archaeomagnetic analyses. Both field direction and intensity are derived two give a complete vector description of the field in 1785 at the site. The problem of magnetic refraction is considered in detail and a model is proposed that, for the first time, is capable of quantitatively explaining the effect. The model allows for an

adjustment in direction with no corresponding deviation of the intensity and the resulting low intensity derived from the feature is found to be consistent with late 18th C intensities from France, raising the possibility of a dipole low during this period. Chapter 15 gives an overview of the archaeointensity results, comparing them with previously obtained data and considering the geophysical implications. The possibility of using archaeointensity as part of a dating strategy is explored, highlighting periods where such an approach might be appropriate.

The thesis contains two chapters that, as published or submitted papers, have co-authorship. Chapter 4 (Suttie et al. 2010) is included because it forms the natural conclusion to the arguments put forward in chapters 2 and 3. Specifically, whereas chapter 3 calculates the energy density in an unperturbed microwave cavity and argues that a similar distribution should be expected when the perturbation is small, chapter 4 uses the perturbation theory to develop an experiment in which the presence of the sample within the cavity is accounted for. Importantly, having questioned the existing theory of microwave demagnetisation and the interpretation of experimental evidence for its efficacy in chapters 2 and 3, chapter 4 gives experimental proof of the concept. The co-authors, Prof. Shaw and Dr. Hill primarily assisted with form and structure of the paper. Prof. Shaw assisted with certain technical aspects of the experiment, particularly the measurement of sample temperature. Chapter 6 has been submitted to *Earth and Planetary Science Letters*, with co-authors Dr. Holme, Dr. Hill and Prof. Shaw. It is included as it not only gives an insight into the epistemology of archaeointensity, but further quantifies the likely errors and therefore has implications for the application of archaeointensity to scientific dating. The assistance of Dr. Holme in writing the necessary FORTRAN code is acknowledged as well as his useful insights into methods of data analysis. The analysis was carried out solely by the author. Dr. Hill and Prof. Shaw provided some assistance with structure and tone of the paper.

Chapter 2

Microwave demagnetisation I: electromagnetic theory and the absorption of microwaves by matter

In this chapter the theory of electromagnetism and its application to problems of absorption will be reviewed. The aim is to outline all the possible mechanisms by which microwaves may be absorbed by commonly used palaeomagnetic and archaeomagnetic materials. For this reason conductors will not be considered in detail. Firstly the macroscopic theory of electromagnetism will be used to examine the bulk absorption of microwaves. This will be extended to deal with absorption by small particles. Special attention will then be given to absorption by magnetic particles and involving the magnetic component of the microwave field. Theories of magnetic absorption that have been developed specifically within the field of palaeomagnetism will be critically reviewed.

2.1 Electromagnetic theory

There is no completely uncontroversial way to introduce the field quantities that will be used to develop the theory of microwaves and their interactions with matter. While there is little argument over the correct microscopic form of the Maxwell equations, their extension to bulk properties of matter has long been debated (Bohren and Huffman 1983:13). Here we will only briefly mention the alternative interpretations of field quantities and equations. We take the macroscopic form of the Maxwell equations to be

$$\nabla \times \mathbf{H} = j + \frac{\delta D}{\delta t} \qquad 2.1$$

$$\nabla . \mathbf{D} = \rho \qquad 2.2$$

$$\nabla . \mathbf{B} = 0 \qquad 2.3$$

$$\nabla \times \mathbf{E} = \frac{\delta B}{\delta t} \qquad 2.4$$

where E is the electric field , B is the magnetic flux density, H is the magnetic field and D is the electric flux density. D is related to E and H is related to B by the constitutive relations

$$\mathbf{D} = \varepsilon \mathbf{E} \qquad 2.5$$

$$\mathbf{B} = \mu \mathbf{H} \qquad 2.6$$

where μ and ε are the magnetic permeability and the electric permittivity respectively. Some explanation is needed here although it is rarely given. In particular the relationship between B and H is often misunderstood. Perhaps the simplest way of considering the constitutive relations is the following, due to Sommerfeld (1964). A charge density ρ gives rise to a field D. D is a measure of quantity: an amount of something. The field E is a measure of the intensity of the resulting field. Similarly a current j gives rise to a field H: H is a measure of the amount of excitation. B is the intensity of the resulting field. The product of an amount and an intensity in general gives an energy. For example, by way of an analogy, a spring may be extended an amount and the resulting force is found by the spring constant, a constitutive relation. The potential energy is found by taking the product of the extension and the force. Pressure and volume would be another example of a constitutive pair, one being an amount, the volume, and one being intensity, the pressure. Thinking of the magnetic field in terms of the spring analogy, H is the extension and B the force, or by the pressure analogy, H is the "volume" of magnetisation and B the "pressure", although an experimental attempt to refute this interpretation has been made (Whitworth and Stopes-Roe 1971). The important point is that equations represent spatial averages of the microscopic equations where it is the vectors **E** and **B** that are averaged over the material (Russakoff 1970).

When the field quantities vary with time, complex notation will be employed. The time dependence is always $e^{i\omega t}$ so there is no need to include this factor in the expressions for the fields. It is to be understood that when a field is described by a complex vector, a phasor, the complete time dependent description of the field can be found by multiplying by $e^{i\omega t}$ and taking the real part. For example when a field is described by $\mathcal{F}(x,y,z,t) = Re(F(x,y,z)e^{i\omega t}$, only the phasor *F* will be expressed. If *F* is real then the field has cosine time dependence. If F has an imaginary part there will be an out-of-phase part to the field. It should be stressed that the use of complex variables is a matter of convenience and that sine and cosine expansions would yield the same results.

By choosing a $e^{i\omega t}$ time dependence, the driving force has the phase cos ωt . Returning to the spring analogy, one can imagine a spring being driven by a force with cos ωt time dependence. If ω is the natural frequency of oscillation of the spring, the displacement will grow ever larger. In the absence of losses it will be unbounded, and in phase with the driving force. In reality there will always be a loss mechanism that limits the displacement of the spring and this is due to the out of phase response. This is one of the advantages of

the complex notation: loss mechanisms can easily be incorporated simply by adding an imaginary part to the constitutive relations. These are usually expressed as complex variables at high frequencies: $\varepsilon = \varepsilon' - j\varepsilon''$ and $\mu = \mu' - j\mu''$ where the real part represents dispersion and the imaginary part represents the absorption.

The loss at any given frequency is often characterised by the dielectric loss tangent, $\tan\delta_e = \varepsilon''/\varepsilon'$ and the magnetic loss tangent, $\tan\delta_m = \mu''/\mu'$. Dividing ε' by the permittivity of free space, ε_0 , gives the dimensionless relative permittivity ε_r so that $\varepsilon/\varepsilon_0 = \varepsilon_r(1 - j\tan\delta_e)$. Similarly dividing μ' by the permeability of free space, μ_0 , gives the dimensionless relative permeability μ_r so that $\mu/\mu_0 = \mu_r(1 - j\tan\delta_m)$. Some values of ε_r and ε'' for commonly encountered minerals and other materials are given in table 2.1. It has often been claimed that when microwaves are employed in palaeomagnetism, they interact with the titanomagnetite grains through a magnetic resonant absorption mechanism (e.g. Walton et al. 1996, Brown et al. 2007). Before tackling this subject the different ways in which matter can absorb electromagnetic energy will be outlined and some terminology will be defined. In the vast majority of materials absorption occurs due to the time varying electric field inducing a polarization within the material. This will be called electrical absorption. A note of caution: throughout this chapter the term magnetic absorption will be used to describe cases where absorption occurs due to the interaction with the magnetic field component, not absorption due to a high displacement current, as defined by some authors (e.g. Landau and Lifshitz 1984). The discussion of electrical absorption here will be limited to the case of a bulk dielectric of volume V in a time varying field **E** of frequency ω. The rate of dissipation of energy (W)is (e.g Sommerfeld 1964, Landau and Lifshitz,1984)

$$W = \frac{\omega}{2}\varepsilon'' \iiint_V |\boldsymbol{E}^2| dV \qquad 2.7$$

Table 2.1 Some values of ε_r and ε'' for certain minerals and other common materials. Values marked with asterisks, include the conductivity in the imaginary part of the permittivitty

Material	**ε_r**	**tanδ**	**ε'' (pF/m)**	**Frequency (GHz)**	**Reference**
Basalt(1)	7.9	0.056	3.9	9.37	Zheng et al. (2005)
Basalt(2)	7.55	0.0744	4.9	9.37	Zheng et al. (2005)
Pyroxene	7.9	0.057	4.0	9.37	Zheng et al. (2005)
Olivine	8.05	0.0072	0.5	9.37	Zheng et al. (2005)
Plagioclase	6.56	0.049	2.8	9.37	Zheng et al. (2005)
Fused quartz	3.78	0.0001	0.003	10	Rizzi (1988)
Magnetite (bulk)	≈100	≈1.2	≈1000*	3	Fannin et al.(2007)
Magnetite (nanoparticles)	36.8	0.46	150*	3	Fannin et al.(2007)
Vanadic titano-magnetite	343	0.17	513*	9.37	Zheng et al. (2005)
Alumina	9.6	0.0001	0.008	10	Rizzi (1988)
Mica	5.4	0.0003	0.01	10	Rizzi (1988)
Wood (dry balsa)	1.2	0.1	1.0	10	Rizzi (1988)
Water	76.7	0.157	106	3	Rizzi (1988)

It is the quadrature permittivity that determines the dissipation of energy in the material as explained above. It is clear from the values in table 2.1 and equation 2.7 that the dielectric heating effect in, say, a basalt, composed of plagioclase and pyroxene will be very much larger than that for quartz, although Walton and Boehnel (2008) specifically uses the low observed loss in quartz to argue against dielectric heating in basalt. Much of the work in this project will concern ceramics. It is noted that low loss of porcelain makes it a useful material for constructing capacitors and it might be expected that some fine ceramics will have relatively low loss. Equation 2.7 will only be strictly true for a homogenous medium of uniform dielectric constant; the absorption of individual grains requires a more sophisticated treatment (see Bohren and Huffman 1983). The literature concerning microwave demagnetisation in palaeomagnetism does not generally address the issue of

dielectric heating in detail. Instead attention has been focussed on mechanisms of magnetic absorption.

2.2 Magnetic absorption

Having briefly described the electrical absorption of energy in a sample irradiated with microwaves attention is turned to magnetic absorption mechanisms. The first thing to note is that these are comparatively rare and less well understood than the electrical effects. They also cease to become important at relatively low frequencies (Landau and Lifshitz 1984) whereas electrical effects extend into the optical bands and beyond. If the susceptibility is known then the absorption in low fields can be calculated in much the same way as in the case of dielectrics. There is an important difference however: dielectric absorption at microwave frequencies is due to Debye relaxation whereas in the magnetic case this occurs at much lower frequencies (Chen et al. 2004). The magnetic susceptibility may then exhibit resonant (Lorentz) behaviour at microwave frequencies, and so vary rapidly with frequency, whereas the dielectric function will only vary slowly and will not exhibit resonance. The everyday heating of food in a microwave oven, for instance, is not a resonant absorption, but simply Debye relaxation.

At its simplest, a ferrimagnetic mineral can be thought of as an ordered array of electronic spins. Although it is not strictly correct to describe electron spins in classical terms, as the spin is a purely quantum mechanical quantity, it is still a useful approach. When the frequency of the driving force is close to the precession frequency of the electronic spins, the spin system will become coupled with the r.f. field and absorb energy. When all the spins precess in phase the mode of excitation is called the uniform mode. As the energy of the system increases the uniform mode breaks down into spin-waves or magnons. These can be thought of as wave like disturbances of the phase angle of the electron spins (or the corresponding magnetic moment in a given direction). Stacey and Banerjee (1974) offer the analogy of waves in a field of barley on a windy day. Under certain conditions non-uniform modes may be directly excited by the microwave field.

The dispersion of the susceptibility at microwave frequencies has a Lorenztian form (Morrish 1980, Chen 2004). No empirical data relating to the dispersion of the susceptibility of magnetite could be found in the literature, presumably because its high dielectric loss (see table 2.1) makes it experimentally difficult. The real and imaginary parts of the susceptibility of maghaemite have been determined at frequencies up to 12.2 GHz, and

show a broad peak in the imaginary part at frequencies between 2 and 6 GHz (Vastyn et al. 1962). Similar behaviour is predicted theoretically for magnetite (Morrish 1980, Draine and Lazarian 1999).

At lower frequencies the dielectric absorption decreases if there is no great frequency dependence of the dielectric function. At a frequency of 2.45GHz it has been possible to examine the effect of both the magnetic and electric field on magnetite. Interestingly, electron microscopy and XRD of the crystal structure of magnetite heated by magnetic absorption showed a different structure, with a decrease in long range order and a unique microstructure, when compared to crystals that had been heated dielectrically (Roy et al. 2002). These experiments show that bulk magnetite couples strongly with the magnetic component of the microwave field at 2.45GHz, but there are no experiments on the very small grains that form the magnetic carriers in palaeo and archaeomagnetism. During this project the only microwave source was 14-14.5GHz, which is considerably higher than the frequency of the peak susceptibility of magnetite.

2.3 Microwave demagnetisation

The possibility of demagnetising palaeomagnetic samples using microwave was reported by Walton (1991).There had been attempts to use microwave heating in the analysis of lunar samples previously, but this was an attempt to use the ohmic heating of the conductive portions of the lunar fines (Hale et al. 1978). The approach of Walton et al. (1991) was different in that it attempted to use the magnetic component of the microwave field to transfer energy directly to the magnetic grains and so avoid bulk heating of the matrix. Initial attempts used 2.45GHz as this was easily available. Later an 8.2 GHz system was developed (Walton et al. 1993). Walton et al. (1996) claimed that this was capable of directly generating spinwaves without exciting the uniform mode although it is not clear how this was established. This interpretation has nevertheless been widely accepted and cited in the palaeomagnetic literature (e.g. Brown et al. 2009). Later higher frequencies were used apparently because of experimental evidence that they could demagnetise material more efficiently (Walton 2002), but the dielectric contribution to heating was considered negligible. The suggestion was that spinwaves in small grains must have a short wavelength and could then only be excited by correspondingly high frequencies. In particular it was claimed that spinwaves could be directly excited in the absence of a large bias field (a steady field applied at the same time as the time varying microwave field) and that this led to massive absorption of energy in the magnetic grains. In an experiment

where the temperature of samples in a microwave cavity was monitored, pure magnetite and basalt, containing about 0.1% magnetite, showed similar temperature rises in a microwave cavity (Walton et al. 2004a). The resulting absorption was claimed to be firstly, largely independent of the amount of magnetic material, and secondly, a broadband absorption above a certain critical frequency (Walton and Boehnel 2008).

Here, a less esoteric theory concerning the absorption of microwaves by magnetite will be developed. To understand previously published experimental findings a fuller understanding of the operation of a microwave resonant cavity will be required. This is given in Chapter3. For the time being, certain inconsistencies in the theory of microwave demagnetisation (Walton et al. 2004a, Walton et al. 2004b) will be highlighted.

The magnetic properties of ferrites other than magnetite are used in various microwave applications. In most cases they have large saturating steady fields applied, known as a bias field, and their response to the microwave field is usually given as a function of the bias field, rather than the frequency. Microwave engineers make the distinction between two types of power loss in ferrites, an effect that they are usually trying to avoid. Firstly, there is low field loss which occurs when the ferrite is magnetised below saturation and secondly there are effects due to high power non-linearity which occur in the presence of a strong bias field(Baden Fuller 1987: 222). The maximum angular frequency (ω_{max}) at which low frequency loss can occur is given by $\omega_{max} = \gamma(H_a + B_s/\mu_0)$, where γ is the gyromagnetic ratio, H_a is the anisotropy field and B_s is the saturating field(Baden Fuller 1984:226). Using typical values of 20kA/m for the anisotropy field and 200mT for the saturating field (Dunlop and Özdemir 1997) gives a maximum frequency of 6.3GHz. Microwave palaeointensities have used frequencies of 8.2GHz, 14Ghz and 16GHz, well above the upper limit for low field loss in magnetite.

We will not attempt to give the mathematical theory concerning the generation and propagation of spinwaves (see Suhl 1956) as it is highly complex and would dwarf the present work. Instead we will develop a simple argument that shows that it is not possible to have very large absorption across a range of frequencies in the absence of a large bias field. To do this we will introduce the concept of the complex frequency.

2.4 The complex frequency

The quantities ε and μ have been introduced as complex-valued functions of the real variable ω. Instead, we can account for the in phase and out of phase response by

introducing the complex angular frequency $\omega = \omega' - j\omega''$ and considering the susceptibility, $\chi(\omega)$. Take the integral of $\oint \frac{\chi(\omega)}{\omega - s} d\omega$ around the contour shown in figure 2.1, where s is some fixed frequency at which the susceptibility is to be evaluated and the path marked 1 is at infinity. It can be shown that as long as the response in the time domain is a linear function of the applied field, then $\frac{\chi(\omega)}{\omega - s}$ is analytic in the half-plane, hence $\oint \frac{\chi(\omega)}{\omega - s} d\omega = 0$. Adding up the contributions from 1,2,3,and 4 so that they equal 0, it can easily be shown that

$$\chi'(s) = \frac{2}{\pi} \int_0^{\infty} \frac{\omega \chi''(\omega)}{\omega^2 - s^2} d\omega \qquad 2.7$$

$$\chi''(s) = -\frac{2s}{\pi} \int_0^{\infty} \frac{\chi'(\omega)}{\omega^2 - s^2} d\omega \qquad 2.8$$

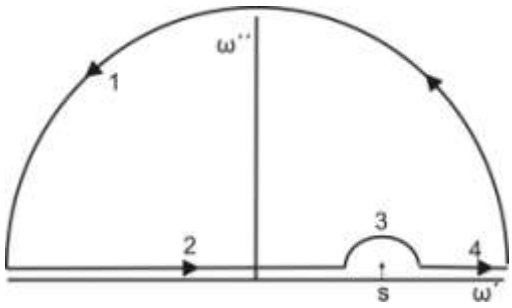

Figure 2.1 The contour of integration in the complex plane used to derive the relations 2.7 and 2.8.

The real and imaginary parts of a response function are not independent but satisfy what are known as the Kramers-Kronig relations (Bohren and Huffman 1983). These relations are very useful when looking for absorption mechanisms because anything that leads to absorption anywhere in the frequency spectrum should show up in the real part of the response. In fact they appear not to have been used in rock magnetism despite the promise of great utility. As an example imagine the static susceptibility of a mixture of superparamagnetic and multi-domain grains. We see that $\chi'(0) = \frac{2}{\pi} \int_0^{\infty} \frac{\chi''(\omega)}{\omega} d\omega$ which, as the frequency appears in the denominator suggests that the susceptibility should be dominated by the grains with low frequency loss. This is indeed the case; superparamagnetic grains will tend to dominate the susceptibility of an assemblage (Dunlop and Özdemir 1997) but here it has been demonstrated simply by using the properties of complex variables without appealing to the physics of the problem at all. The

Kramers Kronig relations are especially useful in magnetism because the susceptibility tends to zero at relatively low frequencies (Landau and Lifshitz 1984)so there is no need to complete the integral beyond a convenient upper limit yet they are rarely , if ever, used.

These relations effectively limit both the amount of absorption that can occur and the frequency range over which it occurs. If there was, for instance, the possibility of strong absorption across a large range of frequencies, this would have to be apparent in the real part of the susceptibility, unless there is a violation of the Kramers Kronig conditions: causality and linearity. While we may look for non-linear aspects to the response function, causality must be maintained. A non-linear response can be associated with large absorption mechanisms because the Kramers Kronig relation need not apply. This may be achieved by applying a saturating bias field as a saturated specimen effectively has 0 susceptibility below a certain critical threshold, or by applying alternating fields of sufficient magnitude to impose a non-linear response. From this argument it can be seen that the sort of broadband, large scale absorption that has been suggested (Walton and Boehnel 2008) cannot occur in low bias fields, unless the alternating field is very large. Nor can the absorption be independent of concentration unless the real part of the susceptibilty is similarly independent, which is clearly not possible. The actual magnitude of the fields in a microwave cavity during a palaeointensity experiment have, as yet, not been quantified. This omission is rectified in chapter3.

Of course there will always be some amount of absorption and scattering of incident electromagnetic radiation for any non-zero susceptibility, electric or magnetic. What is being argued here is that there are no mechanisms at work at high frequencies in zero bias field that cannot be explained by classical theories of electromagnetism. In the next chapter an understanding of microwave transmission will be developed so that the results of previous experiments, interpreted as demonstrating new physical phenomenon (Walton 2004a), can be parsimoniously explained.

Chapter 3

Microwave Demagnetisation II : Material characterisation and measurements

In this chapter the practicalities of applying microwaves to real samples are explored in detail and methods for measuring their absorption are developed. In particular it will be shown how the introduction of a sample to a resonant microwave cavity affects the cavity's characteristics and how transmission line measurements can be used to understand the processes by which the sample absorbs microwaves. After reviewing transmission line theory, resonant cavities and perturbation theory, some experimental results are considered in detail in order to resolve some of the controversies that were raised in the previous chapter.

3.1 The wave guide

Before considering the microwave cavity in detail, it is worth looking briefly at the waveguide which is used as a transmission line at the GHz frequencies used here. The resonant cavity is essentially a shorted length of waveguide so it is natural to consider this first. In addition the only measurements that can easily be made when operating the microwave system are taken on the transmission line, rather than in the cavity and so understanding waveguide theory, or more generally transmission line theory is going to be important in developing an understanding of the theory of microwave demagnetisation.

At its simplest a transmission line is used to transfer power from one point to another and, at low frequencies, can consist of two wires. At microwave frequencies wires can no longer be used as they radiate more power than they transmit and waveguides or coaxial cable are used. The wave guide is a hollow metal tube along which power is transferred. Only two shapes of waveguide need be considered here: those with rectangular cross-section and those with circular cross-section. The microwave system uses a rectangular waveguide to transmit power from the amplifier to the cavity and a short length of circular waveguide as the cavity resonator. The mathematical theory of waveguides is given in a great many text books (e.g. Pozar 2004, Rizzi 1988) and there is no need to repeat it here. Instead their operation will be described in simple terms and only some important quantities that will be of use later will be defined.

When a waveguide is excited by some power source power may be transmitted along the guide if certain conditions are met. One can think of electromagnetic waves being reflected by the conducting walls of the waveguide as they travel along it. Waves being reflected by opposite walls will interfere resulting in a characteristic pattern of electric and magnetic fields within the waveguide. A particular pattern of fields is known as a *mode* and there is a useful nomenclature for describing them. Modes are divided into two basic types; ones with longitudinal electric field components but only transverse magnetic fields, and ones with longitudinal magnetic field components but only transverse electric fields. These are known as transverse magnetic (TM) and transverse electric (TE) respectively. Waves whose E-field and H-field are both perpendicular to the direction of power flow, as are seen in plane waves in free space, cannot exist in waveguides. Two parameters are then required to fully describe a mode in either rectangular or circular waveguide. In rectangular wave guide we define n as the number of field variations along the broad wall of the wave guide and m as the number of field variations along the narrow wall. A mode can then be described conveniently in the form TE_{nm} or TM_{nm}. In circular wave guides n is defined as the number of azimuthal field maxima and m as the number of radial field maxima. In this work we shall deal almost exclusively with TE modes. The wave length in the waveguide is the distance between peak electrical fields and we denote this as the guide wavelength, λ_g. The propagation constant (β) is $2\pi/\lambda_g$. In general we will use complex variables to describe wave propagation so that a wave propagating in the z direction along the waveguide can be described by $E(x,y)e^{-i\beta z}$ and $H(x,y)e^{-i\beta z}$. All the field quantities will have a $e^{-i\omega t}$ time dependence which will not be explicitly expressed. Loss in the wave guide can easily be accommodated by the use of a complex propagation constant: $\gamma=\beta+i\alpha$. β is always smaller than the free space wavenumber k; the guide wavelength is longer than the wavelength in free space.

For any given mode the waveguide has a cutoff frequency, below which microwaves cannot propagate and we denote the corresponding cutoff wavenumber as k_c. At this frequency the guide wavelength becomes infinite. In rectangular waveguide the cutoff wavlength of the dominant TE_{01} mode is simply twice the width of the waveguide. β is related to k and k_c by the relation $\beta=\sqrt{(k^2- k_c^2)}$. From this it can be seen that when k less than k_c, the propagation constant becomes wholly imaginary and the fields decay exponentially along the line. Such fields are called evanescent.

Describing the fields in circular waveguides requires solving Maxwell's equations in cylindrical co-ordinates. A family of functions known as Bessel functions naturally arise in differential problems with circular symmetry so before examining circular waveguide it is helpful to review some of their properties. By convention Bessel functions of the first kind are denoted by $J_n(x)$, where n is the order of the Bessel function. When considering a TE_{nm} mode in a circular waveguide, $J_n(r)$ describes the radial variation of some field components, where r is the radius, and the derivative $J_n'(r)$ the other components. An important constant is the m^{th} stationary point of $J_n(x)$: the m^{th} zero of $J_n'(x)$ which we will denote q. We will only consider m=1 modes (modes with one radial maximum) so will only need to consider the first stationary point of the corresponding Bessel function. Figure 3.1 shows the first two Bessel functions of the first kind and the line x/2 which can be used to approximate $J_1(x)$ for small values of x.

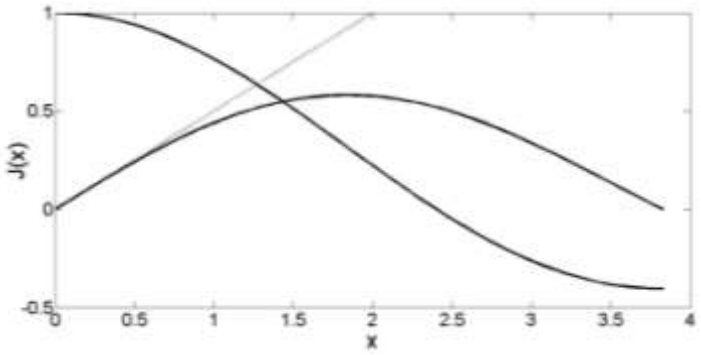

Figure 3.1 The first two Bessel functions of the first kind and the line x/2 which can be used to approximate $J_1(x)$ for small values of x.

The general formula for a Bessel function of the first kind is $J_n(x) = \sum_{m=0}^{\infty} \frac{-1^m (x/2)^{n+2m}}{m!(n+m)!}$.

From this it is easy to show that $J_1(x) = J_0'(x)$ and for small x, $J_1(x) \approx \frac{x}{2}$. The first zero of $J_0'(x)$ is 3.832=q for n=0. The line x/2 is shown in figure and it can be seen that it is a good approximation up to q/5. These facts will be used to simplify the calculation of energy in samples later on. If a waveguide has radius a, then the cutoff wavenumber is q/a. In the TE_{01} mode that will be chiefly discussed when considering cavity resonance, the electric field varies radially as $J_1\left(\frac{qr}{a}\right)$.

Another useful concept is that of surface resistance : the effective resistance of a conductor in a microwave field. At high frequencies , electromagnetic fields only penetrate a very small distance into a conductor and the characteristic distance is known as the skin depth, δ_s. The effective surface resistance R_s is then $1/(\sigma\ \delta)_s$, where σ is the conductivity. All the waveguides and components used in this work are made of brass and a value of R_s of

0.0466Ω has been calculated for brass at 14GHz. Table 3.1 lists all the quantities that will be used when discussing microwave propagation

Table 3.1 List of the terms and symbols used to describe waveguide transmission

Quantity	Symbol	Definition	Notes
Frequency	f	Cycles per second	
Wavelength	λ	Peak to peak distance of wave in free space	
Angular frequency	ω	2πf	
Wavenumber	k	2π/λ	
Cutoff wavenumber	k_c	Minimum wavenumber at which a given mode can propagate	q/a in circular waveguide , radius a.
Guide wavelength	λ_g	Peak to peak distance of wave in waveguide	Always longer than λ
Propagation constant	β	$2\pi/\lambda_g$	$=\sqrt{(k^2- k_c^2)}$. Replace with γ=β+iα for lossy transmission.
Surface resistivity	R_s	$\sqrt{(\omega\mu/2\sigma)}$	0.0466Ω for brass at 14GHz
Stationary point of Bessel function	q	J'(q)=0	3.832 for TE01 1.8 for TE11
Impedance of free space	η	E/H for a plane wave	$\sqrt{(\mu_0/\varepsilon_0)}$
Quality factor	Q	Stored energy/ energy lost per cycle	

Other than the peculiarities of waveguide transmission listed above, waveguides can be treated much as any other transmission line. Some of the general properties of transmission line are now reviewed. Imagine the simplified schematic of a transmission line shown in figure 3.2. It is customary to denote distance along the line as z (lowercase) and impedance as Z (uppercase).The voltage ($\mathcal{V}$(t,z)) and the current($\mathcal{I}$ (t,z))are functions of both distance along the line (*z*) and time. The time dependence is assumed to be $e^{i\omega t}$ and will not be shown so that the voltage and current can be described by the cosine based phasors V and I as explained in chapter 2. Here they are of course phasor scalar quantities rather than the phasor vectors used to describe the E and H fields.

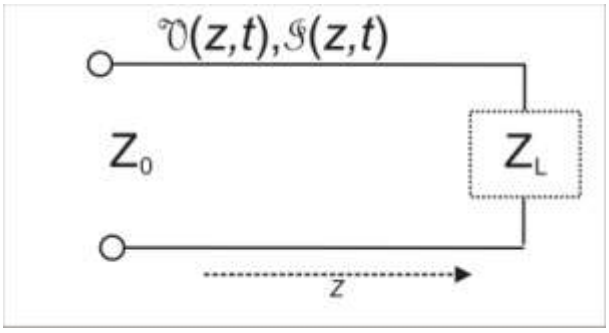

Figure 3.2 Schematic of the simple transmission line referred to in the text.

The solutions of the well-known telegrapher equations can be written

$V(z) = V^+e^{-i\beta z} + V^-e^{i\beta z}$ and $I(z) = I^+e^{-i\beta z} + I^-e^{i\beta z}$ which can be seen to represent two travelling waves, one in the forward direction and one in the reverse direction. The ratio

$\frac{V^+}{I^+} = -\frac{V^-}{I^-} = Z_0$ is called the characteristic impedance of the transmission line. Now imagine that some load with impedance Z_L is put across the line at the point z=0. Now the ratio V/I at the point z=0 must equal Z_L. Hence $Z_L = \frac{V^+ + V^-}{V^+ - V^-}Z_0$ or rearranging $V^- = \frac{Z_L - Z_0}{Z_L + Z_0}V^+$. There is a reflected wave the amplitude of which depends on the load impedance. In the case of a short circuit or an open circuit the reflected wave is the same amplitude as the forward wave. When the load impedance is equal to the characteristic impedance, there is no reflected wave and the load is said to be matched to the line. The ratio of the amplitude of the reflected wave to the forward wave is called the reflection co-efficient, Γ. Using this definition, it is possible to write the voltage as

$V(z) = V^+e^{-i\beta z}(1 + \Gamma e^{2i\beta z})$. Thus the magnitude of the wave is modulated along the line, with maxima and minima occurring every half wavelength. The ratio of maximum amplitude to minimum amplitude is called the voltage standing wave ratio (VSWR). At microwave frequencies it becomes impractical to make measurements of voltage or current on the line. Instead it is usual to measure power; at its simplest a microwave power meter can consist of a strong absorber such as water and a thermometer. The system used here allows the measurement of both the forward and reflected power by using directional couplers and power meters. When standing wave ratios (SWRs) are used they will refer to power standing wave ratios, rather than VSWRs. It is possible to measure the SWR on the transmission line and hence the magnitude, but not the phase of the reflection co-efficient, which will in general be complex. One further useful result is given without proof: if a

transmission line of length *l* is terminated in a short circuit, the input impedance is $iZ_0 \tan \theta l$ (e.g Pozar 2004).

If a section of lossless transmission line is short-circuited at both ends it will be able to support standing waves if the line is an integral number of half wavelengths long. Power incident on one end will be totally reflected due to the mismatch, travel to the opposite end and so forth. If the system is excited continually the fields will increase without limit. Clearly the notion of a completely lossless line is physically unrealisable as there will always be both series and shunt conduction losses. These losses will limit the size that the fields can reach. Such a system is called a resonator and provides an effective means of amplifying a signal. If the transmission line is made of waveguide, the system is called a cavity resonator. Here circular waveguide was used to make a cylindrical cavity resonator.

The waveguide is terminated by a slot coupled to the cavity resonator. It is the impedance of this slot that determines how much of the power is reflected. Calculating this is not a simple problem and the shape of the slot was determined by trial and error. The terminal impedance was found to depend strongly on whether the cavity was empty or not as well as the resonant frequency and mode of the cavity. Before considering these issues in detail, the operation of a cylindrical cavity resonator will be examined.

3.2 The microwave cavity

All the work contained in this thesis was carried out in a 30mm diameter brass cylindrical cavity, operating between 14 and 14.5 GHz with an adjustable end plate that allowed its length(l) to be varied. The mode in which a cavity resonates can be describe using the same notation as was used for waveguides, but with an additional suffix, $p=2l/\lambda_g$, the number of half wavelengths that span the length of the length of the cavity. The mode of the cavity can then be given as TE_{nmp}. The cavity is exited via the slot which terminates the waveguide. This slot acts as a magnetic dipole so that the resulting mode in the cavity must be a TE mode as a longitudinal magnetic field is being excited. For this reason TM modes will not be considered, although they may be present to some small degree. It is convenient to use cylindrical co-ordinates to describe the fields in the cavity. Figure 3.3 shows all the variables used in the field equations.

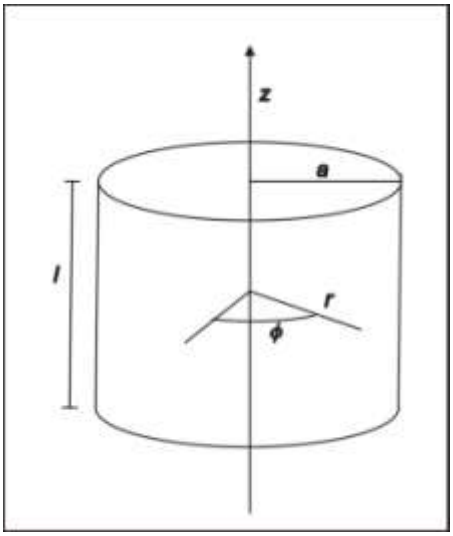

Figure 3.3 The geometry of the cylindrical cavity, showing all the spatial variables used in the field equations

As it is the magnetic field in the cavity that is primarily of interest, it makes sense to describe the fields within the cavity in terms of the maximum H-field, H_0;

$$E_\varphi = H_0 \frac{ik\eta a}{q} J_n'\left(\frac{qr}{a}\right) \cos n\varphi \sin \frac{p\pi z}{l}$$

$$E_r = \frac{ik\eta a^2 n}{q^2 r} H_0 J_n\left(\frac{qr}{a}\right) \sin n\varphi \sin \frac{p\pi z}{l}$$

$$E_z = 0$$

$$H_z = H_0 J_n\left(\frac{qr}{a}\right) \cos n\varphi \sin \frac{p\pi z}{l}$$

$$H_\varphi = H_0 \frac{-\beta a^2 n}{q^2 r} J_n\left(\frac{qr}{a}\right) \sin n\varphi \cos \frac{p\pi z}{l}$$

$$H_r = H_0 \frac{\beta a}{q} J_n'\left(\frac{qr}{a}\right) \cos n\varphi \sin \frac{p\pi z}{l}$$

In TE_{011}, the mode that was apparently used in all previous microwave palaeointensity experiments the electric field equations simplify to

$$E_z = E_r = H_\varphi = 0$$

$$E_\varphi = H_0 \frac{ik\eta a}{q} J_0'\left(\frac{qr}{a}\right) \sin \frac{\pi z}{l}$$

$$H_z = H_0 J_0\left(\frac{qr}{a}\right)\sin\frac{\pi z}{l}$$

$$H_r = H_0\frac{\beta a}{q}J_0'\left(\frac{qr}{a}\right)\sin\frac{\pi z}{l}$$

This makes it fairly straightforward to calculate the electrical energy density in a sample although this never appears to have been done, other than in Suttie et al. (2010). As $J_1(x) \approx J_0'(x)$, $E \propto J_1(\frac{3.83r}{a})$, where a is the radius of the cavity. For small x, $J_1(x) \approx \frac{x}{2}$, so the electric field increases linearly with radius if the sample is less than about one fifth the radius of the cavity. The heat generated by the electric field in the sample is given by (2.7)

$$\frac{\omega}{2}\varepsilon'' \iiint_S |\boldsymbol{E}^2| dV$$

It is possible to calculate the magnitude of the fields in the empty cavity by considering the power dissipated in the cavity walls by conduction (P_c).To do this we integrate the magnetic field components across the surface of the cavity. The power loss in a conducting sheet (s) is found by a surface integral

$$P_c = \frac{R_S}{2}\int_s H^2 ds$$

where H is always tangential to the surface and R_S is the surface resistivity (see table 3.1). In a TE_{011} cavity we integrate H_z around the circumference and H_φ over the two endplates.

The conductive power loss in the wall is straightforward to calculate. For brass at 14GHz R_S=0.0466Ω (see table), l=2cm,a=1.5cm, q=3.832 and $J_0(q)$=-0.40:

$$P_{wall} = \frac{R_S}{2}\int_{z=0}^{z=l}\int_{\varphi=0}^{\varphi=2\pi} H_z^2\,(r=a)a\,dzd\varphi$$

$$= \frac{R_S}{2}2\pi H_0^2 J_0^2(q)a\int_{z=0}^{z=l}\sin\frac{\pi z}{l}dz$$

$$= \frac{R_S}{2}\pi H_0^2 J_0^2(q)al = 3.5\times10^{-6}H_0^2$$

Similarly, the power absorbed at the two end plates can be calculated

$$P_{ends} = R_S \int_{r=0}^{r=a} \int_{\varphi=0}^{\varphi=2\pi} H_r^2\,(z=0) r\, dr d\varphi$$

$$= R_S 2\pi H_0^2 \left(\frac{\beta a}{q}\right)^2 \int_{r=0}^{r=a} (J_0')^2 \left(\frac{qr}{a}\right) r\, dr$$

The integral can be solved by substituting $J_1(x) = J_0'(x)$

then using the identity

$$\int x J_n(kx) dx = \frac{x^2}{2} \left(J_n^2(kx) - J_{n-1}(kx) J_{n+1}(kx)\right)$$

whence

$$\int_{r=0}^{r=a} (J_0')^2 \left(\frac{qr}{a}\right) r\, dr = -\frac{a^2}{2} J_0\left(\frac{qr}{a}\right) J_2\left(\frac{qr}{a}\right) = 0.081 a^2$$

We find

$$P_{ends} = 2 \times 10^{-6} H_0^2$$

$$P_c = P_{ends} + P_{wall} = 5.5 \times 10^{-6} H_0^2$$

These formulae give the power in Watts absorbed over the cavity for a given field in A/m at the centre of the cavity. The first thing to note is that the fields generated in the empty cavity are very large; if the cavity is absorbing 1W of power the magnetic field is 426A/m, which is over 0.5mT. It should be noted that the magnetic field only increases as the square root of the power so that at the full power of 80W, the H-field is still less than 5mT. There is also a theoretical maximum field that can be generated before the accompanying E-field causes the dielectric breakdown of air. The field required for this is about 3×10^6V/m and as the impedance of space is 378Ω, the maximum possible magnetic field will be 10mT. Such fields could in principle exceed the coercive force of some of the magnetic grains but in practice these fields are never reached. This is because the main limitation on the size of the field when a sample is placed in the cavity is, in general, due to absorption by the sample rather than conductive losses in the cavity. To see why this is so we calculate the dielectric loss in a typical sample, assuming that ε'' is known. For the time being, the energy dissipated in the sample will be calculated assuming that the fields in the cavity are not changed by its presence. This assumption will be discussed in more detail later.

Imagine a sample of radius R, thickness Z in the centre of a cavity of radius a. If the sample is thin (< 1/5 the length of the cavity), the axial variation of the electric field can be ignored. Assuming that the presence of the sample does not significantly disturb the fields within the cavity and that the radius of the sample is less than 1/5 that of the cavity we can write, as $J_0'(x) \cong \frac{x}{2}$ for small *x*

$$|\mathbf{E}| = E_\varphi \cong H_0 \frac{ik\eta a}{q}\left(\frac{qr}{2a}\right)$$

$$|\boldsymbol{E}^2| = \frac{1}{4}H_0^2(k\eta r)^2$$

We can use this to compare the dielectric loss in a sample with the conductive loss in the brass walls of the cavity.

$$P_d = \frac{\omega}{2}\varepsilon'' \int_{z=0}^{z=Z}\int_{r=0}^{r=R}\int_{\varphi=0}^{\varphi=2\pi} |\boldsymbol{E}^2|\, r\, dz d\varphi dr = \frac{\omega}{2}\varepsilon''\, 2\pi Z \frac{1}{4}H_0^2(k\eta)^2 \int_0^R r^3\, dr$$

$$= \frac{1}{16}\varepsilon'' V \omega H_0^2 (k\eta R)^2$$

where V is the volume of the sample. This is a very useful result that allows the amount of dielectric heating to be quantified .For a basalt disc 2mm thick of radius 2.5mm, with ε'' of $4\text{x}10^{-12}$ F/m this gives a dielectric loss of

$$P_d = 6.6 \times 10^{-5} H_0^2$$

over an order of magnitude greater than the conductive wall losses. Even samples with relatively low dielectric loss will contribute as much to the damping of the cavity as the losses in the walls. From this it can be seen that it is quite wrong to compare the heating effect in different samples in order to draw conclusions about their efficiency at absorbing microwave radiation, whether by dielectric or magnetic absorption. In a lossless resonator the fields are essentially unbounded. It is the loss mechanisms that determine the magnitude of the fields within the cavity. A lossy sample may exhibit exactly the same heating effect as a lower loss sample simply because the lossy sample limits the fields to which it is exposed. Figure 3.4 shows how the power generated in a sample varies with its dielectric loss, for a given input power. Above a certain value, about 3 pF/m, increasing the dielectric loss does not result in an appreciable increase in heating of the sample as the sample is already absorbing most of the available power.

Figure 3.4 The percentage of incident power absorbed by a sample of quadrature permittivity ε'' in the centre of a TE_{011} cavity.

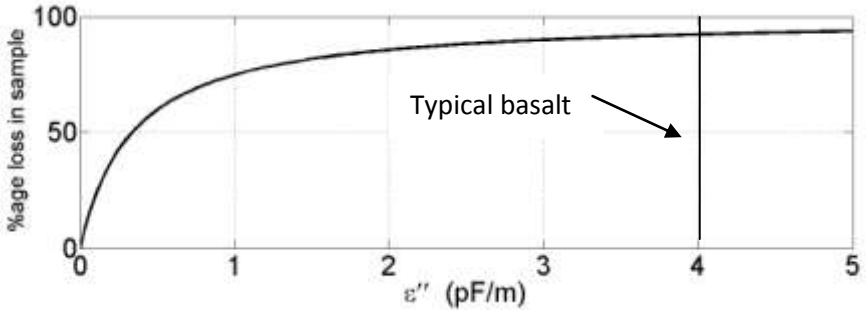

This helps to explain why the two samples, one pure magnetite and the other basalt, studied by Walton et al. (2004a)(see chapter 2) showed such a similarity in their heating profiles. If the bulk of the absorption was in the sample rather than in the cavity walls then it is to be expected that the samples would exhibit the same temperature rise even if they possessed very different characteristics. This was interpreted as showing that absorption was independent of concentration of magnetic (absorbing) medium (Walton et al. 2004a, Walton and Boehnel 2008).One problem with this interpretation is that Walton(2004a)calculated the power dissipation in the sample from the observed temperature rise and found it to be around one third the total power incident on the cavity. Unfortunately the apparatus was not described in detail (in particular the return loss was not specified) and it is not possible to say whether the missing two thirds of the power was being absorbed in the cavity or externally as part of the coupling mechanism. Given the calculations presented here it is very difficult to see how the cavity walls could be responsible for the majority of the power being dissipated, unless the samples had a tan δ of less than 10^{-3}. This is certainly not true for either magnetite or basalt although it must be noted that the calculations given here are approximations based on the fields in an empty cavity. It is not possible to explicitly calculate the fields in a cavity with a sample in it. The temperature measurements were made using an infrared thermometer attached to a hole in the side of the cavity. As a hole in the side of a TE_{011} cavity cuts a line of current, it would be expected to contribute to the loss, and actually radiate microwaves. For this reason the approach is not to be recommended. Without more experimental information the analysis here cannot be exhaustive, but still provides a realistic alternative interpretation of the published experimental results that does not involve magnetic absorption at all. When this

piece of evidence is removed the case for absorption occurring due to the spread of the wave vector in phase space is considerably weakened. It would seem more parsimonious to assume that the observed heating effect in these experiments was due largely, if not entirely, to dielectric absorption. This interpretation allows us to overcome many of the inconsistencies that were outlined in the previous chapter, in particular the apparent violation of the Kramers-Kronig criteria.

It could be further argued that there is little evidence for a magnetic absorption mechanism at 14GHz in naturally occurring titanomagnetites at all. The main argument for this was reported by Walton (2002) and the experiment reported therein can now be analysed using the results derived above. It is to be regretted that many of the published works on microwave demagnetisation do not give the dimensions of the cavities used making it difficult to assess the validity of some of the interpretations of experimental data that has been gathered over the years. Consider figure 3.5 (from Walton 2002). It shows how the magnetic moment of a sample decreases as microwaves of increasing power are absorbed by a cavity. This was interpreted as proof that magnetic particles within the sample absorb power more efficiently at higher frequencies. Yet once again the dielectric heating of the sample does not appear to have been properly considered. As Suttie et al. (2010) point out, all basalts will exhibit considerable dielectric loss due to plagioclase and pyroxene in the groundmass.

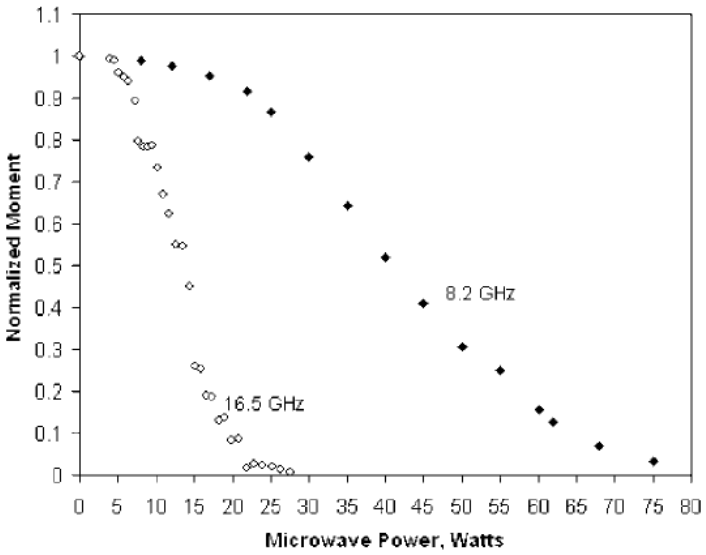

Figure 3.5 A copy of figure 2 from Walton (2002). Demagnetisation of two samples of basalt at 8.2GHZ and 16.5GHz. This was interpreted as showing that higher frequencies can demagnetise samples more efficiently.

Looking at figure3.5, it could be argued, given the similar profiles of the demagnetisation curves, that at 16.5 GHz the sample was heated about 3 times more than at 8.2 GHz and that demagnetisation was solely the result of dielectric heating. Using the results obtained

above it is possible to calculate the difference in dielectric heating in each case, assuming the samples were identical (this is not clear from the paper). In the absence of information regarding the dimensions of the cavity we assume that at 8.2GHz the sample was in a 5cm diameter cavity as described by Hill (2000) while at 16.5GHz it was in a 3cm diameter cavity as was used in this study. Using the formulae derived above and remembering to recalculate the surface resistivity of brass at each frequency, it is possible to ask what type of sample would give the results shown if the only source of heating was from the electric field. We find that a value of about 2pF/m for ε'' would satisfactorily explain these results. This is a little lower than might be expected for a sample of lava, although it is not clear whether the lava was, say, highly vesicular and once again we point out that the analysis presented here is not exact. Another effect that may be important is the dependence of ε'' on temperature. This has been ignored up until now but any loss mechanism that is due to Debye relaxation, such as is exhibited by matter at microwave frequencies, will tend to increase with temperature. It is certainly not possible to interpret this experiment as unequivocal proof that magnetic grains absorb more energy at 16.6 GHz than at 8.2GHz. It is also quite impossible to say for sure that magnetic absorption was the cause of the demagnetisation in either case without making the kind of detailed measurements explained in Suttie et al. (2010).

It has been established that previous experimental work may be based on flawed assumptions. The results in Suttie et al. (2010) are difficult to argue with as very detailed measurements were made to establish whether the sample was being demagnetised by interaction with the magnetic or electric microwave field. The temperature measurements may however be slightly inaccurate for the same reasons as above: just as Walton et al. (2004a) measured the temperature of the edge of a sample where it was subjected to a circumferential E-field, Suttie et al. (2010) measured the bottom of a sample in a TE_{112} cavity where it would be subjected to a radial electric field. Such fields can cause rapid localised heating. Walton (2004) suggested that the principle cause heating, and hence of alteration of palaeomagnetic samples in a microwave experiment was the decay of magnons into the phonon system and that this could effectively be stopped by using high microwave powers. During this project it was noticed that temperatures high enough to cause melting could occur at high power levels. It was further noticed that the melt spots always occurred at the location of strong electric fields: on the edge of the sample in TE_{011} and on the top or bottom in TE_{112}. If microwave demagnetisation is affected only by the electric field it would make sense to set up the cavity in such a way to make this field

uniform over the sample. There is, it turns out, a way to measure the energy being dissipated in the sample without making direct temperature measurements. To do this perturbation theory must be employed.

The previous calculations have all assumed that the geometry of the fields in the cavity are not strongly perturbed by the presence of a sample and for this reason may not be entirely accurate. There is in general no way to explicitly calculate the field in a cavity filled with an inhomogenous medium, but Suttie et al. (2010) showed how perturbation theory could be used to verify that the fields were not strongly perturbed. Perturbation theory is a mathematical method of finding approximate solutions to system of differential equations where exact solutions cannot be found but are known for a closely related system. In particular it allows the eigenvalues of an unsolvable system to be found if the eigenfunctions are close to the eigenfunctions of an exactly soluble system. Rather than examine the general perturbation method here it is developed with respect to fields in the sample loaded cavity. In this case the known eigenfunctions are the fields within the empty cavity and while it will not be possible to describe the fields in a cavity containing a sample, the eigenvalues, that is the resonant frequencies, can be found. Suttie et al. (2010) argued that if the measured eigenfrequencies of the system agreed with the predictions of perturbation analysis, then the assumption that the eigenfunctions must be close to the unperturbed eigenfunctions must be justified. Several authors give derivations for equation 2 in Suttie et al. (2010)(e.g Slater 1946, Baden Fuller 1987,Chen et al. 2004, Carter 2001). Here we rewrite it as

$$\frac{\Delta\omega}{\omega} = \frac{\iiint_{Sample}[\Delta\mu H \cdot H - \Delta\varepsilon E \cdot E]dV}{\iiint_{Cavity}[\varepsilon_0 E \cdot E \ - \mu_0 H \cdot H]dV}$$

This can be taken as the master equation governing the change in resonant frequency when a sample is placed in to the cavity. The quantities in the integrands in equation are clearly energies, but the minus signs require some explanation. In the resonant cavity the electric and magnetic fields are out of phase so that the stored energy within the cavity changes from electrical to magnetic and back again. The minus sign actually sums the two contributions to the energy, taking into account the phasor nature of the field variables. Suttie et al. (2010) actually used complex conjugates to describe equation by using the fact that $H.H - E.E = H.H^* + E.E^*$. It can be seen that the fractional change in frequency of

the resonant cavity when a sample is placed in it is equal to the energy in the sample divided by the total energy in the cavity. This forms the basis of the resonant cavity perturbation (RCP) method of material characterisation at microwave frequencies (Chen et al.2004, Baden Fuller 1987). This is quite different from reflection cavity methods commonly used in ferromagnetic resonance experiments (e.g. VaLstyn et al. 1962, Suhl 1956) where the absorption spectra are observed directly. In the RCP method, the absorption of energy by the cavity is determined by the impedance of the slot that couples the cavity to the waveguide, which in turn depends on a number of factors, such as the geometry of the slot, the frequency and the permittivity of the medium within the cavity. The dielectric properties of ceramics from the British Isles may be very different from those of igneous rocks, say or ceramics from other parts of the world that have been produced under different firing conditions. One of the problems encountered here was matching the cavity to the transmission line as the original matching had been done with cavity loaded basalt.

Despite the mathematical complexity of the perturbation method there is a straightforward interpretation of the result in terms of equivalent circuits. A tank circuit, consisting of a capacitor and an inductor in parallel, makes a useful analogue for a cavity resonator. At resonance it develops very high voltages with minimal current flow i.e it has a very high impedance. This is similar to the cavity which develops very large electromagnetic fields from a small input of power, with low conduction loss. It makes intuitive sense therefore to picture a cavity resonator as a tank circuit (see figure 3.6)

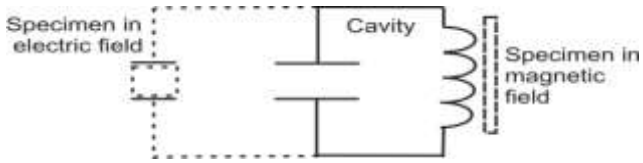

Figure 3.6 A resonant cavity envisaged as tank circuit

The introduction of a dielectric sample to the cavity is equivalent to increasing the capacitance, while a magnetic sample would be analogous to increasing the flux in the inductor. In either case the resonant frequency of the circuit would drop. As in a cavity resonator the voltage across a tank circuit is limited by the losses occurring within the circuit. The Q of the circuit decreases as the size of the resistance gets smaller. Placing a lossy dielectric in a cavity should have the same effect (see figure 3.7).

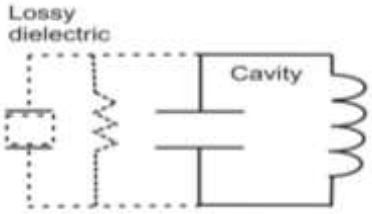

Figure 3.7 A resonant cavity envisaged as tank circuit with a lossy dielectric sample shown as a shunt resistance

Using the result of the perturbation analysis it is possible to consider the loss in the sample as a function of the Q of the cavity. Instead of considering loss in the sample, the eigenfrequency can be replaced with a complex frequency ($\omega_0=\omega'+i\omega''$) because the eigenfunctions are themselves complex. Consider the tank circuit shown in figure 3.7 as a resistor (impedance R), a capacitor (impedance $i\omega C$) and a inductor (impedance $=1/i\omega L$)in parallel. It has impedance given by

$$\frac{1}{Z}=\frac{1}{R}-\frac{i}{\omega L}+i\omega C$$

a resonant frequency $\omega_0=\frac{1}{\sqrt{LC}}$ and a Q given by $Q=\frac{R}{\omega_0 L}$. These results are unchanged by removing the resistor from the circuit and introducing a complex resonant frequency with $\omega''=\omega'/2Q$ (e.g. . Rizzi 1988). We now postulate that this result is true for the cavity resonator (see Chen et al. 2004)so that if inserting a sample into a cavity of Q_1 changes it to Q_2, it would be expected that the difference would be related to the loss in the sample:

$$\frac{1}{Q_2}-\frac{1}{Q_1}\cong\frac{2(\omega_2''-\omega_1'')}{\omega_0}=\varepsilon''\frac{\iiint_{Sample}|\boldsymbol{E}^2|dV}{\iiint_{Cavity}|\boldsymbol{E}^2|dV}$$

where for clarity it has been assumed that the magnetic loss is negligible compared to the electric loss. It has also been assumed that the change in the real resonant frequency of the cavity is small and that Q is large i.e $\omega'>>\omega''$. Thus $\frac{1}{Q_2}-\frac{1}{Q_1}$ is a measure of the energy dissipated in the sample. This remarkable result means that it is actually feasible to calculate the power dissipated in, and hence the temperature rise of, a sample in a microwave cavity by making measurements on the transmission line, rather than in the cavity itself.

If the resonant frequency is not changed then Q is proportional to the bandwidth of the SWR. There is a practical problem to overcome however: if the resonant frequency changes by more than a few MHz or if the matching of the cavity to the line changes a meaningful comparison of the Q cannot be made. These problems can be overcome by retuning the

cavity and including an impedance matching device in the transmission line if necessary. We now demonstrate the value of these results with a practical example. Suttie et al. (2010) (see chapter 4) made detailed measurements of the temperature of a basalt sample in two positions in a TE_{112} cavity in an effort to establish whether it was possible to demagnetize a sample without using the electric component of the microwave field. The initial temperature rise was found to be 92K/s in the E-field at 10W and 29K/s in H-field at 15W. From this it was apparent that the sample dissipated about 4.7 times the power in the E-field as in the H-field. Data concerning the matching of the cavity to the line was not published although it had been recorded. The SWR was measured across the frequency spectrum with an empty sample rod in the middle of the cavity, then with the sample attached (in the H-field maximum) and finally with the sample in the E-field maximum. To keep the (real) resonant frequency the same the cavity was retuned by unscrewing the end cap about one third of a turn when the sample was placed in the E-field maximum, dropping the resonant frequency by about 200MHz. The results are shown in figure 3.8.

Figure 3.8 The Q of the cavity measured during the experiment in Suttie et al. (2010), chapter 4.

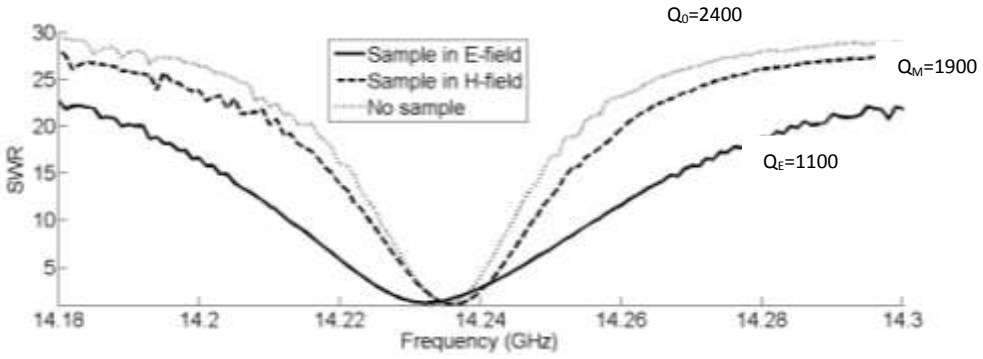

From the calculated values of Q we can estimate the relative amount of heating in each position. In the H-field, $1/Q_M - 1/Q_0 = 0.00011$ and in the E-field $1/Q_E - 1/Q_0 = 0.00049$. From these measurements alone and the preceding perturbation analysis, we can predict that the sample would heat up 4.5 times more in the E-field than in the H-field. This agrees fairly well with measured temperature rise and it is possible to envisage a system where, after suitable calibration, accurate determination of the Q could be used to monitor temperature remotely. This is just one example of the power of the theoretical methods

that have been developed here which provide a sound theoretical framework for future workers to study microwave demagnetisation.

The main conclusion of Suttie et al. (2010) was that it was possible to demagnetise a sample of basalt using the H-field component of a 14.2GHz microwave field and that this did not cause significant heating. As this result is very different from previous experimental investigations where the heating was found to be significant and independent of the concentration of the absorbing medium (Walton et al. 2004a, Walton and Boehnel 2008) the mechanism for the demagnetisation still remains to be explained. We will make no firm statement concerning the dispersion of the susceptibility of magnetite at frequencies above 14GHz, but point out that the nature of the Kramers Kronig relations (see chapter2) and the Lorentzian form of the susceptibility (e.g. Chen et al.2004) mean that the real part of the susceptibility must in fact be negative in a region above the resonant frequency. It has been suggested that this could lead to a form of absorption in magnetic materials similar to that observed in dielectrics with a negative permittivity and that this may explain certain aspects of the cosmic microwave background radiation by the magnetic dipole emission and absorption from iron oxides in the interstellar dust (Draine and Lazarian 1999). The thorough study of these questions is left for future investigation.

Chapter 4

Direct demonstration of microwave demagnetisation of a whole rock sample with minimal heating

The following paper (Suttie et al. 2010) that forms this chapter reports an experiment that makes practical use of the theory developed in chapters 2 and 3.

Neil Suttie, John Shaw and Mimi J. Hill Dept. Earth and Ocean Sciences, University of Liverpool, UK

Chapter published as:

Direct demonstration of microwave demagnetization of a whole rock sample with minimal heating

Neil Suttie, John Shaw, Mimi J. Hill

Earth & Planetary Science Letters

292 (2010) 357-362

Doi:10.1016/j.epsl.2010.02.002

Abstract

Microwave demagnetization has been employed in a number of palaeointensity determinations and has been shown to produce equivalent results to thermal methods, yet the degree of demagnetization caused by the magnetic component of the microwave field, rather than dielectric heating, has never been fully established. Here we present results that show unequivocally that a sample of basalt may be demagnetized by the microwave magnetic field with minimal heating. The fields within a resonant cavity are described quantitatively and the possibility of perturbation due to the sample is accounted for. This allows direct comparison of the demagnetizing effect of the electric and magnetic field components. While the magnetic field can demagnetize the sample it is shown that without careful control of the sample's shape and placement, the effects of the electric field become dominant.

4.1.Introduction

It has been argued that microwave demagnetization has the potential to reduce thermal alteration during palaeointensity experiments (Walton et al. 1992, Hill and Shaw 1999) and this has been demonstrated in studies of geological material (e.g. Hill et al. 2002, Hill et al. 2005) and archaeological material (e.g. Casas et al. 2005). It is however also possible to have rapid heating to very high temperatures in a microwave field if lossy dielectrics are present. Common minerals with high dielectric loss include pyroxene and plagioclase feldspar, which tend to dominate the matrix of basalt, the rock most frequently used in palaeointensity studies. Walton et al. (2004a) argued that, in experiments on both synthetic magnetite and basalt, dielectric heating could be neglected although the electrical energy density in the region of the sample was not given. The possibility of selectively demagnetizing grains of various sizes by the application of different frequency

microwaves has been mooted (Walton et al. 2004b) and even explored as a dating technique (Walton and Bohnel 2008), but as the heating effect of the electric field increases with frequency, this would have to be eliminated before such an approach could be practically applied.

Previous theoretical work has concentrated on the interactions between the microwave magnetic field and the magnetic grains within the specimen at the microscopic level by making various assumptions about the mode of absorption and the nature of the excitation within the magnetically ordered phases (Walton et al. 1996). Here a different approach is used. This paper aims to distinguish between absorption caused by the electric component of the microwave field and that produced by the magnetic component and so to establish whether the magnetization can be reset without the influence of dielectric heating of the matrix. Furthermore, we aim to describe the fields in terms of measurable parameters and so provide a sound theoretical framework for further study of microwave demagnetization.

4.2 Background

In order to understand the absorption of microwaves by a specimen placed within a cavity it is useful to review the characteristics of the electric field (**E**) and the magnetic field (**H**) in a resonant cavity. Cylindrical cavity resonators can support a number of different shapes of oscillating electromagnetic field, which are divided into two basic types: ones with longitudinal electric field components (H_z= 0), and ones with longitudinal magnetic field components (E_z=0), where the subscript z denotes components parallel to the axis of the cylindrical cavity. These are known as transverse magnetic (TM) and transverse electric (TE) respectively. A mode is then specified by three numbers *n, m, p* where n is the number of azimuthal wavelengths, m the number of radial maxima and p is the number of half wavelengths along the axis of the cavity. Practical microwave palaeointensity studies at the University of Liverpool use cylindrical samples of approximately 5mm diameter and 3mm thick in a right cylindrical cavity resonating at between 14 and 14.5 GHz in the TE_{011} mode. Here we use the TE_{112} mode which allows us to place the sample very precisely in the node of the electric field or the magnetic field and hence compare the effects of the electric and magnetic fields on the magnetization of the sample (see figure 4.1 for the field distributions in these two modes).

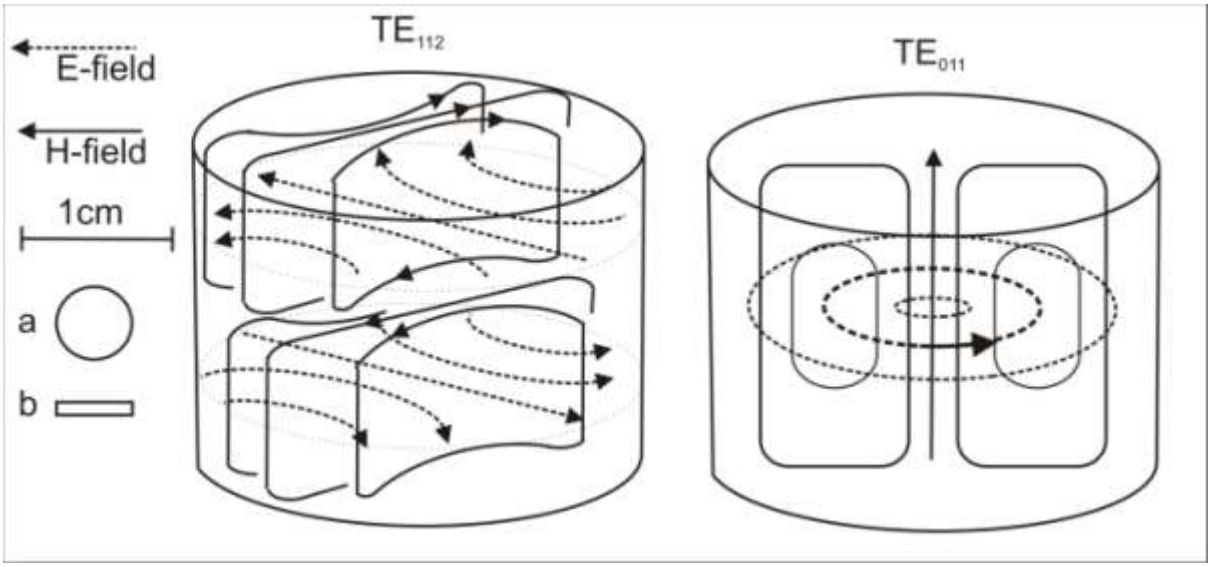

Figure4.1. Scale drawing of the electric and magnetic fields within a TE_{112} and a TE_{011} cavity, showing a plan view (a) and side view (b) of the sample used in this study. In the TE_{011} cavity the heavy dashed line shows the position of the electric field maximum and the faint dashed lines show the half-maximums. Note that in TE_{011} the sample would be exposed to an electric field in excess of half its maximum value. The representations of the fields are based on those of Baden Fuller (1987).

The reason for using TE_{112} in this study is that the fields vary in strength along the axis of the cavity so a thin slice of material can be placed in either the electric or magnetic fields by moving it along the axis of the cavity. This allows us to measure the dielectric heating of the sample in the electric field maximum and then calculate the contribution of the dielectric loss to the power generated within the sample when it is placed in the magnetic field maximum. In the TE_{011} mode commonly used in microwave palaeointensity studies the electrical field increases radially from the centre, reaching its maximum value at just under half the radius of the cavity. The electric field (E) varies with radius (r) as a first order Bessel function (J_1) of the first kind: $E \propto J_1(\frac{3.83r}{a})$, where a is the radius of the cavity. For small x, $J_1(x) \approx \frac{x}{2}$, so the electric field increases approximately linearly across a sample placed in the centre of a TE_{011} cavity. In a cavity of diameter 30mm, the electric field increases to 61% of its maximum value by a radius of 3mm and a 6mm diameter sample could experience considerable dielectric heating around its circumference. Previous studies using cavities and samples of these dimensions (Walton et al. 2004a, 2004b) argued that the dielectric heating was negligible and concluded that the heating was due to the strong absorption of microwaves by the magnetic grains.

A time varying magnetic field in a sample must be accompanied by a time varying electric field around the sample, the size of which depends on the cross-sectional area of the

sample normal to the magnetic field. Decreasing the sample size reduces the electric field for a given power but for any given shape of sample in any particular cavity there will be some dielectric heating that can be increased by increasing the applied power. To ensure that the dielectric contribution is accounted for it must be measured separately but this would be difficult to achieve in TE_{011} mode as there is no obvious way of placing the sample in a uniform electric field, with negligible magnetic field. If a non-magnetic material of similar electrical properties to the sample can be found, this could be used as a control, but here we choose to use a different mode (TE_{112}) which allows a direct comparison between the effects of the magnetic and electric fields to be made (see figure 1).

The electrical field of the TE_{112} varies along the axis of the cavity as $\sin\frac{2\pi z}{l}$, where *l* is the length of the cavity and *z* the distance along its axis. The resonant frequency (f_r) is given by $f_r = \frac{1}{2\pi\sqrt{\mu\varepsilon}}\sqrt{\left(\frac{1.84}{r}\right)^2 + \left(\frac{2\pi}{l}\right)^2}$ (4.1), where r is the radius of the cavity and μ and ε are the magnetic permeability and the electric permittivity of the medium within the cavity respectively. If specimens are placed within the cavity, the effective values of μ and ε will change and the resonant frequency of the cavity will shift. The fields within empty or uniformly filled cavities can be derived from first principles by solving Maxwell's equations (Pozar 2004, Rizzi 1988) but if a specimen of differing electrical and magnetic properties from the surrounding medium is placed in the cavity, exact solutions are not generally available. If the effect on the fields is small it can be accounted for using perturbation theory by considering the macroscopic electric and magnetic properties of the specimen (Slater 1946). We will demonstrate that such an approach is consistent with our observations of the cavity response and hence show that the fields in the neighbourhood of the specimen can be adequately described.

The magnetic permeability μ and the electric permittivity ε are defined by the constitutive relations $\mathbf{B} = \mu\mathbf{H}$ and $\mathbf{D} = \varepsilon\mathbf{E}$ respectively, where **B** is the magnetic flux density, **H** is the magnetic field, **D** is the electric flux density and **E** is the electric field. As the specimen will not in general be homogenous we use the spatial averages of **B**, **H**, **D** and **E** over the specimen in these relations to give what are usually called the effective permittivity and permeability. These are usually expressed as complex variables at high frequencies: $\varepsilon = \varepsilon' - j\varepsilon''$ and $\mu = \mu' - j\mu''$ where the real part represents dispersion and the imaginary part determines the absorption.

The loss at any given frequency is often characterised by the dielectric loss tangent, $\tan\delta_e = \varepsilon''/\varepsilon'$ and the magnetic loss tangent, $\tan\delta_m = \mu''/\mu'$. Dividing ε' by the permittivity of free space, ε_0, gives the dimensionless relative permittivity ε_r so that $\varepsilon/\varepsilon_0 = \varepsilon_r(1 - j\tan\delta_e)$. Similarly dividing μ' by the permeability of free space, μ_0, gives the dimensionless relative permeability μ_r so that $\mu/\mu_0 = \mu_r(1 - j\tan\delta_m)$.

Following the usual perturbation method (Slater 1946, Baden Fuller 1987, Pozar 2004) it can be shown that if a small perturbing specimen is introduced to the cavity, the angular frequency (ω) changes according to

$$\frac{\Delta\omega}{\omega} = \frac{\iiint_S(\Delta\varepsilon \boldsymbol{E}\boldsymbol{E}^* + \Delta\mu \boldsymbol{H}\boldsymbol{H}^*)dV}{\iiint_C(\varepsilon \boldsymbol{E}\boldsymbol{E}^* + \mu \boldsymbol{H}\boldsymbol{H}^*)dV} \qquad (4.2)$$

where **E** and **H** are the complex electrical and magnetic fields, ε and μ are the permittivity and permeability of the empty cavity, $\Delta\varepsilon$ and $\Delta\mu$ the change in permittivity and permeability due to the specimen. The integral in the numerator is taken over the volume (V) of the specimen and the integral in the denominator is taken over the volume of the cavity.

Carter (2001) gives a full review of the assumptions underlying perturbation theory as applied to microwave resonators, one of which is that the specimen must be homogenous so that the fields within it are entirely constrained by the fields at its boundary. While this is not strictly the case for a palaeomagnetic sample, we show that the use of effective permittivity as defined above gives results consistent with the small perturbation analysis. The relationship given by (2) states that the relative change in resonant frequency is equal to the relative change in electromagnetic energy within the cavity. The frequency has real and imaginary components, the change in the real part being governed by the change in the stored energy and the change in imaginary part reflecting the change in the dissipated energy. The change in the imaginary part of the frequency can be measured if the Q of the cavity is determined with enough precision, but due to changes in the external Q when the specimen is inserted this can be difficult. If we define the frequency, f, as Re {ω/2π} and only consider changes due to a dielectric then taking the real parts of (2) gives

$$\frac{\Delta f}{f} = \frac{\varepsilon_r - 1}{2} \frac{\iiint_S |\boldsymbol{E}^2| dV}{\iiint_C |\boldsymbol{E}^2| dV} \quad (4.3)$$

where ε_r is the relative permittivity of the specimen. The factor of 2 appears in the denominator because at resonance the electrical energy is equal to the magnetic energy and so is half the total electromagnetic energy in the cavity (see Chen et al. 2004). This relation can be used to ensure that the fields within the cavity are not significantly perturbed by the presence of a sample by measuring the change in frequency and comparing it with the predicted value. An analogous relation to (3) exists for a magnetic specimen in the magnetic field but as the magnetic susceptibilty of a palaeomagnetic specimen is small compared to the electric susceptibilty the effect of the change in magnetic energy can be ignored (see section 3).

4.3 Basalt sample characteristics

Zheng et al. (2005) obtained values of between 7 and 8 for the relative permittivity (ε_r) of basalts at 9.37 GHz with tan δ_e of between 0.05 and 0.08. No data appears to be available for the complex permittivity of basalt at 14GHz (the frequency used for this study), but in the absence of strong resonant effects we can assume that these values are fairly typical of basalts up to and beyond 14GHz. The dispersion of the permeability of an assemblage of magnetic particles at this frequency is not well understood (Baden Fuller 1987) but as the concentration of magnetic minerals is small, $\mu_r \ll \varepsilon_r$ and the effect of the magnetic properties of the basalt on the real part of the resonant frequency is negligible, although tan δ_m may be large enough to have some observable effect which would be manifested in the imaginary part of the resonant frequency.

The basalt sample used in this study came from the Jianguo sequence, China (Zhu et al.2004; Davies 2009). Transmitted light microscopy revealed a groundmass of pyroxene and plagioclase feldspar with titanomagnetite inclusions, typically 20µm across. Thermal demagnetization experiments showed around 90% of the NRM to be removed by 250°C interpreted as indicating the remanence being carried by high titanium titanomagnetite. The sample used for this study has a susceptibility at 470Hz of 0.025 SI and showed a frequency dependence of susceptibilty of 3.5% when the frequency was increased to 4700Hz. The ratios of saturation remanence to saturation magnetization (M_{rs}/M_s) and

remanent coercive force to ordinary coercive force (H_{cr}/H_r) were measured as 0.1 and 3.0 respectively, placing the bulk magnetic grain size in the pseudo-single domain field (Day et al. 1977, Dunlop 2002).The frequency dependence of susceptibilty suggests a substantial superparamagnetic fraction and microscopy identified grains of multi-domain size, suggesting that the M_{rs}/M_s and H_{cr}/H_r ratios reflect a mixture of grain sizes from superparamagnetic to multi-domain grains.

4.4 Method

A signal generator provides a signal between 14 and 14.5 GHz to a power amplifier capable of delivering 80 W. A section of waveguide delivers the power to a cylindrical cavity of radius 15mm, coupled via a slot. The orientation of the slot is chosen so that only TE modes are excited. In general the waveguide, a hollow rectangular brass tube, when excited will have waves propagating in both directions along it. These are called the forward and reflected waves and can be measured using directional couplers connected to power meters. The forward power is controlled by the computer with the gain automatically adjusting to give the requested power. The proportion of the forward power reflected, however, depends on the coupling between the cavity and the waveguide and cannot be controlled by the computer. At frequencies away from a resonant frequency of the cavity the waveguide termination is essentially a short circuit with all the forward power reflected and the power dissipated as standing waves in the waveguide. At resonance, the cavity will absorb energy but there will still be reflected power and standing waves in the waveguide unless the admittance of the cavity is equal to the admittance of the waveguide. Matching these values under various conditions is one of the challenges of the microwave palaeointensity method as the admittance of the slot changes as specimens and sample holders are placed in the cavity. It may sometimes be necessary to use impedance matching devices in the waveguide but in this instance the cavity was found to be adequately coupled to the waveguide throughout the experiment, with no more than 10% of the forward power being reflected. The cavity has a small hole in either end allowing a 5mm quartz tube to be inserted. The tube is used so that a sample may be held by vacuum making adhesives, which often have strong dielectric properties, unnecessary. The sample can be moved up and down along the axis of the cavity by a computer controlled worm driven carriage (see figure 2). A steady magnetic field can be applied by coils surrounding the cavity, which for clarity are not shown in figure 2. The cavity is mounted above a Tristan Technologies, Inc. DRM-300 SQUID magnetometer and the sample may be moved into the

magnetometer for measurement of its magnetic moment and then returned to its original position in the microwave cavity after measurement. The assembly of cavity and coils is housed within a mu-metal shield (not shown in figure2) ensuring that the ambient field within the cavity is no more than a few nT.

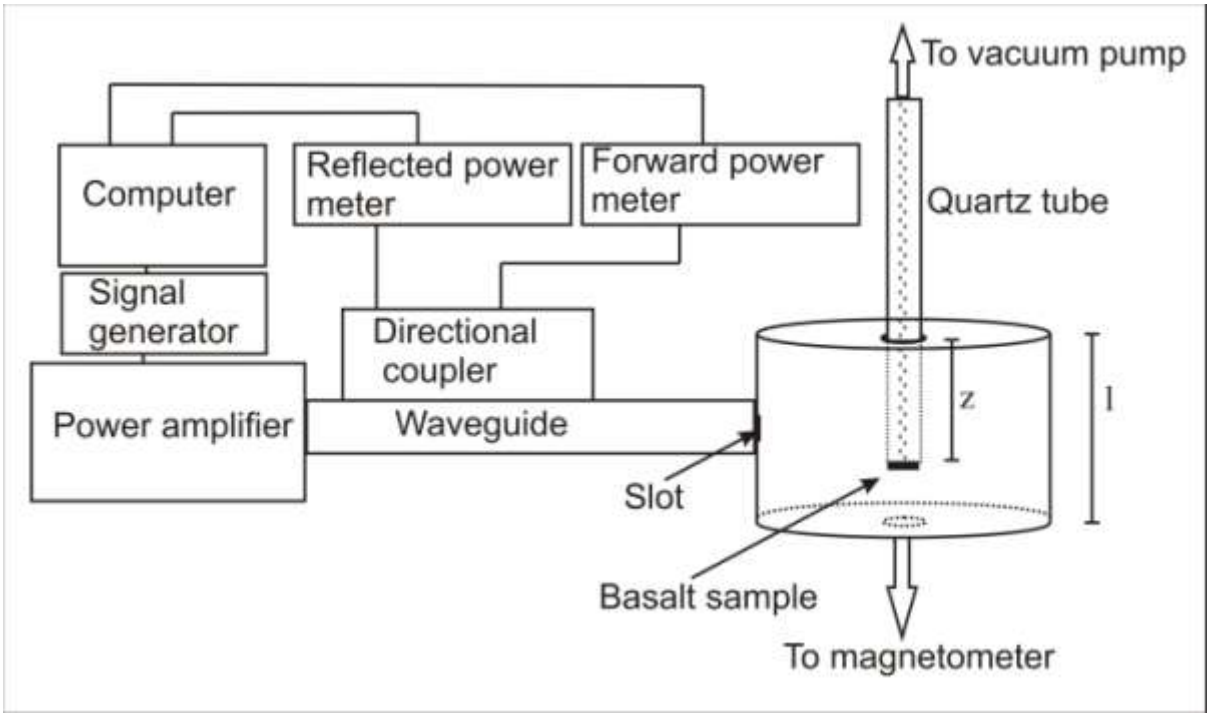

Figure 4.2 Schematic of the apparatus used in the experiment. In the first part of the experiment the cavity was placed between Helmholtz coils capable of providing a steady magnetic field, within a mu-metal shield. These were removed when the temperature measurements were made. An infra-red thermometer was placed in the aperture at the bottom of the cavity. Also shown are the length of cavity (l) and the length of rod (z) referred to in the text.

The cavity has an adjustable end cap allowing its length to be varied. From equation (1) the TE_{112} mode is found to be resonant at 14.8 GHz with the length set at 22mm. The introduction of a quartz tube causes the frequency to drop below 14.5 GHz, within the range of the amplifier. The resonant frequency of the cavity is measured as the tube is lowered incrementally into the cavity. The change in resonant frequency is then used to identify the regions of minimum and maximum electrical energy within the cavity. A thin disc 0.8mm thick and 5mm in diameter was taken from the well-characterised basalt. This was mounted on the end of the rod and the frequency measured again as the rod was moved into the cavity. After measuring the natural remanent magnetisation (NRM), the sample was placed in the antinode of the magnetic field, where the electrical energy is a minimum, and demagnetized using 15W of power for 3s. It was remagnetized in a 50μT

field, using 10W for 3s, and then demagnetized using the same power to ensure that the remanence imparted in the applied field could be completely removed. The sample was then positioned in the electrical field maximum, one quarter of the way into the cavity and remagnetized in a 50μT field once again using 10W for 3s. The TRM gained in the electric field was then removed with the sample placed in the magnetic antinode, first at 10W for 3s, then at 15W for 3s. The total energy absorbed by the cavity was calculated for each step by monitoring the difference between forward and reflected power with time.

The cavity was then removed from the magnetic shielding to allow a Fluke 80T infrared thermometer to be placed at the bottom aperture of the cavity. The thermometer was calibrated using a thermocouple attached to a miniature oven placed in the cavity at both positions used for demagnetizing the sample. Microwaves were applied at the same powers with the sample positioned as before and the temperature monitored. To check for consistency this was carried out four times for each of the two sample positions. The total energy absorbed by the cavity in each case was measured to ensure consistency with the first part of the experiment. Having achieved this it can be assumed that the sample temperature measured was the same as experienced during the first part of the experiment. Ideally the thermometer would be used to measure the temperature directly during the demagnetization steps, but owing to the need to remove the thermometer to allow the sample to be lowered into the magnetometer after each microwave application, this was impractical.

4.5 Results and Discussion

When the rod is placed a distance *Z* into the cavity of length *l* resonant in the TE_{112} mode, the change in resonant frequency is given by

$$\frac{\Delta f}{f_0} = 0.0475\left(\frac{\varepsilon_r - 1}{2}\right)\left(\frac{Z}{l} - \frac{1}{4\pi}\sin\frac{4\pi Z}{l}\right) \qquad (4.4)$$

where f_0 is the resonant frequency of the empty cavity. The derivation of (4.4) is given in the appendix. Figure 4.3 shows the experimentally determined variation of f_r with position for both the empty quartz tube and the quartz tube with basalt sample attached, along with the change predicted using (4.4) for a tube with relative permittivity of 3.5 and f_0=14.8GHz. Pozar (2004) gives ε_r of 3.78 for fused quartz at 10GHz. We were unable to find any data for 14GHz and it is not clear whether the slightly lower value obtained here is due to dispersion, impurities within the quartz or slight misalignment of the tube with the

axis of the cavity. There is good agreement between the measured and predicted values and this confirms that the cavity is operating in the correct mode and there is little disruption to the fields in the cavity, although the data shows a small change in f_r at the centre of the cavity where the electrical energy is predicted to be zero.

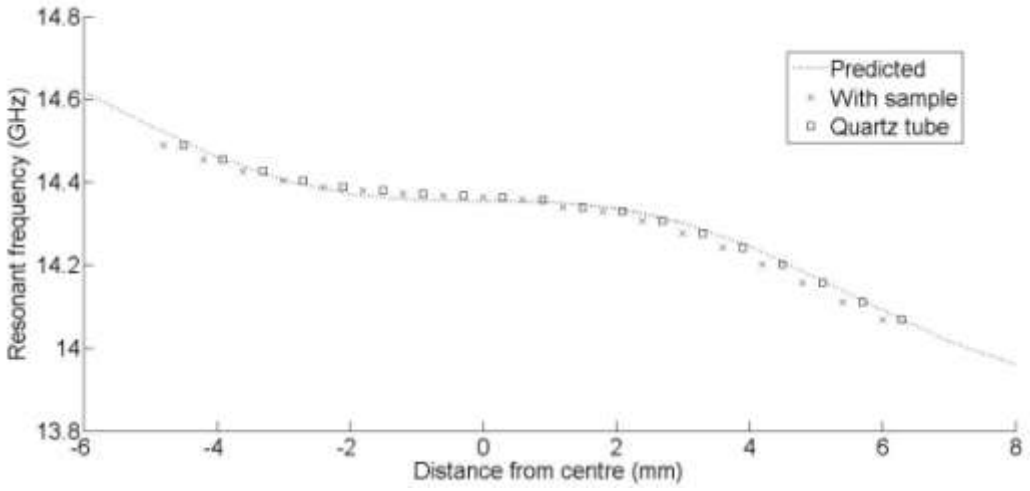

Figure 4.3. The resonant frequency of the cavity with a length of quartz tube inserted along its axis. The figure shows the measured value for an empty quartz tube and for the same tube with the 0.8mm thick basalt sample on the end. Also shown are the values predicted by perturbation theory for the empty quartz tube, with relative permittivity of 3.5.

There is a slight change in the behaviour of the resonant frequency when the basalt is attached to the quartz tube because of the higher permittivity of basalt. This is consistent with the basalt having a relative permittivity value of around 7, in good agreement with available data (Zheng *et al.* 2005). It should be noted that there is no discernable effect on the resonant frequency due to the magnetic susceptibilty of the sample, although previous studies have suggested that there may be such an influence (e.g. Walton et al. 1996). Palaeomagnetic samples rarely have low frequency susceptibilities much larger than 0.1 SI units and the electrical term in equation (4.2) will always tend to dominate.

Table 4.1 shows the results of the demagnetization experiment. Initially the sample had a magnetic moment of 705 x10^{-9} Am^2, its natural remanent magnetization. The first demagnetization step, carried out at the node of the electric field removed over 90% of the magnetization. The table also shows the total energy absorbed by the cavity and sample during each step. This is repeatable to within 2-3% for a given power and position. The total energy absorbed drops when the sample is placed in the electric field maximum because the cavity is less well coupled than when the sample is in the magnetic field maximum.

Table4.1 Table showing the magnetic moment of the sample after each step. Shaded rows indicate a TRM imparted in an applied field of 50 μT. All other rows are demagnetization steps in zero field. The power was applied for 3 s in each case. The TRM gained in the electric field at 10W can be removed in the magnetic field at 15W. Note that the moment changes are vector differences and the applied field was not parallel to the NRM.

Energy absorbed (J)	Power (W)	Field component	NRM remaining ($Am^2 \times 10^{-9}$)	TRM gained ($Am^2 \times 10^{-9}$)	TRM remaining ($Am^2 \times 10^{-9}$)
25.77	10	Magnetic	60		
25.89	10	Magnetic		256	
25.35	10	Magnetic			16
25.51	10	Electric	48		
21.65	10	Electric		443	
25.57	10	Magnetic			148
39.63	15	Magnetic	46		Removed

The total electrical field energy at a given position within the cavity is proportional to the change in frequency as the quartz tube passes through that point. Figure 4.4 shows the rate of change of resonant frequency with length of quartz tube and is therefore, by differentiating (4.3), a graph of the electrical energy density along the axis of the cavity. It can be seen that the electrical energy at an antinode is about 10 times that at the minimum, taken over a 0.8mm slice. The TRM gained in the electrical field maximum at 10W for 3 s was removed entirely at the electrical field minimum at a power of 15W for 3s. The electric field energy was in this case certainly less than one fifth of the energy which produced the TRM and the sample was therefore largely demagnetised by the interaction with the magnetic component of the microwave field. Clearly the effect of the two field components is dependent on the sample, and the results given here are not intended to be universal, but they do highlight the danger of excessive dielectric heating if the sample is exposed to a high electric field. The difference in heating is clearly demonstrated when the sample temperature was monitored.

Figure 4.4 The rate of change in resonant frequency per length of perturbing rod ($\Delta f_r/\Delta z$) plotted against the position of the end of the quartz rod. The change in frequency per length is proportional to the electrical energy density along the axis of the cavity. The two positions that the sample was placed in, at the node and antinode of the electrical, field are shown. The sample at the electrical field maximum experiences at least 10 times the electrical energy compared to the sample at the electrical field minimum.

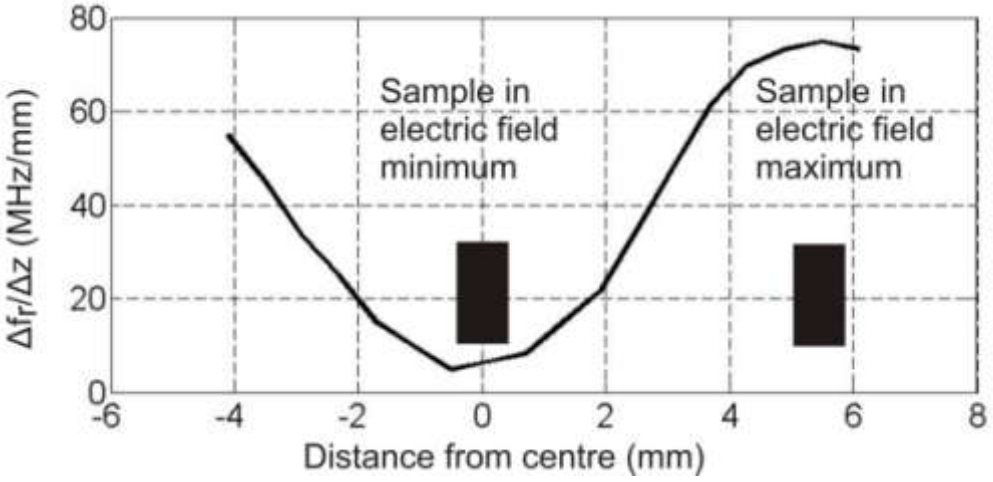

Figure 4.5 shows the temperature of the sample as microwaves were applied for 3s at 10W with the sample at the electric field maximum and as microwaves were applied for 3s at 15W with the sample in the magnetic field maximum, averaged over four runs in each position. The energy absorbed by the cavity in each case was close to that in the demagnetization experiment and the temperatures shown can be taken as realistically representing the temperature attained when the sample was being demagnetized. Careful positioning of the sample at the electric field minimum eliminates most of the heating of the bulk matrix. As the magnetic field energy is dissipated either within or around the magnetic grains, the temperature of these grains may be higher than the observed temperature, but it is not possible to draw firm conclusions about the process by which the magnetic field energy is absorbed or the temperature that the magnetic grains reach. The large spread in the temperature data for the magnetic field most probably reflects the difficulty in achieving the correct position. As the electrical energy increases rapidly either side of this point a small change in position can cause a large difference in the dielectric heating and it is possible that dielectric heating might account for some of the temperature rise seen. At the electrical antinode a small displacement has less of an effect.

Figure 4.5 The temperature measured with the sample in each of the two positions. In the electric field 10W was applied for 3s and in the magnetic field 15W was applied for 3s. Both resulted in the same change in magnetization but this was at much lower temperatures in the magnetic field. The dotted line indicates when the microwave field was switched off.

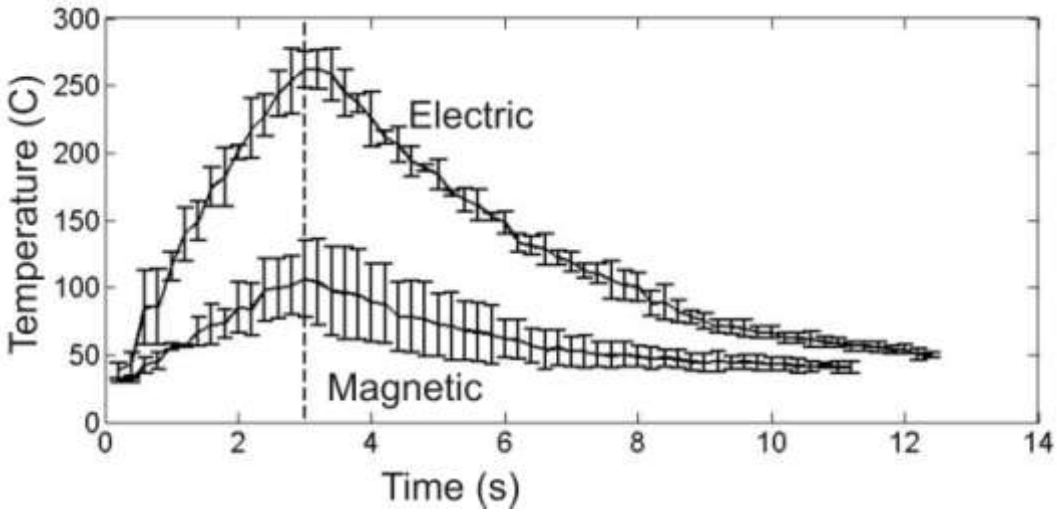

The initial temperature rise can be used to estimate the power dissipated in the sample. The temperature rises at 92K/s in the electric field and 29K/s in the magnetic field. If the electric field varies sinusoidally along the axis of the cavity and the sample was placed precisely at the electric field maximum and minimum positions then the dielectric heating at the electric field minimum should be less than 0.5% of the heating at the electric field maximum. In this case we find that the electric field heats the sample 4.7 times more effectively than the magnetic field. It is very probable, however, that there is some dielectric heating due to inexact positioning of the sample at the node of the electric field, or possibly due to perturbation of the fields within the cavity and some of the heating seen in the magnetic field is most likely dielectric in origin. The magnetic grains constitute about 1% of the sample so it is to be expected that the bulk temperature rise in the sample as a result of magnetic absorption would be much lower than any dielectric heating, even if the magnetic grains are being heated to their Curie temperature. As the infra-red thermometer measures the temperature of the bottom surface of the sample, where the electric field is highest, it may be that the bulk heating due to magnetic absorption is actually a small fraction of the total heating observed, although the magnetic grains are absorbing enough energy to be demagnetised.

As the mode most commonly used in palaeointensity is TE_{011} ,it is of some interest to consider how much dielectric heating the sample would experience if placed in the centre of a cavity operating in this mode. The electric field increases radially to a little over one

half of its maximum value from the centre of a 5mm diameter sample to its edge, as shown in figure 1. Allowing for all the uncertainties in the experiment, it is possible to say that the dielectric heating would be at least of the same order as the heating due to magnetic absorption if this sample was demagnetized in a TE_{011} cavity. This result is very different to that of Walton et al. (2004a) who found that dielectric heating of a 6mm diameter lava core was negligible compared to the heating caused by magnetic absorption in a TE_{011} cavity, despite the large electric field around the sample, although they did not say how this was established. All basalt samples would be expected to show similar dielectric loss due to the plagioclase feldspar and pyroxene in the groundmass, but different basalts may exhibit different amounts of magnetic absorption. It should be noted that magnetite itself has a non-negligible conductivity and may itself contribute to the electric loss, both by free-electron and dielectric processes, so the effect of dielectric heating should also be taken into account when considering absorption of microwaves by synthetic magnetite in a lossless matrix. Here we have only considered the dielectric heating by integrating the electrical energy over the sample volume. There is, however, a further complication in the case of a sample of this size in a TE_{011} cavity where the E-field is zero at the centre and large around the edge of the sample. As the dielectric loss tends to increase with temperature, the sample may experience increasingly rapid dielectric heating around its edge, leading to a large temperature gradient across the sample. This should be kept in mind when making deductions about the nature of microwave absorption by samples in a TE_{011} cavity and meaningful study of the demagnetizing effect of the magnetic field must include realistic estimations of the dielectric loss.

4.6 Conclusions

It has been conclusively demonstrated for the first time that whole rock samples may be demagnetised by the magnetic component of a microwave field without excessive heating of the matrix. It has also been shown that the high dielectric loss of basalt will lead to thermal demagnetization if the sample experiences a microwave electrical field. The dielectric heating can be avoided by operating the resonant cavity in a suitable mode and we find no evidence that the magnetic component of the microwave field can cause significant heating of the bulk matrix of a rock sample. If conclusions about the nature of magnetic absorption of microwaves are to be drawn from observations of sample heating, detailed measurement of the dielectric heating within the sample must be made. It has

been shown that the fields within a cavity containing a palaeomagnetic sample can be adequately described using the resonant cavity perturbation method, allowing the dielectric heating to be minimised and providing a framework from within which microwave demagnetization may be studied.

Appendix

The electric field components of a cavity in TE_{112} with radius *a* (15mm) and length *l* (22mm) are, in cylindrical co-ordinates with radius *r* and azimuth *φ*

$$E_\varphi = E_0 J_1'\left(\frac{qr}{a}\right)\cos\varphi \sin\frac{2\pi z}{l}$$

$$E_r = \frac{a}{qr}E_0 J_1\left(\frac{qr}{a}\right)\sin\varphi \sin\frac{2\pi z}{l}$$

where q=1.8412 is the first maximum of a first order Bessel function of the first kind, J_1. The change in frequency when a tube of bore radius R_1, outer radius R_2 and relative permittivity ε_r ,is inserted a length *Z* along the axis of the cavity is from (2)

$$\frac{\Delta f}{f_0} = \frac{\varepsilon_r - 1}{2}\ \frac{\int_{z=0}^{Z}\int_{\varphi=0}^{2\pi}\int_{r=R_1}^{R_2}\left(E_\varphi^2 + E_r^2\right)rd\varphi dr dz}{\int_{z=0}^{l}\int_{\varphi=0}^{2\pi}\int_{r=0}^{a}\left(E_\varphi^2 + E_r^2\right)rd\varphi dr dz}$$

$$= \frac{\varepsilon_r - 1}{2}\ \frac{\int_{z=0}^{Z}\sin^2\left(\frac{2\pi z}{l}\right)dz\int_{r=R_1}^{R_2}\left(J_1'^2\left(\frac{qr}{a}\right) + \left(\frac{a}{qr}\right)^2 J_1^2\left(\frac{qr}{a}\right)\right)rdr}{\int_{z=0}^{l}\sin^2\left(\frac{2\pi z}{l}\right)dz\int_{r=0}^{a}\left(J_1'^2\left(\frac{qr}{a}\right) + \left(\frac{a}{qr}\right)^2 J_1^2\left(\frac{qr}{a}\right)\right)rdr}$$

A well known integral identity (Pozar 2004) gives

$$\int_{x=0}^{q}\left(J_1'^2(x) + \frac{1}{x^2}J_1^2(x)\right)xdx = \frac{q^2-1}{2}J_1^2(q)$$

$$= 0.405$$

The integral in the numerator can be evaluated by expanding the Bessel functions and ignoring higher order terms as R_1 and R_2 are small. For small *x*,

$$J_1(x) \approx \frac{x}{2} - \frac{x^3}{16} \quad \text{and} \quad J_1'(x) = J_0(x) - \frac{1}{x}J_1(x) \approx \frac{1}{2} - \frac{3x^2}{16}$$

$$\int \left(J_1'^2(x) + \frac{1}{x^2}J_1^2(x)\right) x dx \approx \frac{x^2}{4} - \frac{x^4}{16}$$

Evaluating this integral between R_1=1mm and R_2=2.5mm gives 0.019. Hence 4.75% of $|E|^2$ within a cross-section of the cavity is found in the quartz walls of the tube. Evaluating the remaining integrals using $\int \sin^2(\frac{2\pi z}{l})dz = \frac{z}{2} - \frac{l\sin(\frac{4\pi z}{l})}{8\pi}$ we get equation (4.4)

$$\frac{\Delta f}{f_0} = 0.0475\left(\frac{\varepsilon_r - 1}{2}\right)\left(\frac{z}{l} - \frac{1}{4\pi}\sin\frac{4\pi z}{l}\right)$$

Acknowledgements

John Share is acknowledged for his help and support during many years of developing the microwave systems. Rixiang Zhu is thanked for supplying the basalt sample. Neil Suttie is supported by a NERC CASE (with English Heritage) studentship tied to grant NER/S/J/2006/14310. The microwave system was developed using a NERC grant NER/ NE/B50572X/1. Two anonymous reviewers are thanked for their valuable comments.

Chapter 5

Archaeointensity methods

5.1 The archaeointensity method

All the archaeointensity measurements presented in this study are essentially derived by variations of the Thellier method (Thellier and Thellier 1959). The sample is heated up and cooled down in a known field to remove the natural remanent magnetisation (NRM) and impart a thermoremanent magnetisation (TRM). Since it has become possible to create zero field environments within the laboratory , either the Coe (1967) or the Aitken (1988) variants of this method are commonly used, where a heating step in zero field is followed by a heating in an applied field or vice versa. For the purposes of introducing the method, no distinction is made between heating the sample in a conventional thermal demagnetiser and exciting it with microwave radiation. The essence of the method is to heat the sample in small increments of temperature, cooling it down each time first in zero field then in an applied laboratory field. As the TRM gained is proportional to the inducing field, the ratio of the TRM gained to the NRM lost at each stage should remain constant, and be equal to the ratio of the laboratory field to the ancient field of interest. The results are usually interpreted by means of a TRM/NRM plot, sometimes known as an Arai plot (Nagata 1963). The ordinates are the NRMs recorded after each zero-field heating and the abscissae are the TRMs gained in the subsequent heating in an applied field.

The Thellier method requires that the remanent magnetisation acquired by a sample is proportional to the applied field and that the constant of proportionality does not change. It further requires that the law of additivity holds: the magnetisation blocked, or unblocked, over a temperature range is the sum of the individual magnetisations blocked or unblocked, over incremental temperature steps. The constant of proportionality will alter if the magnetic minerals are altered during the heating of the sample. The law of additivity will only hold for assemblages of single-domain grains that obey the Neél theory of thermoremanence (Neél 1949)(e.g. Fabian 2001). One of the advantages of the Thellier method and its variants is that it is possible to incorporate various checks for non-ideal behaviour within the experiment. Two such checks were routinely used during this study: partial TRM (pTRM) checks and so-called tailchecks. The pTRM check formed part of the original procedure of Thellier and Thellier (1959) and was further discussed by Coe (1967).

The check is designed to detect alteration of the sample by repeating a previous in-field step after a higher temperature zero field step. If the sample has not altered the TRM gained will be the same as that gained during the first in-field step at that temperature because of the additivity of pTRMs. The motivation for the tailcheck (Riisager and Riisager 2001) is to detect multi-domain behaviour. After an applied field step, the zero-field step is repeated to ensure that the remaining NRM has not changed. In particular if there is a component of magnetisation in the direction of the laboratory field that is not removed (a "tail"), this can be an indication of multi-domain grains, with an attendant violation of the law of additvity. Both checks can easily be incorporated into the TRM/NRM plot. The NRM/TRM plot gives a useful visual indication of the success of an experiment. It also allows the ancient field to be calculated from which ever section the experimenter sees fit, which introduces some degree of subjectivity to the procedure. In addition to the TRM/NRM plot, a vector endpoint diagram is plotted to check that the magnetisation is trending towards the origin after each zero-field step. Any non-linearity, or change in direction of the NRM is a sign that the magnetisation has more than one component. Secondary, viscous components can often be removed at a low temperature.

Various authors have suggested guidelines for the interpretation of these diagrams that may be used to select the most reliable results. For instance, Selkin and Tauxe (2000) require a minimum of four points on the NRM/TRM plot, that the standard error of the slope of the trendline does not exceed 10% of its value and that the maximum angle of deviation (M.A.D.)(Kirschvink 1980) of the NRM vector does not exceed 15°. Another commonly used criterion is the correlation co-efficient (r): Laj et al. (2002) suggest $r>9.8$, whereas Yamamoto et al. (2003) use a stricter $r>0.995$. Summary statistics such as r should never replace visual examination of the data (Anscombe 1973) but there is a real enthusiasm for them in palaeointensity and archaeointensity.

The most commonly used suite of descriptive statistics is that devised by Coe et al. (1978) which attempt to describe all the salient features of the NRM/TRM plot. The statistics quoted for each of the determinations in this study are briefly described. The proportion of the NRM which is used to determine the ancient field is denoted f. The distribution of the data points is described by the gap factor, g. The ratio of the standard error of the gradient best fit line to the gradient is usually denoted β but it has been omitted from the results given here, to avoid overly crowded tables. It can be found by dividing the standard error

by the field estimate and the common criterion that it should not exceed 0.1 (e.g. Selkin and Tauxe 2000) can be easily checked by inspection. Perhaps the most widely quoted of the Coe (1978) statistics is the quality factor, q. This is simply the product of f and g divided by β. Coe (1978) further suggested that the reciprocal of q could be taken as a reasonable estimate of the uncertainty in a measurement. This has been given in all the results tables as the Coe error, along with the standard error. If more than one sample from the same feature are not available, it is clearly unrealistic to quote an experimental error, but as shown in the meta-analysis presented in Chapter 6, an estimate of around 10-12% appears to be reasonable, but should be use cautiously in field modelling because expressing uncertainty as a proportion of measurement may introduce bias. When an artefact or site yields a number of results the mean value may be taken as best estimate. Some workers have chosen to weight individual results (Coe et al. 1978, Chauvin et al. 2000) to obtain a weighted mean. It is not clear however that the weights truly reflect the uncertainty in the individual results and in this study weighting is not used. Another consideration is whether averaging should be carried out at the site or specimen level. This is considered in chapter, where it is shown that the choice should be made according to the main source of variance in the assemblage. Having estimated the mean it would seem to make sense to give the uncertainty of this estimate as the associated error. In general, most workers and compilers of databases prefer to give the estimate of the standard deviation as an indicator of uncertainty (Donadini et al. 2009, Genevey et al. 2008). The origin of this practice is unclear, and it is assumed that it is done as a tacit acknowledgement that the experimental error is only a small part of the error budget (see chapter 6), although multiplying the experimental error by the square root of the number of samples cannot be a good way to account for a systematic error. In this study, where there are enough samples to provide a mean estimate of the ancient field, the standard error of the mean will be quoted as the associated uncertainty.

The estimation of both the mean and its error will ultimately be determined by the selection of results. Some of the criteria used to make this selection have already be outlined above. In addition to these the success or failure of the pTRM and tailchecks must be considered. Various schemes have been proposed for this, for example tailchecks should differ by no more than 10% of the pTRM being removed (Riisager and Risager2001) and pTRM checks should agree to within 5% (Pick and Tauxe 1993). Another suggestion is that pTRM checks should agree to within 10% of the total length of the trendline being used to

calculate the intensity (Selkin and Tauxe 2000). As well as considering individual checks, pTRM checks that consistently fail with the same sign can give grounds for rejection of a result (e.g. Kissel and Laj 2004). Rather than adopt a rigid set of criteria at the outset each case here will be considered on its merits. For instance the low magnetisations in the sandstone studied in chapter require a relaxation of the criteria to allow for instrumental error.

5.2 Experimental methods

Prior to the archaeointensity experiments, the magnetic mineralogy of all materials was determined using a Magnetic measurements variable force translation balance (MM VFTB). Small chips weighing 100-150mg are placed in the instrument and their magnetisation can be measured in fields of up to 750mT. The IRM acquisition, coercivity, hysteresis and behaviour of the saturation magnetisation during heating and cooling (the thermomagnetic curve) were measured for all samples. With weakly magnetic samples it was not possible to obtain IRM acquisition data as the remanent magnetisations were too weak. Susceptibilities were measured on a Bartington MS2 susceptibility bridge.

Essentially the results reported in this study were obtained by two different experimental methods: microwave archaeointensity and Thellier. The apparatus for the microwave experiments is described in Suttie et al. (2010), although many of the results were obtained before the vacuum pump system of sample mounting had been developed. In these case the sample, a 5mm diameter core of approximately 3mm in length was glued to a quartz rod using heat resistant cement (Unifrax Fixwool®). After the development of the vacuum pump system the sample, of the same dimensions, could be directly mounted onto the sample tube, without the need for adhesive. After mounting the sample a computer controlled worm driven carriage lowers the sample into the three Tristan SQUID magnetometers for measurement of the NRM. The sample is then automatically withdrawn and positioned in the centre of the microwave cavity. Microwaves can then be applied at a given power for a set amount of time. The magnetisation is measured and the process repeated. Once the sample's magnetisation is seen to fall a TRM can be imparted using the triple axis field coils that surround the cavity. This field can be applied in any direction. To minimise the effects of anisotropy, it was applied parallel to the NRM in all of the experiments reported here. High powers were avoided as the large electric fields produced could damage the sample (see chapter 3) and consequently it was not always possible to fully demagnetise the sample. To minimise the effect of any differences in the applied

power at each step, it is best if the applied field has a magnitude similar to that of the ancient field, although obviously this can only ever be an approximation.

Conventional Thellier experiments were carried out using a Magnetic Measurements thermal demagnetiser. A solenoid wound around the furnace allows a field to be applied using constant current supply. The field was set by measuring with a fluxgate magnetometer. Samples were prepared as 1" diameter cores. Measurement of the sample moment was done on either an Agico JR6 or an FIT Squid magnetometer. During these experiments the field could only be applied along the axis of the furnace, corresponding to the axis of the cylindrical sample. This makes it necessary to determine the anisotropy of TRM. Anisotropy of TRM was measured after completely demagnetising the samples by applying a field in each of 3 perpendicular directions and cooling the samples down from 470°C, repeating the procedure in anti-parallel directions. After cooling three 3 components of magnetisation gained were measured allowing the tensor components of anisotropy to be estimated. Details of the procedure are given in chapter 13.

The decision to measure anisotropy of TRM after completing the archaeointensity experiment runs the risk that the samples may have altered during the high temperature stages of the experiment. For this reason some workers prefer to determine anisotropy before the sample has been completely demagnetised (Chauvin et al. 2000, Hill et al. 2007), though the six repeated heatings risk damaging the sample before the completion of the experiment. In general the anisotropy measurements did not appear to be very successful. Some degree of the failure may be due to alteration although the holder that was manufactured for the purpose of positioning the samples in the furnace was somewhat crude in design, so the orientation might have been less than perfect. Anisotropy did not in general need to be considered in the microwave archaeointensity experiments because the direction of the applied field with respect to the sample could be precisely controlled (e.g. Le Goff and Gallet 2004).

A further consideration that could not be fully resolved is that of the cooling rate. The TRM gained by a specimen depends slightly on the rate at which it cools down. Essentially, a slower cooling rate allows magnetic grains to equilibrate with the ambient field at a lower temperature than a faster cooling rate. As their spontaneous magnetisation is higher at the lower temperature, there is a shift in the partition function that determines the position of the magnetic equilibrium. An increase in TRM of about 5-6% for every order of magnitude difference in the rate of cooling has been predicted on theoretical grounds for an

assemblage of single domain grains (Dodson and McLelland-Brown 1980) and observed experimentally (Fox and Aitken 1980). A thermally insulated furnace, capable of maintaining a temperature of 700°C for several hours, cooled down over a period of about two days, when switched off. After the anisotropy measurements samples were placed in this furnace in an applied field of 50μT and cooled down slowly. After measurement of the TRM, they were heated and cooled in the faster cooling furnace to check that the TRM thus gained was not substantially different from that gained during the main experiment. In general these experiments did not give reproducible results. Attempts to quantify the cooling rate correction appropriate to the microwave archaeointensity experiments are reported in chapters 10 and 11.

Chapter 6

Consistent treatment of errors in archaeointensity implies a rapidly decreasing dipole

N. Suttie, R.Holme, M.Hill and J.Shaw.

Chapter published as:

Consistent treatment of errors in archaeointensity implies rapid decay of the dipole prior to 1840

Neil Suttie, Richard Holme, Mimi J. Hill, John Shaw

Earth & Planetary Science Letters

304 (2011) 13-21

Doi:10.1016/j.epsl.2011.02.010

Abstract

We present a meta-analysis of 223 archaeo and palaeointensities spanning the period 1840-1990 and compare these data with the geomagnetic field model gufm1 (Jackson et al. 2000). We find that the principal source of uncertainty in all the data, regardless of experimental method or number of samples, is due to systematic error. This error is quantified and it is shown that the data is capable of estimating the magnitude of the geomagnetic field for the period with reasonable accuracy, but only if errors are estimated on the basis of the true field strength, rather than the measured intensity. The findings are then applied to archaeointensity data from the period from 1590-1840 and it is shown that the most likely behaviour of the field was a decay of the axial dipole at a similar rate as for the period since 1840. We show that serious underestimation of the field's magnitude can be an artefact of inconsistent error estimation.

1 Introduction

The strength of the geomagnetic field is a subject of both scientific and public interest, with the decay over the past 160 years leading to speculation as to whether we are entering a geomagnetic reversal (e.g. Olson 2002). Prior to 1832, there was no capability for direct measurements of geomagnetic field strength; to investigate the field strength at this time, palaeomagnetic and archaeomagnetic determinations must be made. Recently, Gubbins et al. (2006) used a database of all available palaeointensity measurements to constrain the evolution of field strength from 1590 to 1840; directional information was taken from the gufm1 model of Jackson et al. (2000). They concluded that the most likely scenario prior to 1840 was for no strong decay in the field strength. A similar interpretation

was given by Finlay (2008) who employed a variety of modelling strategies, but also noted that the weight given to the archaeointensity data had a strong effect on his models.

Estimates of uncertainty are an integral part of any scientific study, but the assignment of uncertainty to palaeointensity has been largely ad hoc. A protocol for estimating uncertainty in the palaeointensity derived from an individual sample was proposed by Coe et al. (1978) and this may be taken to weight each measurement, if more than one are available from the same site. The standard error of the weighted mean can then be used to express uncertainty (Coe et al.1978) although it was recognised previously that systematic errors make this a dubious measure of accuracy (Coe 1967a). Others have preferred to use weighted mean palaeointensities according to the type of experiment or the material used, as well as the number of samples per site, and express the uncertainty as the standard deviation of this value (e.g. Chauvin et al. 2000). The standard deviation of a suite of palaeointensity determinations, rather than the standard error of the mean, is often regarded as an appropriate measure of uncertainty. Experiments based on the method of Thellier and Thellier (1959) and its variants are often considered to be most reliable (Selkin and Tauxe 2000) although in some cases alternative methods appear to have been more effective (e.g. Yamamoto et al. 2003, Oishi et al. 2005). In the compilation of data sets it is common to assign quality values to a set of measurements, depending on factors such as the experimental protocol, corrections for anomalous behaviour or the spread of the data. Such factors were used to assign minimum errors ranging from 6% to 20% of the measured intensity to the data compiled by Korte et al. (2005). In an analysis of 315 archaeointensity results from 1600 to 1840, Gubbins et al. (2006) used the data and uncertainties from Korte et al. (2005) to show that it was possible to describe the change of the axial dipole as a linear function of time over the period and found that such a model gave a χ^2 probability of 99%. While testing a hypothesis with χ^2 is a one tailed test, with a model being rejected if the probability falls below a certain value, very high probabilities generally indicate that the errors have been overestimated (Barlow 1989). In the case of the data studied by Gubbins et al.(2006), there was less than a 1% probability that data with the given uncertainties would agree to the extent that was found and the allocation of errors within the database used must be called into question. We show that the choice of error can have a considerable effect on inferences drawn from the data, which have in turn been applied to a range of geophysical questions; not only are the resulting models used to study core

dynamics (e.g Hulot et al. 2010) but are becoming increasingly important in evaluating records of solar variation (e.g. Bard et al. 2007).

The aim of most archaeointensity study is to illuminate the behaviour of the past geomagnetic field. In general, it is the main core field rather than local variation which is the quantity of interest and the fidelity of data as a record of this will be affected by factors other than experimental uncertainty. Volcanic rocks are invariably extruded in regions of large magnetic anomaly and fired archaeological artefacts are by definition made in areas of industrial activity. The field recorded by such materials can only be regarded as an approximation of the main core field. While experimental uncertainty can be reduced by repetition and recent progress in the experimental determination of archaeointensity (e.g. Chauvin et al. 2000, Genevey and Gallet 2002, Gomez–Paccard et al. 2008) and palaeointensity (e.g. Biggin et al. 2007, Dekkers and Böhnel 2006) has gone a long way to reducing systematic errors, there is a limit to the precision with which such measurements can quantify the main field. There is a tacit acknowledgement of this fact in the adoption of the estimate of the standard deviation, $\hat{\sigma}$, of a set of data as a measure of the uncertainty of the mean value (e.g. Donadini et al. 2009, Genevey et al. 2009). The assumption appears to be that the experimental uncertainty is a small contribution to the total error budget and so the uncertainty cannot be reduced by averaging. The reason for this is never explicitly stated, nor have the additional contributions to the uncertainty been quantified. In terms of geomagnetic field modelling, it is desirable to have a spot measurement of the field with an associated uncertainty. This measurement will usually be derived from a number, N, individual determinations from a site. Given enough data, the central limit theory ensures that the mean will always have a normal distribution, whatever the distribution of the data, with a standard deviation of $\sigma/\sqrt{N}$. If, however, the experimental error is small compared to the total error budget, as seems to be implied by the choice of $\hat{\sigma}$ as the uncertainty, then it is natural to ask how best to describe the total uncertainty.

The aim of this paper is to find a realistic estimate of uncertainty for archaeointensity determinations and to apply this to the problem of determining the field strength prior to 1840. 223 data from 1840 until present, from 62 studies are compared with the field model gufm1 (Jackson et al. 2000), which is assumed to be a good representation of the Earth's magnetic field from 1840 until present .The justification for this is , following the argument of Gubbins et al. (2006), that the strength of the magnetic field at all points on the surface of the Earth can be determined by one measurement if the direction of the field is known

precisely at all locations (Hulot et al. 1997). The fit of the model gufm1 to the observatory data compiled by Malin and Bullard (1981) is excellent as far back as 1840 (see Jackson et al. (2000), figure 11).By studying the distribution of data around the main field value the uncertainty inherent in the measurements can be estimated. Once this has been established, the data prior to 1840 can be re-examined and the effect of different estimates of uncertainty on inferences of the past field can be studied.

One problem with archaeointensity data is the presence of outliers which can often mask the underlying distribution. Testing data for normality is at best a haphazard affair and can be practically impossible when outliers are present and if the alternative distribution is not known explicitly. In this study we rely mainly on graphical methods, particularly quantile-quantile plots, and goodness-of-fit tests. The presence of outliers will almost always cause the hypothesis of normality to be rejected. The data were analysed before and after the rejection of outliers that showed extreme values. Reasons for the rejection of outliers are discussed on a case-by case basis. After describing the data used in section 2, tests for normality and the rejection of outliers are considered in section 3. In section 4 various subsets of the data are compared to determine which materials and methods are the most reliable. In section 5 archaeointensities for the period 1840-1990 are shown to be informative enough to infer the decay of the dipole field seen over this period but the choice of error estimate is shown to be critical. The conclusions regarding uncertainty are then applied to the data for the period from 1590 to 1840 in section 6. Both the data from ArcheoInt 2009 (Genevey at al. 2008) and the data set used by Gubbins et al. (2006) and Finlay (2008) are considered in detail and both are shown to be consistent with decay in the main dipole field of a similar magnitude to that observed since 1840.

2 The post 1840 dataset

All 205 archaeo and palaeointensities dating from 1840 to 1990,with an age uncertainty of less than 20 years, found in the ArcheoInt2009 database (Genevey at al. 2008) were compared with intensity values for each of the locations represented, taken from the model gufm1. The majority of the data have age uncertainties of much less than 20 years and the uncertainty in intensity due to this in no case exceeds 600nT and is usually much less, so can be considered negligible. For each of these data, f, the corresponding value of gufm1, g, at the site location for the expected age was found. At first, to investigate the strength of various estimates of error associated with each measurement, only those data

with a defined non-zero estimate of error, s, were considered. For these 186 data a χ^2 sum, $\chi^2 = \sum \frac{(g-f)^2}{s^2}$,of 4260 was formed using the model values and the published uncertainty. Such a value of χ^2 for 186 degrees of freedom is so unlikely as to be practically incalculable. Of these data, 156 had an error defined as the estimate of their standard deviation. Using this as an estimate for s gave a χ^2 sum of over 3500 and again a probability of 0. The published errors appear to account for only a small fraction of the misfit between the data and the model so it was decided to consider the larger data set of 205, including those data with no estimate of error. One of these was removed from the analysis as being such an egregious outlier, an intensity of 144μT, that its inclusion would completely dominate the results. The presence of this outlier could be easily determined by a casual glance at the data and so its removal seems justified. Furthermore, the original report (Domen 1977) gives the intensity with a question mark, although whether this is because of some suspicion regarding the archaeointensity experiment or simply because of the clearly wayward result is not clear. The data are taken from 56 different studies using a variety of different palaeointensity techniques including 118 from Thellier and Thellier type methods (Thellier and Thellier 1959, Coe 1967b), 27 from Shaw and derivative (Shaw 1974), 18 Wilson (Wilson 1961), 5 microwave (Shaw et al. 1996) and 34 derived from the ratio of NRM to TRM. In addition to these a further 19 data were included from 6 different studies on 13 lava flows dating from 1878 to 1983 (Yamamoto et al.2003, Calvo et al.2002, Oishi et al.2005, Mochizuki et al.2004, Michalk et al.2008, Biggin et al. 2007) making a total data set of 223.

3 Describing the distribution

If the experimental uncertainty is small compared to other sources of error, the choice of variate must be considered carefully. Essentially we are interested in the distribution of data (f) around the modelled field (g), but if the given error (s) only accounts for part of the error budget, the usual choice of normalised variate (f-g)/s is not appropriate. Describing the uncertainty as a percentage of the measured field (e.g Korte et al. 2005) amounts to choosing (f-g)/f as the variate of interest. If the expectation <f>=g , the variate (f-g)/f is biased because in general <g/f> will not equal one. More recently databases have used an absolute value of uncertainty of, say, 5μT (e.g. Donadini et al. 2009). Such a choice of error would be appropriate if the precision was determined by the sensitivity of the measuring

apparatus, but it seems unlikely that 5μT is the maximum sensitivity attainable. Furthermore, applying an absolute value of error to the data results in the underweighting of data from lower latitudes where the field is weaker. Recent archaeointensity studies in Brazil (Hartmann et al. 2010), not included in this analysis, have successfully measured archaeointensity as low as 25 μT, with experimental errors as low as 200nT. To assign an uncertainty to this data of 5μT, as well as to archaeointensities from more northerly latitudes that may be three times as high, does not seem justified. If the source of uncertainty in the data is due to the presence of magnetised bodies in the environment in which they cooled it can be argued on physical grounds that the uncertainty will be a function of the strength of the inducing field. Similarly it might be expected that uncertainty arising from the experimental method will also reflect the magnitude of the original field as instrumental precision is not a significant factor; the uncertainty in setting the applied laboratory field in a Thellier experiment, for instance, or the precision of the magnetometer will not usually contribute greatly to the error budget. For these reasons the distribution of the scaled variate $(f-g)/g$ is studied here. The choice to scale the misfit by the main field value means that its expectation is 0 when f is a true measure of g and, furthermore, that data from lower latitudes will have the same weight as those from higher latitudes when deriving the coefficients for the expansion of the potential. The effect of describing the errors in terms of the measured field value when g is not known a priori will be considered in detail in section 5.

A quantile-quantile plot of this variate against a normal distribution was used to test the data for normality (see figure 1). Dividing a normal distribution of zero mean and unit variance into the same number of quantiles as the data, and plotting one against the other, should show a straight line relationship, if the distribution is normal. There are clearly a large number of outliers and two studies were found to be particularly prevalent among the most extreme values. Three of the largest overestimates of the field come from archaeological artefacts from Sternberg (1989), a fact that may be attributable to the use of iron kiln furniture over the period (Sternberg1989) although outliers due to this and other local field distortions throughout the industrialised period must be likely in the European archaeological data as well.

Figure 1 Quantile-quantile plot of all 223 data from 1840-1990, expressed as normalised misfit ,(f-g)/g, against a standard normal variate (i.e a normal distribution is divided into 223 equal cumulative intervals and plotted against the 223 data). Inset is a histogram of the data. The dotted line is the best fit straight line through the points: its slope is an estimate of the variance of the data. For a normal distribution , all points would lie on the dotted line.

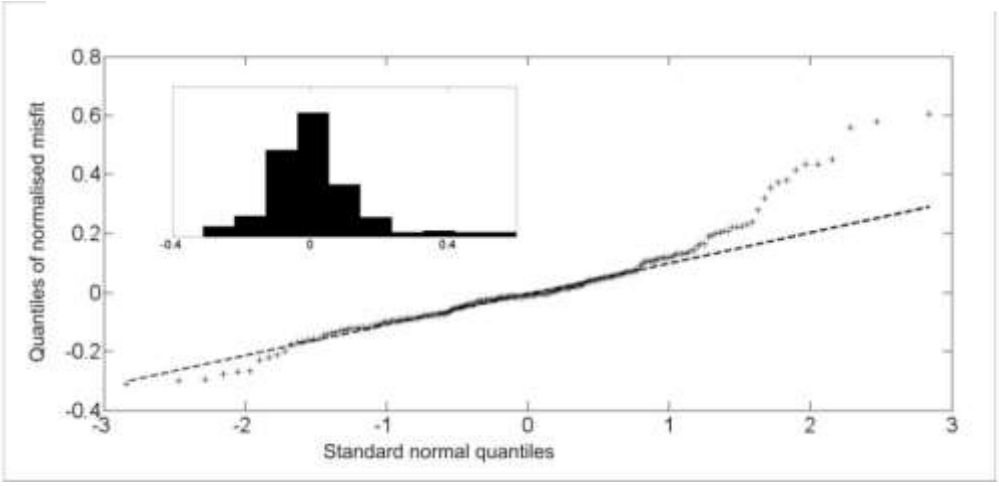

Also, results from Tulloch (1992), which accounts for 47 of 223 data, show a distribution which is much wider than that for the data set as a whole. To avoid having the results heavily biased by one unpublished study focussing on lavas from Mount Vesuvius and the Canary Islands, the results from Tulloch (1992) are excluded, along with the ten from Sternberg 1989, leaving 166 data, henceforth referred to as the reduced data.

Figure 2 Quantile-quantile plot of the reduced data set of 166 left after removal of two studies (see text) , expressed as normalised misfit ,(f-g)/g, against a standard normal variate. The dotted line represents the best fitting straight line through the data. Inset is a histogram.

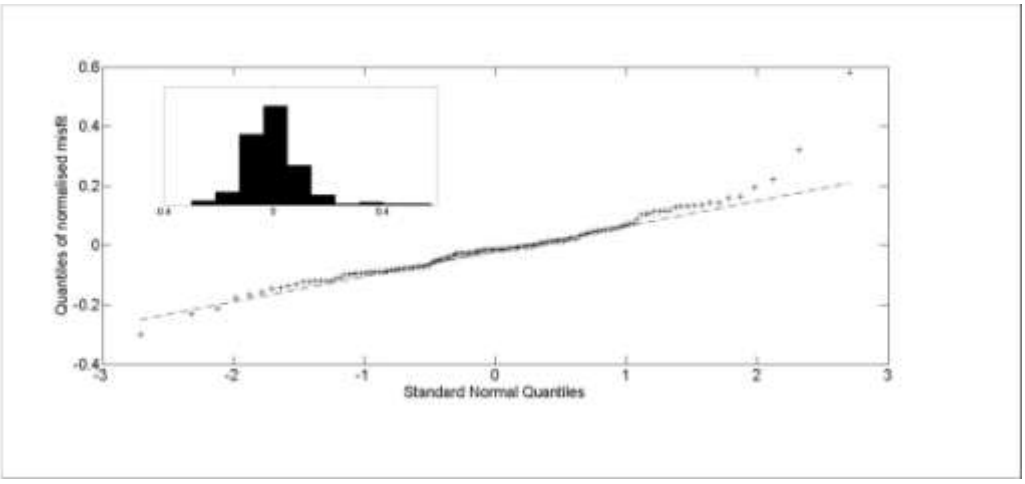

Figure 2 shows quantile-quantile plots of the variate (f-g/g), for this reduced dataset. The distribution is skewed with three points representing overestimates of over one third of the modelled field value: an overestimate of 24.5μT in Kovacheva et al. (2009) one of 12.9 μT in Yamamoto et al.(2003) and one of 16.2 μT in Calvo et al.(2002). The mean value is -0.2% with a standard deviation of 11%. The removal of the three values that exceed 1/3 leaves a distribution that approaches normality with a χ^2 probability of 22% and we cannot reject the hypothesis that these 163 data are normally distributed. The mean value is -1% with a standard deviation of 9.3%. From this analysis it is concluded that the data are normally distributed, although outliers are present, have a mean value indistinguishable from the modelled field value and about 10% of the field is a reasonable estimate of the error in the archaeointensity dataset.

It is worth considering the uncertainty in the data before the removal of the outliers because this is more likely to resemble the situation faced when using archaeointensity data to construct a field model. Notwithstanding the problem that the data are unlikely to be normally distributed it is legitimate to estimate the variance of the original dataset of 223. The variate (f-g)/g is found to have a mean of 1.2% and a standard deviation of 14.6% but this ignores any information contained in the original estimates of uncertainty. Another approach is to consider the variate (f-g)/S, where S is an estimate of dispersion that takes account of the original estimates of error. A minimum value of S, in terms of g, can be chosen so that the variate (f-g)/S has unit variance. This is found to be achieved by applying a minimum error to the data of 11.5% of the modelled field value and retaining original error estimates that exceed this. From this it can be seen that ignoring the published estimates in uncertainty does decrease the information content of the data slightly. This suggests that when the published estimate of error is large it does reflect an unreliable result and should be taken into account. This can be summarised in terms of three basic scenarios: data that are free of outliers can be described as having errors of 10% of the field, where the data have a wider dispersion and outliers may be present a minimum error of 11-12% of the true field is appropriate, and where the data have a wide dispersion and there is no original estimate of error an error of 14-15% of the field should be used. These values are appropriate for the data set as a whole, but it is possible that certain subsets of data may exhibit more or less dispersion than this. This is examined in the next section where a more exact analysis of the variance is given. It should be noted than in every case the mean misfit is not significantly different from 0.

4 Quality factors

It is possible to evaluate the importance of various quality factors by considering the distribution of the data derived with and without certain tests and protocols. Again, the data are restricted to the reduced dataset of166. The following criteria are considered: whether the material is volcanic or archaeological, whether anisotropy and cooling rate corrections have been applied, whether pTRM checks (Thellier and Thellier 1959, Coe 1967b) have been used and if the archaeointensity was derived from Thellier and Thellier type experiment. As the resulting datasets are reduced in size it becomes difficult to make robust inferences about their distributions. For this reason the data are presented in the form of box and whisker plots (figure3). Outliers, which we have defined as any data more than 1.5 times the interquartile range above or below the interquartiles, are shown as crosses outside the main distribution. Despite the overall similarity of the distributions certain notable features are worth commenting on. The volcanic data has a greater spread than the archaeological data but has fewer outliers. Whether outliers in the archaeological data can be ascribed to the common use of ferrous kiln furniture through the period can only be speculation but a possibility.

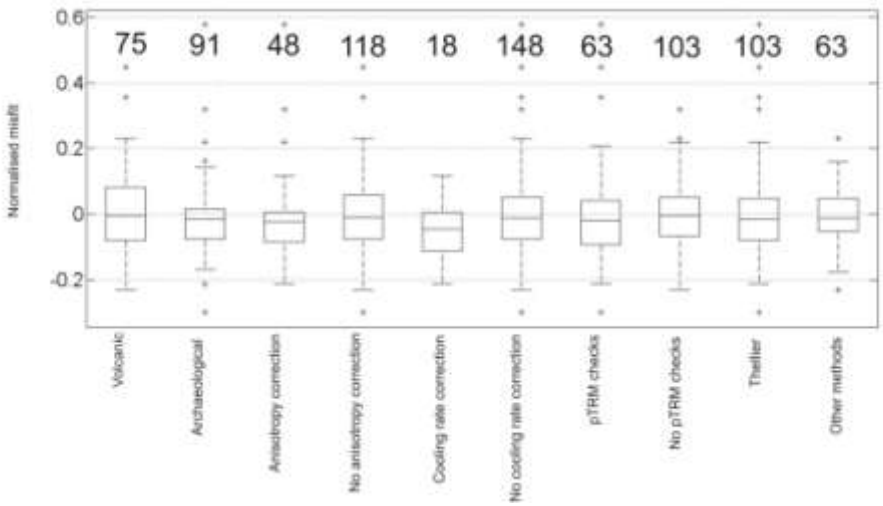

Figure 3 Box- and –whisker plots of subsets of the data, showing the normalised misfit. The reduced data set (see text) of 166 is divided by some criterion and two box plots are drawn representing the data in each category. Five criteria are applied giving ten distributions which are labelled accordingly. Boxes span the interquartile range(IQR), with the median shown. Whiskers extend to the last datum within 1.5 times the IQR above the upper quartile or below the lower quartile. Data lying outside this range are marked by crosses. The number in each group is shown above the boxes.

It is difficult to discern any real improvement in any of the data sets due to any of the factors considered and the distributions are remarkable for their similarity. Some groups of data may be closely correlated: anisotropy corrections are usually only applied to archaeological artefacts and the apparent difference in the spread of the anisotropy corrected data may simply be a reflection of the difference seen in the volcanic and archaeological data sets. The only distribution with a mean that can be regarded as significantly different from the others is the data that has been cooling rate corrected. In this case the null hypothesis that the data come from a distribution with zero mean can be rejected at the 5% significance level using a t-test (with a significance of 2.9%). In all other cases the data are consistent with a mean misfit of zero. It appears that the cooling rate corrections that have been applied are simple estimates, rather than empirically determined, so it would be premature to draw any conclusions regarding the validity of cooling rate corrections in general. The ratio of the variances of each pair of distributions was also considered to ascertain whether there were any significant differences. In only one case was the difference found to be significant; the variance of the results obtained by Thellier type methods was found to be larger than that for results obtained by other methods. Strictly speaking a ratio of variance test (or F-test) as well as a t-test are only exact tests when the distributions are normal but it has been shown that even fairly large departures from normality should not result in serious error (Cochran 1947). Even after removal of the two largest outliers in the Thellier type data, the difference in the variances of the Thellier type and non-Thellier type data sets is still significant at 6%, however, as five different datasets have been compared this should be interpreted cautiously. From the point of view of field modelling, it is not clear that it is beneficial to weight certain data on the grounds of experimental protocols. This is not to say that exacting archaeointensity protocols are not capable of reproducing the field accurately (e.g Genevey and Gallet 2002, Genevey et al.2009), but that certain sources of uncertainty are beyond experimental control.

Another factor that was considered was the number of individual measurements contributing to a palaeointensity determination. Considering the rationalised misfit, (f-g)/g, as before, it was found that increasing the numbers of measurements did not significantly improve precision and it was impossible to distinguish between the distributions of data on the grounds of number of samples analysed. This, along with the fact that the standard error of the mean does not represent the uncertainty (see Genevey et al.2009, Donadini et al.2009) shows that a key source of error is systematic, rather than random. Yet the mean

misfit with gufm1 is indistinguishable from 0, so the systematic errors are evenly distributed around 0 and can be treated as a random variable whose variance can be estimated. Again the data are normalised by the modelled main field value, g. For the i^{th} datum, $z_i = (f_i - g_i)/g_i$ and $S_i = s_i/g_i$, the variance of the systematic error (V) can be estimated by $V = \frac{1}{N-1}\sum_1^N (z_i - \bar{z})^2 - \frac{1}{N}\sum_1^N \frac{S_i^2}{n_i}$, where n_i is the number of individual samples used to determine the i^{th} intensity, with standard deviation s_i. For a useful estimate data is required that has both a large enough n for a reasonably precise estimate of s, but without excluding so many data that the variance of z cannot be found. A good compromise was found to be n>7 which left N=27 data in the analysis. The total standard deviation was 10.5% of the predicted field value, with the standard deviation due to systematic error 9.3%. Removal of the largest datum, an apparent anomaly, left a standard deviation of 8.0%, 6.4% of which was due the systematic error. These values proved quite robust after removal of more extreme values and it can be concluded that the experimentally observed spread in intensity from one feature can only account for around 20% of the total dispersion seen in the data. Systematic effects are not necessarily due to inadequacies in the palaeointensity methods, but include local magnetic sources, and also any error in the model. To summarise the analysis, the palaeointensities have an inherent uncertainty due to systematic effects of around 6-7% of the magnitude of the field, and this cannot be reduced by increasing the number of measurements from a single feature. The procedure used here could be used to incorporate the observed variance of a palaeointensity into an overall estimate of uncertainty but as half of the 166 data have fewer than 3 individual measurements, a good estimate of the individual dispersion is not usually available. For this reason, in the analysis that follows, the heuristic estimate of uncertainty found in section 3 is preferred.

The possibility remains that an absolute error estimate, of say 5μT , may be more appropriate but the range of the data studied here does not allow for this to be tested. Recently published archaeointensities from Brazil from the late 19th and early 20th century of around 25 μT (Hartmann et al. 2010), not included in the previous analysis, were compared with the models gufm1 and IGRF. These three data have negligible experimental uncertainties and are found to be below the modelled field by between 4 and 6%. This confirms the estimate of the systematic error and the appropriateness of giving it as a proportion of the field magnitude.

5 Information in the data

Each of the sets of data considered so far have a mean misfit with the palaeofield of close to 0, so it is expected it would be possible to estimate the true behaviour of the field from the data. The task is made somewhat easier by the fact that g_1^0 has decayed approximately linearly since 1840. Following the method of Gubbins et al. (2006), all the intensity measurements are converted to the corresponding values of g_1^0 (see figure 4) and a straight line relationship between age and g_1^0 is sought.

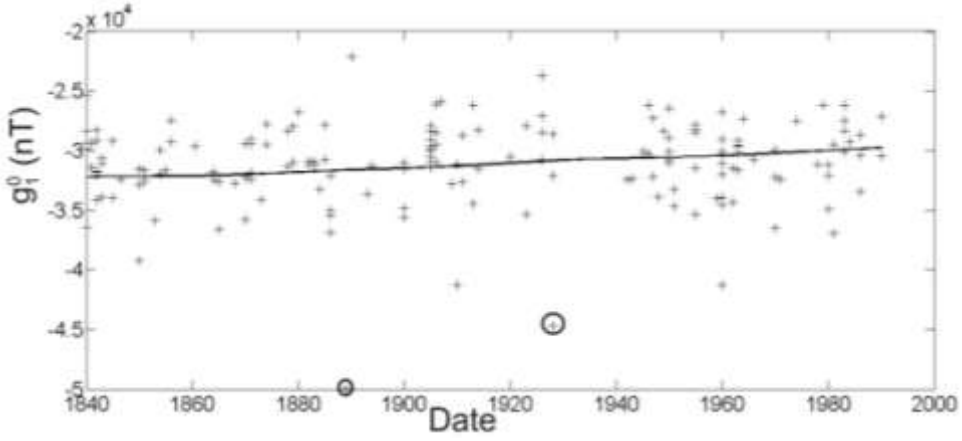

Figure 4 The reduced data set of 166 from 1840 to 1990, after being converted to the corresponding value ofg_1^0, via the field model gufm1. The value of g_1^0 from gufm1 is shown for reference. Two outliers that were removed from the analysis are circled.

Two outliers, the point at 1889 (Kovacheva et al. 2009) and 1928 (Calvo et al.2002) discussed previously, were removed. As the morphology of the field changes with time, the derived value of g_1^0 for each measurement site depends on both the intensity and the age. For this reason the age uncertainty cannot easily be incorporated into the calculation of likelihood as was done by Gubbins et al. (2006) so the age uncertainties, which are in every case less than 20 years, have been ignored. The errors introduced through the uncertainty in age are negligible compared to the total error. To study the bias introduced by defining errors as a percentage of the measured intensity rather than the modelled field, maximum likelihood estimates of a straight line through the data are given for both cases. Firstly both the gradient and height of the line are allowed to vary using error estimates as 10% of the

measured intensity (a) and 10% of the modelled field (b) (see figure5).

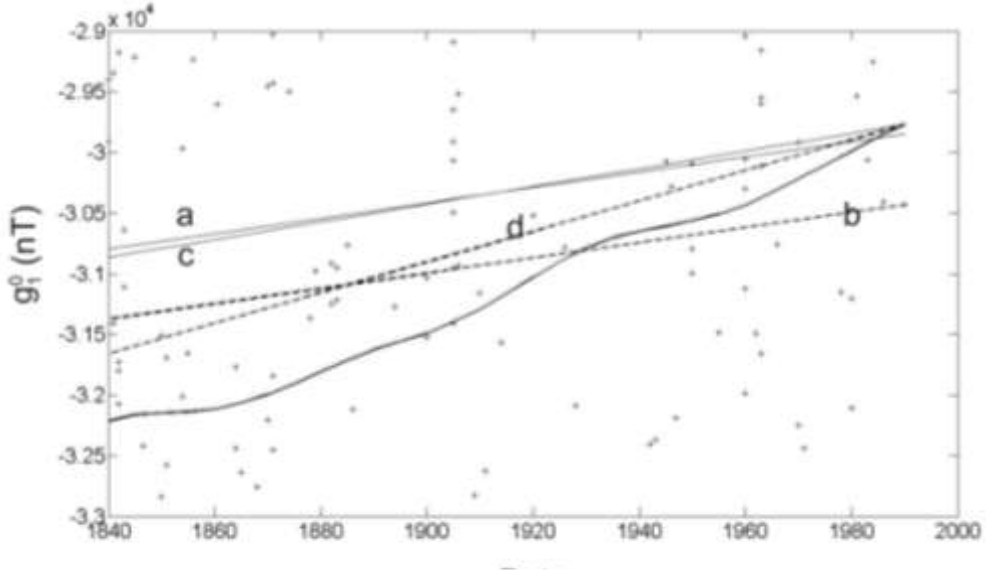

Figure 5 Four best fitting straight lines compared to the model gufm1. The four cases are (a)two free parameters, errors estimated from measured intensity, (b) two free parameters, errors estimated from model intensity, (c) one free parameter, errors estimated from measured intensity, (d) one free parameter, errors estimated from model intensity. Data are shown as crosses, but note that the range shown is smaller than in figure 4 for clarity, so not all the data shown in figure 4 is seen.

In both cases the gradient is approximately the same but the magnitude of the field is better estimated if errors of 10% of the modelled field are used (see table 1). A different method, used by Gubbins et al. (2006), is to fix the line at a known point and then find the gradient that maximises the likelihood. The same algorithm was used here although the age uncertainties were set to zero for the reasons outlined above, with the line being fixed at the value given by gufm1 at 1990. In this case the best fitting lines had gradients of 7.3nT/year(c) and 12.6nT/year (d) for the two estimates of error, as compared to the average of 15nT per year of gufm1. Once again giving the error in the measurements as a fraction of the true field value improves the estimation of the field strength with the root mean squared misfit with gufm1 improving by a factor of two. There is no way, however, of establishing the uncertainty in these parameters, as the model has already been used to estimate the probable uncertainty. Despite the fact the uncertainties in the data are of a similar magnitude to the total change in field strength over the period, the data is still informative enough to reasonably reproduce the decay of the field and correctly identifies

the mean magnitude. A significant bias is introduced, however, if errors are assigned as a fraction of the measured intensity, rather than the field strength. This will always tend to cause underestimation of the field strength for a combination of two reasons. Firstly, lower estimates of field strength will have lower associated errors than higher estimates and are therefore preferentially weighted. Secondly, as long as f has a symmetric distribution about g, with expectation g, the expectation <g/f> will be greater than 1. These two factors combine to push the model towards lower field values.

6 The field prior to 1840

Having established a reasonable estimate of error the behaviour of the field prior to 1840 can be reassessed. The ArcheoInt database (Genevey et al. 2008) gives 316 intensities from between 1590 and 1840, with age uncertainties of less than 20 years. After these have been converted to their corresponding g_1^0 values via the model gufm1, a visual inspection of the data reveals one obvious outlier. This datum comes from Sternberg (1989) which was discussed previously in section 3. This study and that of Tulloch (1992) are removed to make the data as consistent with the previous analysis as possible. This leaves 261 data that are shown in figure 6. Two obvious outliers, one high and one low, can be rejected leaving 259 data. It makes sense to try to constrain the field with all of this data because the accuracy of a similar data set has been established in the previous section. Even if the data is of limited precision, as long as it is accurate and numerous enough, it should be capable of elucidating some aspects of the behaviour of the field. An alternative approach has been adopted by Genevey et al. (2009), who consider a much smaller data set of far greater experimental precision and used this to scale the evolution of the dipole via the model gufm1. There is some danger inherent in such an approach: because of the limited spatio-temporal distribution of the data, it is difficult to know which features represent the true behaviour of the field, and which are artefacts of local effects and inadequacies of the model being used. For instance, 7 individual potsherds from the period 1818-1848 were found to give a very precisely determined mean that was however some 3μT below the intensity predicted by gufm1 for the locations at 1840. It may be possible that the strength of the dipole did decrease by some 7% in a dozen years, but equally there may be an issue with the model, or some local effects, causing this discrepancy. By taking all the data available globally, any such discrepancies should be averaged out. Here a large, accurate data set of lesser precision is preferred to a few data of high precision, although it is acknowledged that the outstanding precision now being achieved in archaeointensity (e.g.

Genevey et al. 2009, Hartmann et al. 2010) is making the experimental uncertainty all but negligible.

The maximum likelihood algorithm, again with age uncertainties set to 0,is applied to find the best straight line fit , tied to the value of g_1^0 for 1840 taken from gufm1. Following the heuristic approach to error estimation in section 3, the published error is retained when this is larger than 12% of the measured value.

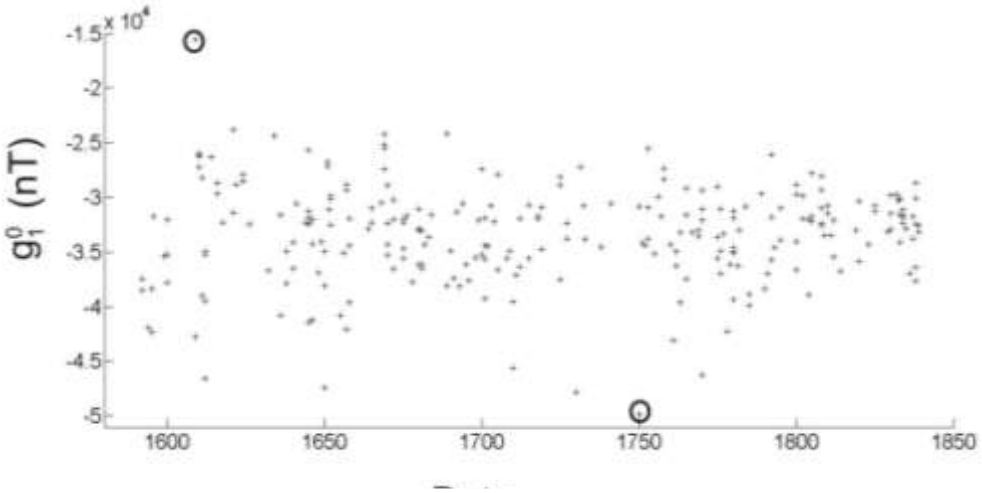

Figure 6 The 261 data used to reconstruct the field strength previous to 1840, converted to g_1^0.The highest and lowest extreme values are shown (circled) but were removed from the analysis.

The best fitting straight line is found to have a gradient of 0.1nT per year with a χ^2 of 270 giving a χ^2 probability of 30%. But now consider what happens if the errors are assigned on the basis of the main field value, which is unknown. An iterative approach is used, calculating the associated errors for a given rate of change of the dipole field, then forming the likelihood and finally choosing the gradient with the minimum χ^2 sum. If a minimum uncertainty of 12% of the field is used, the maximum likelihood is found to be a decay of 11.9 nT per year with a χ^2probablity of 12%. Gradients outside of the range 6 to 18 nT per year would be rejected at the 5% level by a χ^2 goodness of-fit -test. This is remarkably close

to the average fall of 15nT per year observed since 1840 (Barraclough1974).

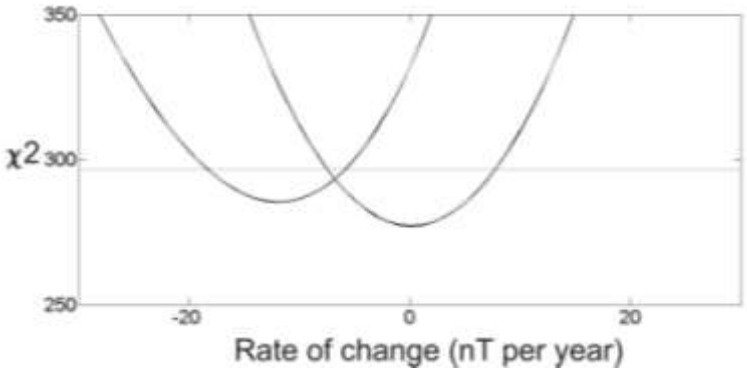

The χ^2 sum is plotted against the rate of change of the field in figure7. χ^2 is closely related to the log likelihood so is useful for picturing the dispersion of a parameter estimated by maximum likelihood. It would be a fallacy to give an actual error estimate on the rate of decay, as this would require that it had been established that the decay was indeed linear but it is possible to say which linear decays are improbable. The horizontal line represents a χ^2 probability of 5% on 258 degrees- of- freedom. It is far from clear whether a straight line fit should be accepted or not but the effect of the hidden bias in estimating errors as a fraction of the measured value is clearly seen.

It is of some interest to reanalyse the dataset of Korte et al. (2005) that was used in the analysis of Gubbins et al. (2006) and Finlay (2008). This consists of 315 data spanning the period 1590 to 1840; over half have errors assigned as 20% of the measured intensity and over one quarter have errors assigned as 10% of the measured intensity. Applying the same maximum likelihood algorithm as Gubbins et al. (2006), following the method of Williamson (1968), and this time keeping the age uncertainties but changing the uncertainties in the intensity data, reveals the importance of consistent error estimation. After confirming the estimate of 2.28nT per year found by Gubbins et al. (2006), uncertainty in the intensity is replaced with estimates of 15% of the measured intensity and of the derived field value. 15% was found to be a reasonable estimate of uncertainty in section 3, when the original estimates of uncertainty were ignored. As the data in this case have had ad hoc estimates of uncertainty ascribed to them and the original estimates cannot easily be recovered, this is considered the best analogy. When errors are assigned

as 15% of the measured intensity, the data are best explained by no change in g_1^0 (χ^2=257). When the error is given as 15% of the expected field value the maximum likelihood is given by a decay of 15.3nT per year (χ^2=255), very close to the average change in g_1^0 since 1840.The conclusion persists: while a linear decay may not be the best model, if errors are assigned on the basis of the derived field value, the field tends to show behaviour very similar to the decay observed since 1840. The χ^2 sums are plotted against the rate of change of g_1^0 in figure 8, with the 95% χ^2 probability indicated. The range of acceptable values is rather large and the importance of removing outliers must be stressed, if meaningful inferences about the behaviour of the field are to be drawn. This was not done with this data set in order that a true comparison with previous studies could be made. Clearly, the choice of the magnitude of uncertainty has no effect on the maximum likelihood estimate of the rate of decay, as long as it is applied to all the data. The size of the bias introduced by assigning uncertainties as fractions of the measured value is determined by the width of the underlying distribution of the data about the actual field. We also note that similar values for the decay are obtained when each of the intensities is given a set error of say 5μT, but feel that such an error estimation scheme is unjustified on physical grounds.

Figure 8 χ^2 sums for linear decays of different rates using 2 different estimates of error in the 315 archaeointensities from Korte et al. (2005) The horizontal line represents a χ^2 probability of 5%. The curve on the right shows χ^2 sums as found by Gubbins et al. (2006). When errors are estimated as a fraction of the hypothesised field, the χ^2 sums are given by the curve on the left.

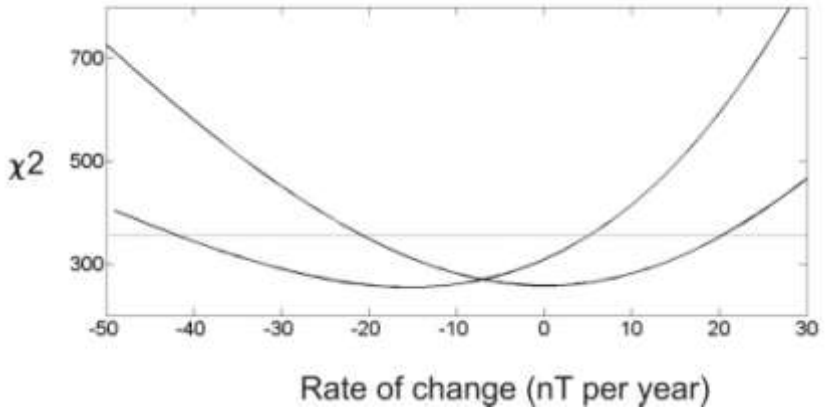

The effect of assigning uncertainties on the basis of the measured value is surprisingly large. It is a simple matter to verify the magnitude of the effect by using simulated data. Ages and age uncertainties were taken from the data set used by Gubbins et al (2006). For each of the 315 ages, intensity was assigned, assuming a linear decay of the main dipole field of 11.9nT per year, the rate shown to be most likely in the analysis above. A random number, drawn from a normal distribution of mean 0 and standard deviation of 15% of the intensity, was added to this value to give a simulated measured intensity. The maximum likelihood algorithm of Gubbins et al. (2006) was then applied, first to the data with errors given as 15% of the simulated measured intensity, then as 15% of the intensity. This was repeated 500 times and the mean value for the rate of change of g_1^0 found for each case as well as the standard deviation of the results. When the errors were estimated from the measured intensity, the mean result was a decay of 2.3 nT/year with a standard deviation of 3.2 nT /year. When errors were given as 15% of the actual intensity the result was 13.7nT/year, with a standard deviation of 3.2nT /year. If the age uncertainties were set to zero the results were a decay of 1.6 and 11.7 nT/year for the two cases. From this it can be seen that the result of 2.28nT/year (Gubbins et al 2006) is in fact an artefact of the method of assigning uncertainties to the data. The most probable rate of decay, when the errors are estimated from the likely field value is about 12nT/year.

The analysis presented above demonstrates that when a simple linear decay of the dipole field is constrained by the available archaeo and palaeointensities for the period 1590 to 1840 the most likely scenario is a decay close to that for the period since 1840, but it is not clear whether such a simple model is justified and a simple visual inspection of the data does little to inspire confidence in a straight line fit. Before the results are accepted some visual confirmation should be sought. In a case such as this where the data exhibits a great deal of dispersion it is useful to bin the data according to age. The data is grouped into periods of 40 years and for each group the distribution of g_1^0 is shown as a box and whisker plot (figure 9).

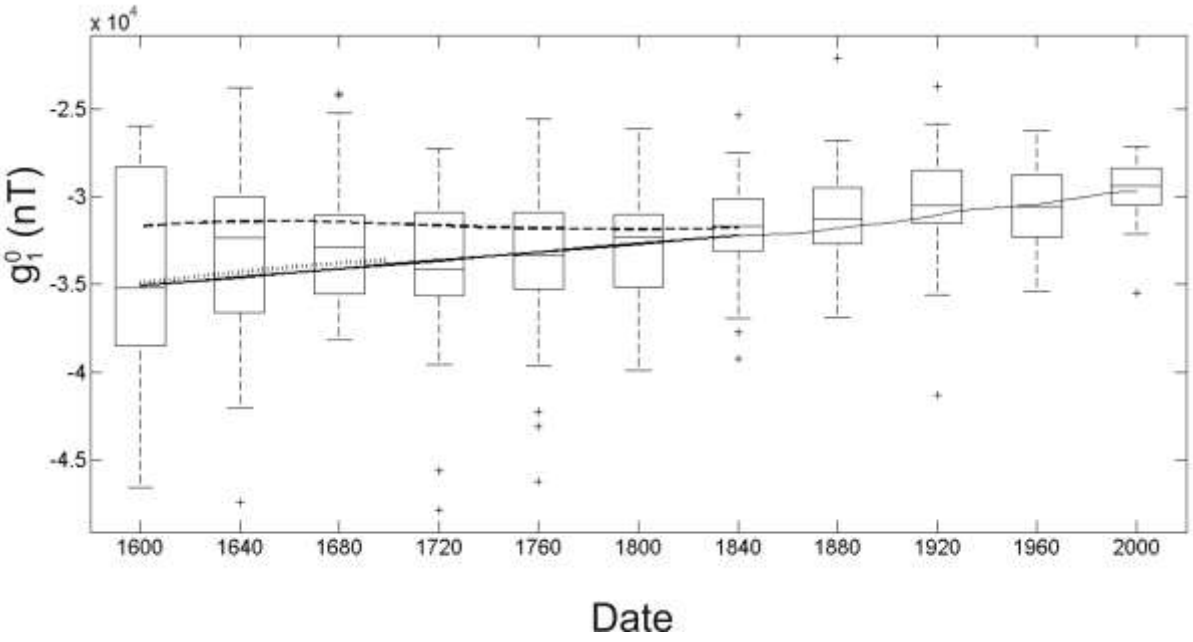

Figure 9 Box-and -whisker plots of the data from ArcheoInt2009 from 1590-1990, along with the additional studies mentioned in section 2, converted to g_1^0 and grouped in 40 year intervals. Also shown is g_1^0 from gufm1 from 1840-1990 and its extrapolation back to 1600 assuming a decay of 11.9nT/year. The proposed value of g_1^0 close to the median of each group back as far as 1720, and is very close to the values given by the archaeomagnetic model of Hongre et al. (1998) (dotted line). Also shown is the axial dipole from CALS7K.2 (Korte and Constable 2005), (dashed line).

The value of g_1^0 from gufm1 is shown, with a linear extrapolation assuming a decay of 11.9nT /year back to 1590. The median of each group from the present back until 1700 lies on or close to the model, which confirms that our findings are valid at least as far back as then. The data for the 17th century diverge from the model somewhat but it must be noted that the model itself may be less reliable during this period when there were few inclination data. It may be that the large dispersion seen in the earliest data is in some part due to inadequacies in the model. The evolution of the axial dipole proposed here shows clear continuity with the purely archaeomagnetic model of Hongre et al. (1998), but less so with CALS7K.2 (Korte and Constable 2005).

7 Conclusions

If archaeointensity errors are given as between 10 and 15% of the actual field value if they are capable of reproducing the recent behaviour of the field from1840-1990 when

combined with the field model gufm1. Archaeo and palaeointensities from the database are normally distributed around the modelled field value, although the presence of outliers can obscure this. If outliers can be rejected, an error estimate of 10% of the expectation is appropriate; otherwise the estimate increases to 12-15%. We found no evidence that this estimate is affected by the method, protocol, or the use of anisotropy or cooling rate corrections and we conclude that despite some imprecision, all archaeointensity and palaeointensity data should be considered as accurate. Although it is clearly desirable to reduce the experimental uncertainty as far as possible, the principal contribution to the error budget is not experimental and consequently cannot be reduced by averaging. Estimating the error in a measurement as a fraction of the measurement unavoidably introduces a significant bias into the data set and should be avoided. Such a procedure will always tend to produce underestimates of the field.

When these factors are considered in relation to archaeointensity data from 1590 to 1840, the data are seen to be consistent with a dipole field decaying at a similar rate to that observed since 1840. The data are most consistent with a linear decay of 11.9nT per year, although there is no reason to suggest that this value did not vary around this value over the period. The trend can be clearly seen by grouping the data by age and plotting the median and inter quartile range of each group. This reveals that the present decay in the dipole field can be seen as part of a long term process that started at least as early as 1700. Certain inconsistencies between the model and the data, particularly throughout the 17th C, highlight the need for a greater number of globally distributed data, and for greater dialogue between modellers and experimentalists concerning the most effective sampling strategies to adopt.

Chapter 7

Whitby Abbey Cliff

7.1 Background

During excavations at Whitby Abbey Cliff (54.5°N, 0.6°W) carried out by English Heritage Centre for Archaeology a number of fired clay features were uncovered. These were associated with the original Anglo-Saxon Abbey. A small piece of a fired clay floor (context 40818) was provided for archaeointensity analysis by Paul Linford of English Heritage after the feature had been dated archaeomagnetically to 7^{th} or 8^{th} centuries (see Linford 2002).The period is of interest from a geomagnetist's viewpoint because of the high field strengths found in archaeointensity studies from French sites (Genevey et al. 2002). Despite the rather uncertain date of the context, this fact in conjunction with the high precision achieved in the directional analysis (α_{95}= 1.9°) made the material worthy of further study. In particular, from the point of view of field modelling a complete vector description of the field at a point in space is highly informative, even in the absence of precise dating. The clay obtained for this study was not orientated so directional checks to the archaeointensity analysis could not be made. Both microwave and conventional heating was used to derive archaeointensity estimates and while the results are of a rather poor quality, the importance of the period in terms of understanding the evolution of the geomagnetic field, make them of some interest.

7.2 Magnetic properties

A fragment of the clay was analysed using an MM VFTB. The IRM acquisition, co-ercivity, hysteresis and thermomagnetic data are shown in figure 7.1. The hysteresis loop is narrow and the IRM saturates in a field of 200mT. This would indicate magnetite as the main magnetic phase but the magnetisation does not completely disappear until around 600°C, a little above the Curie temperature of magnetite. A high Curie temperature would often suggest the presence of haematite but there is no sign of this in the IRM or hysteresis data. The thermomagnetic curve is reasonably reversible with the cooling curve is slightly less than the heating curve although this can be caused by a slight lag between the sample temperature and the thermocouple in the instrument.

Figure 7.1 IRM acquisition and backfield coercvity (top) and hysteresis and thermomagnetic curve (bottom) for the fired clay. Arbitrary units (a.u.) of magnetisation have been used.

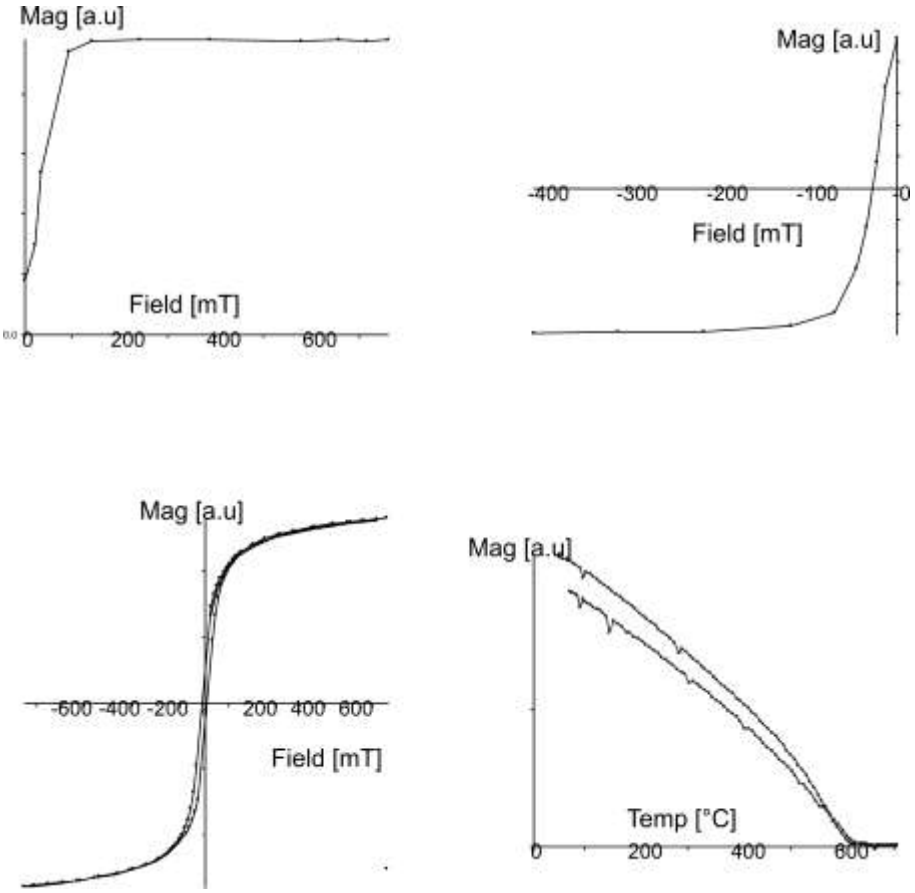

7.3 Thellier archaeointensity method and results

The archaeomagnetic dating report for this feature had already demonstrated a stable primary remanence but as the material used here was unorientated there was no opportunity to make any directional comparisons. For conventional thermal archaeointensity, 1" cylindrical specimens were prepared for by setting plugs of the clay, approximately 7cm^3 in volume in heat resistant cement (Unifrax Fixwool, a mixture of sodium silicate and calcined clay) in cylindrical moulds. Four samples were prepared in this way but one became damaged after being wedged in the oven at an early stage of the experiment and will not be discussed further. The mounting was done so that the axes of the cylinders were approximately perpendicular to the NRM. These were then heated first in a zero-field then in an applied field of 50μT along the axes of the cylinders in an MM thermal demagnetiser. Zero field and applied field steps were carried out at 150, 250, 300, 350, 390, 430, 470, 500, 530, 560 and 590°C with tailchecks and pTRM checks carried out at 250, 390 and 500°C. The samples were weighed before the experiment and the magnetic susceptibility measured on a Bartington MS1 susceptibility bridge. This was repeated after the 150, 300,390, 430 and 590°C applied field steps. Each sample was found to have lost 2% of its mass during the experiment, but how much of this was from the actual clay and how much from the fixative was not determined. In one case (Sample 3) the susceptibility was found to vary by almost 10%. The susceptibilities of the whole sample, including fixative are shown in figure 7.2. Owing to the presence of a non-magnetic fixative, the susceptibilities are shown in arbitrary units. The mass susceptibilities were of the order of 1-2 x 10^{-5} m^3/kg.

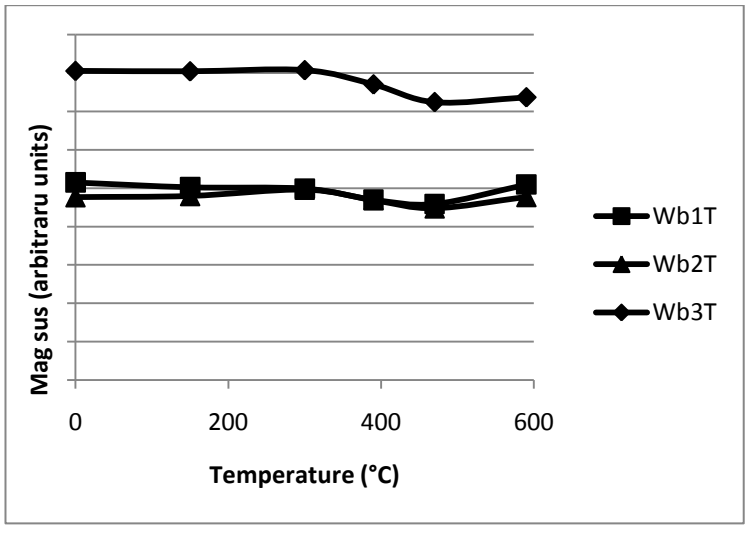

Figure 7.2 Susceptibility measured after selected temperature steps during the experiment. Each sample shows a similar profile.

NRM/TRM plots for the three samples are shown in figure 7.3 along with vector endpoint diagrams of the zero-field steps. The abscissae of the tailchecks is the difference in the z-component of the two zero field steps in each case. This can be negative, showing the z-component actually decreased or positive, which may be interpreted as being due to multi-domain behaviour. By showing only the component in the direction of the applied field, it is possible to get a true indication of how much of the discrepancy is due to multi-domain behaviour.

Figure 7.3 NRM/TRM plots and vector endpoint diagrams for the three samples. The maximum angle of deviation (M.A.D.) is given for the range selected to determine the intensity.

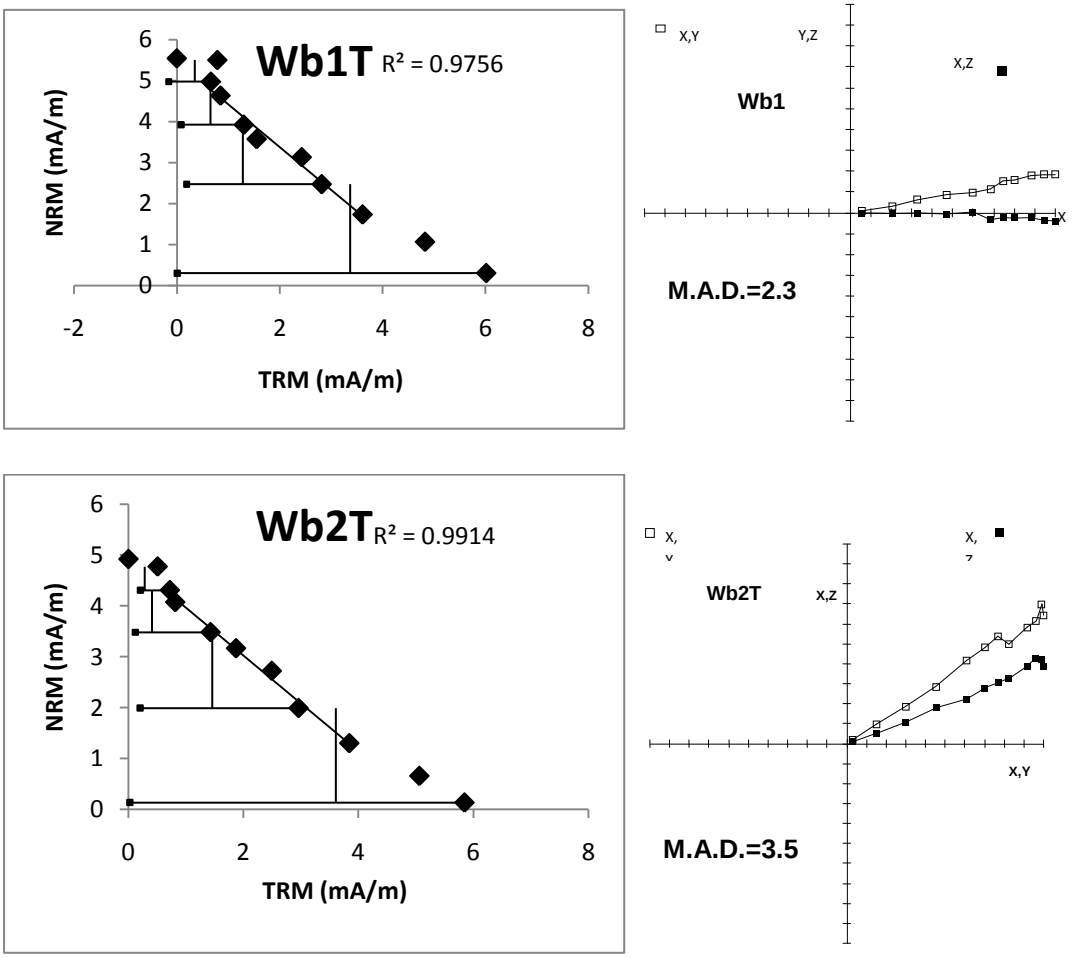

Figure 7.3 continued

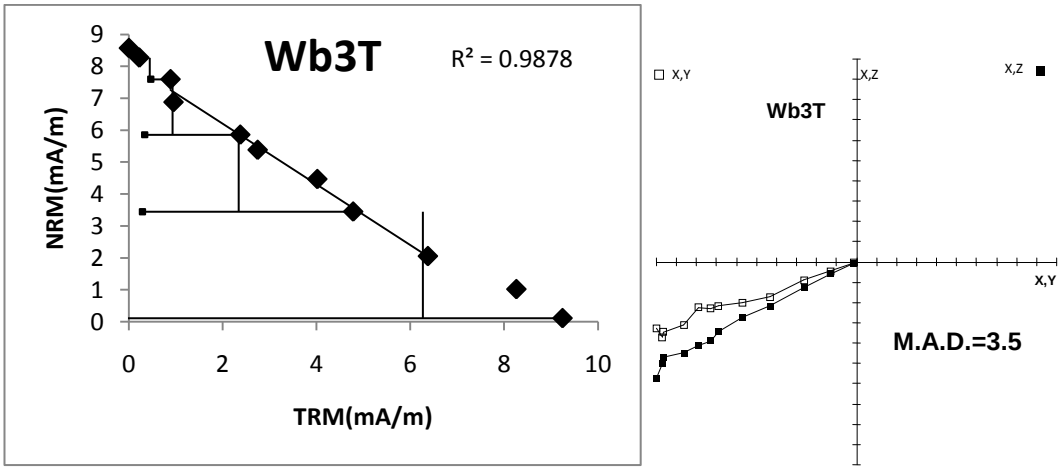

The z component of the NRM is small so any multidomain effects should be easily seen either in the tailcheck or in the demagnetisation plots. The overall quality of the results is low, with the final pTRM check failing in all three samples, and is summarised in table 7.1.

Table 7.1 Coe (1978) statistics and field estimates for the three samples in figure 7.3

Sample	Number of points	f	g	q	Ancient Field (μT)	Standard Error (μT)	Coe Error (μT)
Wb1T	7	0.58	0.82	6.8	52.7	3.7	7.7
Wb2T	7	0.61	0.81	11.9	47.2	2.0	4.0
Wb3T	7	0.65	0.82	10.7	47.8	2.4	4.5

7.4 Microwave archaeointensity method and results

Microwave archaeointensities were obtained by mounting fragments of the clay, approximately 100-150mg in weight, on to glass rods using the Fixwool adhesive. A total of five samples were mounted, but two of these fell off when they were introduced to the microwave cavity. The clay itself is quite friable and no attempt was made to consolidate the samples. The three remaining samples were subjected to an archaeointensity analysis using a field parallel to the sample NRM. Fields of 40 or 50μT were used, although there is

evidence that the ancient field may have been much higher during this period (Genevey et al. 2002, Donadini et al. 2008). The first sample did not confirm this assertion, so lower fields were used. The cavity was found to heat the samples sufficiently to demagnetise about ¾ of their moment using 20-30W of power. No attempt was made to demagnetise them completely because their irregular shape was thought to make dielectric breakdown likely to occur at higher powers. The NRM/TRM plots for the three samples are shown in figure 7.4 along with vector endpoint diagrams of the zero-field steps.

Figure 7.4 NRM/TRM plots and vector endpoint diagrams for the three samples. The maximum angle of deviation (M.A.D.) is given for the range selected to determine the intensity.

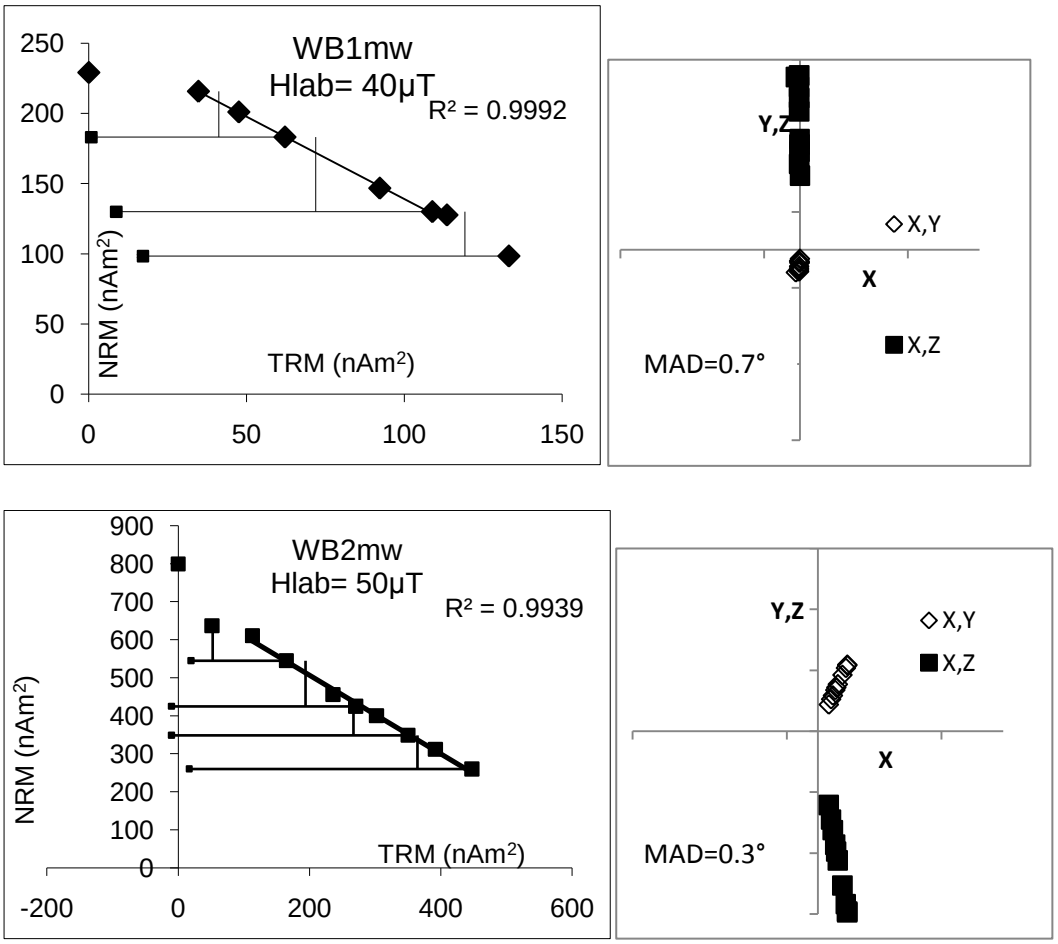

Figure 7.4 continued

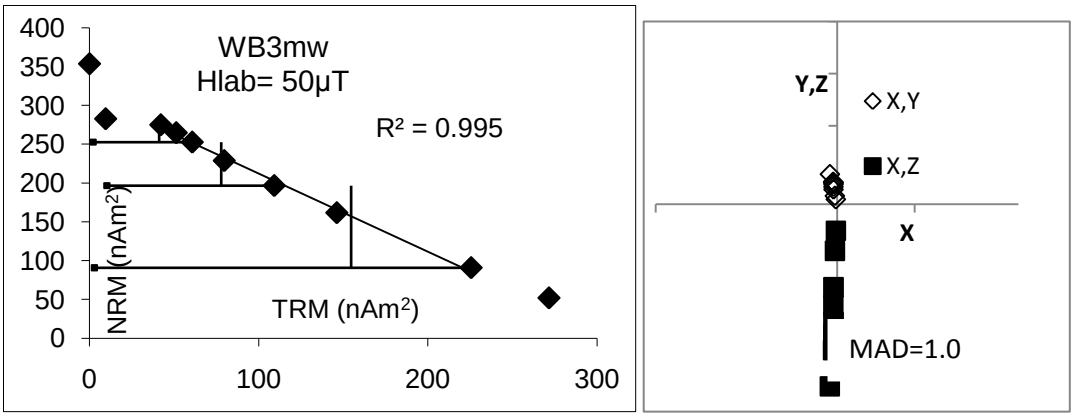

Again the overall quality of the results is poor, with pTRM checks failing badly in specimens 1 and 3. There is however a general agreement with the thermally derived archaeointensities. Also note that the MADs for the microwave samples are all less than 1°, showing the precision that can be achieved with the triple axis SQUIDs. Coe statistics and the field estimates are shown in table7.2.

Table 7.2 Coe (1978) statistics and field estimates for the three microwave samples in figure 7.4

Sample	Number of points	f	g	q	Field (µT)	Standard Error (µT)	Coe Error (µT)
WB1mw	5	0.37	0.71	16.2	46.9	0.8	2.9
WB2mw	8	0.44	0.83	11.4	51.9	1.7	4.5
WB3mw	7	0.52	0.76	12.5	50.5	1.6	4.0

We will consider the assemblage of all six results, three thermal and three microwave, despite some reservations about their quality. The six results have a mean of 49.5µT , with a standard deviation of 2.5 µT. There was no indication that the material was strongly anisotropic and the difference in the applied field directions, with one experiment having the field applied parallel to the NRM and one experiment applying the field perpendicular to the NRM, should have countered any effect of this nature. No cooling rate correction was carried out, but there is a difference in cooling rate between the thermally derived results and those from the microwave. If a large cooling rate correction was needed it would be expected that the results would differ on this account. Multi-domain material

may underestimate the field strength when cooled quickly, as opposed to single domain which will tend to yield overestimates. There does not appear to be a systematic difference between the two sets of results.

If the results here are taken at face value they have some important consequences for our understanding of the geomagnetic field. It has been suggested that the Dark Ages saw a large increase of in the strength of the field sometimes referred to as an archaeomagnetic jerk (Gallet et al. 2003). Furthermore, the coincidence of this event with climatic change has led to the proposal that there is a link between the geomagnetic field and climate (Gallet et al. 2005). To compare the intensity recovered from Whitby with the data from France that showed this large increase in field strength, the intensity was relocated to Paris, assuming a purely dipolar field with poles calculated from the archaeodirection of the Whitby floor. The resulting intensity is superimposed on figure 2a from Gallet et al. (2005) (see figure 7.5).

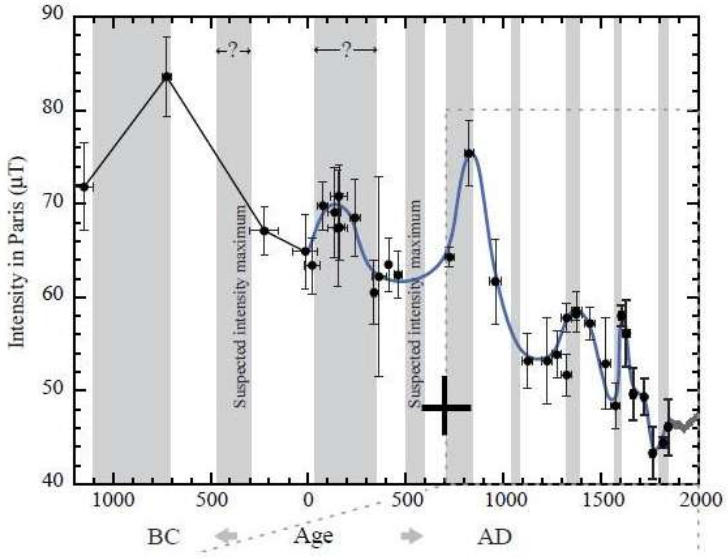

Figure 7.5 The archaeointensity derived from Whitby Abbey Cliff, relocated to Paris and superimposed on figure 2a of Gallet et al. (2005).

For consistency the errorbars on the Whitby data point have been given as the standard deviation of the data, a custom often used in archaeointensity papers, and these are shown on the other data in the graph. Whatever the uncertainty in the data, there is clearly a very large discrepancy between the intensity derived from Whitby floor and the data from France. This may be because the data presented here is of rather dubious quality, but the size of the discrepancy is still surprising. There is no simple explanation for this; the geomagnetic field models during the period are poorly constrained so it is not possible to estimate the size of the non-dipole components with any accuracy but it seems unlikely

that they could give rise to a deviation of this magnitude between Britain and France. Until the existence of a dipole high during the Dark Ages is confirmed by more archaeointensity data, preferably with a wider spatial distribution, arguments for archaeomagnetic jerks and attendant climatic effects may best be treated cautiously.

Chapter 8

Microwave archaeointensity from clay tobacco pipes

8.1 Background

In this chapter results from microwave intensity experiments on post-Medieval clay tobacco pipes are presented. These artefacts have the great advantage of often being well-dated owing to the common occurrence of makers' marks which have been well studied. In fact they are often used as a convenient way of giving *terminus post quem* for archaeological contexts. In addition there is little evidence from Britain of iron kiln furniture within the small kilns that were used to produce these pipes and the stands that held them during firing appear to have been formed from clay (Peacey 1996). As recorders of the magnitude of the geomagnetic field they are far from ideal, however: the stems are strongly anisotropic (Games and Baker 1981), and the white clay from which they are invariably made is, at best, weakly magnetic. Within this chapter the problems encountered as a result of these feature will be looked at in some detail and an account of the instrumental developments needed to overcome them will be given. Five fragments of pipe were originally chosen for analysis, one of which, made by J.Williams in Bristol in 1856, proved to have such a weak magnetisation that it could not be measured on the microwave system. This was unfortunate as it had been chosen because it came from a date shortly after direct observations of field strength were first made, so could have served as a check. The other pipes studied here came exclusively from Marlborough (51.4°N, 1.7°W), an important centre for pipe making in the 17th and 18th centuries. Two fragments (1 and 2) were made by John Greenland, working from 1700-1737, one was made by Thomas Hill, 1690-1710, and one was made by Thomas Hunt, 1667-1696.

8.2 Sample preparation and archaeointensity method

Stems of the clay pipes were cut into short cylindrical sections of approximately 3mm length that were then be attached to the sample holder with adhesive. Two samples were prepared from each fragment, apart from John Greenland, 2, which had a longer stem than the others and was able to provide three samples. Note that the development of an adhesive free system did not come about until after these experiments had taken place although as the pipes clearly have holes passing through them, there would be some difficulty in holding them in place with a vacuum pump. The remanent magnetisation of a

small section of pipe was usually of the order of 10 nAm^2 . The noise level of the SQUID magnetometers in the microwave system was generally of the 0.2 nAm^2 on the x and y axis magnetometers and a little less on the z-axis, so it would seem that an archaeointensity experiment would be possible, but on occasions quite large deviations due to noise did occur. These appear to have been caused by mechanical noise from the cooling pump that keeps the liquid helium below boiling point. On turning the cooling system off it was discovered, after rewriting a subroutine in the control software that made it possible to eliminate drift caused by the changing temperature of the SQUIDs, that a noise level of less than 10pA m^2 could be achieved. Unfortunately the procedure could only be maintained for around 15 minutes before a rapid outgassing from the Dewar rendered the equipment unusable. While work continued to find a solution to the problem of the "blow-up effect", it was decided to work with the cooling pump running and correspondingly less precise measurements. Some of the strict selection criteria (see chapter 5) were relaxed for these artefacts to allow for the high noise level.

The anisotropy is principally accounted for by applying the laboratory TRM parallel to the NRM. This can be done easily using the triple axis field programmable field coils as long as the sample is in the centre of the coil configuration. If the sample is very strongly anisotropic there will still be some error in the estimate of the ancient field strength: the NRM will be in a direction closer to the maximum principal axis of anisotropy than the ancient field and if a laboratory field is applied in this direction the resulting TRM will be nearer still to this axis. Hence applying the laboratory field parallel to the NRM will consistently lead to an underestimation of the field. This can be overcome by monitoring the direction of the magnetisation of the sample as the experiment progresses. If the direction of the TRM gained changes significantly from that of the applied field a first order correction to the direction of the laboratory field can be made. Such a procedure will ensure that the effect of anisotropy on the field estimate does not exceed one or two percent (Le Goff and Gallet 2004). Some of the more detailed analysis of anisotropy is best illustrated with reference to specific samples.

8.3 Magnetic properties of clay tobacco pipes

As they are only weakly magnetic it was not possible to ascertain detailed rock magnetic properties of the clay using the available instruments. An MM VFTB provided a reasonable hysteresis and thermomagnetic analysis but the IRM and coercivity of the clay was not clearly defined (figure8.1). As there was no discernible difference in the rock magnetic

parameters obtained from different pipes only one example is given here. It is likely that all pipe makers in the Marlborough area exploited the same source of clay.

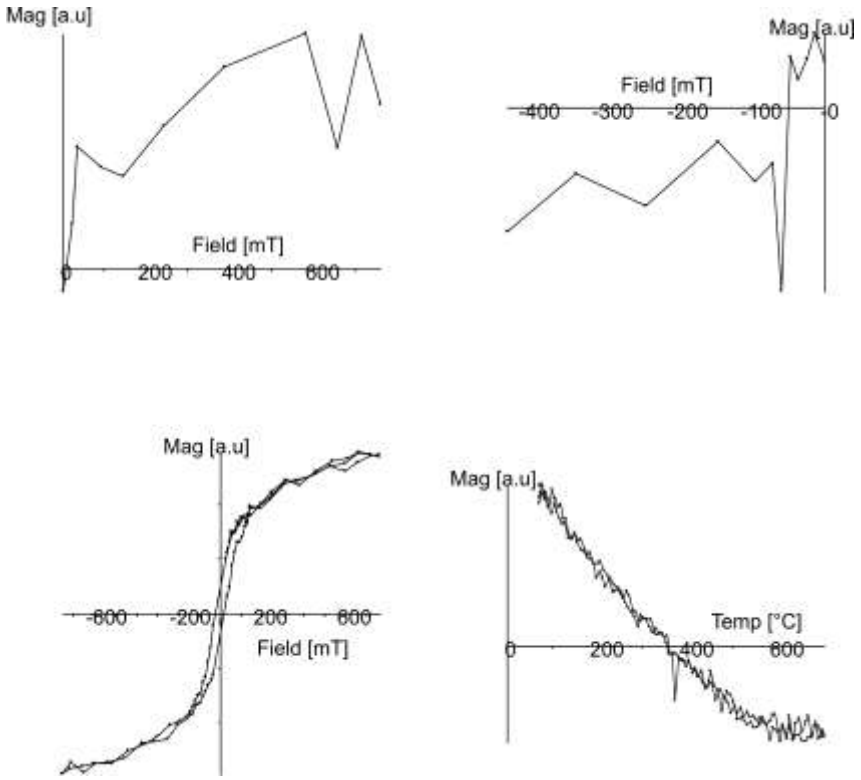

Figure 8.1 IRM acquisition and backfield coercivity (top) and hysteresis and thermomagnetic curve for a fragment of John Greenland pipe, fragment 2. Magnetisations are in arbitrary units(a.u.)

The remanence measurements are rather too noisy to draw any clear conclusions from, but the in-field measurements alone provide some useful information. The thermomagnetic curve appears to be reversible and at high temperatures it is dominated by a negative magnetisation. This may be because paramagnetism is temperature dependent, while diamagnetism is not. The hysteresis parameters are found to give ratios of saturation remanence to saturation magnetization (M_{rs}/M_s) and remanent coercive force to ordinary coercive force (H_{cr}/H_r) of 0.19 and 2.0, respectively, placing the bulk magnetic grain size in the pseudo-single domain field (Day et al. 1977, Dunlop 2002). Despite the weak magnetisation, the rock magnetic analysis makes the pipes look like a useful recorder of archaeointensity.

8.4 Microwave archaeointensities

Three of the samples, one each of Greenland (1), Hunt and Hill, failed to demagnetise at all in the microwave cavity. In each case it was not possible to couple the cavity to the waveguide adequately (see chapter 3). Even in the samples that could be made to absorb power, the power levels necessary to demagnetise them were rather high (>50W), suggesting that the pipes have a low dielectric loss. It was not clear what mode the cavity was operating in when it was matched to the waveguide.

Figure 8.2 NRM/TRM plots and vector endpoint diagrams for five samples.

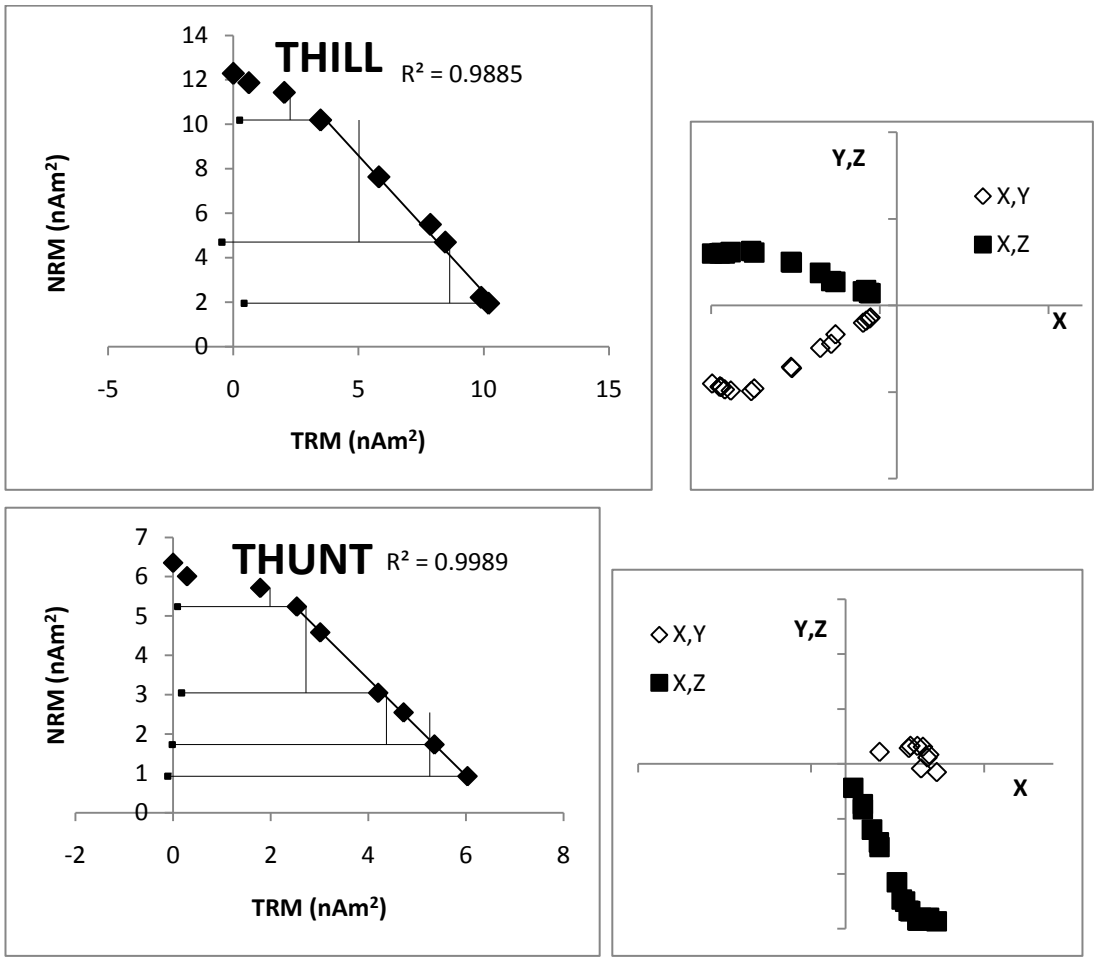

Figure 8.2 continued

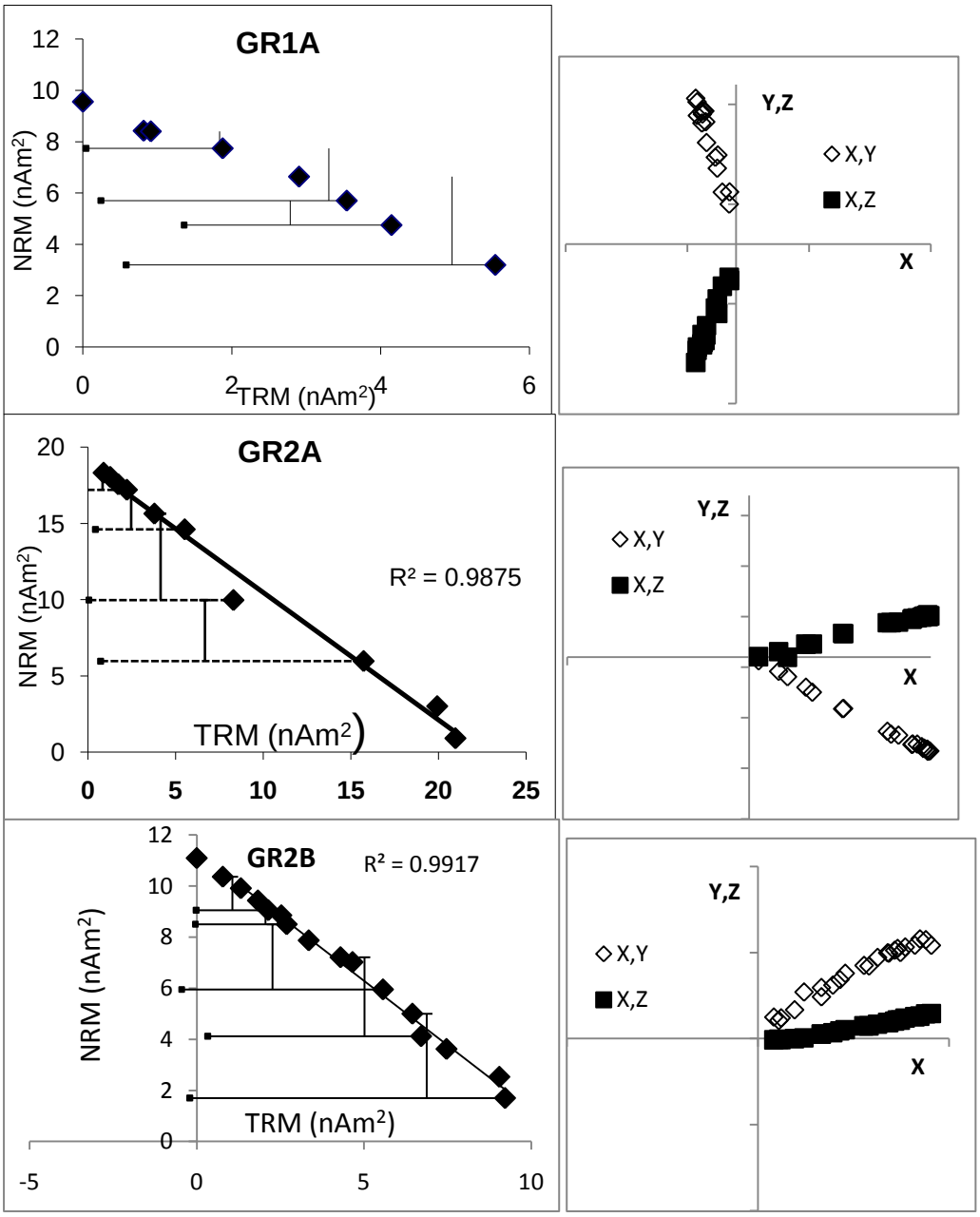

Figure 8.2 continued

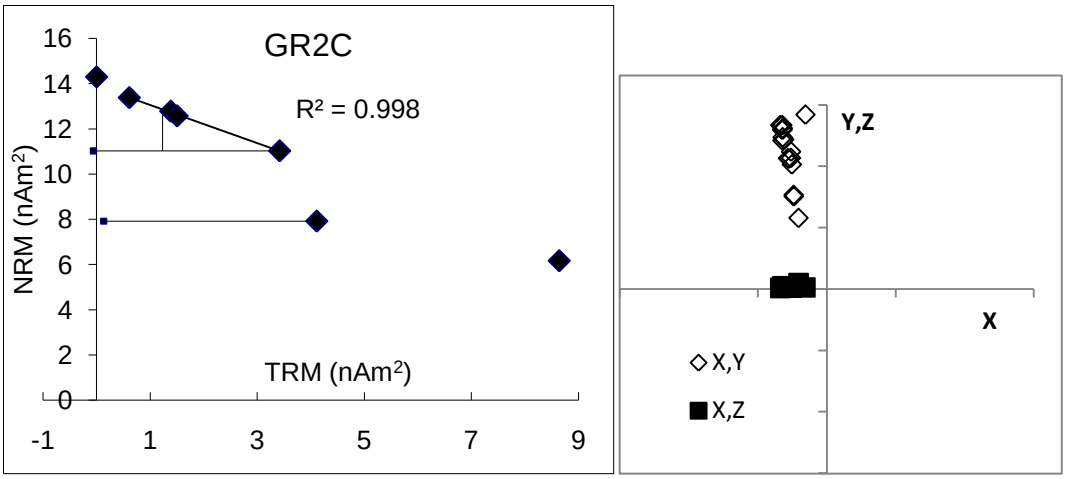

Figure 8.2 shows the NRM/TRM plots for each of the samples analysed, along with a vector endpoint diagram of the zero-field magnetisations at each power. Many of the sample show a secondary component of magnetisation unblocked at a low temperature. This may reflect the custom of throwing used pipes into the fire, but no information regarding the context of the pipes was available. Table 8.1 summarises the statistics for the four samples yielding the best NRM/TRM plots.

Table 8.1 The Coe statistics and field estimates for four samples

Sample	Number of points	g	f	q	Field(μT)	Standard error	Coe error
THILL	6	0.67	0.74	9.2	61.8	3.3	6.7
THUNT	6	0.68	0.77	31.3	61.3	1.0	2.0
GR2A	10	0.92	0.82	19.1	42.1	1.7	2.2
GR2B	14	0.74	0.91	25.5	50.7	1.3	2.0

Of these, the result from the Thomas Hill pipe is deemed unreliable because of the errant pTRM check, although the result is consistent with that from the Thomas Hunt pipe stem which gives fewer reasons to doubt its validity. There is a very large discrepancy between the John Greenland pipe fragments 2A and 2B. One point on the NRM/TRM plot for 2A lies some way from the trendline, a fact that might be explained by noise in the magnetometers if it was not for the fact that a later pTRM check appears to confirm it. It may be that higher power fraction of the NRM/TRM plot is affected by alteration, and that the field has been underestimated for this sample.

For the purposes of constructing a calibration curve, the results from the clay pipes are somewhat disheartening. Only two from the ten samples initially prepared yielded estimates with which we can assign any confidence, and there is no possibility of giving a reasonable estimate of the experimental uncertainty. A minimum uncertainty in cases such as these of 5μT has been suggested (Donadini et al. 2009), which more or less agrees with analysis presented in chapter 6. With the caveat that the results have not been corrected for the cooling rate, the clay pipes give the archaeointensity estimates for Marlborough, 51.4°N, 1.7°W of 1700-1737, 50.7±5 μT and 1667-1696 61.3±5 μT. Despite the attractive features of clay tobacco pipes for studying the geomagnetic field, such as the exact date ranges and their general availability, and despite having equipment capable of overcoming the problems of anisotropy, they were not found to be wholly suitable for microwave archaeointensity. Future workers may, however, wish to re-examine these issues in the light of the analysis presented in chapters 2, 3 and 4 which had not been formulated at the time of these experiments.

Chapter 9

Microwave archaeointensities from bricks: Hindhead kiln

9.1 Background

During works to improve the A3 near Hindhead, Surrey (51.12°N 0.74°W) a brick lined pottery kiln (see figure 9.1) was uncovered and sampled for archaeomagnetic dating by MOLAS. Four bricks from the kiln were obtained for archaeointensity analysis.

Figure 9.1 A section through the kiln during excavation, with 2m scaling rod

Geoquest Associates had obtained a mean archaeodirection for the kiln (declination 346.5°, inclination 73.7°) which they interpreted as being consistent with a date of 1715 to 1735 AD and although there was little material to corroborate this date some late 17th C pottery was recovered from the site. Three of the four bricks were chosen for archaeointensity analysis, the fourth being prone to breaking when drilled. As the material was judged to have potential for further study, it was decided not to risk damaging it any more than was necessary. The three bricks studied were given the codes HH1, HH2 and HH3. An archaeological plan was made available to the author, showing the position of each of the bricks, but a reduction of it was not clear enough to include here.

9.2 Magnetic properties

The susceptibilty of each of the three bricks selected was measured by drilling a 1" diameter core from each and measuring on a Bartington MS1 susceptibilty bridge at 470Hz. The mass susceptibilities were 52, 7.3 and 38 x10^{-8} m^3/kg for bricks 1,2 and 3 respectively. Chips of each brick were analysed using the MM VFTB and the IRM acquisition, backfield coercivity, hysteresis and thermomagnetic behaviour for each are shown in figure 9.2(a-c).

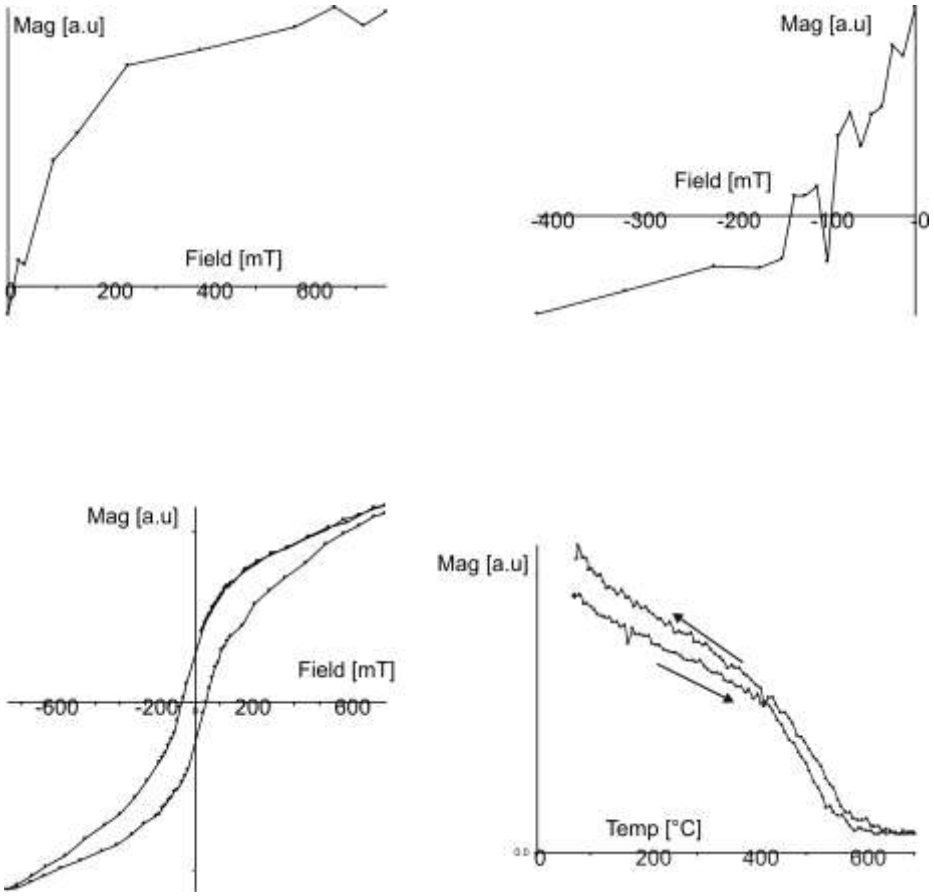

Figure 9.2a. IRM acquisition and backfield coercivity(top) and hysteresis and thermomagnetic behaviour for a chip taken from brick 1. Magnetisations in arbitrary units (a.u.)

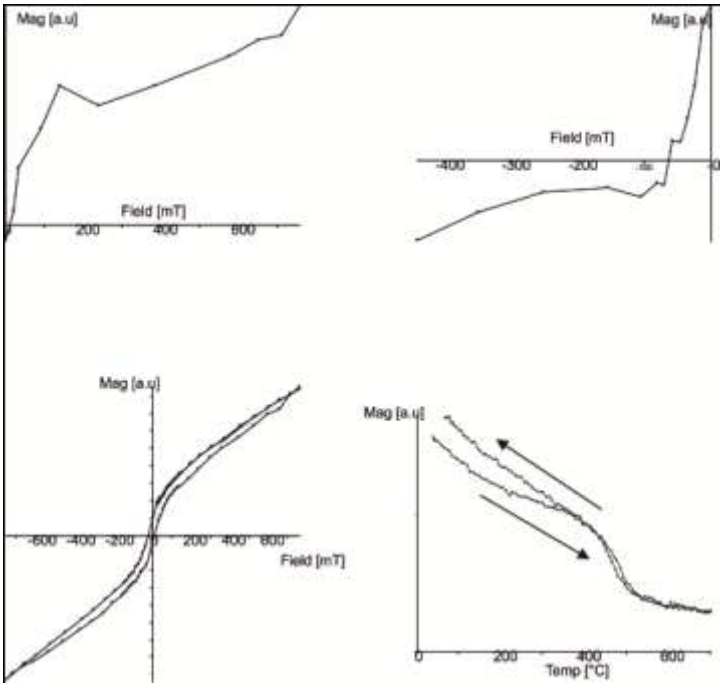

Figure 9.2b. IRM acquisition and backfield coercivity(top) and hysteresis and thermomagnetic behaviour for a chip taken from brick 2.

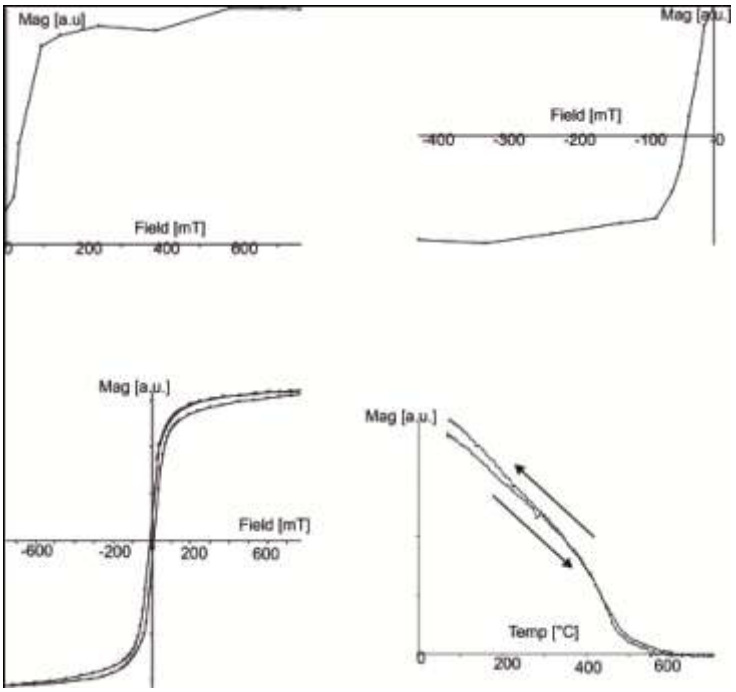

Figure 9.2c. IRM acquisition and backfield coercivity(top) and hysteresis and thermomagnetic behaviour for a chip taken from brick 3.

In all three cases the thermomagnetic behaviour is close to reversible, with a very slight increase in saturation magnetisation on cooling. The three hysteresis loops are quite distinctive. Bricks 1 and 2 are similar in that they do not saturate and have wasp waisted hysteresis typical of an assemblage containing haematite but brick 2 has a lower coercivity, and a strong paramagnetic contribution. Visually these two bricks were identical, with a deep brown red colour. Brick 3, was darker and more purple than the other two bricks. With a Curie temperature of around 580°C, a narrow hysteresis loop and an IRM that

saturates by 100mT, the magnetic assemblage in brick 3 most likely consists of pseudo-single or multi-domain magnetite.

9.3 Archaeointensity results

Four 5mm diameter cores were drilled from each brick and mounted to a sample rod using a non magnetic heat resistant adhesive (Fixwool). Four of the samples failed to yield any result after being lost or damaged during the experiment. In particular the adhesive used to mount the later samples (assigned C and D) seemed prone to fail. There were also some difficulties in matching the cavity to the transmission for some samples. The results of the microwave archaeointensity experiments that ran to completion are shown in figure 9.3.

Figure 9.3 NRM/TRM plots and vector endpoint diagrams for samples of brick from the Hindhead kiln.

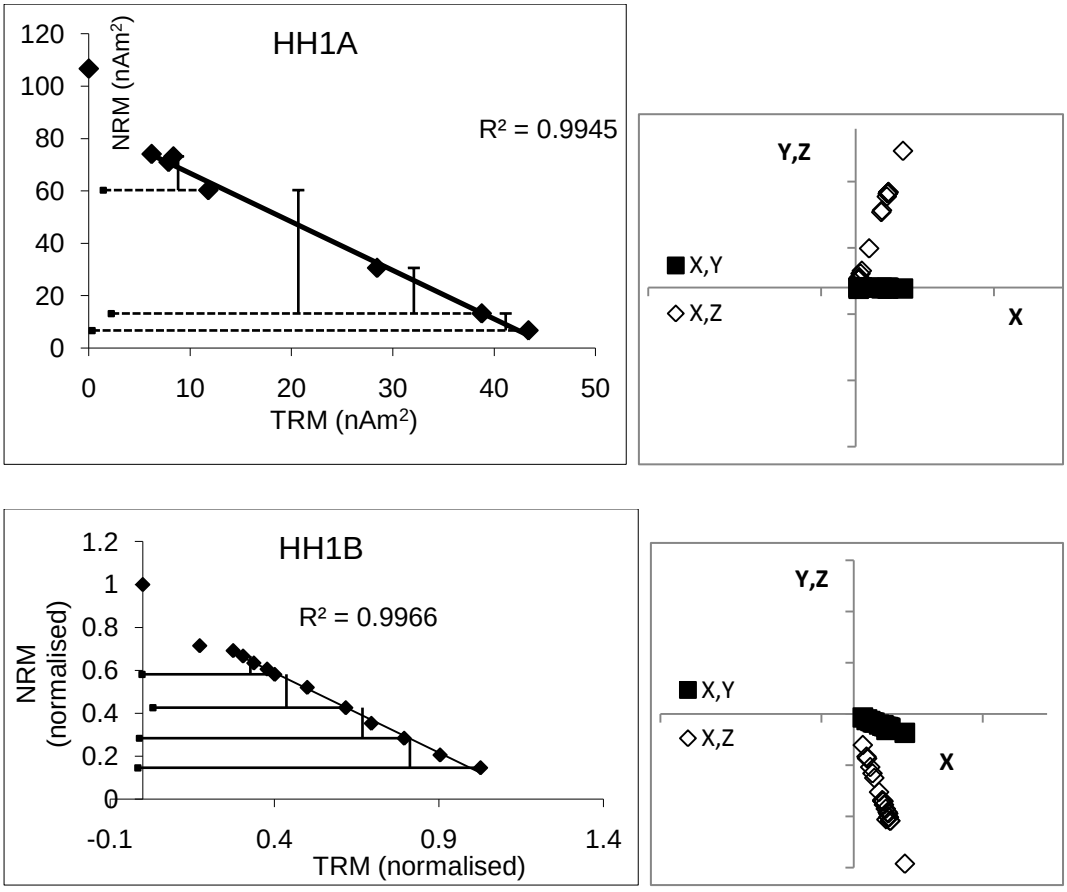

Figure9.3 continued

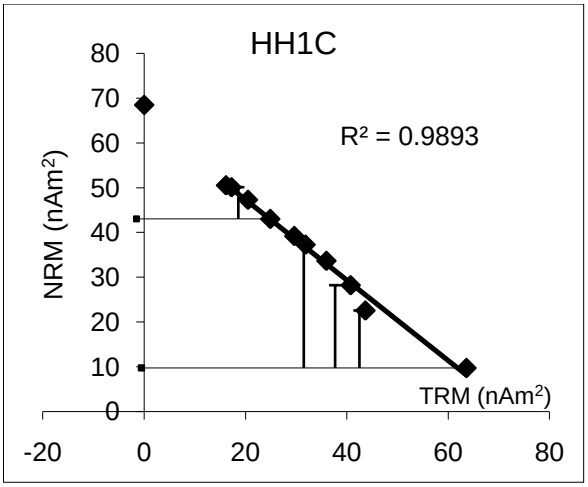

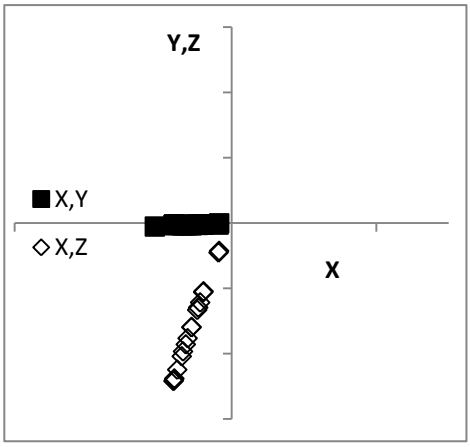

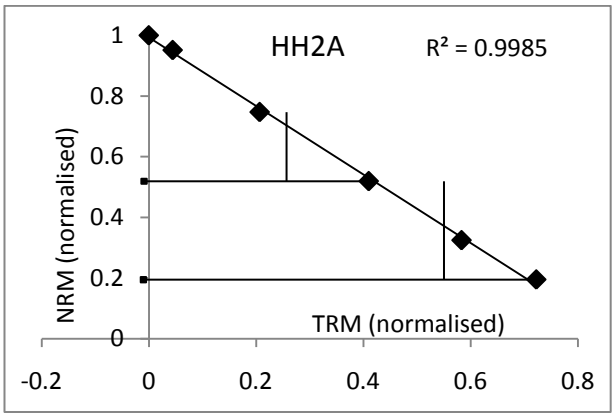

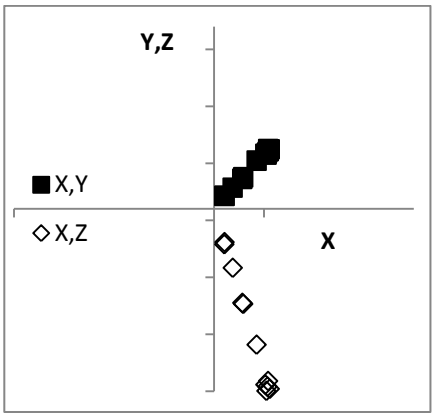

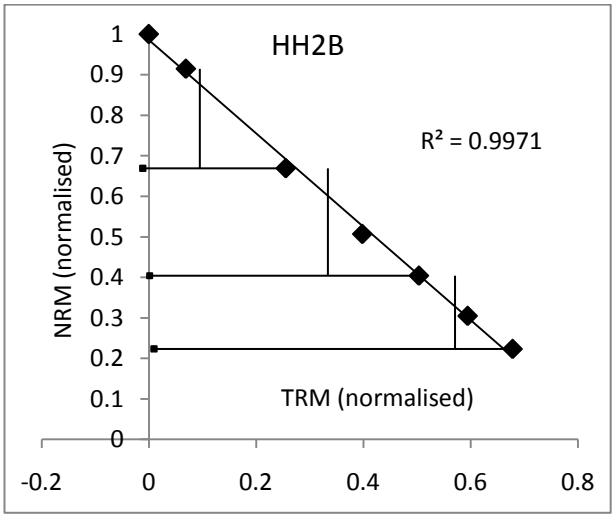

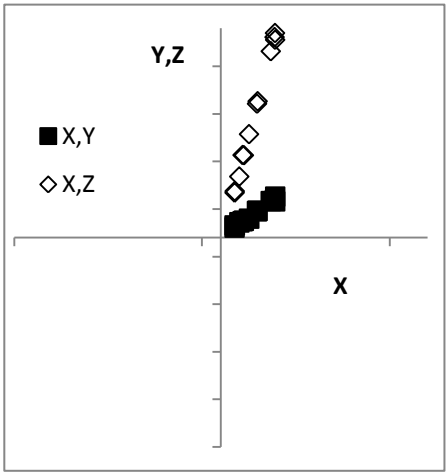

Figure 9.3 continued

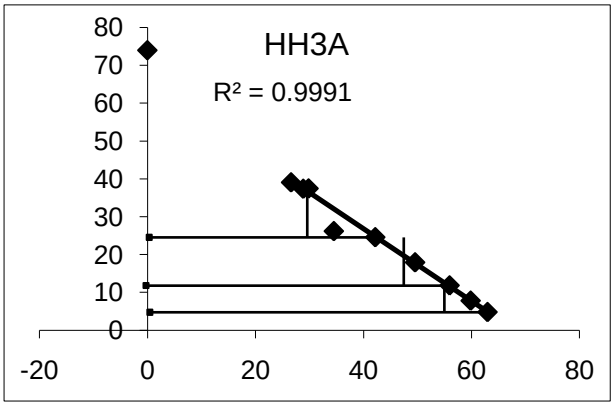

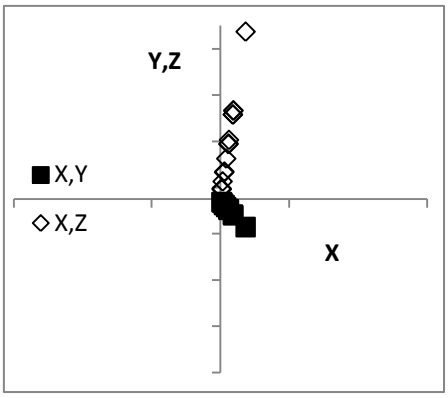

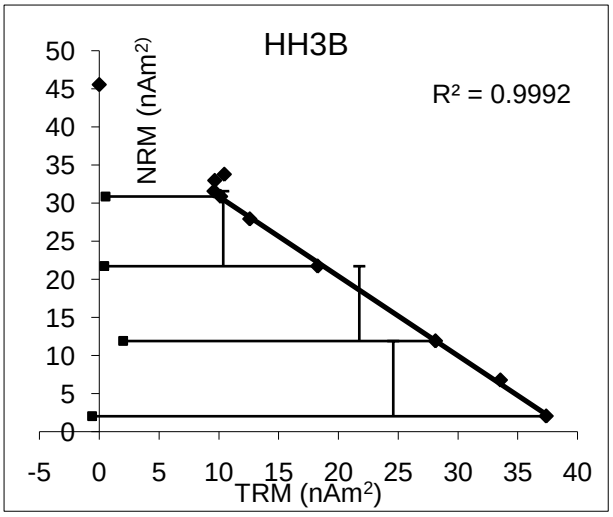

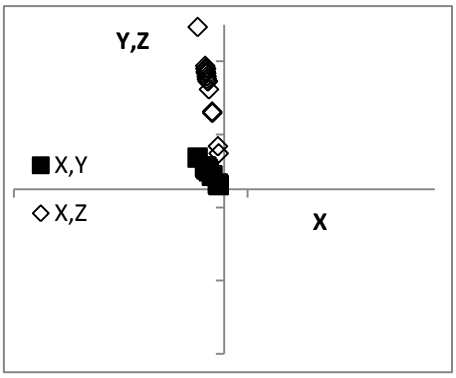

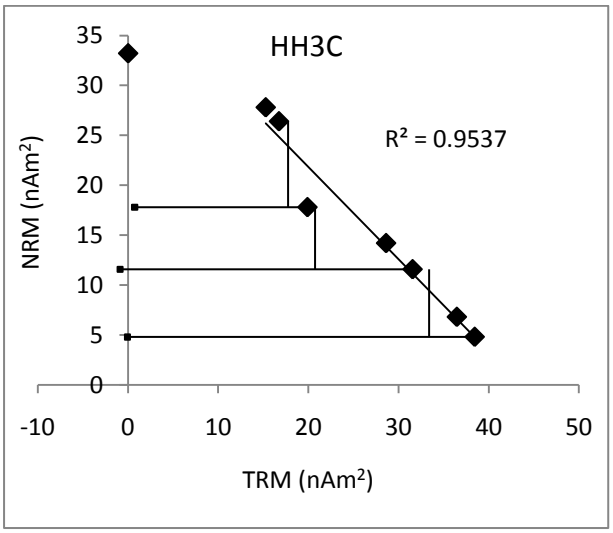

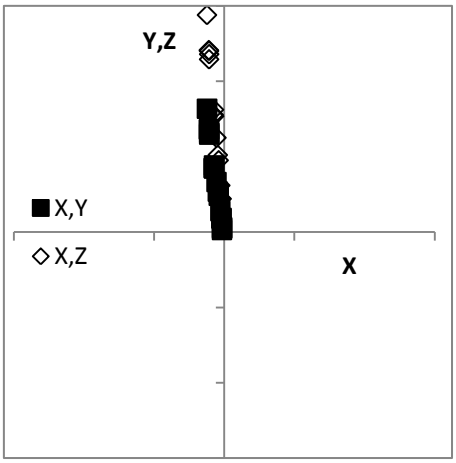

Figure 9.3 continued

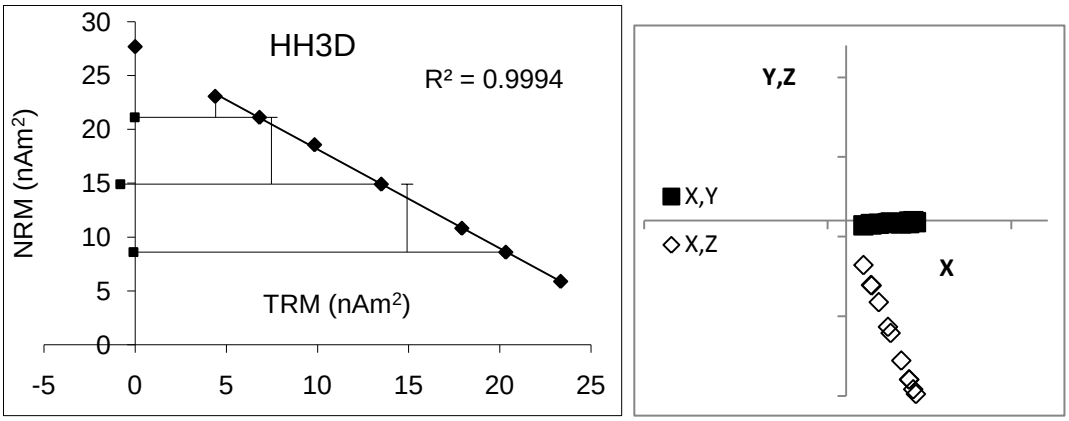

All of the demagnetisation plots show a clear single component with low MADs. Samples 1A, 2A,2B fail to reproduce pTRMs so are rejetcted along with 3C, which has one point falling some way from the trendline and a correspondingly low value of R^2. This point is reproduced in pTRM check, so it seems unlikely to be a simple case of measurement error. Samples 1B,1C, 3A,3B and 3D are now considered in more detail. The statistics for each are summarised in table 9.1. The five samples give a mean value of 64.2μT and have a standard deviation of 5.4μT. The 95% confidence interval for the mean is rather large, exteding from 57.5 to 70.8 μT.

Table 9.1 Coe statistics and estimated field values for selected samples

Sample	Number of points	f	g	q	Field (μT)	Srandard error (μT)	Coe error (μT)
HH1B	11	0.55	0.88	24.8	56.1	1.1	2.3
HH1C	10	0.60	0.83	13.5	67.7	2.5	5.0
HH3A	9	0.53	0.80	7.5	70.1	3.9	9.4
HH3B	7	0.87	0.78	52.9	62.7	0.8	1.2
HH3D	7	0.62	0.82	48.4	64.3	0.7	1.3

The results seem fairly high when compared to other results from the same period (see Genevey et al.2009 and Casas et al. 2005), if the archaeomagnetic dating of the feature is taken to be accurate. One possibility is that the value is an overestimate owing to the rapid cooling rate in the microwave system. When material cools down slowly in a magnetic field, the magnetic grains are able to equilibrate with the field at a lower temperature, increasing

the value of the partition function. This is thought to cause an increase in total magnetisation of around 6% for each order of magnitude difference in cooling rate, for an assemblage of non-interacting single domain grains (Dodson and McClelland-Brown 1980). To investigate this, two of the samples with reasonably high quality factors, 1B and 3C were heated to 650°C in a 62.5 µT field and cooled down slowly over a period of about 30 hours. Both samples were then re-measured on the Tristan microwave system. 1B had a moment that was far higher than the original NRM (101 nAm^2 compared to an original NRM of 61nAm^2) and 3D showed a slight increase (33 nAm^2 compared to an original NRM of 28 nAm^2). The samples were then subjected to the same archaeointensity protocol as had previously been used to derive the historical field estimate. An applied field of 60µT was used for sample 1B but due to an issue with the applied field coils a smaller field of 50 µT was used for sample 1D. The results are shown in figure 9.4.

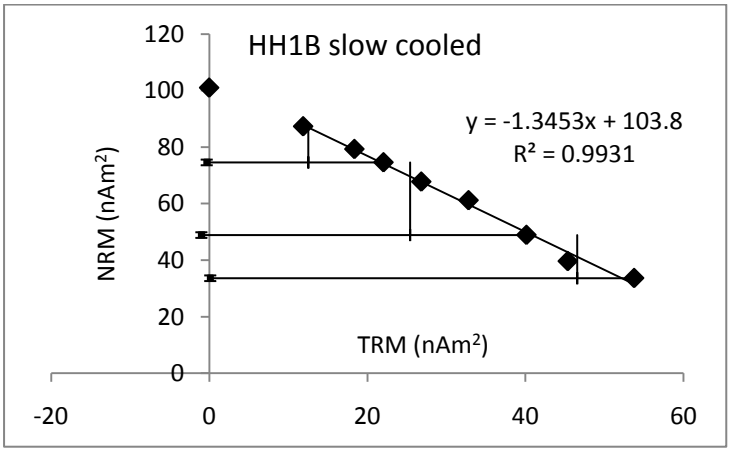

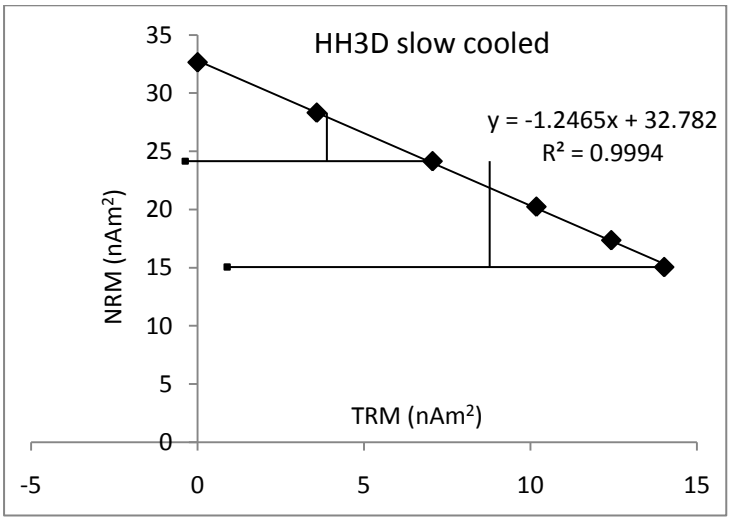

Figure 9.4 NRM/TRM plots for sample HH1B and HH3D after being slow cooled in a 62.5µT field. The applied field in the cavity was 60 c for HH1B and 50 for HH3D. Estimated fields are 80 µT for HH1B and 62 µT for HH3D.

Neither result would be acceptable because of the failure of the pTRM checks however 3D does at least give a correct estimate of the applied field in the oven, which would suggest that the effect of the cooling rate is minimal. In the case of 1B, however, taking the best

fitting straight line results in an overestimate of 28%. This result is difficult to explain: the pTRM checks are increasing, but the result is too high (i.e. the microwave TRMs are too low). If the sample had gained a crystalline remanent magnetisation during the slow cooling stage that was being replaced with a TRM, again the TRM would be expected to be larger than the CRM (Dunlop and Özdemir 1997). It seems likely that if an overestimate of this magnitude could be due to cooling rates, the effect would be seen if the sample was given a TRM in a conventional thermal demagnetiser, with a cooling time of around 20 minutes as this is still around 50 times slower than the cooling of the sample in the microwave cavity. Sample 1B was placed in an MM thermal demagnetiser with a field of 60µT applied and heated up to 650°C held for 10 minutes and cooled to room temperature over 20 minutes. After mounting in the Tristan microwave system, the sample moment was measured as 85 nAm^2. Again the same archaeointensity protocol was applied with an applied field of 60µT, parallel to the sample moment. The result is shown in figure 9.5.

Figure 9.5 NRM/TRM plot for sample HH1B after being cooled in a 60µT field over 20 minutes. The field applied in the microwave cavity was 60µT.

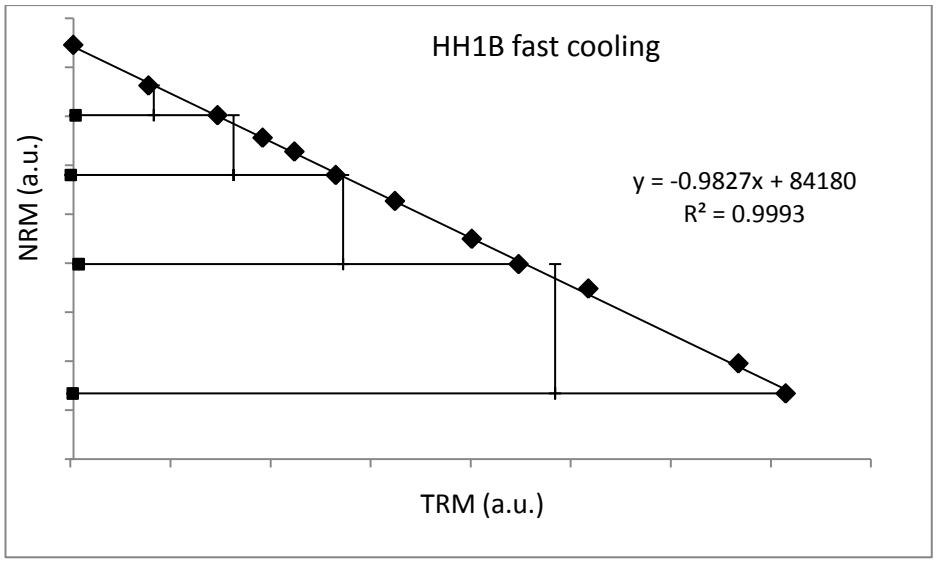

The estimated archaeointensity is 59.0 +/- 0.7 µT. There is no evidence for a cooling rate effect between the microwave TRM and the oven TRM. It seems likely that whatever cooling rate effects there may be, they are fairly small and the large overestimate when the sample was cooled very slowly was due to other factors. In particular failing pTRM checks, showing an increasing trend, must be considered as flags for unreliable results, although the exact causes for this are still unclear.

To conclude, the estimate of 64.2 +/- 2.4μT remains the best estimate for the field strength for this kiln. This may be an overestimate due to the cooling rate effect, but it was not possible to demonstrate this is so and, as shown in chapter 6, cooling rate corrections do not necessarily improve the fidelity of data. As the site was dated archaeomagnetically, it may be best not to assign a date to it for the purposes of geomagnetic field modelling, although the late 17th or early 18th C seem feasible on archaeological grounds. Instead the directional information can be combined with the intensity to give a full vector description of the field, which is useful even without an explicit date.

Chapter 10

Brookhill pottery

10.1 Background

The Museum of Liverpool provided five potsherds from the pottery at Brookhill, Buckley (53.2°N, 3.1°W) for archaeointensity analysis. Brookhill pottery was in production from 1640-1720, producing a wide range of coarse earthenware (Longworth 2006).The sherds analysed here are all black glazed ware and are believed to date from the main period of production 1640-1670. The five sherds, here coded BRH1-5 come from an assemblage with Museum of Liverpool reference code BRC U1/2. As the pottery is believed to have been produced over a brief time interval, the assemblage should, in addition to constraining the geomagnetic field in the 17th C, provide some insight into the source of variance within an archaeointensity analysis. By examining multiple samples from each sherd, it was hoped that it would be apparent whether the main source of variance was within or between the individual samples. Once again, the study was thwarted by an inability to demagnetise certain samples with the microwave equipment. In particular samples taken from sherd BRH1 tended to become damaged before demagnetising for the reasons outlined in chapter 3.

10.2 Magnetic properties

A chip weighing 100-150mg was taken from each potsherd to determine its magnetic characteristics using the MM VFTB. The shape of the potsherds made it inconvenient to measure the low field susceptibility in the usual manner, using a susceptibility bridge and the data shown here has not been calibrated so is given in arbitrary units. IRM acquisition, backfield coercivty, hysteresis and the saturation magnetisation during heating to 700°C were measured. Samples BRH1 and 3 were only weakly magnetic and the resulting datasets were very noisy, so only the data for BRH3 is shown. BRH1 gave very similar results. The data are shown in figure 10.1 In all cases the saturation magnetisation is stronger on cooling than on heating so there is some alteration at temperature, although it was not determined at what temperature this occurred.

Figure 10.1 IRM acquisition, backfield coercivity, hysteresis and thermomagnetic curves for BRH2 and BRH3. BRH1 was very weakly magnetic and gave data that was too noisy for interpretation.

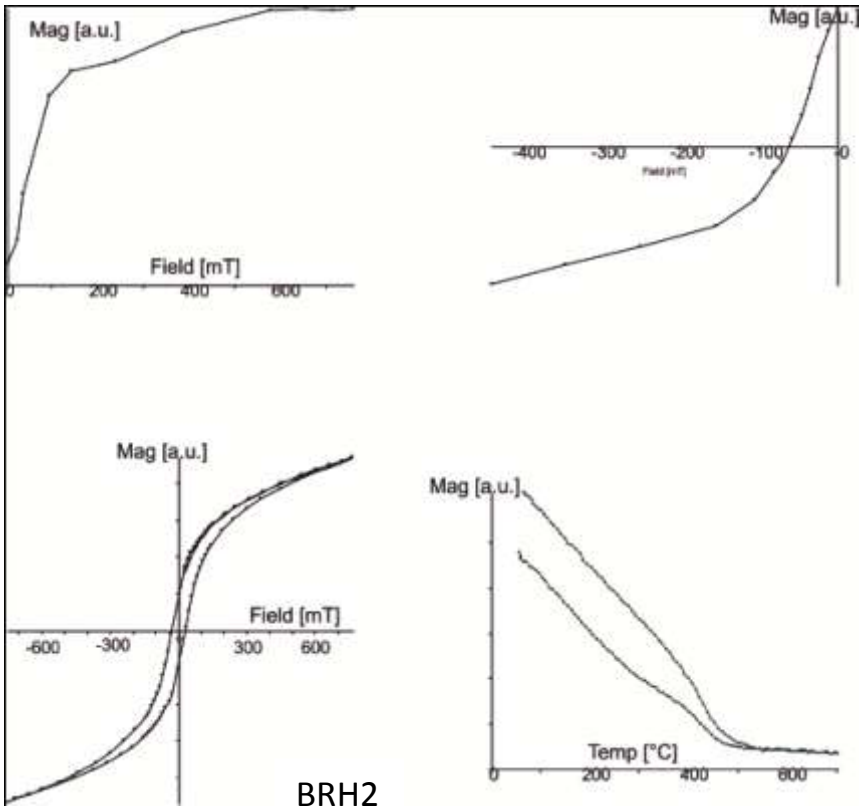

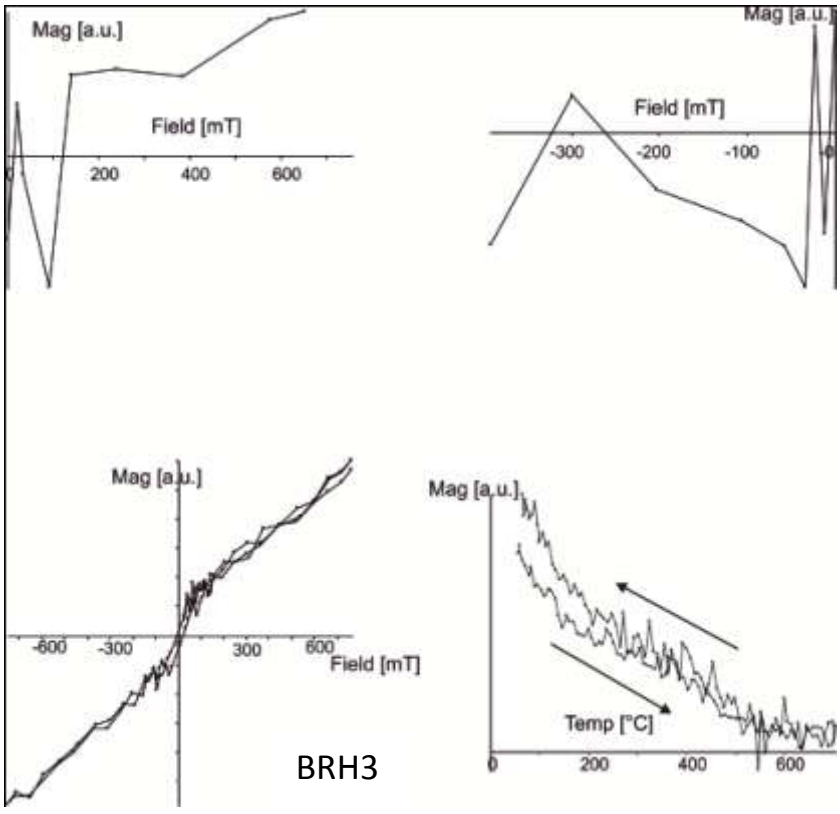

Figure 10.1 continued. IRM acquisition, backfield coercivity, hysteresis and thermomagnetic curves for BRH4 and BRH5.

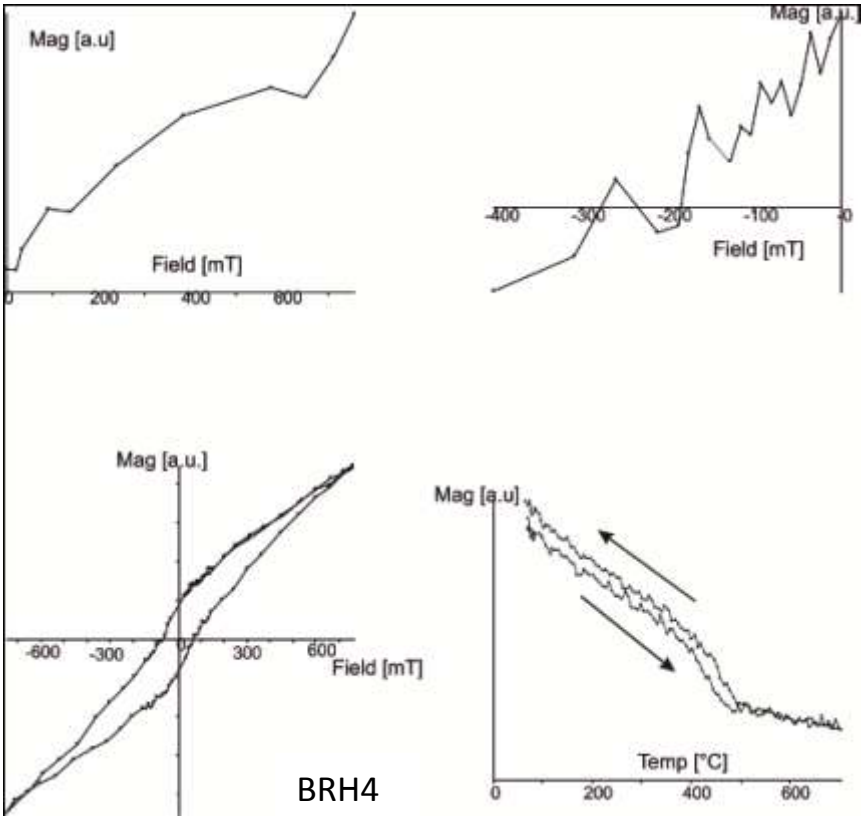

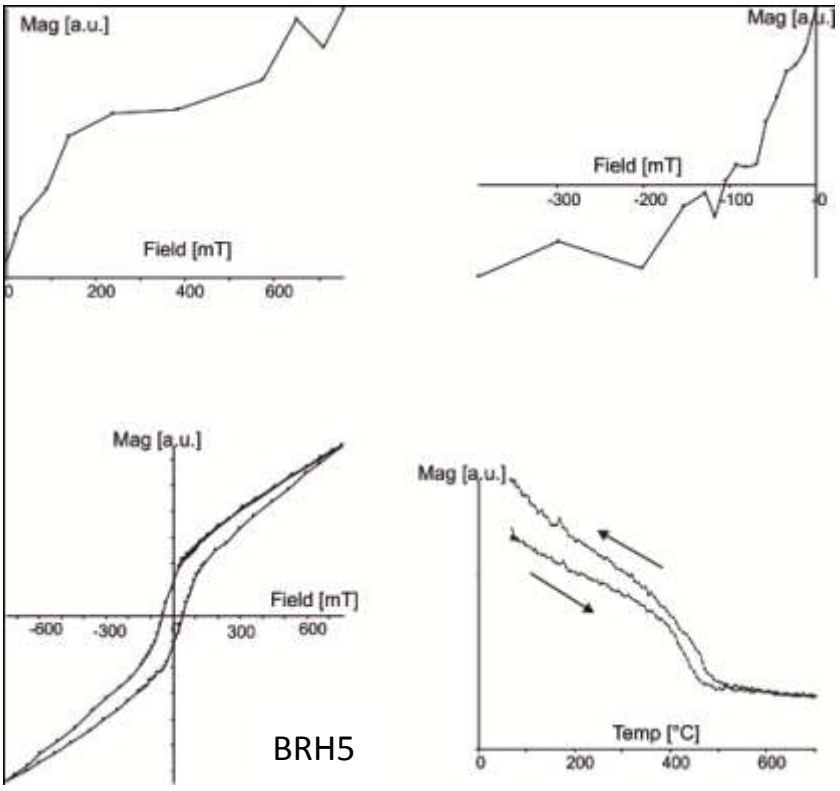

10.3 Microwave archaeointensity

A total of sixteen 5mm cores were drilled and mounted on quartz rods using a heat resistant adhesive, four each from BRH2,4 and 5, which appeared to be the most promising in terms of its magnetic properties, and two from each of 1 and3. Five of these failed to demagnetise and the NRM/TRM plots and the vector endpoint diagrams for the remaining eleven are shown in figure 10.2.

Figure 10.2 NRM/TRM plots and vector endpoint diagrams for the eleven samples that were able to be demagnetised.

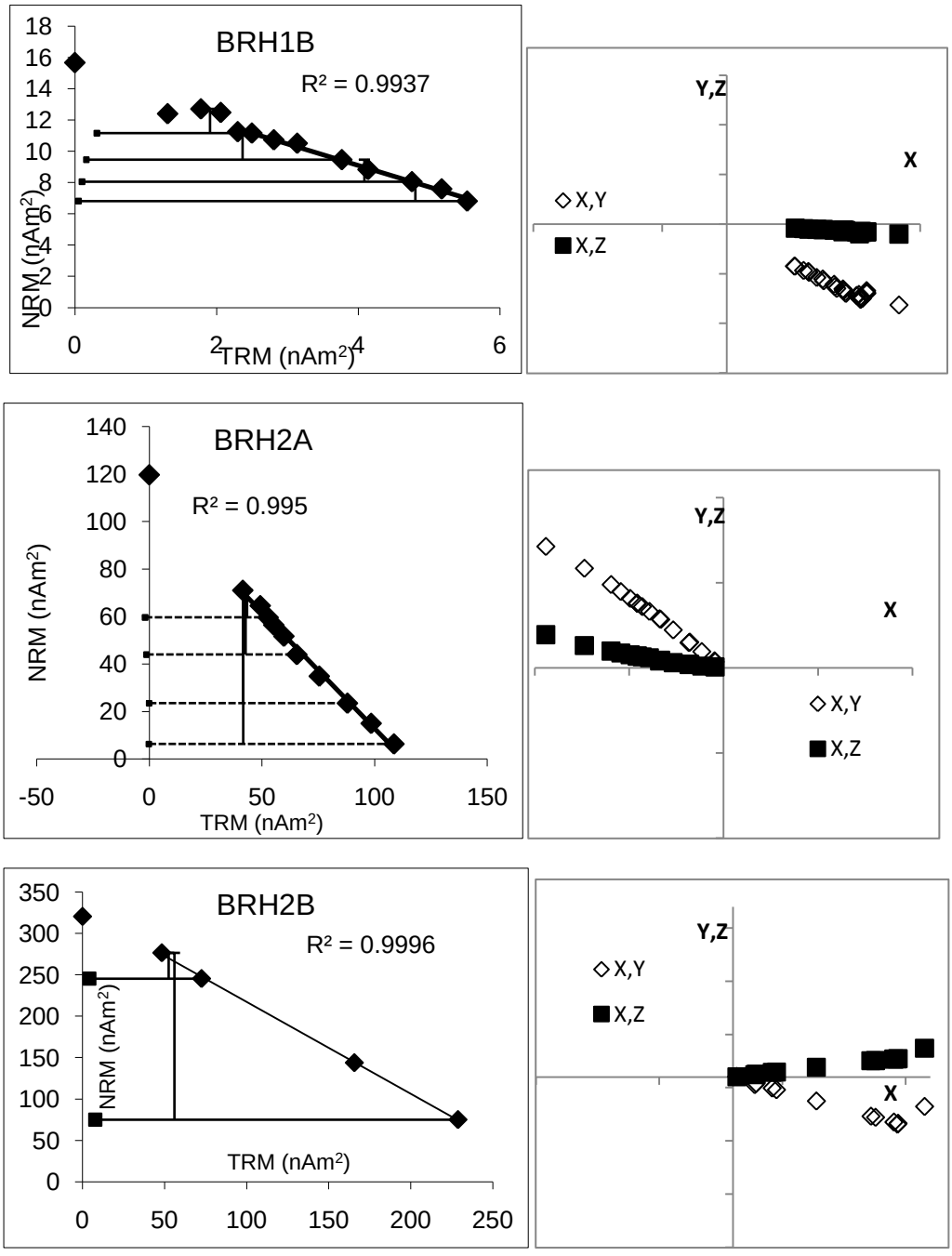

Figure10.2 continued

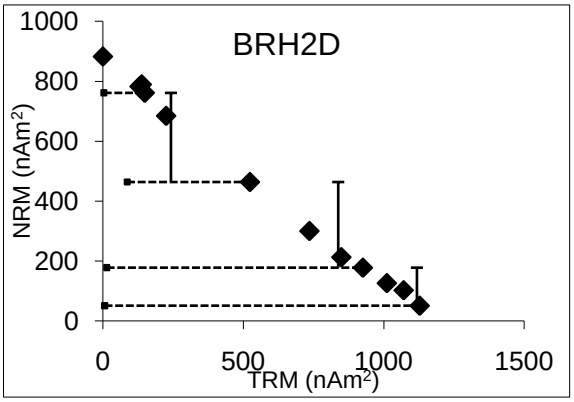

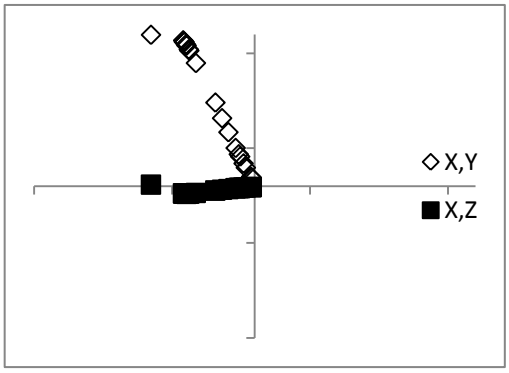

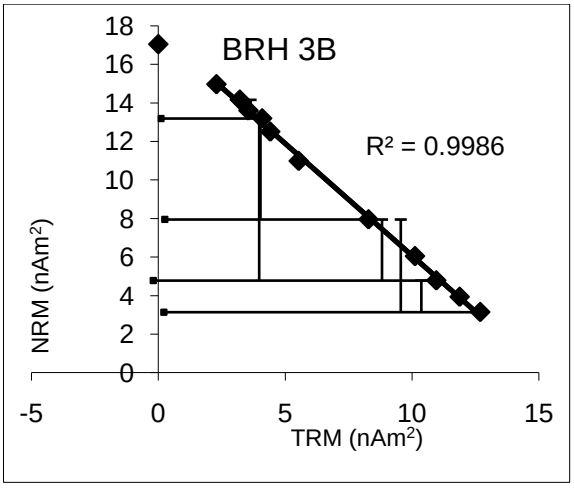

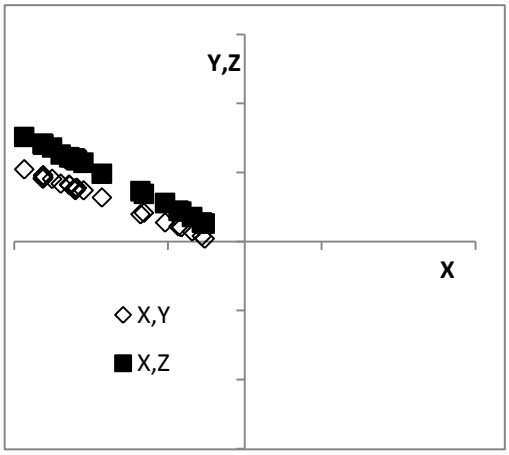

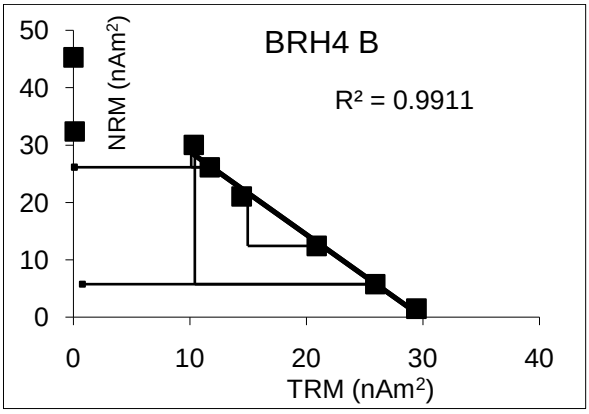

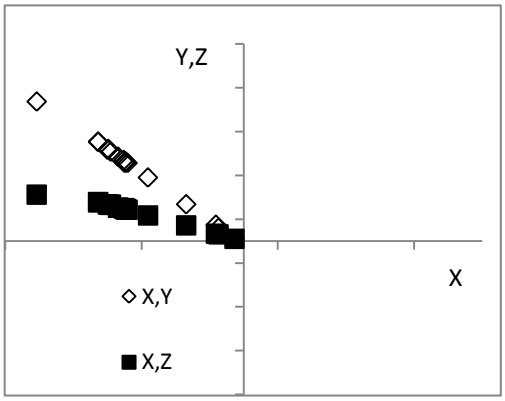

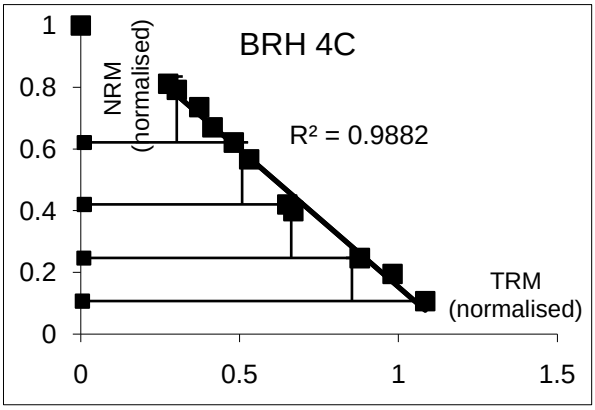

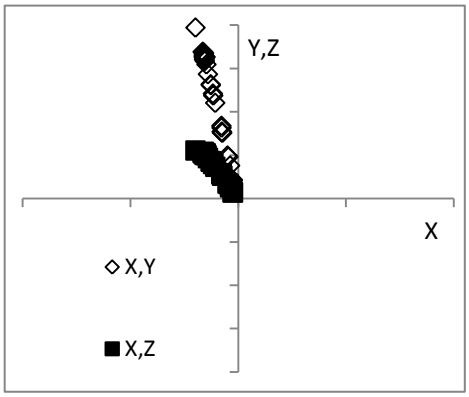

Figure 10.2 continued

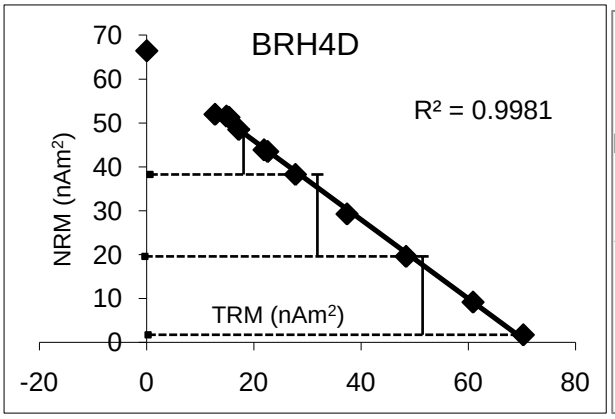

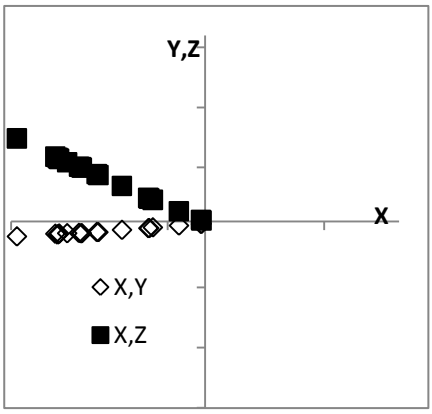

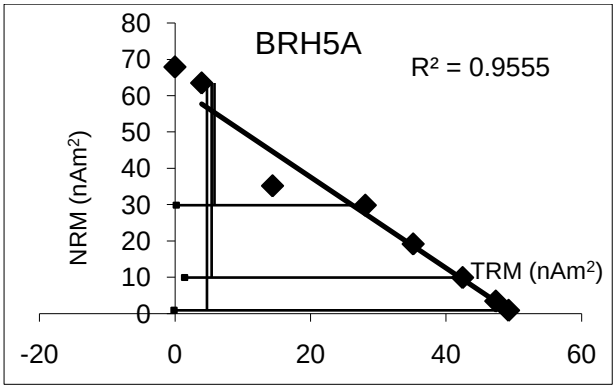

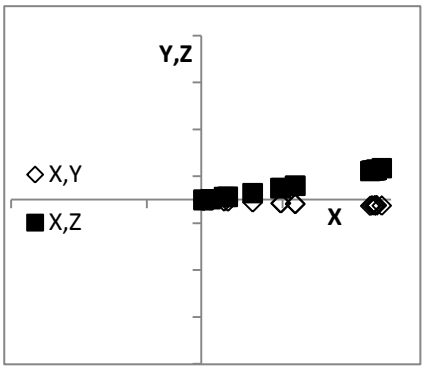

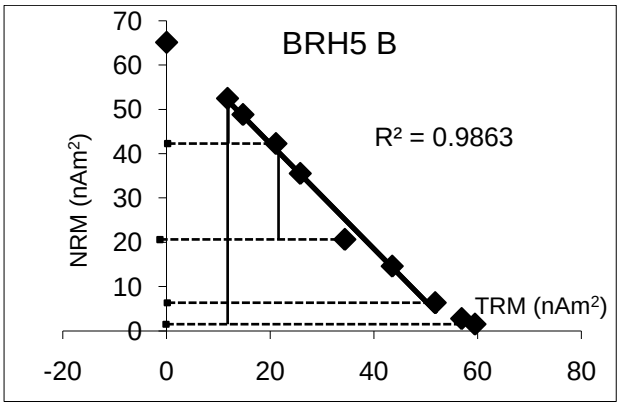

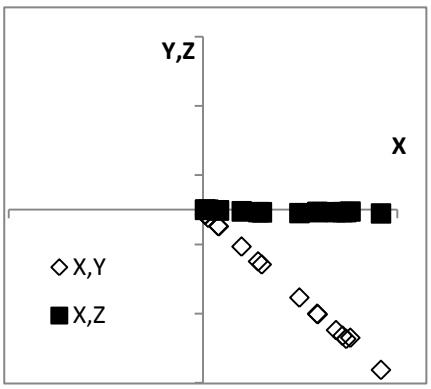

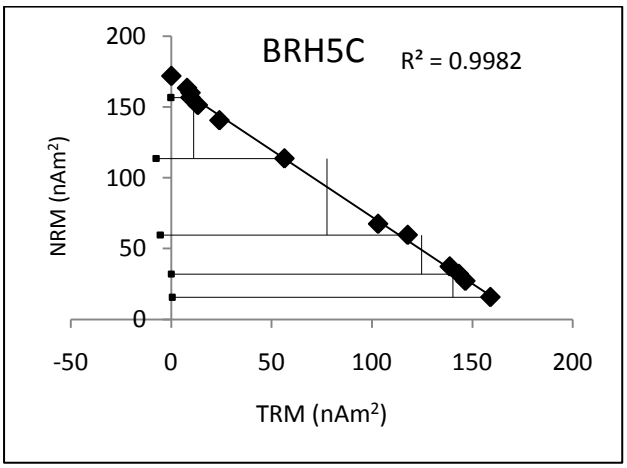

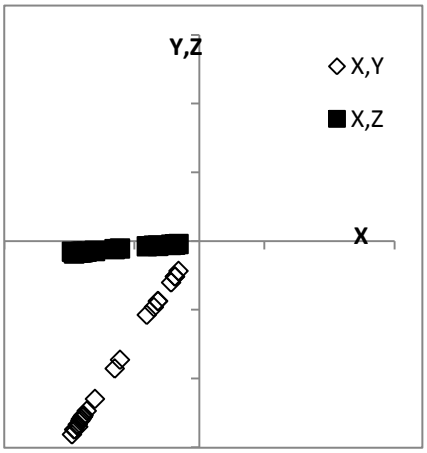

Before discussing the merits of each sample, it is worth looking at the statistics for the whole assemblage. Table 10.1 gives the Coe statistics and the field estimates for all the samples in figure 10.2, other than sample BRH2D, which was judged to have failed the pTRM checks.

Table 10.1 Coe statistics and the field estimates for the ten samples selected.

Sample	Number of points	f	g	q	Estimated field (μT)	Standard error μT	Coe error(μT)
1B	9	0.35	0.84	9.8	55.3	1.7	5.7
2A	10	0.54	0.88	18.9	49.0	1.2	2.6
2B	4	0.63	0.61	27.1	55.4	0.8	2.0
3A	11	0.70	0.86	47.4	58.2	0.7	1.2
4B	6	0.88	0.78	14.6	72.6	3.4	5.0
4C	11	0.70	0.86	16.7	71.7	2.6	4.3
4D	11	0.80	0.84	46.8	63.0	0.9	1.3
5A	7	0.92	0.72	7.0	64.1	6.1	9.1
5B	8	0.76	0.82	12.9	80.0	3.9	6.2
5C	12	0.86	0.83	52.5	75.5	1.0	1.4

It is clear from inspection of table 10.1, without the need for sophisticated analysis of variance that the principal source of variance is between the individual potsherds, not between the samples. The standard deviation of all the ten sherds is 10.1μT, while the standard deviation of the mean value from each sherd is 9.0μT, so almost the entire variance is between the potsherds. One possibility is that the ambient field during firing was variable and that the presence of, say, iron kiln furniture could be responsible for large variance between the potsherds. The pottery of Brookhill appears to have been a small scale industry supplying low grade pottery for the lower ranks in society (Longworth 2006) and there is no good documentary evidence describing the kind equipment that was being used there. It seems more likely however that there is a correlation between the estimated field from each potsherd and its magnetic mineralogy. The results from the weakly magnetic BRH1 and BRH3 are in close agreement. The samples from the higher coercivity BRH4 and BRH5 give means of 69.1 and 73.3 μT respectively, while the lower coercivity BRH2 gives a mean of 52.2 μT.

This observation raises some problems for the choice of a final field estimate for the period. As the individual potsherds record different values, it is the mean of the means for each sherd that should be used as the estimate of the fields. If we take the mean value derived from each potsherd and then take the mean of these, the result is 61.6 μT, with a standard deviation of 9.0 μT. Another approach would be to apply some selection criteria to the data and see if this makes an impact on the result. Tentatively, we suggest that at least half of the NRM should be used to determine the intensity (f>0.5) and $r^2 > 0.99$. BRH5C is rejected on the grounds of a poorly reproduced pTRM check. The remaining

samples are 2A, 2B, 3A, 4A, 4B and 4C. These six samples also give a mean of 61.6 μT, with a standard deviation of 9.3 μT. If instead the average of the mean value derived form sherds BRH2, 3 and 4 is taken the result is 59.8 μT with a standards deviation of 8.6 μT. There is little or no difference in the result derived using various selection strategies and all estimates have large associated uncertainties. For the purposes of the final archaeointensity model, the latter estimate is adopted: 59.8 μT ± 5 μT, using the standard error of the mean of the three potsherds as the uncertainty.

Chapter 11

Tile kiln from Tylers Green, Buckinghamshire

11.1 Background

Excavations at Rose Cottage, Tylers Green (51.6°N, 0.7°W) by Archaeological Services and Consultancy Ltd (ASC) uncovered a series of medieval tile kilns. The tile industry was important during the 14th C, but subsequent archaeomagnetic dating of two of the kilns, sampled by Museum of London Archaeological Services, suggested a later date for their last use (Linford 2004). Samples from one of the kilns, archaeomagnetically dated to 1600±40 years (declination of 9.7°, inclination of 71.9°, α_{95} of 4.3°) were obtained for archaeointensity analysis. The samples consisted of four fragments of plain grey tile and a block of dark grey vitrified brick.

11.2 Magnetic characteristics

Chips taken from one of the tiles and from the kiln lining were analysed in a MM VFTB to determine their magnetic characteristics. IRM acquisition, backfield coercivity, hysteresis and the saturation magnetisation as the sample was heated to 700°C and cooled were measured and the data plotted (see figure 11.1). Absolute values of magnetisation were not calculated.

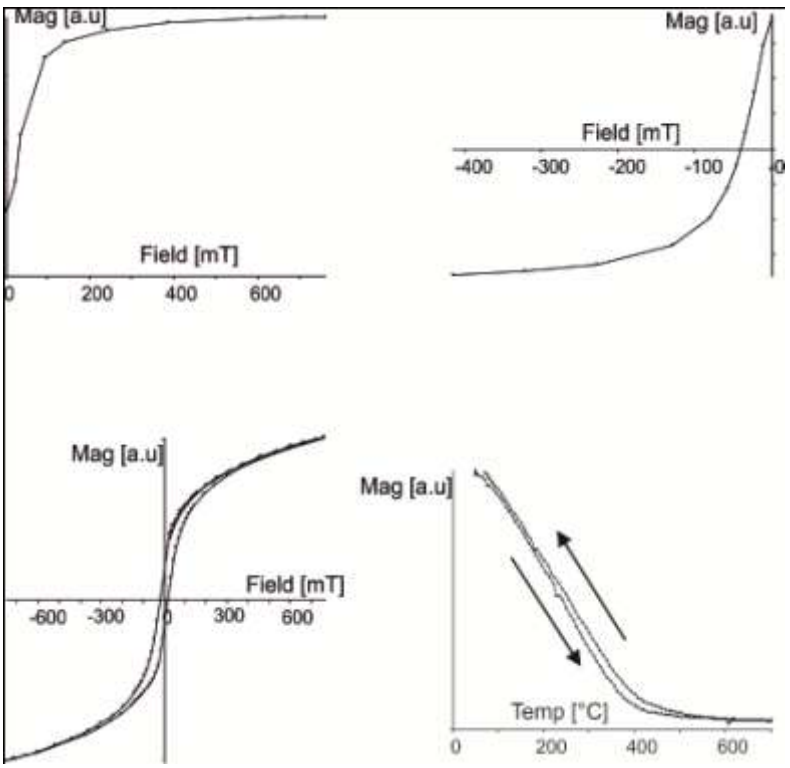

Figure 11.1a IRM acquisition, backfield coercivity, hysteresis and thermomagnetic behaviour for the kiln lining. Magnetisations are given in arbitrary units (a.u).

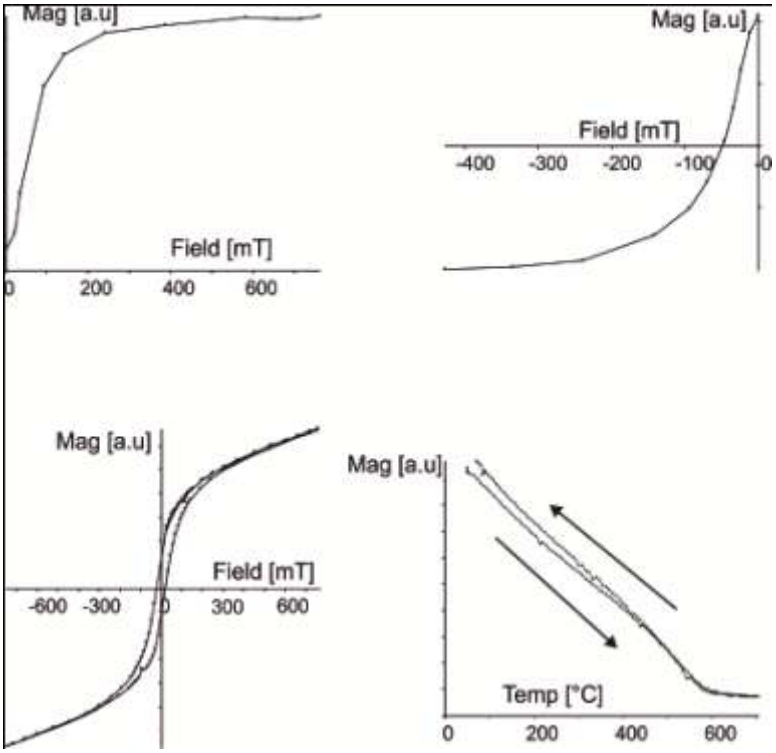

Figure 11.1b IRM acquisition, backfield coercivity, hysteresis and thermomagnetic behaviour for a piece of tile taken from the bottom of the kiln. Magnetisations are given in arbitrary units

Both the kiln lining and the tile have IRMs that are nearly saturated by 300mT, the theoretical maximum for magnetite, and have pot-bellied hysteresis loops suggestive of pseudo-single domain grains. There is little to distinguish between the samples, other than the thermomagnetic properties. The Curie temperature for the tile is about 580°C, so the principal magnetic mineral is probably magnetite. The lower Curie temperature, about 420°C, seen in the kiln lining suggests that the magnetic mineral is not pure magnetite but has some cation substitution. Both show reversible behaviour through the heating cycle making them suitable for archaeointensity.

11.3 Archaeointensity analysis

Three 5mm diameter cores from each tile fragment and the vitrified brick were glued to quartz rods using a non-magnetic high heat resistant adhesive (Fixwool). These were analysed in the Tristan microwave system. Some problems were encountered: two of the brick lining samples and five of the tile samples were lost or damaged early on in the experiment and the tiles required high powers to demagnetise them. It was problems such as these that led to the development of the adhesive-free vacuum pump system for mounting samples (see Suttie et al. 2010). The NRM/TRM plots and the vector endpoint diagrams for the remaining eight samples are shown in figure 11.2. Tailchecks have been plotted as the difference in moment of the two zero field steps at the same power.

Figure 11.2 NRM/TRM plots and the vector endpoint diagrams for the tile samples (A-D) and the kiln lining (K).

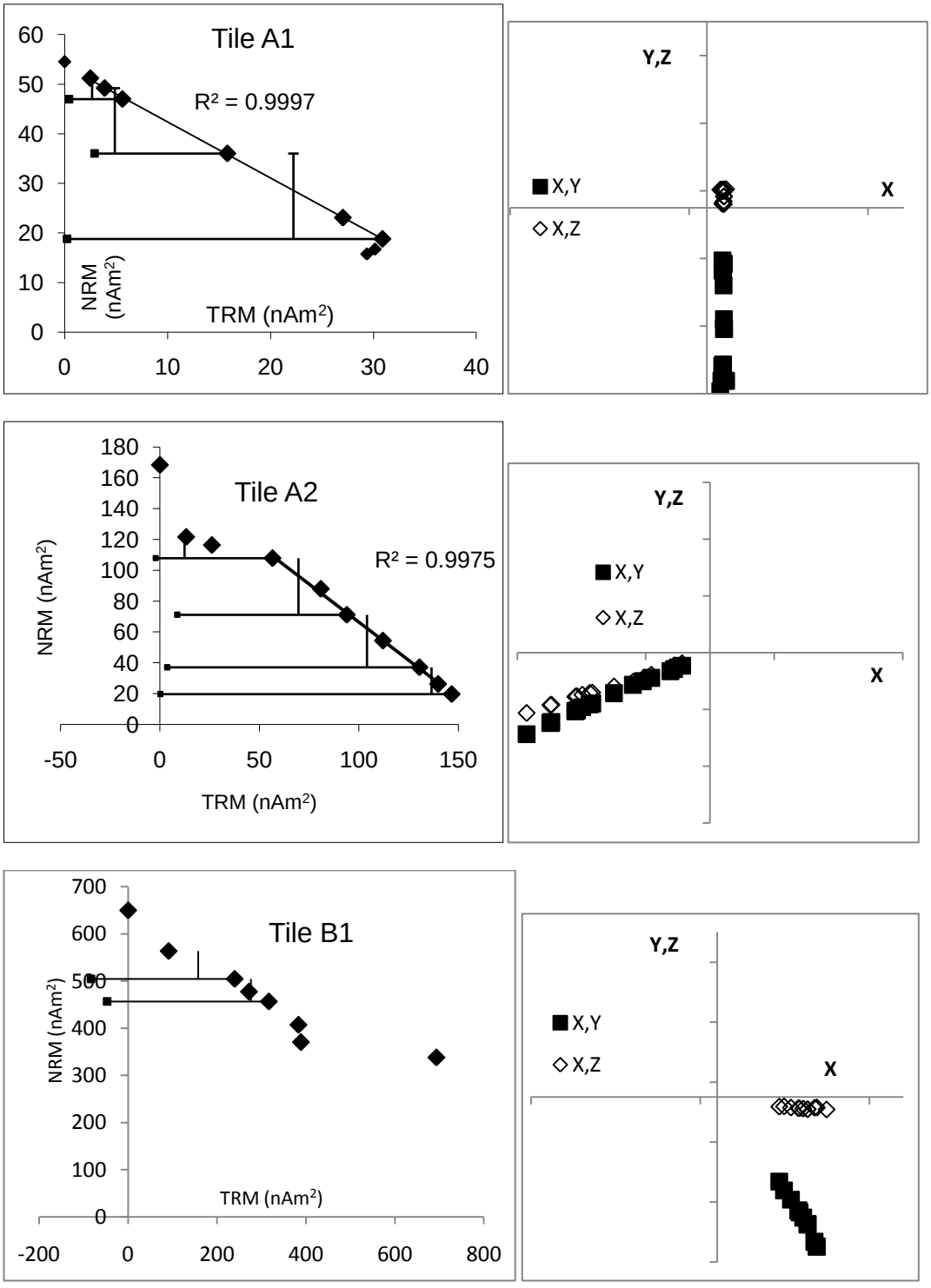

Figure 11.2 continued

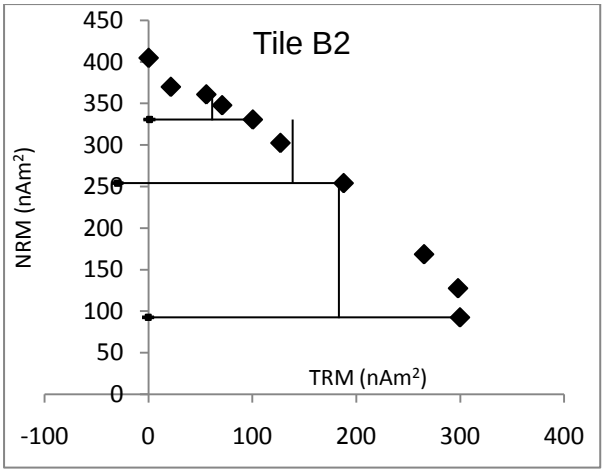

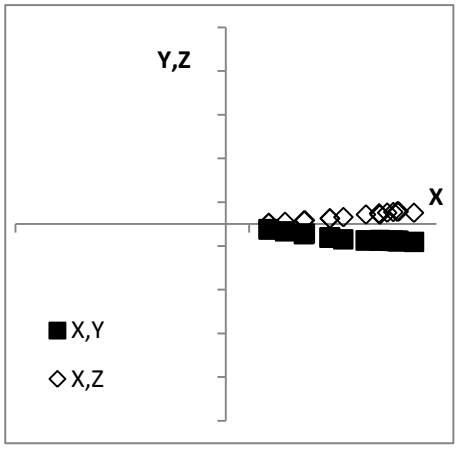

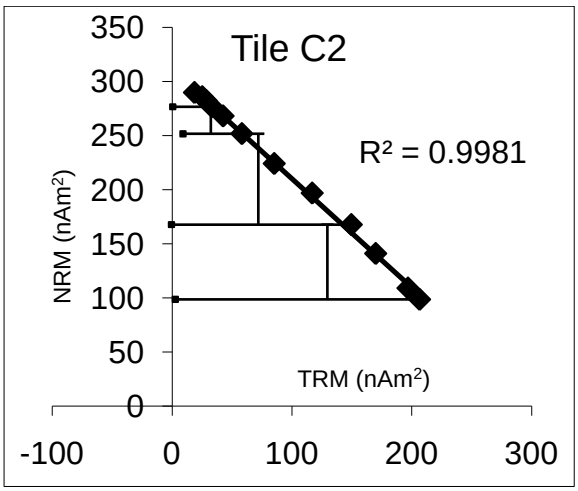

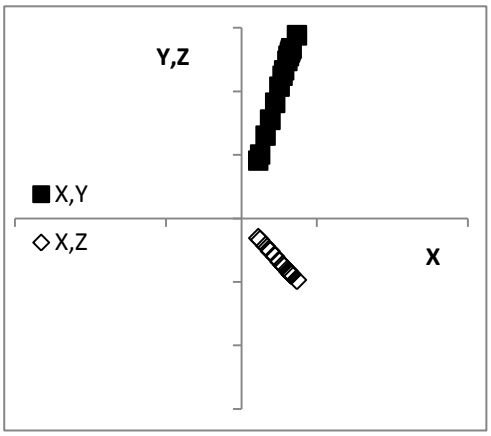

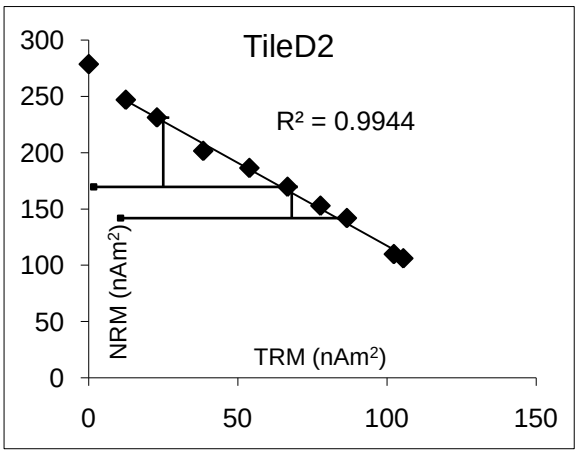

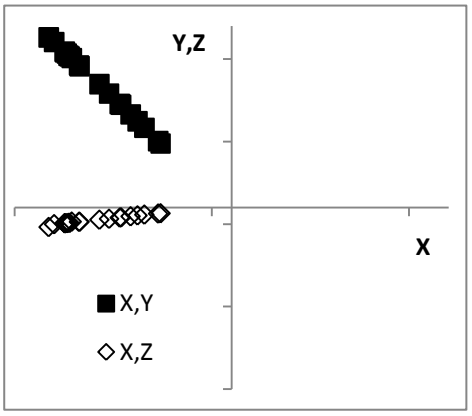

Figure 11.2 continued

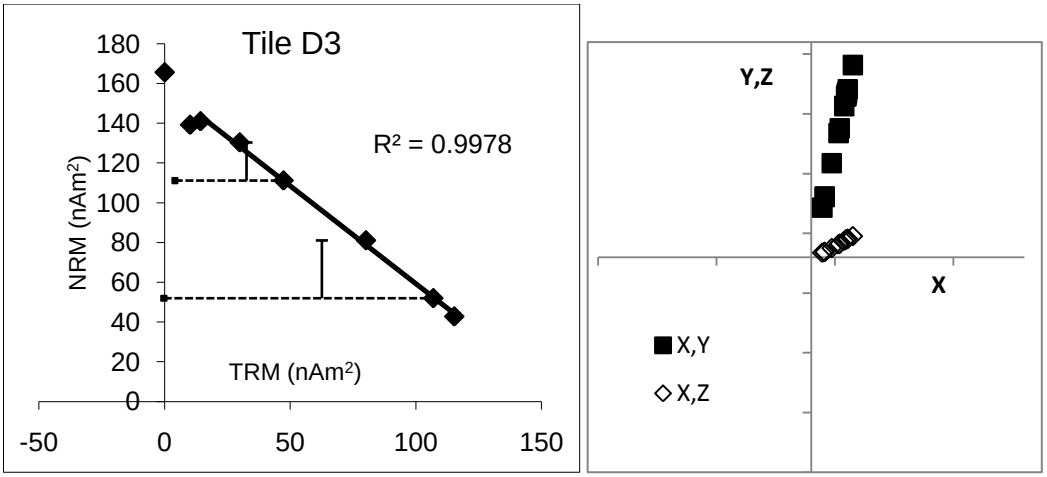

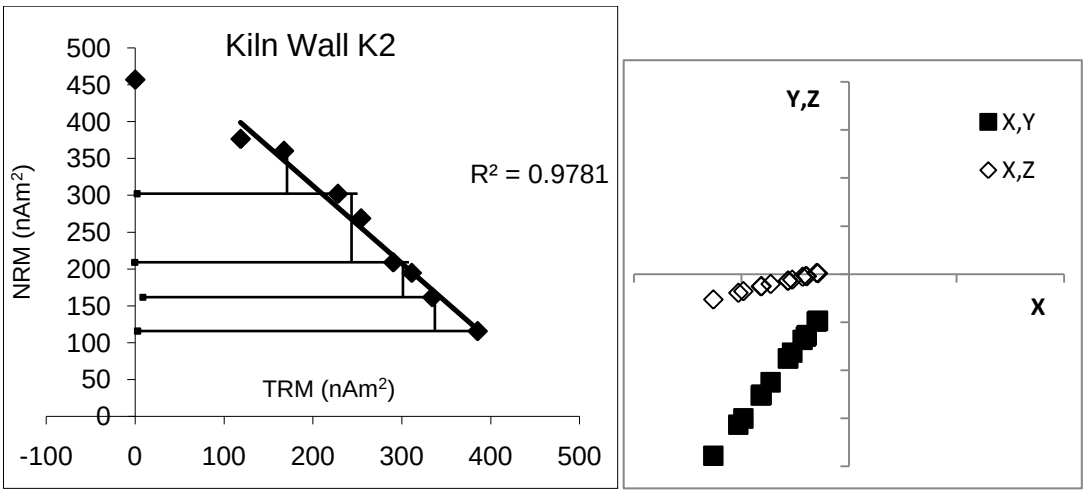

The samples from tile B show some sign of a multi-component remanence and the TRM/NRM plots are non-linear with checks failing badly. Sample A1 has a demagnetisation plot that is not going to the origin and the pTRM and tail checks are poor. The sample from the kiln wall also has a demagnetisation plot that is not going exactly to the origin, although the deviation between the mean direction and the vector direction is only 5 °. This sample will be included tentatively in the analysis shown in table 11.1.

Table 11.1 Field estimates and Coe statistics for the selected samples from the Tyler Green tiles and kiln.

Sample	Number of points	g	f	q	Field (μT)	Standard Error	Coe Error
A2	6	0.48	0.79	15.3	79.0	2.0	5.2
C2	12	0.62	0.87	38.6	70.6	1.0	1.8
D2	9	0.53	0.84	15.9	73.9	2.1	4.7
D3	6	0.60	0.76	19.2	73.9	1.7	3.9
K2	8	0.57	0.83	7.8	74.7	4.5	9.6

The assemblage shows consistently high values with a mean value of 74.4 μT and a standard deviation of 3.0 μT. Sample C2 yields the highest quality result in terms of the pTRM checks, tailchecks, number of points and linearity, but it is notable that it is the lowest value of the assemblage, almost one and one half standard deviations below the mean value. The highest value is from sample A2, where it is noted that the pTRM checks while not individually overly deviant, are all failing in the same way; the pTRMs are increasing. It has been suggested that the cumulative difference between the pTRM checks should be considered and the sample rejected if this exceeds a certain value (Kissel and Laj 2004). In chapter 9 it was shown that some samples gave erroneously high results when the pTRM checks showed this behaviour. While it is still unclear why this should, as progressive alteration leading to larger pTRMs would be expected to decrease the value of the field estimate, there is enough evidence to reject sample A2. The two samples from tile D give the same estimate so the final estimate of the field is taken as the mean of three values: C2, D and K2. The mean is 73.0μT and the standard deviation is 2.1μT. The high value of the field derived from these samples may be anomalous due to some cooling rate effect, but it was not possible to conclusively demonstrate this.

Chapter 12

Microwave archaeointensity from a medieval furnace

12.1 Background

Archaeological investigations at St. John's School, Glastonbury (51.1°N, 2.7°W) in 2003 uncovered a sunken feature consisting of fired clay. The fill of the feature contained fragments of1 1th and 12th century pottery and its form and associated finds suggested that it may have been a bell-casting pit (Linford 2003).The direction of the remanent magnetisation of the feature suggested that the last firing occurred between 1070 and 1120 AD. The direction obtained (declination 20.1°, inclination 63.9°, α_{95} = 2.2°) (Linford 2003) was in excellent agreement with the archaeomagnetic calibration curve of Clark et al. (1988).

A block of collapsed furnace lining (context 173) was obtained for archaeointensity analysis. This material was no longer in the position it had occupied during firing so could not be used for directional analysis. This material was light red fired clay, relatively free from inclusions.

12.2 Magnetic characterisation

A fragment of the clay weighing 120mg was subjected to the usual suite of magnetic measurements in the MM VFTB. IRM acquisition, backfield coercivity, hysteresis and the saturation magnetisation as the sample was heated to 700°C and cooled again were recorded and are shown in figure 12.1. The narrow hysteresis, low coercivity and Curie temperature of about 580° C may be indicative of multi domain magnetite or could point to a substantail superparamagnetic fraction. Generally, material in which the remanence carrier is multidomain does not yield useful archaeointensity, but one of the attractive features of the microwave method is the speed with which an archaeointensity experiment can be carried out.

Figure 12.1 IRM acquisition, backfield coercivity, hysteresis and thermomagnetic curve for a sample of the Glastonbury clay. Magnetisations are given in arbitrary units (a.u.).

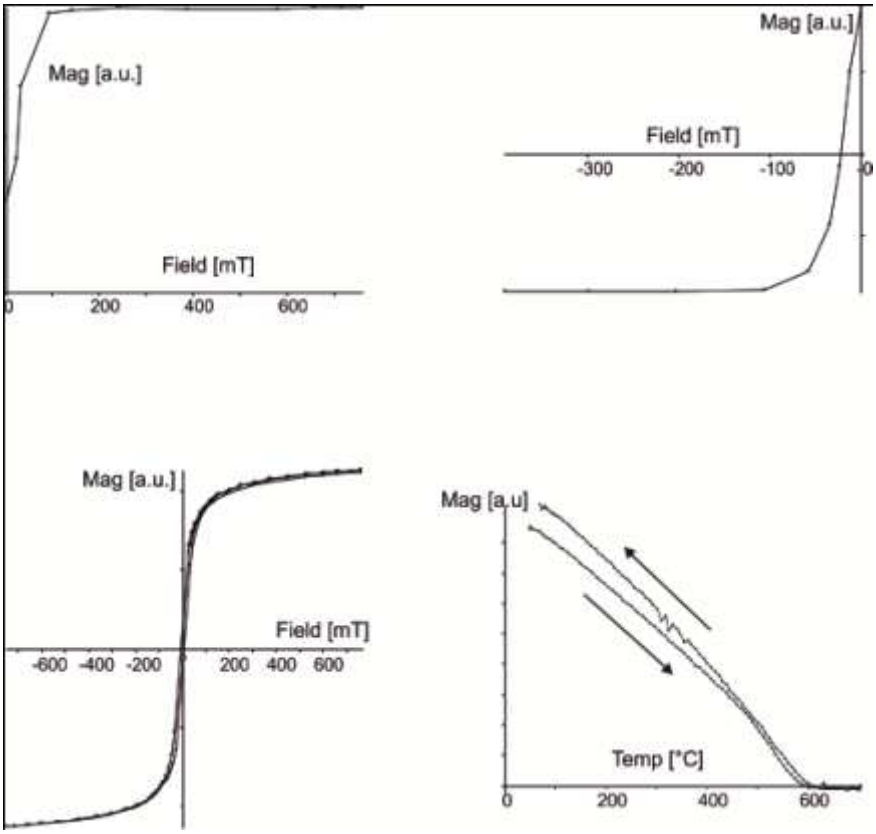

12.3 Microwave archaeointensity

A total of five samples were prepared for measurement on the Tristan microwave system. The sample consisted of fragments of clay, weighing about 150mg, that were broken off the main block with a non-magnetic tool. It was not possible to usefully demagnetise the first four samples, mainly because it was not possible to get the cavity to absorb power. In fact, in at least two of the cases the cavity was probably not operating in the TE_{011} mode (see chapter 3). At the time of the experiment there was still considerable uncertainty regarding the operation of the cavity. It appears that even with cavity in the correct mode, some feature of the dielectric properties of the clay caused the impedance of the system to change substantially. In one case the sample did suddenly couple with a high power microwave field and incurred some damage. It is quite likely that the clay is fairly hygroscopic and it is the very high dielectric constant of water (see table 2.1) that caused this anomalous behaviour. No problems were encountered with the fifth sample. Although it was ostensibly identical to the others, it may simply be that having had longer to dry after

gluing to the sample rod, the moisture content had dropped. The NRM/TRM plot and vector endpoint diagram for this sample (code GL5) are shown in figure 12.2. The applied field was 40μT, which was chosen to reflect low field values previously published for the period in Britain (Game and Davey 1985).

Figure 12.2 NRM/TRM plot and vector endpoint diagram of sample GL5

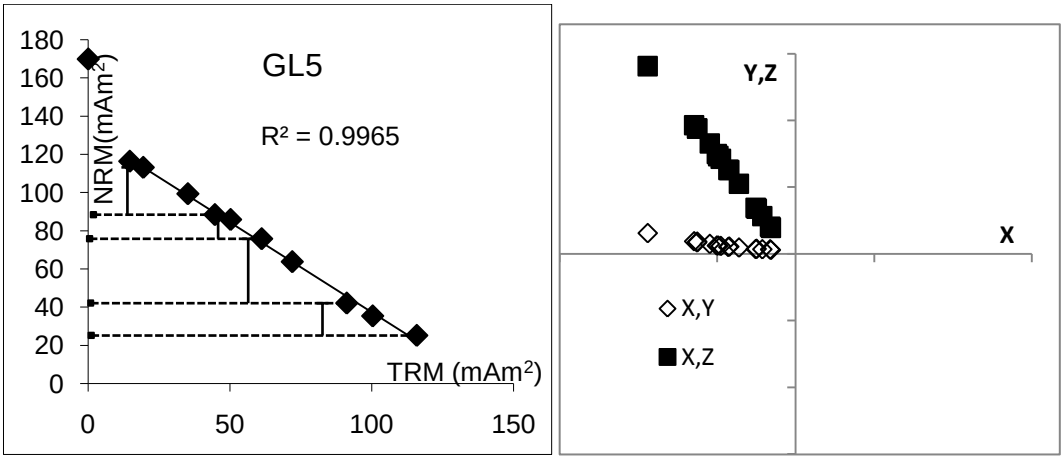

The result is summarised with the Coe statistics in table 12.1.

Table 12.1 Estimated field and Coe statistics for sample GL5

Sample	Number of points	f	g	q	Estimated field (μT)	Standard error(μT)	Coe error(μT)
GL5	10	0.70	0.86	28.6	37.7	0.8	1.3

The tailchecks show good reproducibility despite the clearly multidomain nature of the hysteresis (figure 12.1). The loss of one quarter of the NRM at a low power and the fact that the trendline does not point to total NRM are causes for concern but the result passes the commonly used selection criteria so will be discussed.

12.4 Discussion

One result in isolation cannot be regarded as highly significant indicator off the strength of the geomagnetic field in Norman Britain. When the experiment was carried out a low value of applied field was chosen because the best estimate of the field at the time was thought to be those derived by the Shaw method on Norman ceramics, which gave values of around 40μT (Games and Davey 1985). Arguably the highest quality set of archaeointensity from the medieval period in question is that of Genevey et al. (2009), unpublished at the time of

the experiment. Their results suggest intensity in Paris of between 50 and 55µT at 1200AD, but the data does not extend back to the 11th C. Archaeomagnetic field models (Clark et al. 1988, Lodge and Holme 2008) are consistent in showing the inclination of the field decreasing from the 11th to 13th centuries. Consequently, it is very hard to believe that the field strength could be some 30% lower in 1100, than in the 13th century.

Despite the quality of the result from sample GL5, a number of objections may be raised as to its validity. The clay, while possessing a univectorial primary remanence with no sign of a viscous overprint, may have undergone some amount of diagenesis since firing. It was noted during excavation and sampling of the feature that the ground easily became waterlogged. Another possible explanation is the effect of cooling rate differences between the microwave apparatus and the original furnace. While these would lead to an overestimate for non-interacting single domains (see chapter 10), a multidomain assemblage may show the opposite effect (McClelland-Brown 1984). It therefore seems likely that the low field strength apparently recorded by this feature is anomalous.

Chapter 13

Archaeointensities from heated sandstone

13.1 Background

As there were difficulties in acquiring well-dated archaeological material throughout the project, it was decided to attempt to derived archaeointensity from some less commonly used materials. Sandstone is widely used in both the vernacular and polite architecture of Northern England and Scotland, but as far as can be ascertained, only one study focussing on heated sandstone as a recorder of archaeointensity has been done previously and this was on early Holocene Australian hearth stones (Barbetti 1979). In this chapter, the potential for using fired sandstone from an industrial site for archaeointensity using the Thellier method is examined.

Sandstone from the annealing flue (structure A) and glassmaking sieges (structure B) at Bolsterstone near Sheffield (latitude 53.47°, longitude 1.59°W) were sampled for archaeomagnetic dating for English Heritage (Karloukovski and Hounslow 2006) and 9 samples, 3 from B and 6 from A, were obtained for archaeointensity analysis. The directional analysis, using AF demagnetisation, had identified two phases of use for the each of the two structures; the sieges were dated to 1680-1730 and the flue to 1800-1870 with most probable dates of 1710 and 1840 respectively. As the magnetisations of most samples were of the order of a few mA/m, the material was not suitable for microwave archaeointensity, where the small sample size precludes the use of weakly magnetized material. In most cases it was not possible to obtain particularly meaningful rock magnetic analyses using the MM VFTB for the same reasons. The samples used for archaeointensity were 1" diameter cylindrical cores that had been drilled approximately horizontally out of the walls of the structures. Their remanences were accordingly nearly perpendicular to the axes of the cores. For practical reasons this meant the laboratory field was applied perpendicular to the NRM throughout the experiment. It was decided to retain double heating steps, rather than employ the perpendicular method, however as it was uncertain what degree of anisotropy would be displayed by the sandstone. Magnetic remanence was measured on an Agico JR6 magnetometer. As each sample was close to the standard volume of 11.15cm^3, all remanent magnetisations will be given as volume magnetisations, although it should be realised that this is only approximate. As always, mass magnetisation can be easily found if required. Similarly the bulk volume susceptibility is reported.

13.2 Magnetic characterisation

The bulk susceptibility was measured on a Bartington MS1 susceptibility meter at 470 Hz and 4700Hz where appropriate and is given along with the NRM of each sample is given in table13.1. The specimens clearly divide into two distinct groups on the grounds of their susceptibility, with samples A8A, A11A and A12A having susceptibilities two orders of magnitude greater than the other samples. The Koenigsberger ratio , Q, is calculated as the ratio of the remanence to the induced moment, assuming a field of 50μT.

Table 13.1 Mass, susceptibility NRM and Koenigsberger ratio of the samples studied

Sample Code	Mass(g)	χ(lf)x10^{-6}	χ(hf)x10^{-6}	NRM(mA/m)	Q
A2A	22.91	108		4.16	1.0
A2B	25.89	41		18.74	11.8
A7A	25.54	43		14.82	9.3
A7C	27.68	21		3.65	4.6
A8A	24.45	3850	3740	3123	20.4
A11A	26.31	1590	1450	1155	18.3
A12A	25.72	1680	1590	1328	19.9
A20A	24.60	23		7.94	10.0
B17	26.52	47		9.83	4.9
B18	23.21	27		7.97	6.7
B19	26.71	42		12.59	7.9

The last letter of the sample code indicates the proximity to the top of the original drill core, A being the top. In the original dating report (Karloukovski and Hounslow 2006) it was noted that there was an increase in Q towards the top of the core, consistent with stronger heating at the surface of the structure. Here no such relationship was observed in sample A2 and only slightly in A7. With the exception of A2A, all samples may be expected to hold a thermoremanence on the grounds of their Koenigsberger ratios (e.g. Stacey and Banerjee 1974).

Chips of each specimen were taken and analysed in an MM VFTB. IRM acquisition, backfield coercivity, hysteresis and saturation magnetisation as the sample was heated to 700°C and cooled were measured. The hysteresis and thermomagnetic curves for selected samples are shown in figure 13.1. The measurements of remanence were too noisy to be useful and are not shown.

Figure 13.1 Thermomagnetic curves and hysteresis for selected samples

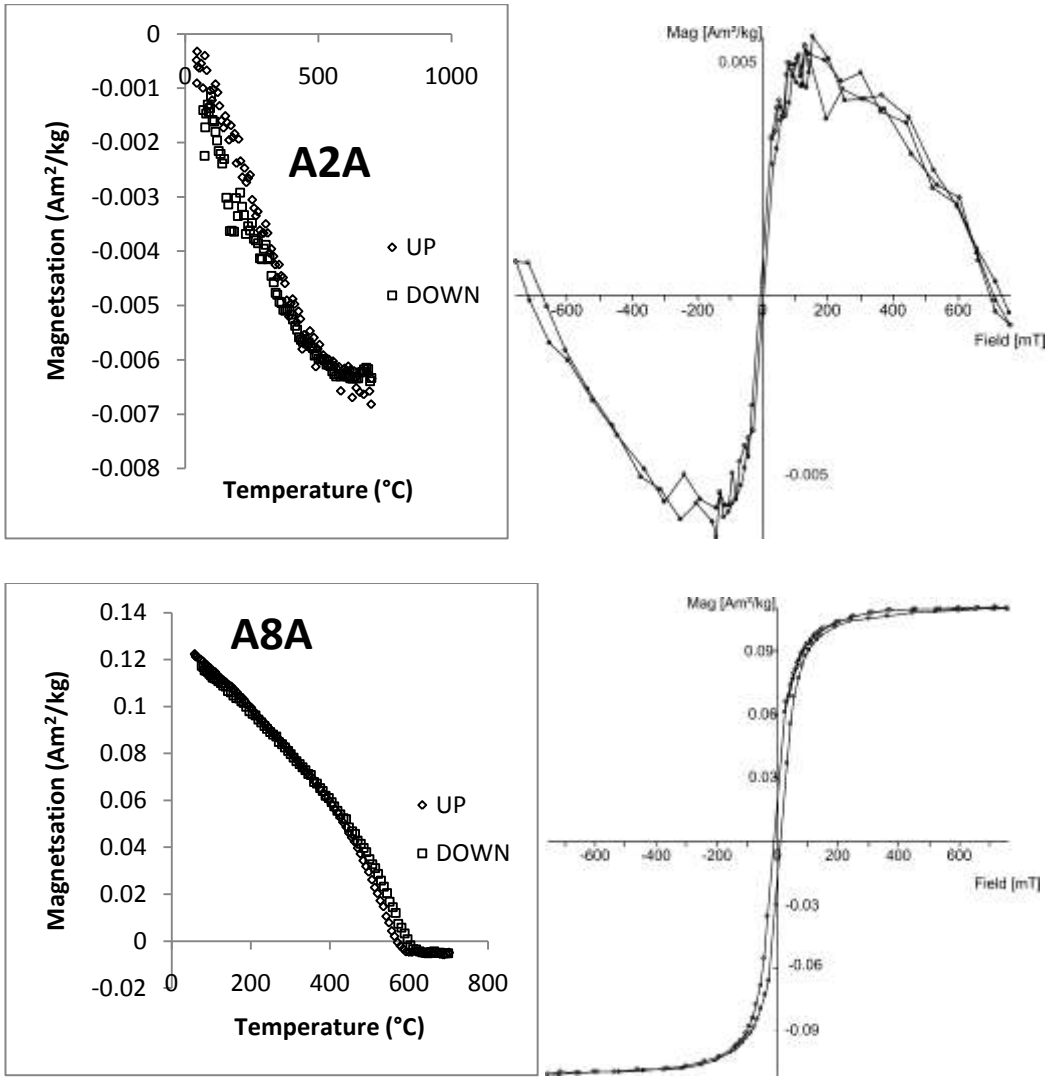

Figure 13.1 continued

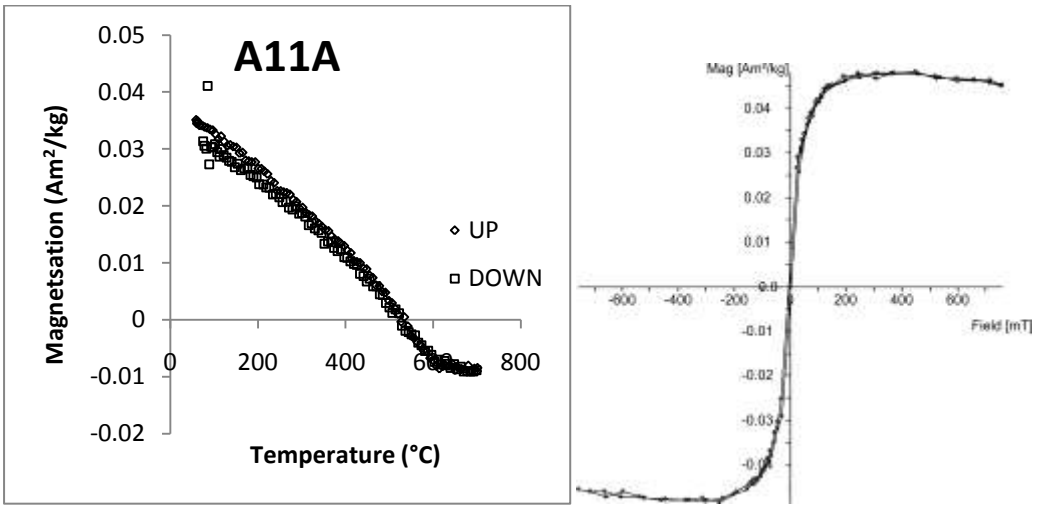

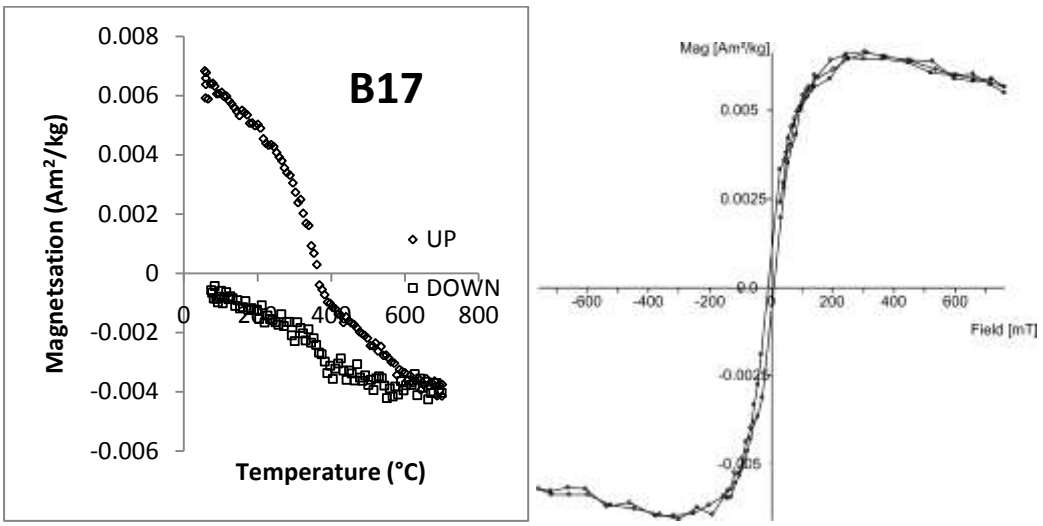

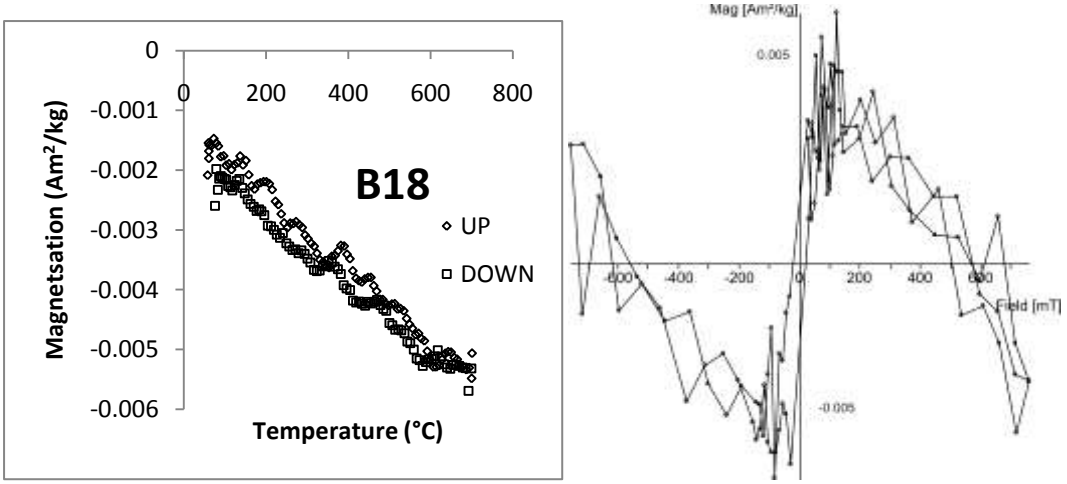

The more strongly magnetic samples have hysteresis typical of multidomain magnetic grains with Curie temperatures around that expected for magnetite. The reversibility of their thermomagnetic curves suggest that an archaeointensity experiment may be fruitful. The less strongly magnetic samples are more difficult to characterise. The hysteresis is dominated by the diamagnetic contribution, most probably from quartz. A2A and B18 have reversible thermomagnetic curves, but it is impossible to identify the domain state owing to the excessive noise in the hysteresis measurement. Note that the thermomagnetic curves give negative magnetisations as the diamagnetic susceptibilty is not dependent on temperature. B17 alters significantly when heated to 700°C , but it was not established whether alteration occurred at a lower temperature. Oddly, the hysteresis of this sample, while still showing some diamagnetic behaviour, is much stronger than its bulk susceptibilty would have suggested and it is likely that there is some heterogeneity within the core. For B17 the ratios of saturation remanence to saturation magnetization (M_{rs}/M_s) and remanent coercive force to ordinary coercive force (H_{cr}/H_r) were measured as 0.11 and 2.4 respectively, placing the bulk magnetic grain size in the pseudo-single domain field (Day et al. 1977, Dunlop 2002).

13.3 Archaeointensity method and results

The samples were heated in a MM thermal demagnetiser and held at temperature for 20 minutes before being fan-cooled to room temperature. Double heating steps were carried out at 150, 200, 250,300, 350, 390, 430, 470, 500 and 530°C , first in zero field and then with a 50µT field applied along the axis of the cylindrical samples. Tailchecks and pTRM checks (see chapter 5) were carried out a t every second temperature step (250, 350 430 and 500°C). The bulk susceptibility was monitored throughout the experiment, being remeasured along with the sample weight after every second heating step. NRM/TRM plots and vector end point diagrams are shown in figure 13.2.

Figure 13.2 NRM/TRM plots and vector endpoint diagrams for each of the samples

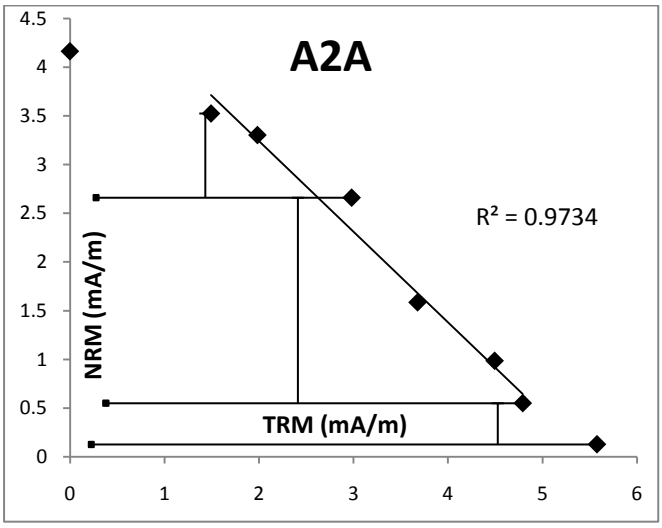

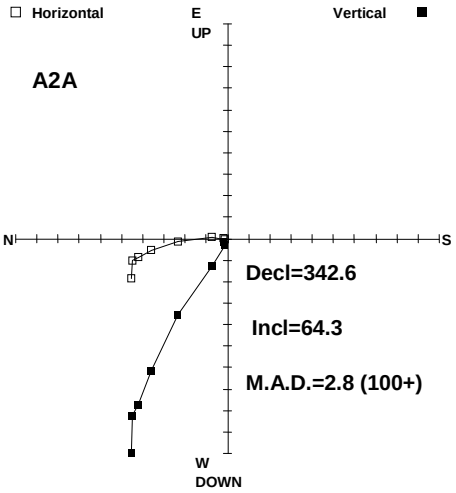

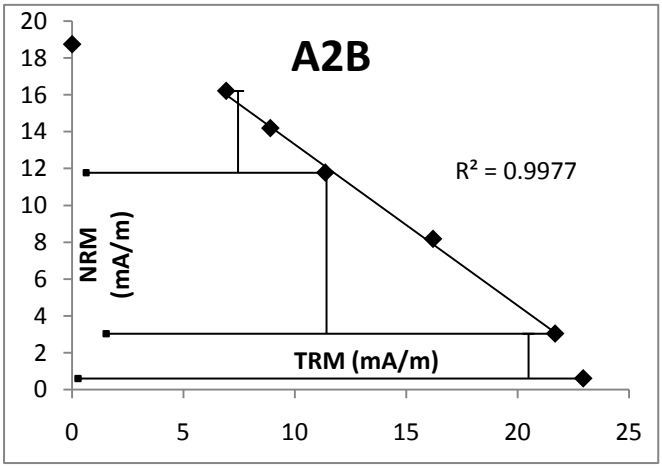

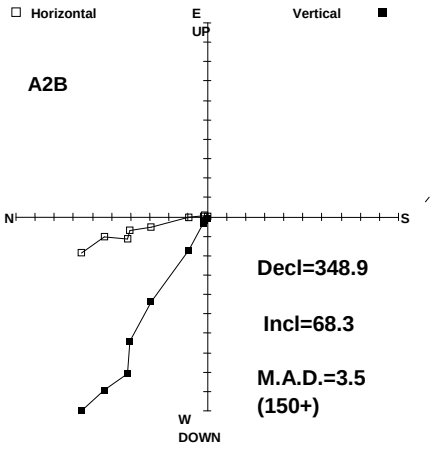

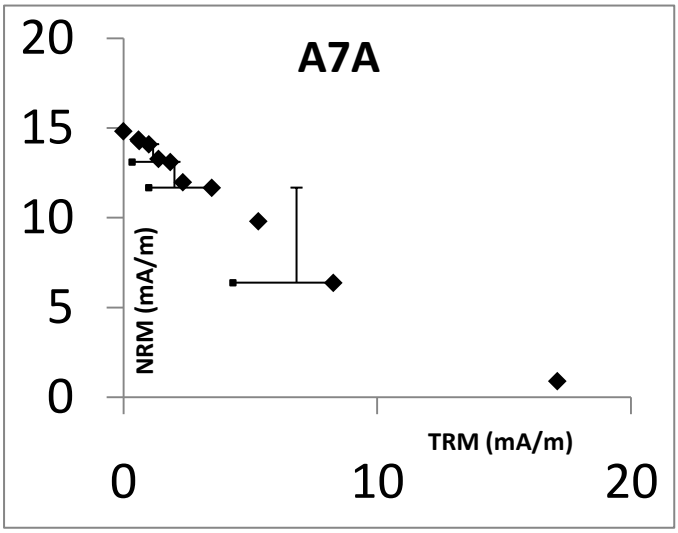

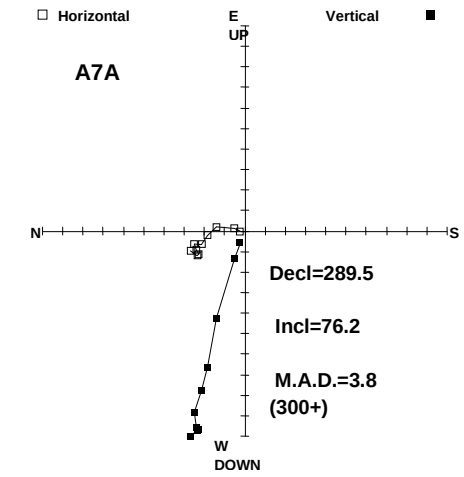

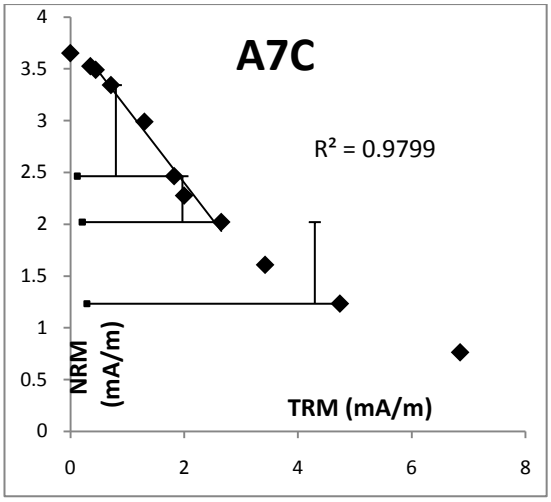

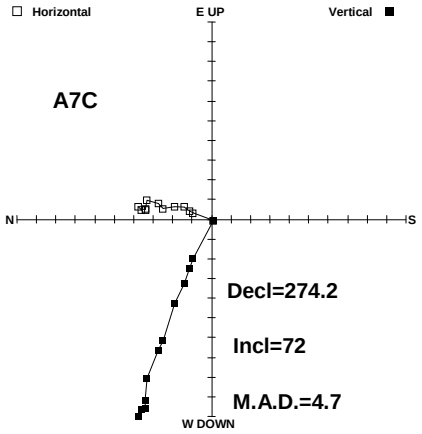

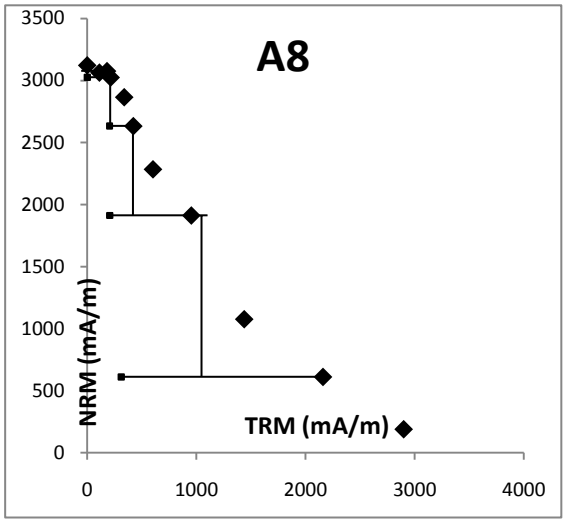

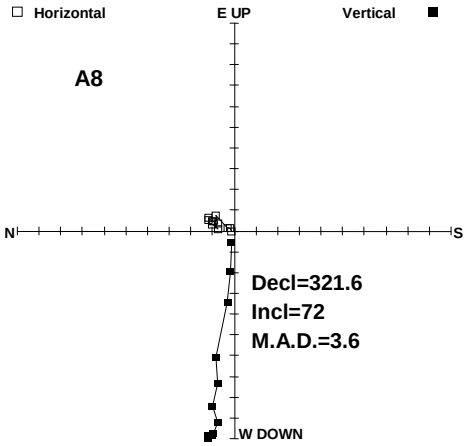

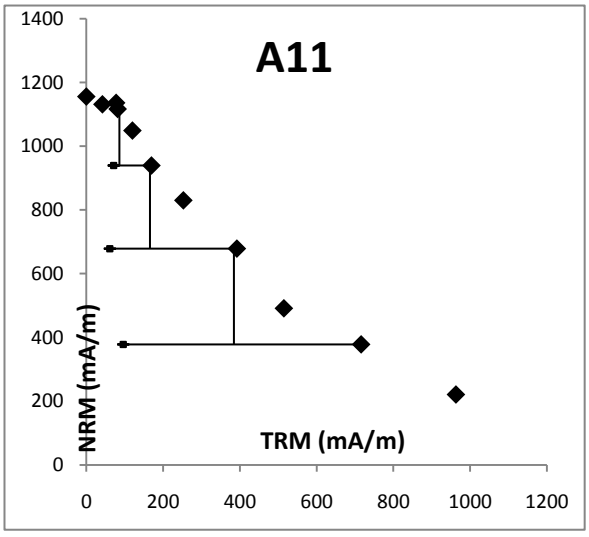

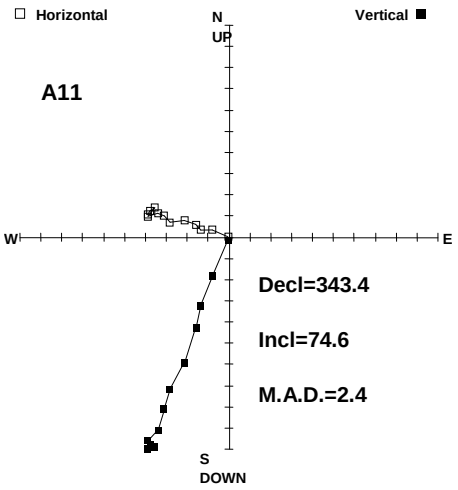

Figure 13.2 continued

Figure 13.2 continued

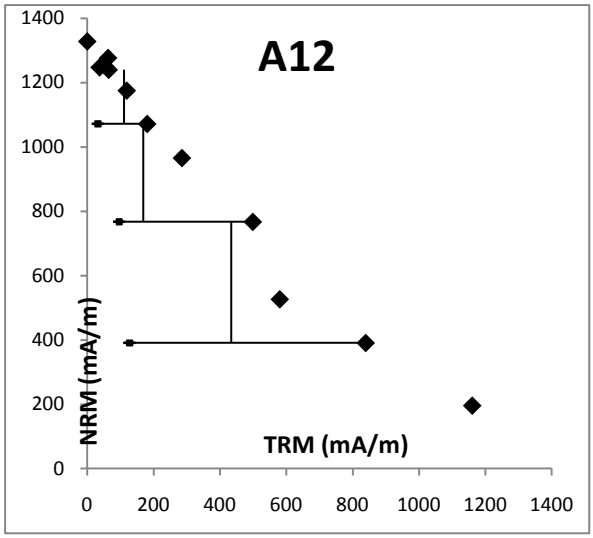

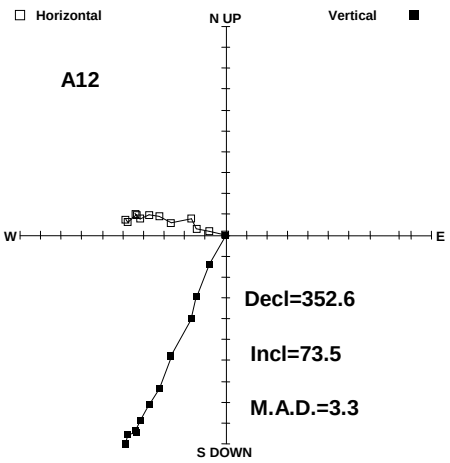

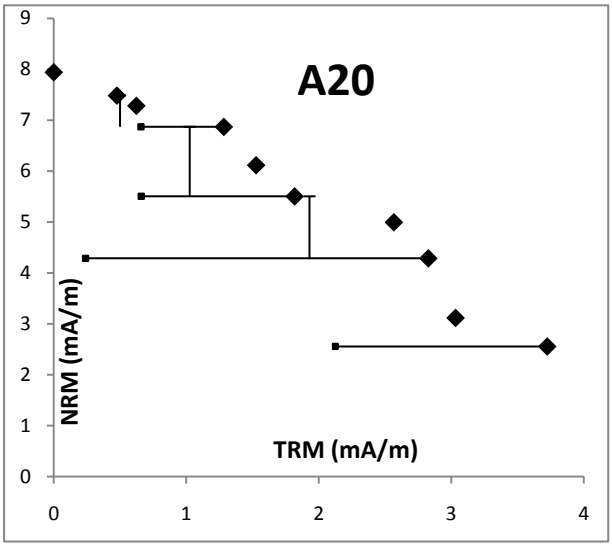

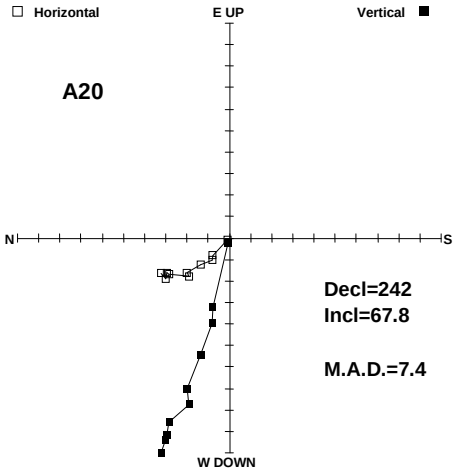

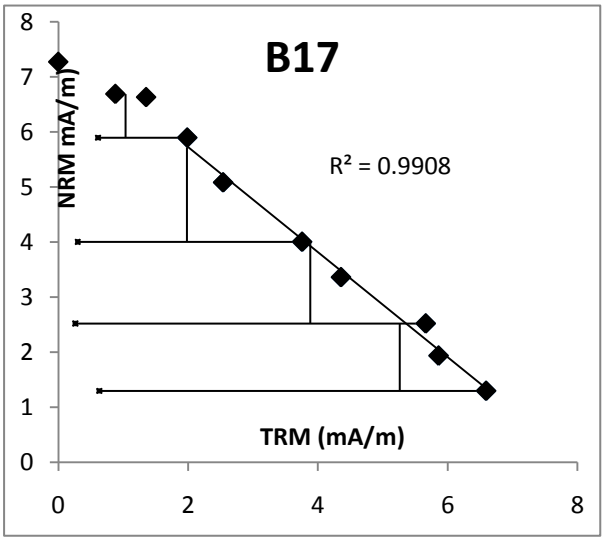

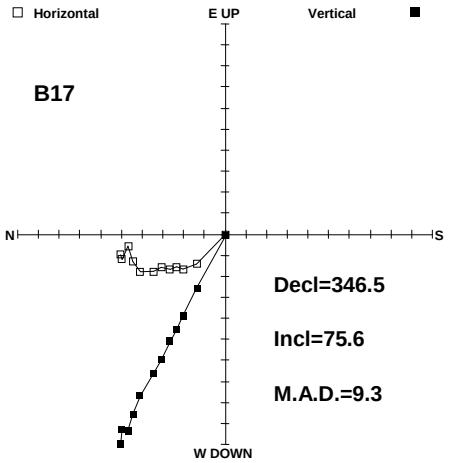

Figure 13.2 continued

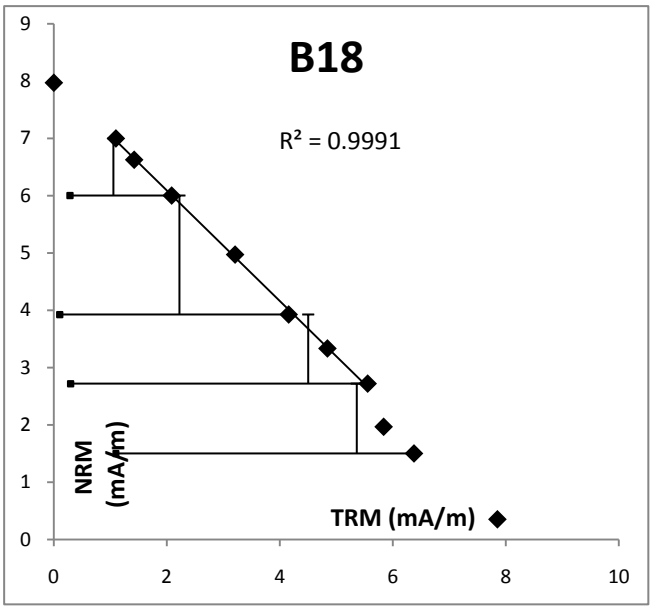

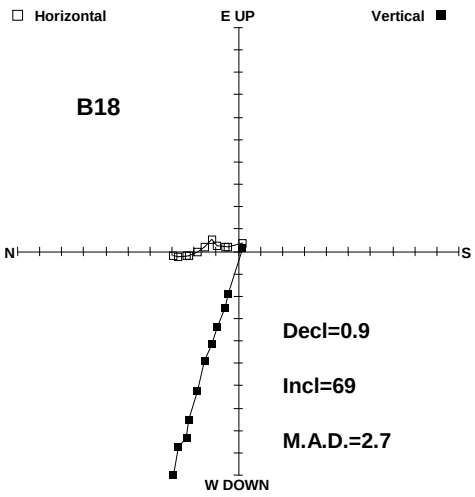

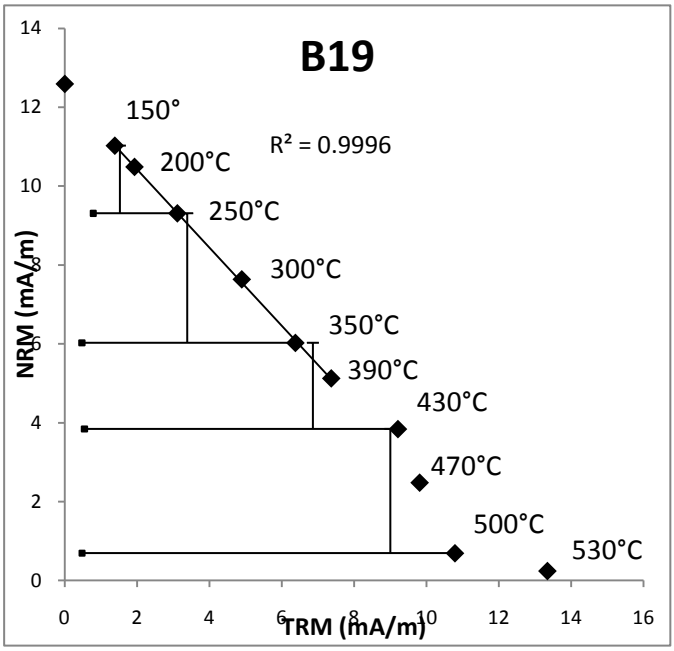

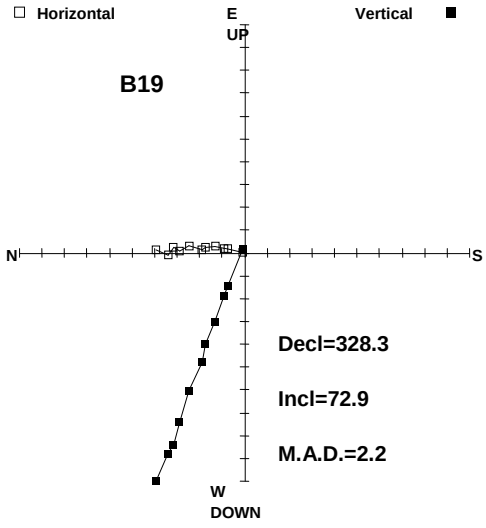

Each vector endpoint diagram in figure 13.2 gives the M.A.D (Kirschvink 1980) for a selected temperature range. There is no universally accepted value of M.A.D in an archaeointensity. In palaeointensity, a M.A.D of less than 15° is sometimes considered appropriate (Selkin and Tauxe 2000) but this seems far too imprecise for archaeointensity. In English Heritage's guidelines for archaeomagnetic dating a maximum of 3° M.A.D is suggested (Linford 2006) although this is for a different purpose where archaeodirection is the quantity of interest. Here we choose to be satisfied with an M.A.D of less than 5°.

The applied field was in the direction of the sample axes, corresponding to the southerly direction in the endpoint diagrams. Any trend in this direction during the archaeointensity experiment can be a sign of a chemical magnetisation developing as magnetic phases are created (Chauvin et al. 2000). This useful check is available as the applied field is nearly perpendicular to the NRM. The directions are in reasonably good agreement with those given in the original dating report. Sample B17 has a multi component remanence but the temperature rage 250-500°C yields a vector with the expected direction and a low M.A.D. 500°C will be taken as the temperature from which the NRM was developed for the purpose of calculating archaeointensity (see Yu and Dunlop 2003), although any result from this sample will need to be interpreted cautiously. The vector representing the high temperature remanence is considerably further east so it may be that this magnetisation derived from the B phase and the lower temperature range is derived from the later reuse of the structure.

An important consideration in assessing the quality of these results is the magnitude of the magnetisation. For this reason the convention of expressing the magnetisation in normalised units on Arai plots has been abandoned. Where the volume magnetisations are of the order of a few mA/m, it is to be expected that tail checks and pTRM checks may fail to be completely reproducible due to greater errors associated with each measurement. In samples A8, A11 and A12 no such appeal can be made and the increasingly wayward tail checks, along with a marked concavity of the data indicates multidomain behaviour and these results are not considered reliable. A7A shows signs of alteration at higher temperatures. Referring to the vector endpoint plot shows that only the NRM blocked above 300°C was unidirectional, so nothing from this sample can be used to determine archaeointensity. A20 is a good example of non-ideal behaviour in every sense, with pTRM checks and tailchecks unequivocally failing, even at low temperatures, and nothing resembling a straight line apparent in the NRM/TRM plot.

There was some change in the susceptibility of some of the samples during the experiment although the low susceptibilities made it difficult to ascertain whether this was real or simply a calibration issue with the susceptibility bridge. Calibration was not carried out but repeat measurements suggest that there was an associated error of at least 5 $x10^{-6}$ SI. B17 showed a continual change in susceptibility throughout the experiment and the alteration visible in the VFTB data appears to accumulate across a range of temperatures. The more strongly magnetic samples (A8, 11, 12) had reasonably consistent susceptibility, although

sample A11 showed a drop of almost 10% by the end of the experiment. Most of the non-linearity in these samples is put down to multidomain behaviour rather than alteration.

The samples yielding reasonably linear NRM/TRM plots are now considered in more detail. Table 13.2 summarises the field estimates and Coe statistics for each sample.

Table 13.2 Field estimates and Coe statistics for selected samples

Sample	N	f	g	MAD	q	Estimated field (μT)	+/-S.E (μT)	+/-Coe error(μT)
A2A	7	0.82	0.69	3.0	9.62	45.14	2.63	4.69
A2B	5	0.70	0.72	4.3	18.09	43.73	1.22	2.42
A7C	7	0.41	0.77	6.6	5.51	35.45	2.04	6.43
B17	7	0.47	0.83	2.4	9.00	47.94	2.06	5.33
B18	7	0.54	0.81	3.7(2.4)	32.86	48.25	0.64	1.47
B19	6	0.47	0.77	3.9	37.31	49.51	0.48	1.33

13.4 Anisotropy

The laboratory field was applied approximately perpendicular to the NRM so it is important to determine the degree of anisotropy. This was done after the 500°C heating step. A total of six TRMs were given to the samples, parallel and antiparallel to each of the x, y and z directions. The averages of these were used to determine a matrix describing the anisotropy of TRM ,

$\boldsymbol{K} = \begin{bmatrix} k_{xx} & k_{xy} & k_{xz} \\ k_{xy} & k_{yy} & k_{yz} \\ k_{xz} & k_{yz} & k_{zz} \end{bmatrix}$ so that $\mathbf{TRM}=\mathbf{K}\boldsymbol{H_{lab}}$. This approach has some drawbacks however; despite a total of 18 measurements being made (x, y and z components of magnetisation in each of the six steps) to determine the 6 elements of the (symmetric) matrix , non-diagonal elements are only poorly determined. That is to say that although the matrix is overdetermined the uncertainty in its orientation is large. Also, pTRM checks are often held to be positive if they agree to within 5- 10% of the TRM that is being reproduced (Selkin and Tauxe 2000). This variation is typically larger than the degree of anisotropy exhibited by many materials so, if anisotropy is going to be determined with any accuracy at all, this must be a bare minimum of reproducibility. As pointed out above, it is not to be expected that the k_{ij} $(i \neq j)$ will have anything like this degree of reproducibility but the

maximum difference between the $k_{ij}\ (i = j)$ determined in each case will be considered an indication of quality of the anisotropy determination. These are given in table 13.3 along with the ratio of the eigenvalues (λ_i) and resulting correction required in the archaeointensity.

Table 13.3 Details of the matrices of anisotropy of TRM for each sample. Also shown is the resulting correction to the intensity

Sample	$\Delta k_{ij(i=j)}$	λ_1/λ_3	λ_1/λ_2	Correction	Corrected Int
A2A	7%	1.20	1.12	+17%	52.8
A2B	14%	1.21	1.10	+3%	44.8
A7C	53%	1.21	1.14	0	35.5
B17	3%	1.24	1.08	+6%	50.8
B18	7%	1.25	1.14	+5%	50.7
B19	11%	1.31	1.16	+8%	53.5

The most striking feature is the large degree of anisotropy, but in the one case where two samples came from the same core (A2), the anisotropy correction leads to quite different results. This is despite the two samples exhibiting similar magnitudes of anisotropy. The reason is due to uncertainty in the orientation of the anisotropy matrix: the two samples may well have the same anisotropy but uncertainties in the off-diagonal terms in the measured matrix make orientation of the ellipsoid highly uncertain. In the case of sample A7C, some considerable alteration has taken place and the anisotropy matrix cannot be considered reliable. Varying degrees of reproducibility are exhibited by the remaining samples. So far only the results of the anisotropy experiment itself have been used to determine the anisotropy matrix. The TRMs gained during the Thellier experiment can themselves be used to check that the anisotropy matrices are reasonable. For each of the 6 samples with a determination of anisotropy the directions of the TRM gained during the experiment are compared to that predicted by the anisotropy matrices in figure 13.3.

Figure 13.3. Circular plots of the actual TRM directions from the Thellier experiment (dots) compared to the direction expected from the anisotropy calculations (crosses) for samples A2A, A2B, A7C, B17, B18 and B19.

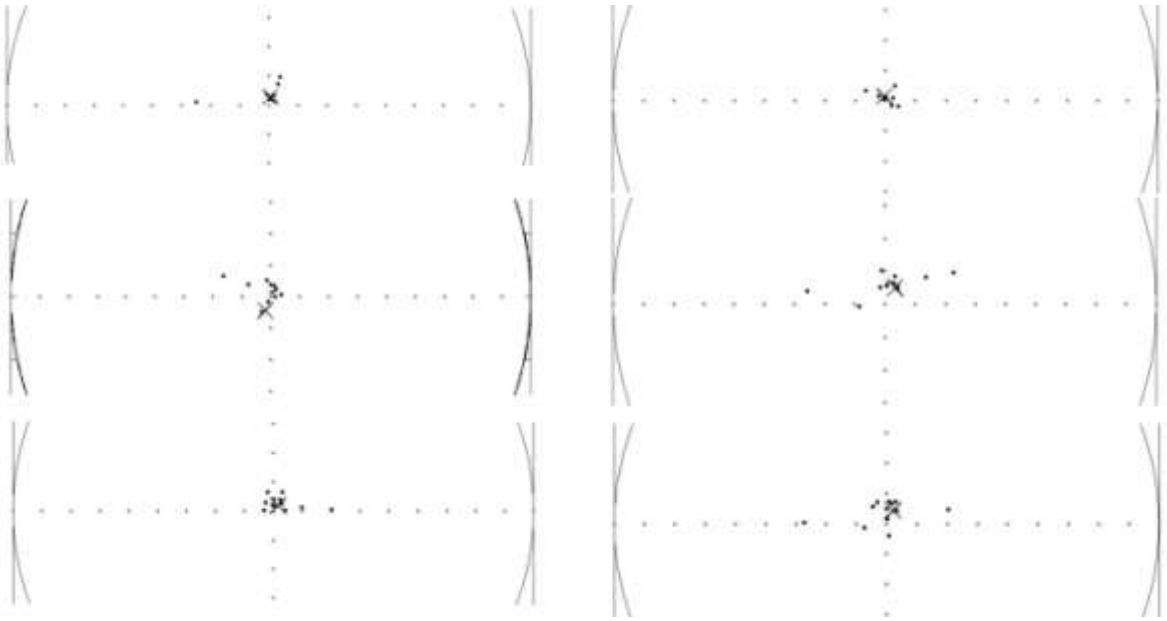

The directions of the TRMs cluster around the predicted direction in all cases other than A7C (middle left), which had already been identified as problematic. Both the estimates for sample from core A2 are consistent with the direction of the TRM despite the differences in the orientation of the ellipsoid. This is because the direction of the applied field is close to one of the principal axes of the ellipsoid in both cases. Commonly, only the best estimate of anisotropy is used to determine the correction to archaeointensity, but given the inherent uncertainties, here this is examined in more detail. In the case of core A2 it is useful to use a Monte Carlo simulation to generate anisotropy matrices around the measured mean values of k_{ij}, using the estimated variance of the k_{ij}. This is done 100 times for each of the anisotropy matrices of A2A and A2B and the directions of the major axes of the ellipsoids shown in figure 13.4.

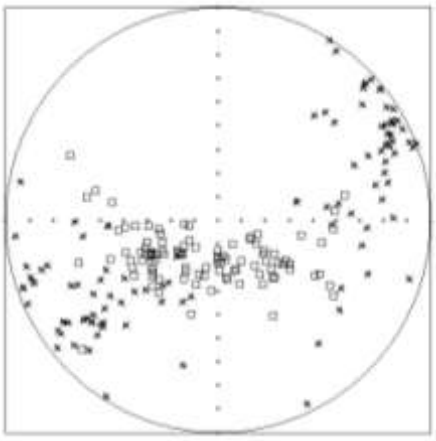

Figure 13.4: Monte Carlo simulations of the direction of the principal component of anisotropy for samples A2A (squares) and A2B (crosses).

The distribution of the anisotropy ellipsoid for A2B is more scattered than that for A2A, but there is a reasonable probability that the directions of the major axes are the same, around 60° down with an azimuth of around 220° (in the uncorrected core coordinates). The most probable directions are quite different in each case and it is this ellipsoid that is used to obtain the anisotropy correction. If it is assumed that both samples have the same ellipsoid of anisotropy, as might be expected from two samples from the same core, then it would be appropriate to take the ellipsoid with the highest joint probability. Similarly, we can also consider the distribution of the correction required as a simple function of the randomly generated anisotropy matrices (see figure 13.5).

Figure 13.5 Histograms of the associated correction factors for the Monte Carlo simulations of the anisotropy matrices in figure 13.4

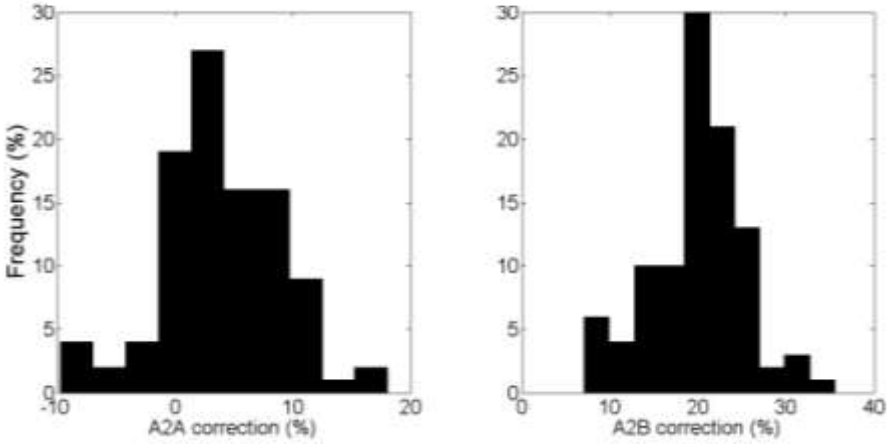

It could be argued that, realistically, the anisotropy correction should be of the order of 10% in both cases, especially when it is understood that this would make no difference to the mean intensity derived from the 2 samples. The associated error becomes extremely difficult to estimate formally and rarely, if ever, appears to have been considered.

These considerations highlight the difficulties faced when correcting for anisotropy and with hindsight it would probably be better to have used a laboratory field as close to parallel to the NRM as possible to minimise these effects, although this was impractical owing to the way in which the samples had been previously prepared.

13.5 Discussion

Notwithstanding the problem of poorly determined anisotropy the results of the archaeointensity experiments can be interpreted in terms of the past behaviour of the geomagnetic field. With samples from structure A, some discussion of which results to accept is necessary. There are many suggestions of "selection criteria" that can be used to identify the most reliable results (see chapter 5), but these are largely subjective and in this case the weak magnetisation and the correspondingly low signal to noise ratio mean many commonly used criteria may not be appropriate. There is no single objective criterion that can be used to reject results. All six of the results being considered pass many of the commonly used criteria but there are grounds for rejecting sample A7C when all are considered together. The results are clearly incongruous and the quality factors, while individually passing the criteria, taken as a whole do not inspire confidence. The MAD is 6.6°, while it is no more than 4.3° for all the others, it has the lowest f value (the proportion of the NRM used to calculate the archaeointensity), and the quality factor q is by far the lowest. This sample was not included in the final archaeointensity determinations which are given in table 13.4 along with the archaeodirections for each structure from the original dating report (Karloukovski and Hounslow 2006) to give a full vector description of the field.

Table 13.4 Archaeointensity determinations from the Bolsterstone sandstoe along with directions from Karloukovski and Hounslow (2006)

Sample	Int	Mean B	± (95%)	± (63%)	Dec	Inc	α95	α63
A2A	52.8(49.7)	48.8	n/a	8.7(1.3)	337.6	71.5	1.8	1
A2B	44.8(48.1)							
B17	50.8							
B18	50.7	51.7	3.9	1.1	350.6	75.1	1.3	0.8
B19	53.5							

The uncertainties quoted in table 13.4 require some explanation. In archeodirections, it is customary to express the uncertainty as a confidence interval, usually at the 95% level,

α95. This is the angle around the best estimate of direction within which there is 95% probability of finding the mean direction. For the sake of consistency, the 95% confidence interval has been given for the intensity of structure B, drawn from a student-t distribution on 2 degrees of freedom, although normally archaeointensities are quoted with their standard deviation, which does not reflect the uncertainty in the mean, as an indicator of uncertainty. For structure A, a 95% confidence limit is too large to be useful as there are only 2 samples. In palaeomagnetism a 63% confidence limit is sometimes used when describing directions (Butler 1992) so this has been given along with the corresponding 63% confidence limits of the mean intensity. The confidence limits and individual intensities from structure A, calculated using the joint probability distribution of the ellipsoid of anisotropy are given in parentheses. While it is accepted that this confidence limit may be somewhat optimistic, mean values can be compared to the geomagnetic field model gufm (Jackson et al. 2000) which is valid over the period of interest. The model does not provide a definite value of intensity for the period prior to 1840, but by choosing to constrain the evolution of the axial dipole according to a favoured hypothesis, the model can be made to predict the intensity. There are essentially two competing hypotheses concerning dipole prior to 1840: the constant axial dipole (Gubbins et al. 2006, Finlay 2008) and the rapidly decaying dipole hypothesis presented in chapter 5. These are shown along with declination and inclination in figure 13.6. Even with the most optimistic estimate of uncertainty, the intensity from structure A is not precise enough to exclude any date after the early 18th century, using any of the models. The mean intensity is certainly consistent with the directional dating suggesting a date in the early 19th century, but given the low variation in intensity seen over the period in the model there is little more that can be said regarding structure A. In the case of structure B, the original dating report, which used a different archaeomagnetic reference curve after relocating the data, gave a date of 1710 +/- 20 years and this was thought to be consistent with historical documents (Karloukovski and Hounslow 2006).

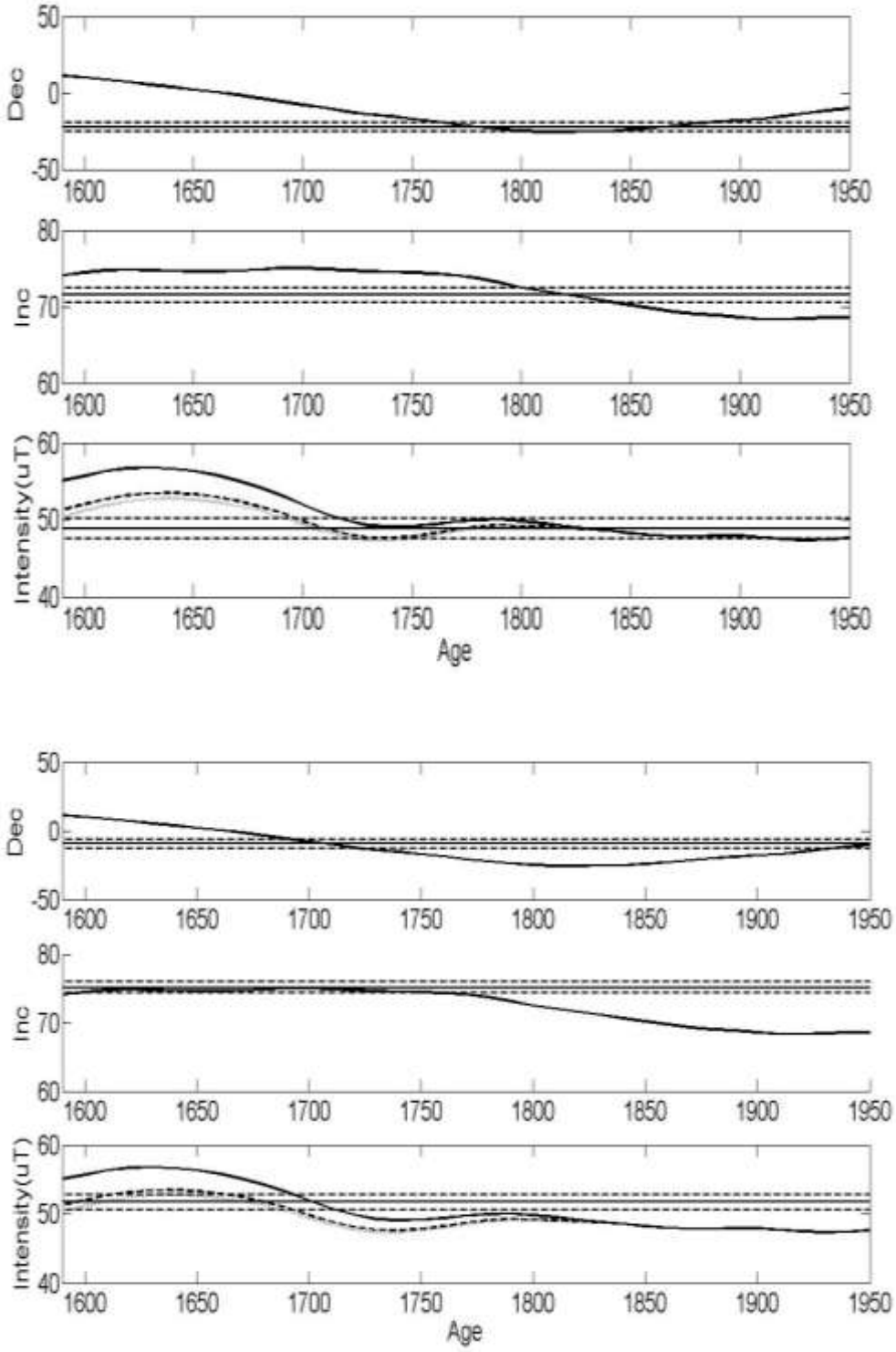

Figure 13.6 Declination, inclination and intensity for structure A (top) and structure B(bottom) plotted with the field model gufm(Jackson et al.2000). The intensity curves before 1840 are scaled according to the suggestion of Gubbins et al. (2006) (bold dotted line), Finlay (feint dotted line) and the 12nT per year decay suggested in chapter 5 (solid line).

This would be confirmed by the intensity derived from structure B, if the rapidly decaying dipole hypothesis was accepted. If either the slow decay (Gubbins et al. 2006) or constant dipole (Finlay 2008) hypotheses were taken to be true the joint probability of the age estimate would be pushed back. It is however, given the uncertainties and the small amount of material analysed in this study, not possible to argue forcefully in favour of any of the competing hypotheses regarding the evolution of the axial dipole over historical times.

To conclude, it has been demonstrated that weakly magnetic burnt sandstone can be used to determine archaeointensity and the field values derived are fully consistent with current hypotheses of the historic field strength. Interestingly, the highest quality results came from very fine grained sandstones that had low susceptibilities and may not naturally have been chosen for archaeointensity. The larger grained material showed signs of multidomain behaviour. Anisotropy must be taken into account when working with this material and, given the difficulties involved in its determination, the laboratory field may be better applied parallel to the NRM. The final results are not by themselves able to elucidate the past behaviour of the field, but show that burnt sandstone from the North of England is a promising material for the investigation of archaeointensity.

Chapter 14

Archaeomagnetism of an 18th C Delftware kiln

14.1 Background

In November 2007 members of the Geomagnetism Laboratory, University of Liverpool were invited to sample a brick kiln floor during North Pennine Archaeology Ltd's excavations at Luneside East, Lancaster (54°N, 2.5°W). Historical documents showed that a Delftware kiln had stood on the site and was operational until 1785. Many tons of broken pottery along with saggars and wastars in pits around the kiln could be firmly identified as being part of the Delftware industry, and there was little doubt that the brick floor was the remains of the kiln. Plaster was poured over the bricks and allowed to set using a Perspex plate and bubble level to ensure a level surface (see figure 14.1).

Figure 14.1 Photograph of sampling procedure, showing plaster with bubble level.

After the plaster set magnetic north was scribed onto the plaster as well as a sunsight when conditions permitted. Subsequent calculations showed the two methods of orientation to be consistent and there is no reason to assume strong deflection of the compass where this was used alone. A total of thirteen orientated monoliths were taken from the kiln floor and flues (see figure 14.2). In addition a further one unorientated brick and a number of fragments of saggars and wastars from the nearby waste heap were taken.

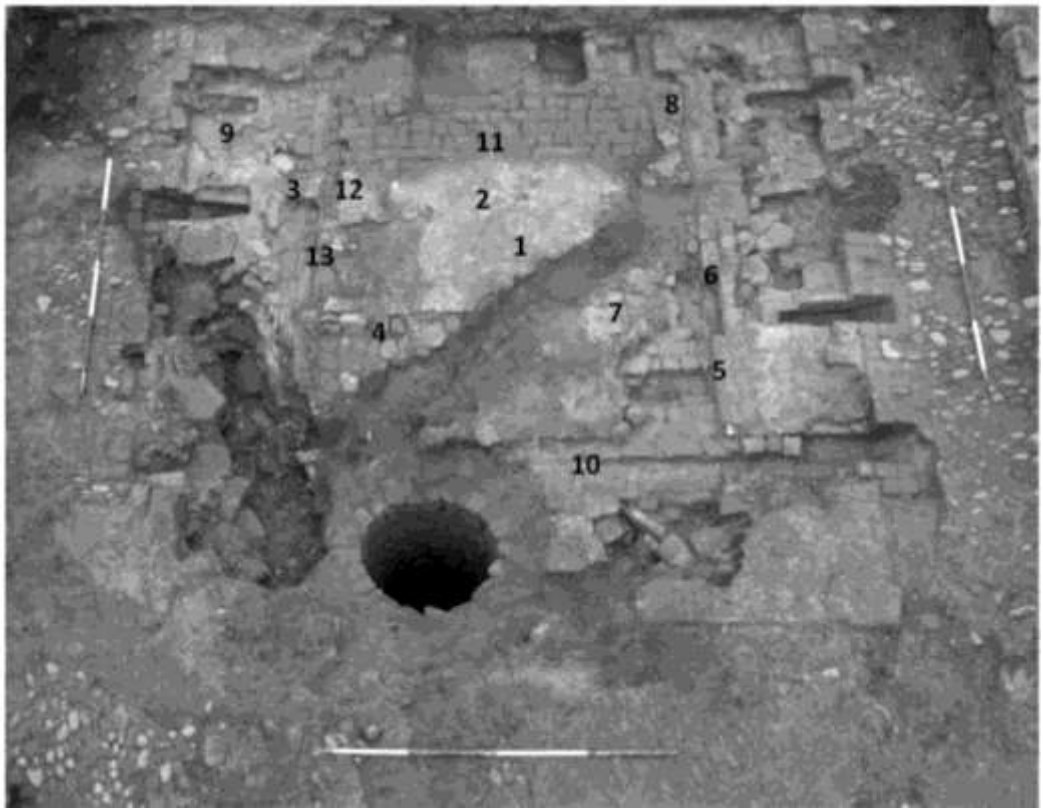

Figure 14.2 Plan photograph of the kiln floor, showing the locations of the bricks that were taken for analysis

As the samples were orientated it was decided to subject them to thermal demagnetisation as the small cores used in the microwave method makes orientation difficult. For this reason it seemed appropriate to carry out a Thellier style archaeointensity experiment.

14.2 Magnetic properties

The bricks themselves displayed a variety of composition and colour with varying degrees of vitrification on the surface. Some proved too friable to drill in the laboratory and in total eight individual monoliths finally provided sixteen cores of enough integrity to measure. The susceptibilty of each was measured on a Bartington MS1 and the remanent magnetisation was measured using either an Agico JR6 or a FIT squid magnetometer. A brief description of each individual sample is given in table 14.1 along with the susceptibility, the NRM and the Koenigsberger ratio, Q. The samples are named firstly by the number of the monolith they were taken from (see figure 14.2), then each core is given a letter and where more than one sample comes from the same core this is given a

number. Cores were of variable size and weight so in this case susceptibilties and NRM are given in mass specific units.

Table 14.1 Description and bulk magnetic properties of each sample

Sample	Description	Susceptibilty ($m^3/kg \times 10^{-6}$)	NRM(mAm^2/kg)	Q
1A	Mauve clay with red inclusions	0.23	0.53	57.4
1B	Purple and green clay with inclusions and some vitrification	1.22	0.75	15.4
2A	As 1A	0.20	0.27	34.9
2B1	As 1A	0.49	1.58	79.9
2B2	As 1A	0.46	1.10	59.2
5A	Dark brown, gritty	6.65	5.29	19.9
6A	Brown, gritty, large,creamy inclusions	2.78	2.15	19.3
6B	As 6A	7.29	5.73	19.6
7A	Reddish brown, sandy with inclusions	2.91	3.64	31.3
7B	As 7A	3.58	3.09	21.6
9A	Orange pink clay with small inclusions	2.13	2.23	26.2
9B	As 9A	2.79	3.46	30.9
10A	As 1A	1.36	0.58	10.6
10B	As 1A	1.54	0.60	9.8
12	Brown red clay with pale inclusions and swirls	1.68	1.19	17.7
13A	Pale yellow /white clay and grit	1.53	1.41	23.1
13B	As 13A	0.65	0.79	30.5
13C	As 13A	0.97	1.22	31.2

The susceptibilities vary by over an order of magnitude, but there is less variability in the Koenigsberger ratios which are all high. The samples come from bricks of very different

material composition and so it may be expected that the magnetic mineralogy is also variable. Such an assemblage is often regarded as a useful recorder of magnetic field intensity because it is less likely to suffer from undiagnosed bias. The magnetic mineralogy was further investigated using an MM VFTB. Chips weighing around 120mg were taken from each brick next to where the cores were taken and subjected to four analyses: IRM acquisition, coercivity, hysteresis and saturation magnetisation as the sample was heated to 700°C and cooled. It should be noted, however that given the large degree of heterogeneity visible in all the cores, the small sample used for this may not perfectly reflect the bulk composition of the sample used for archaeointensity. Some examples of these analyses are shown in figure 14.3.

Figure 14.3 (a-h) : IRM acquisition, coercivity, hysteresis and thermomagnetic behaviour for bricks 2,5,6 ,7, 9,10,12 and 13. Comments on each specimen are given adjacent to each diagram. All magnetisations are given in arbitrary units (a.u.).

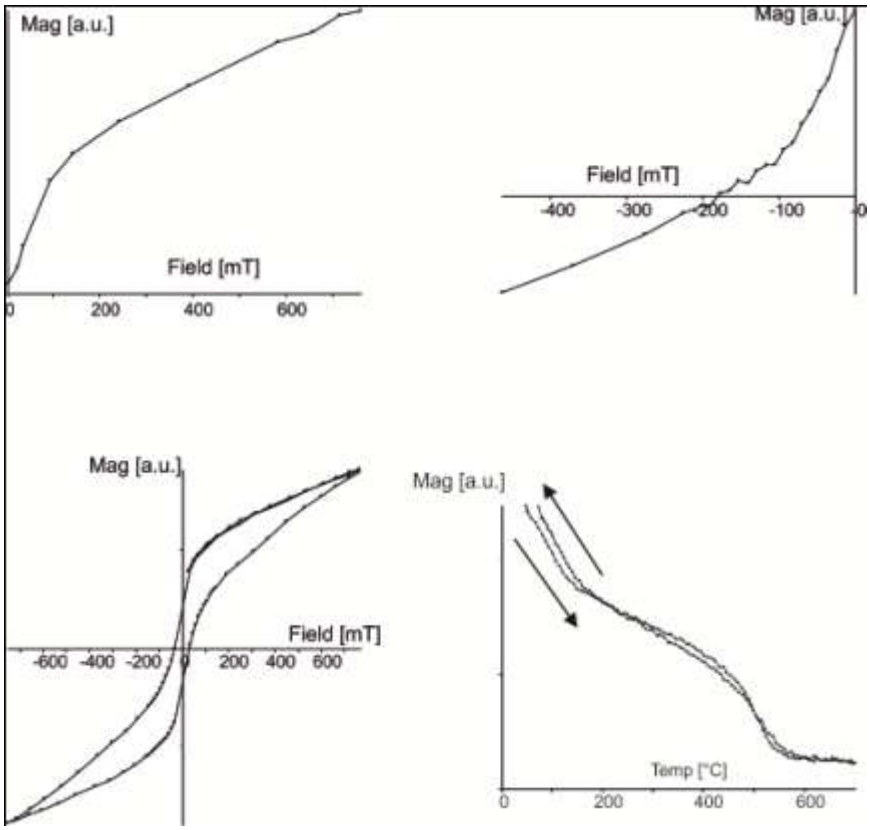

Figure 14.3(a). Rock magnetic analyses for brick 2, showing a reversible thermomagnetic curve and a high coercivity component, most probably haematite.

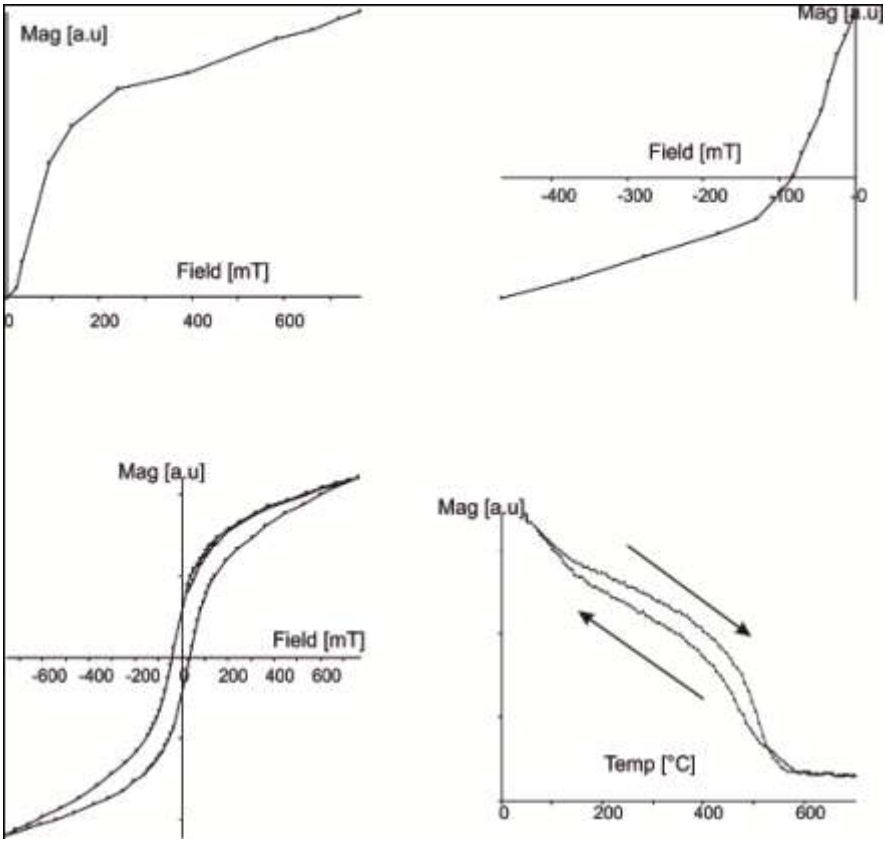

Figure 14.3(b) Rock magnetic analyses for brick 5. The IRM has not saturated by 700mT, indicating the presence of haematite. There is some alteration on heating.

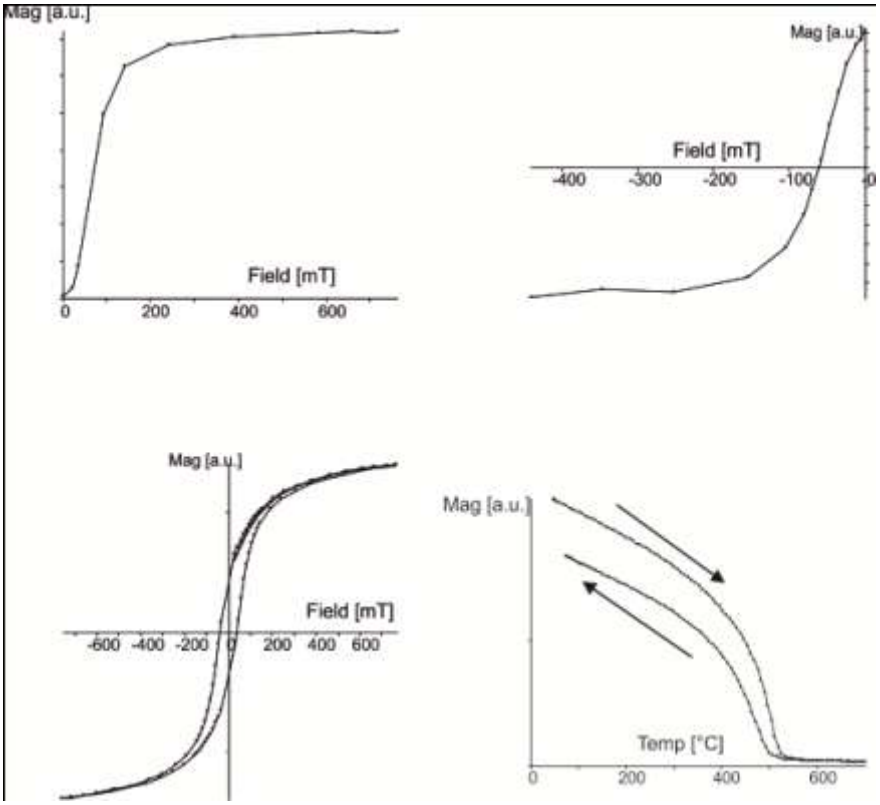

Figure 14.3(c) Rock magnetic analyses for brick 6. The IRM saturates by 300mT. The Curie temperature is too low for pure magnetite.

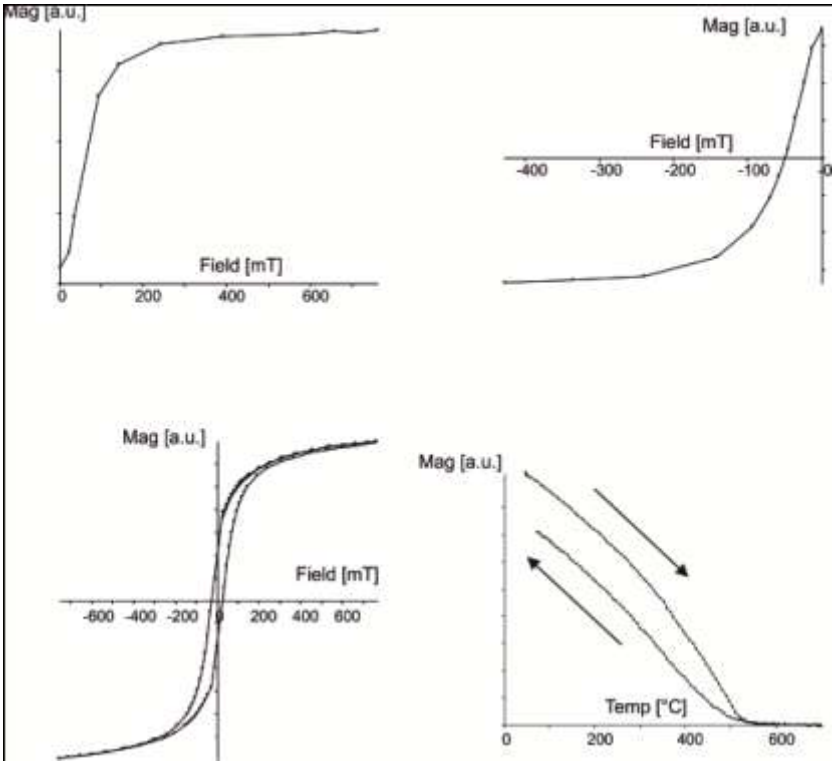

Figure 14.3(d) Rock magnetic analyses for brick 7. The behaviour is similar to brick 6. Note the decrease in magnetisation after heating.

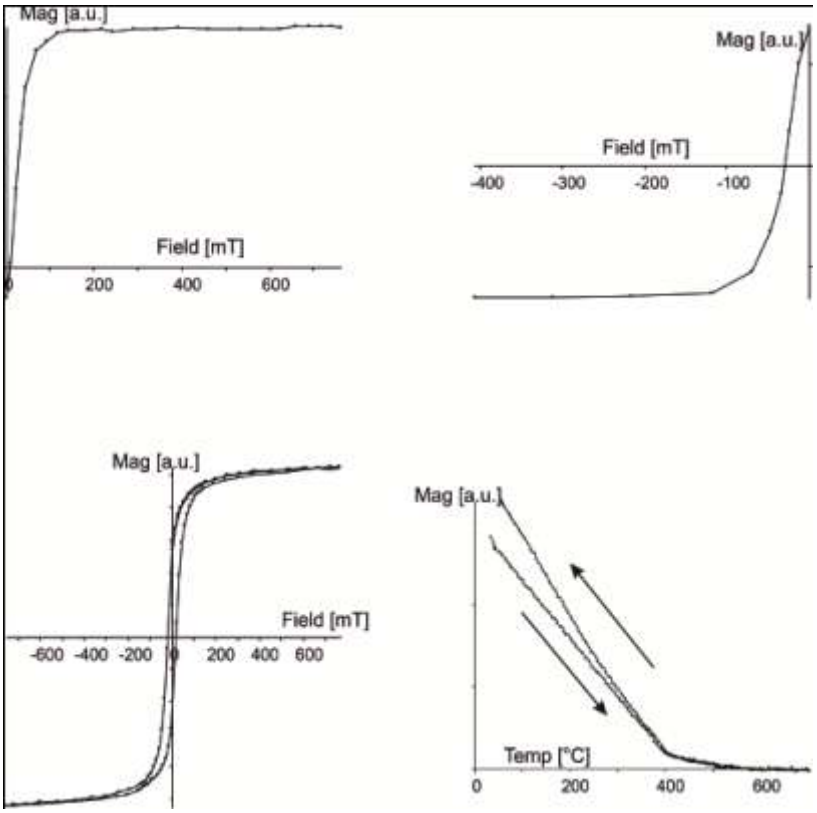

Figure 14.3(e) Rock magnetic analyses for brick 9. The coercivity is much lower than in the other specimens. The thermomagnetic curve shows two distinct Curie temperatures.

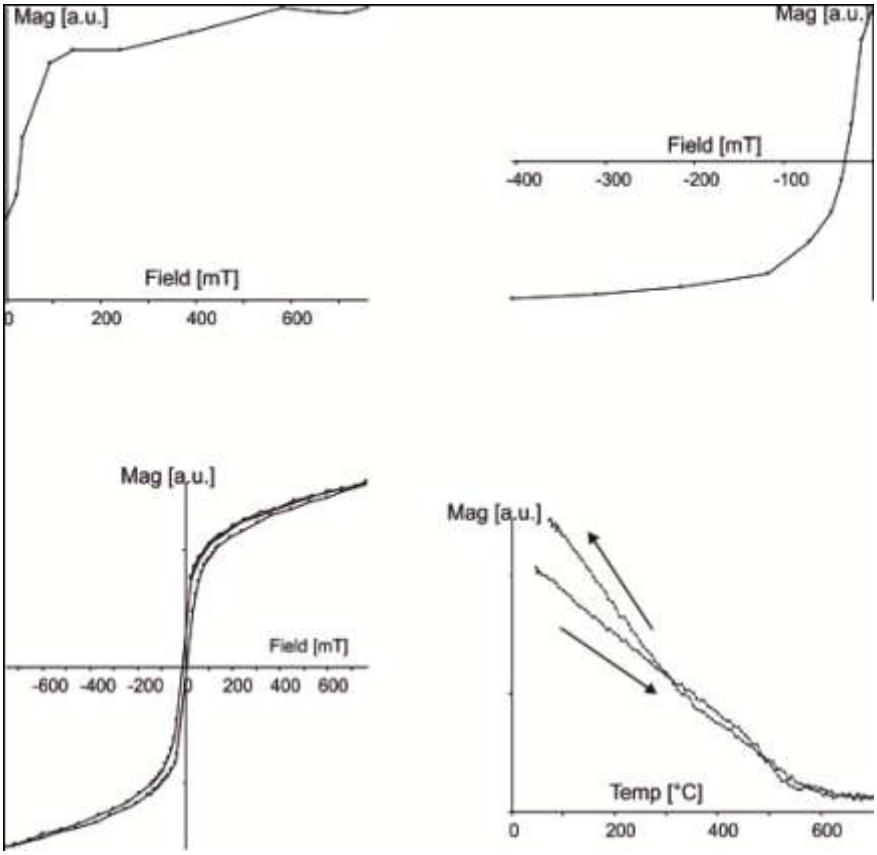

Figure 14.3 (f). Rock magnetic analyses for brick 10. Some small amount of alteration occurs on heating

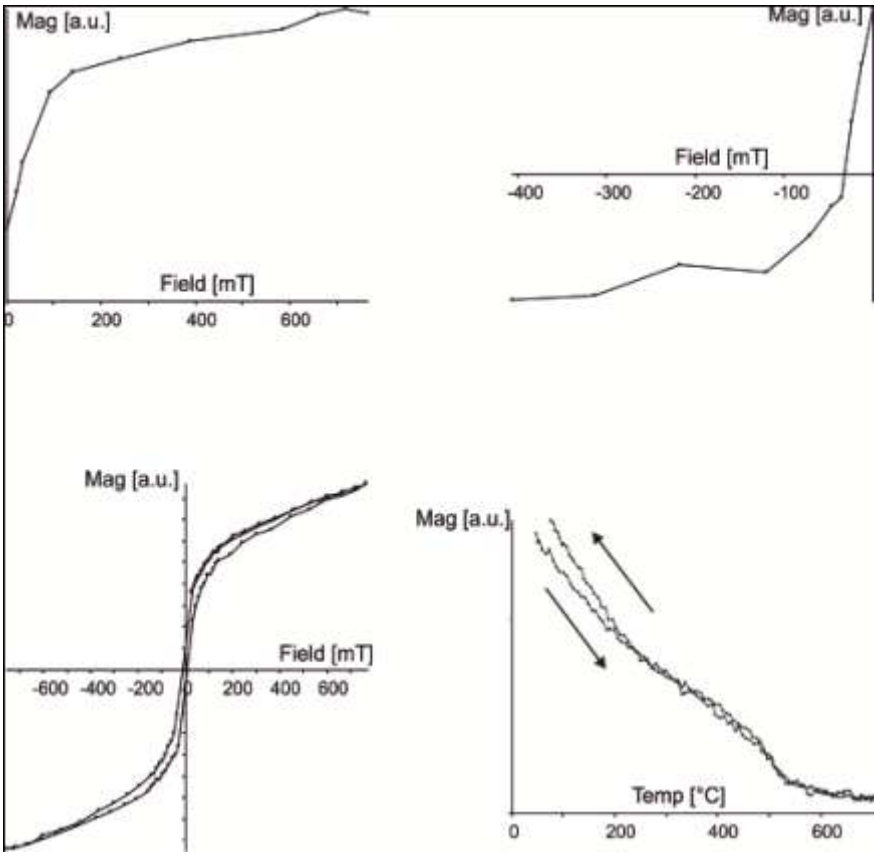

Figure 14.3 (g). Rock magnetic analyses for brick 12. The thermomagnetic curve shows little alteration on heating.

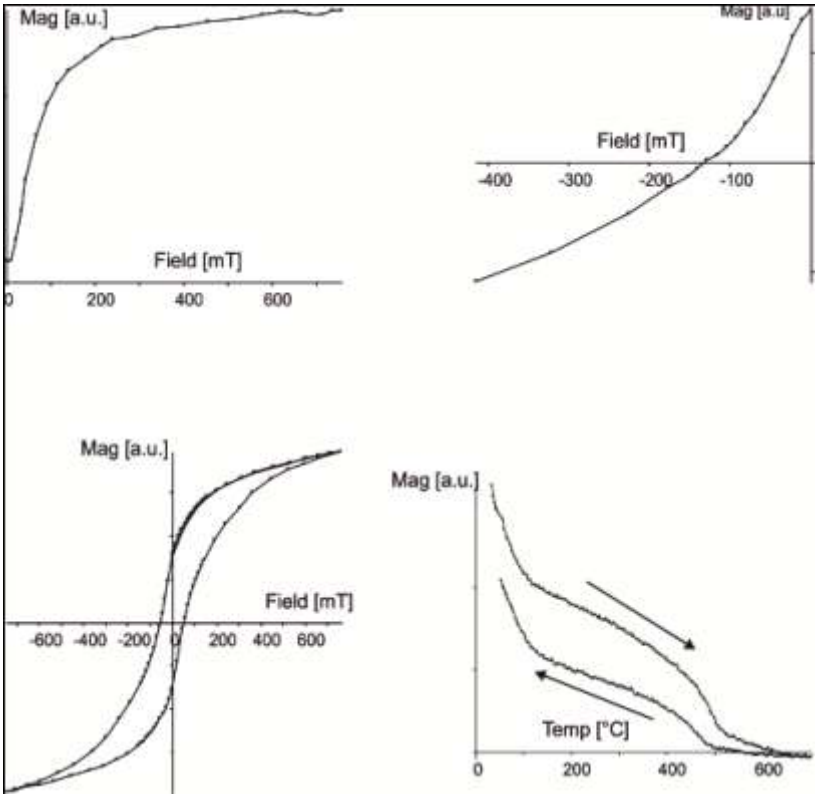

Figure 14.3 (h). Rock magnetic analyses for brick 13. The thermomagnetic curve shows a large decrease in saturation magnetisation after heating.

The analyses reveal a variety of magnetic mineralogies, with some samples saturating quite easily while others are definitely rich in haematite. Many of the bricks failed to give reversible thermomagnetic curves, but as it was not clear at what temperature alteration was occurring it was decided to subject the entire assemblage to Thellier archaeointensity study. The choice of samples was driven more by practicality than mineralogy in that many of the bricks were quite crumbly and a conventional Thellier experiment involves a great deal of manipulation of the samples, with every step requiring the loading and unloading of the oven, so requires samples of reasonable integrity.

14.3 Archaeointensity method and results

The samples were heated in a MM thermal demagnetiser, first in a zero field and then in an applied field of 50µT at the following steps 150°C, 250°C, 300°C, 350°C, 390°C, 430°C, 470°C, 500°C, 530°C, 560°C and 590°C. A zero field step at 200°C was also carried out and any samples that showed an appreciable loss of moment were also given an applied field at this temperature. Samples were held at temperature for 20 minutes. Tailchecks and pTRM checks were carried out at 250°C,390°C and 500°C and 590°C. The anisotropy of TRM was determined by applying a 50µT field at 530°C along the x,y and z axes of the sample. This

was done after the completion of the Thellier experiment so some amount of alteration may have taken place. Figure 13.4 gives the NRM/TRM plots and vector endpoint diagram for the zero field steps for each of the samples.

Figure 14.4 NRM/TRM plots and vector endpoint diagrams for the samples studied

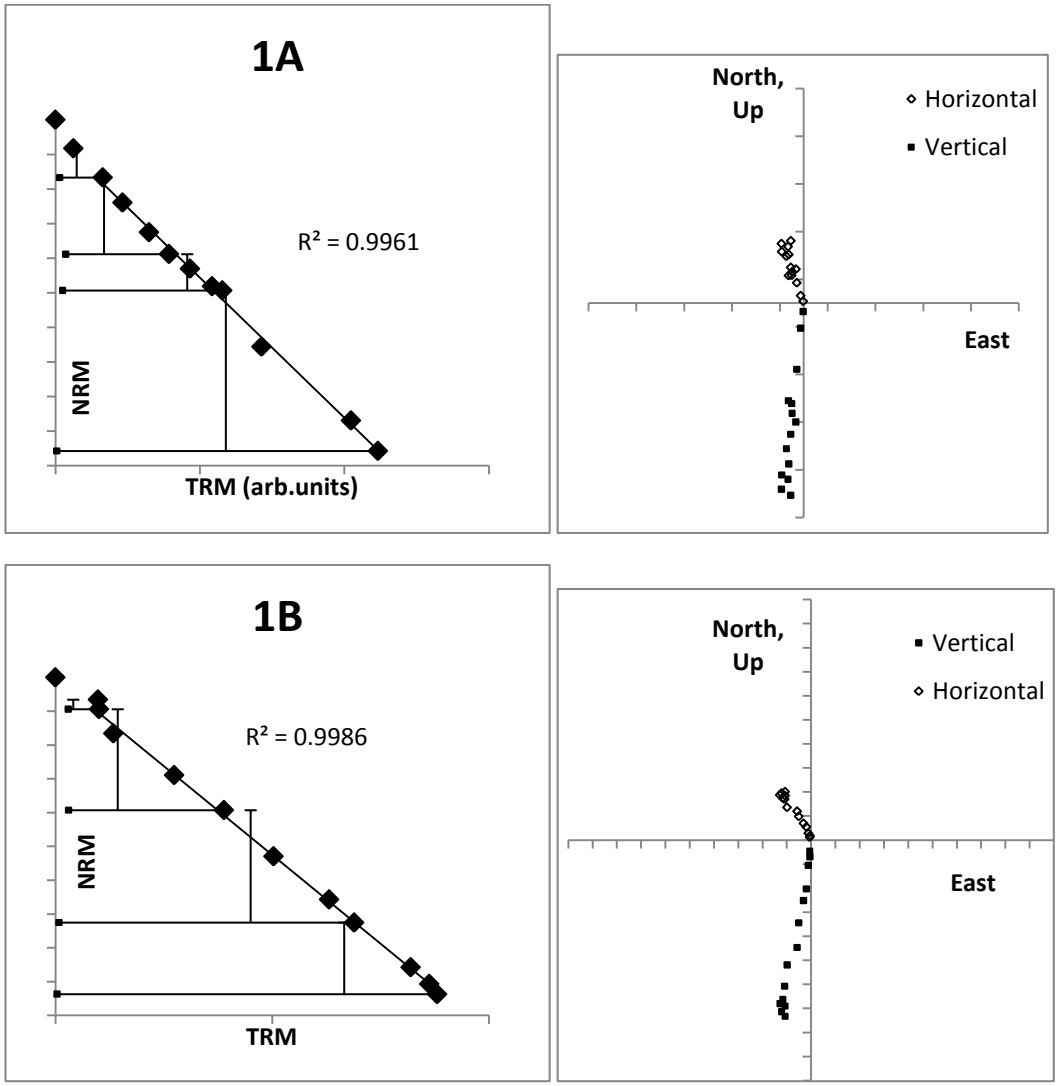

Figure 14.4 continued

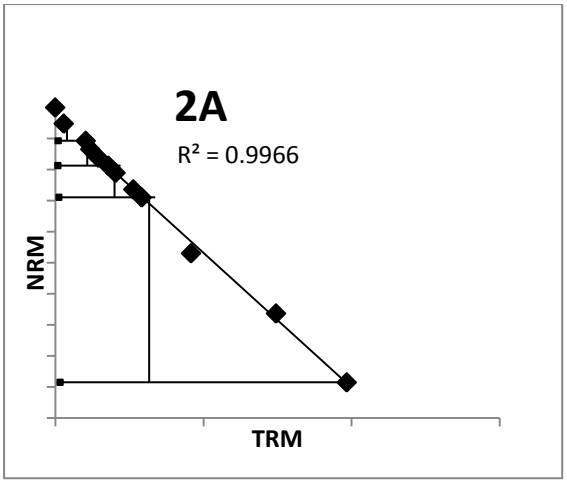

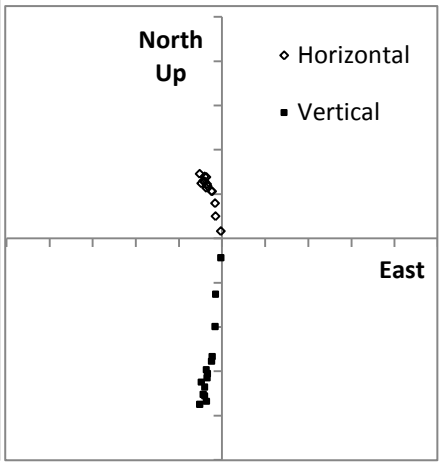

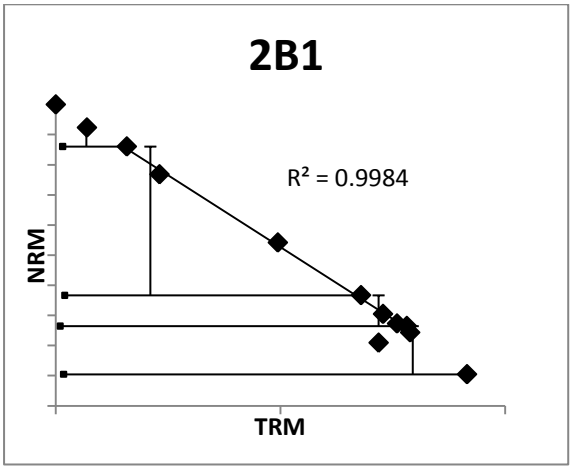

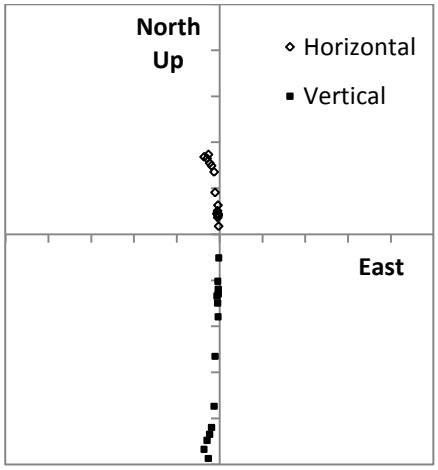

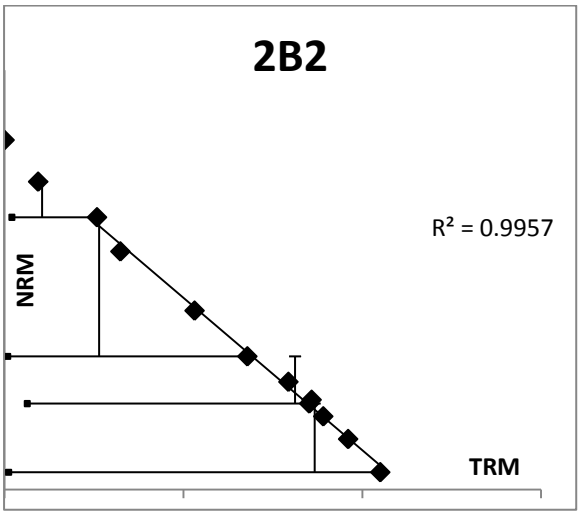

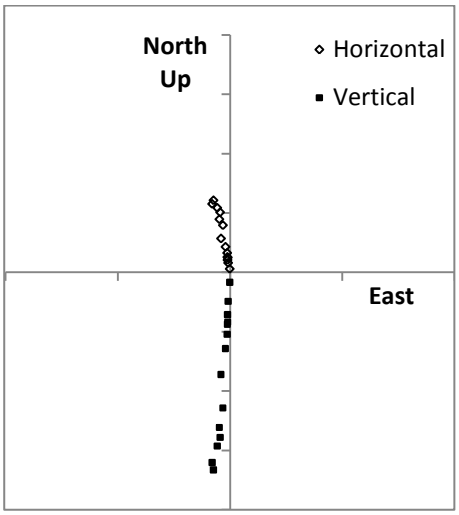

Figure 14.4 continued

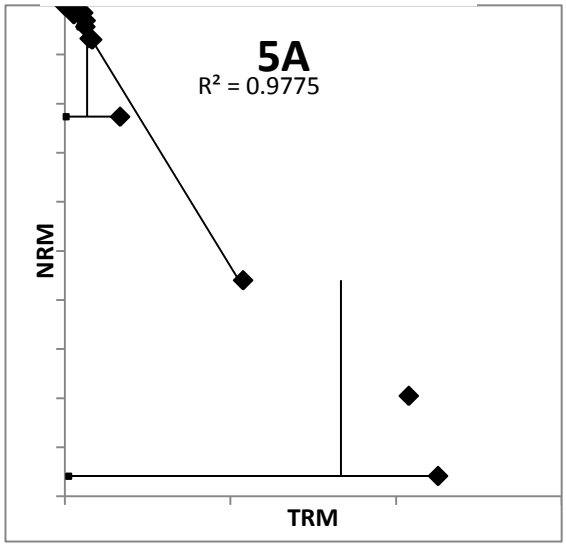

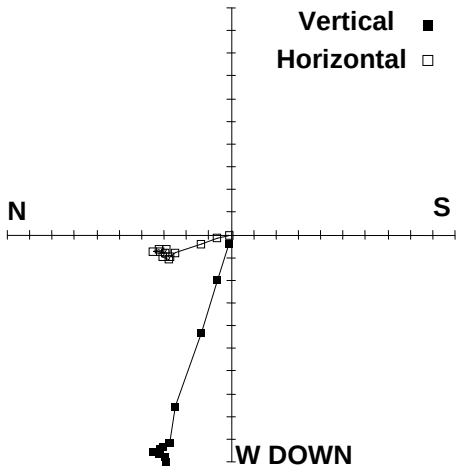

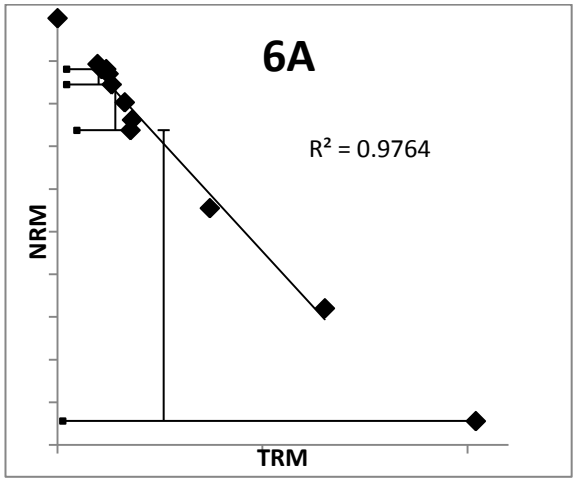

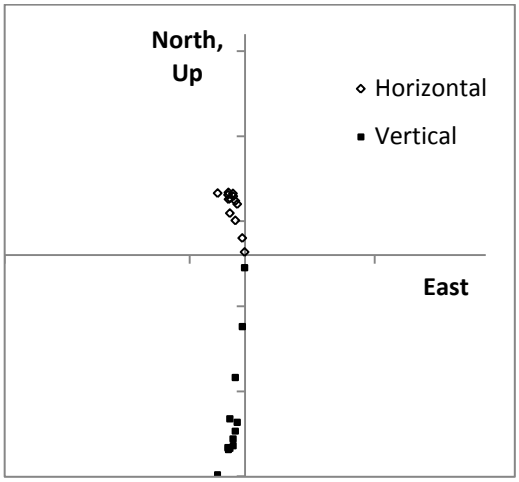

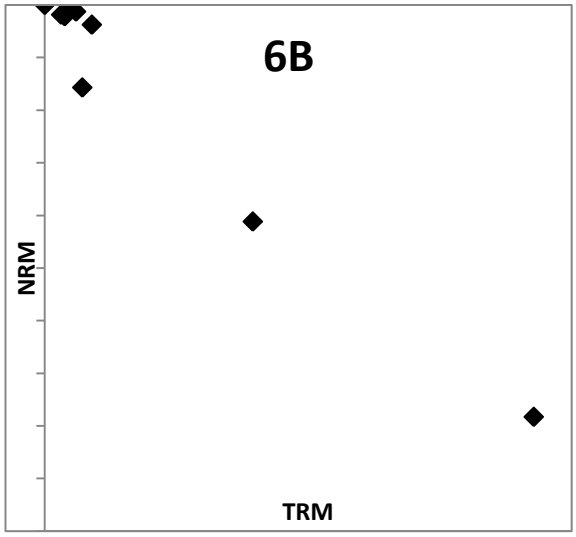

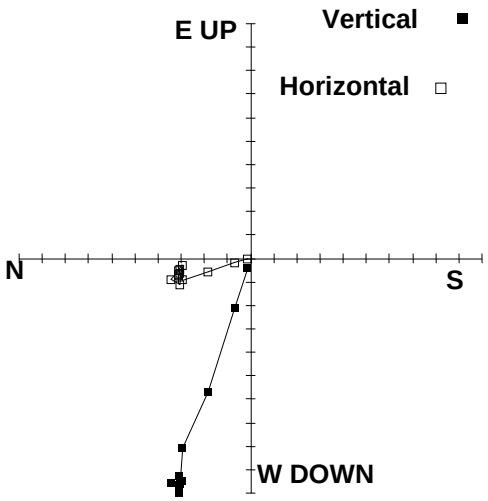

Figure 14.4 continued

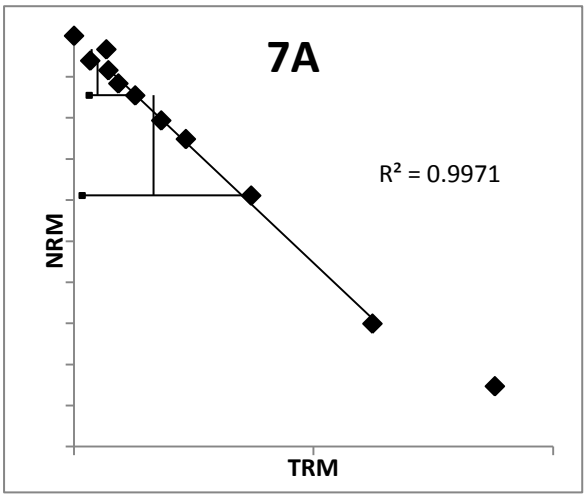

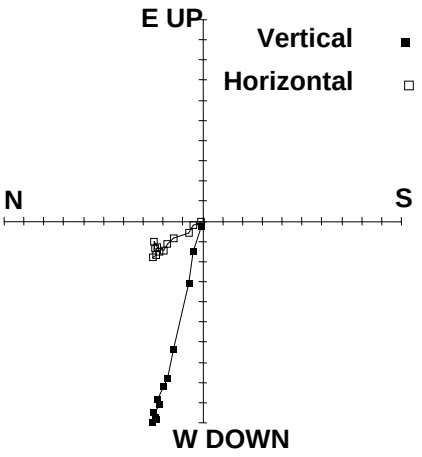

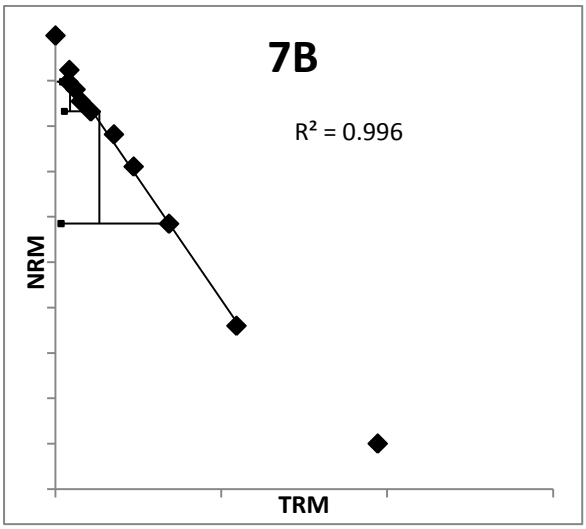

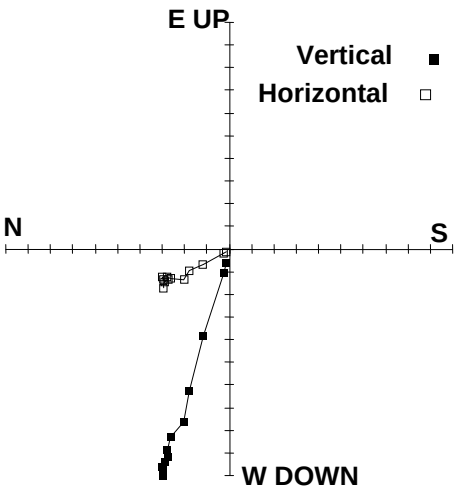

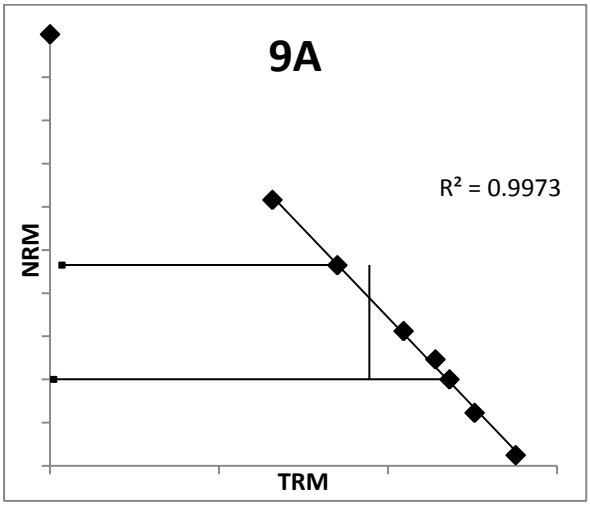

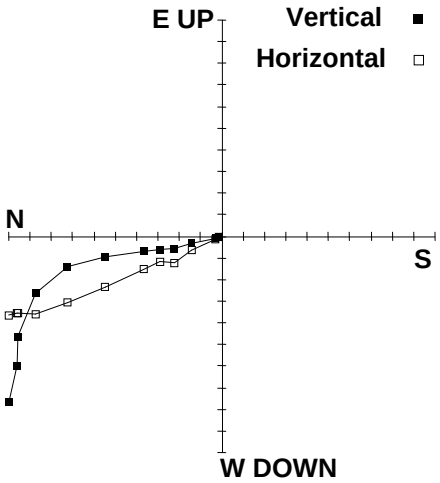

Figure 14.4 continued

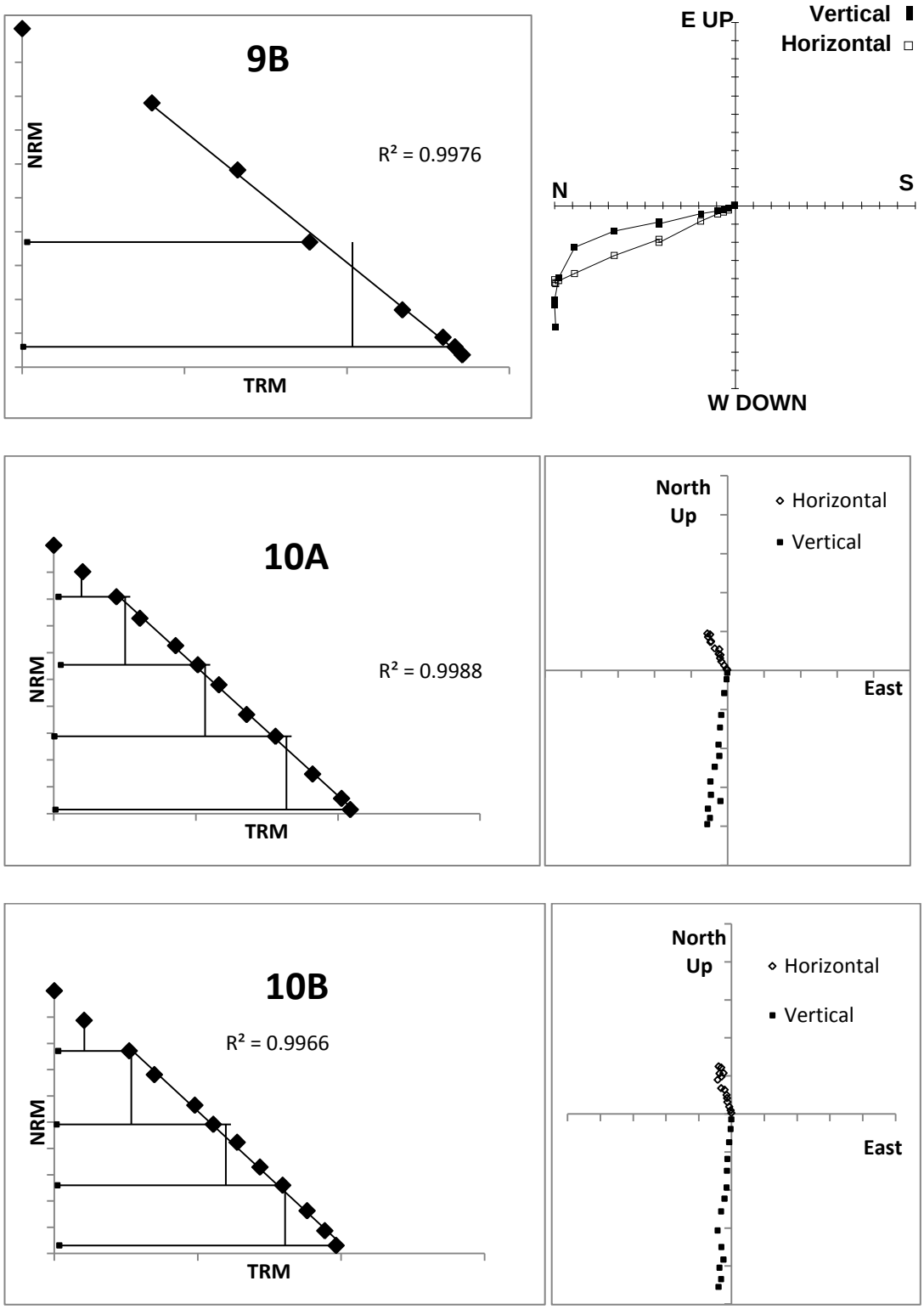

Figure 14.4 continued

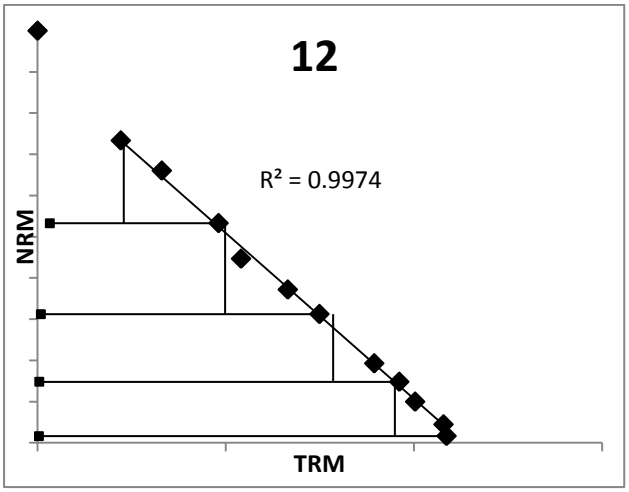

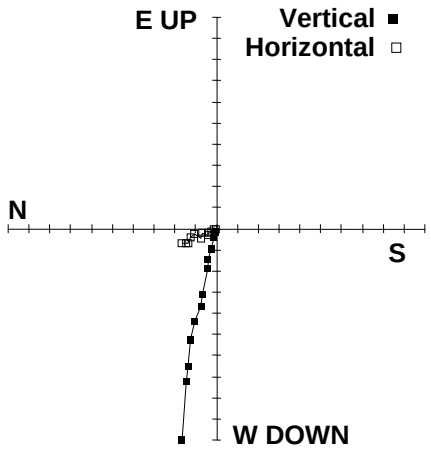

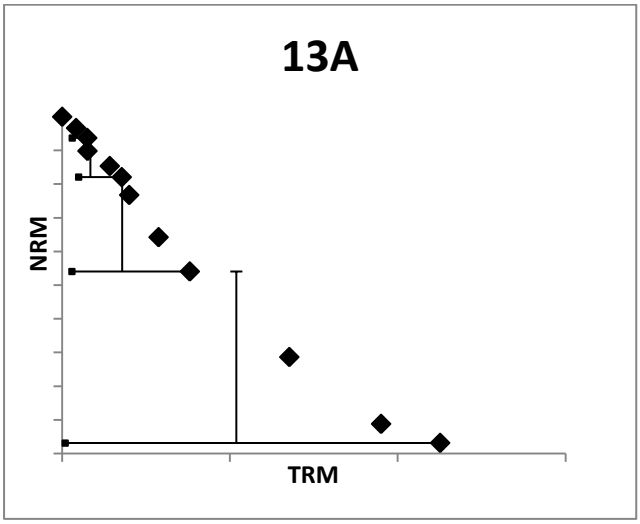

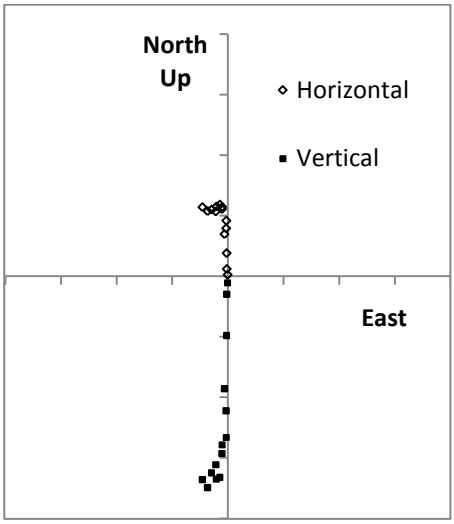

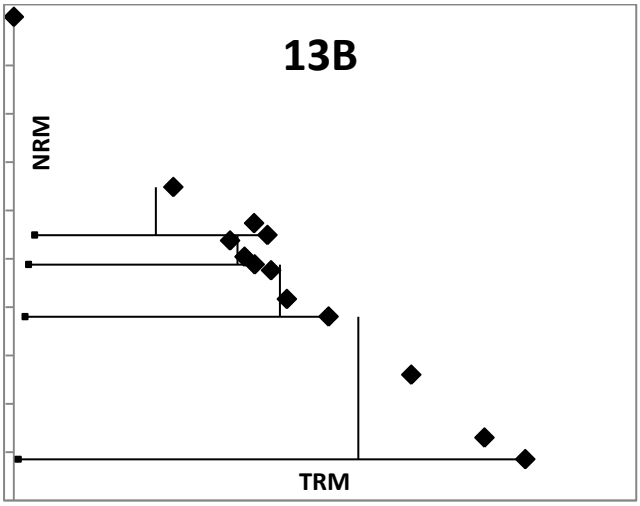

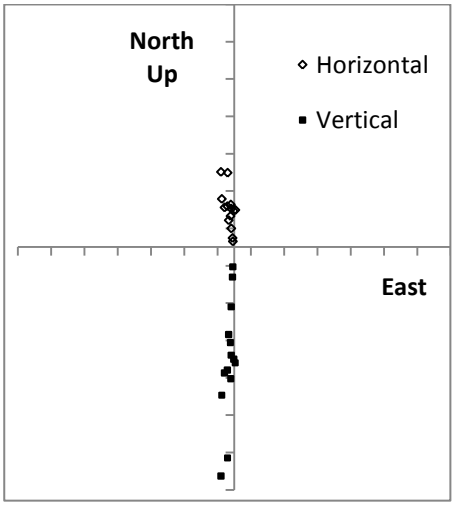

Figure 14.4 continued

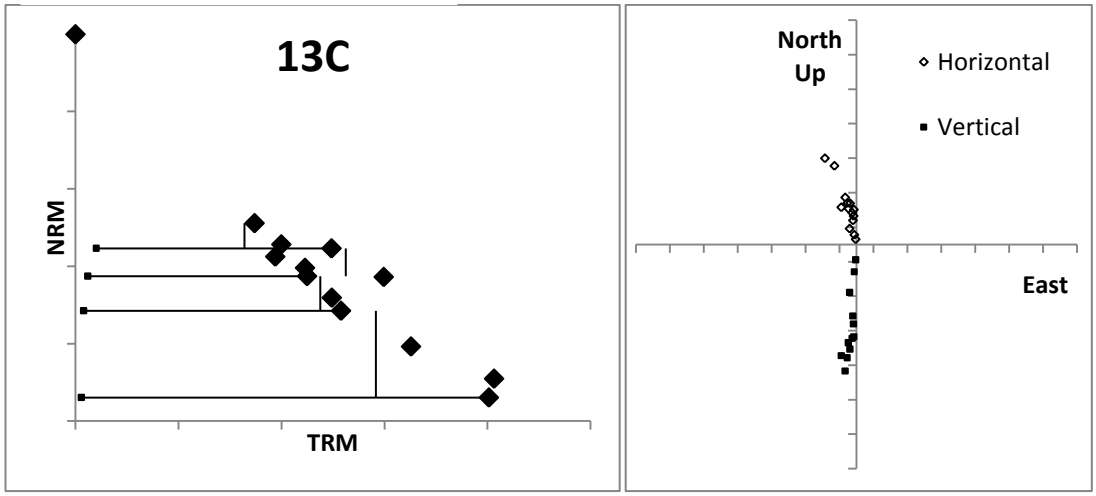

Before the various criteria for acceptance and calculation of results are considered, some of the general features seen in figure 14.4 will be discussed. Cores 1 and 2 appear to give satisfactory results and the anomalous point seen in the NRM/TRM plot for sample 2B1 is associated with a large uncertainty in the magnetometer. Poor results are seen in core 5 and 6, both of which could be described as grit and stones rather than clay. Some of the problem in these cores may be due to the lack of strength and there was some difference in mass between the start and finish of the experiment. In addition sample 6A retained its remanence to a high temperature making it unsuitable for archaeointensity, where a range of blocking temperatures is desirable. Core 13 gave very poor results and while 13A has successful checks at low temperatures, the direction is not stable with a large, probably viscous, overprint. The samples from core 9 have both been insufficiently heated to reset the magnetisation completely, but NRM/TRM plots have been given for the remanence unblocked above 350°C (9A) and 300°C (9B). These will be dealt with separately later. The estimated field and Coe statistics for the remaining samples are given in table 14.2.

Table 14.2 Estimated fields and statistics for selected samples

Sample	Number of points	MAD	f	g	q	Estimated field (μT)	Standard error (μT)	Coe error (μT)
1A	10	3.3	0.79	0.84	29.8	40.63	0.9	1.36
1B	11	2.1	0.87	0.89	49.73	53.34	0.8	1.07
2A	11	3.1	0.83	0.82	36.74	43.59	0.81	1.19
2B1	7	1.0	0.6	0.73	24.29	47.48	0.85	1.95
2B2	10	1.8	0.73	0.85	26.83	43.73	1.01	1.63
5A	7	17.9	0.55	0.54	4.37	55.87	3.76	12.77
6A	10	5.3	0.56	0.7	7.22	52.94	2.88	7.33
7A	7	2.7	0.62	0.67	17.34	55.02	1.32	3.17
7B	8	2.7	0.54	0.74	15.50	53.08	1.36	3.42
9A	7	2.3	0.59	0.8	20.47	40.99	0.95	2.00
9B	7	1.9	0.74	0.76	25.75	38.77	0.85	1.51
10A	10	2.1	0.79	0.88	58.01	48.22	0.58	0.83
10B	10	2.4	0.74	0.88	31.94	50.59	1.04	1.58
12	10	2.6	0.69	0.87	33.47	40.33	0.73	1.21

Sample 7A is a good example of the kind of subjectivity that becomes difficult to avoid when interpreting Thellier experiments. The trendline as shown in figure 14.4 terminates at the penultimate point but it is possible to choose to extend it to the final point or to include one fewer point. Consider the difference that doing this makes to the field estimate (table 14.3).

Table 14.3 Estimated fields and quality factors for different choices of points in the NRM/TRM diagram for sample 7A

Number of points	Field	Standard error	Coe error	q
6	50.37	0.98	4.48	11.3
7	55.02	1.32	3.17	17.3
8	49.65	1.97	3.41	14.6

Choosing seven points gives marginally the better fit, but whether it results in a more accurate estimate of the field is impossible to say. The data set is reduced considerably when the pTRM checks and tailchecks are taken into consideration. A reproducibility of within 10 % of the original is often required, although another suggestion is the DRAT criteria (Selkin and Tauxe 2000) where the difference is normalised by the length of the trendline selected. It might be argued that this length has no physical meaning and this

approach is somewhat ad hoc. Nevertheless, as it is a commonly used parameter it is included here. Firstly we require β, the ratio of the standard error to the field estimate (see chapter 5) to be no more than 5% and the MAD over the range of interest to be less than 5°, thus excluding 5A and 6A (see table 14.4).

Sample	Tailchecks	pTRM	DRAT
1A	9%	13%	5%
1B	8%	16%	5%
2A	5%	10%	2%
2B1	10%	25%	6%
2B2	7%	16%	12%
7A	25%	11%	3%
7B	25%	19%	4%
9A	4%	10%	10%
9B	2%	13%	11%
10A	4%	5%	2%
10B	2%	7%	4%
12	6%	5%	3%

Table 14.4 Maximum percenatge difference in tail and pTRM checks for the assemblage. DRAT is defined by Selkin and Tauxe (2000).

Taking the complete suite of results of samples in table 14.2, other than those from brick 9 whose remanence may predate that of the others, gives a mean of 47.6± 1.7 μT from 10 samples. If we exclude those with tailchecks differing by more than 10% and DRAT greater than 10%, samples 1A, 1B, 2A, 10A, 10B and 12 remain giving 46.1±2.2 μT from 6 samples. The two results are indistinguishable and either may be accepted as a field estimate but here the smaller suite of six results will be considered in greater detail.

It proved impossible to determine the anisotropy of TRM with any precision, and the resulting correction for each of the six results considered was largely negligible in each case. The corrections were -1%,-1%,+1%,4%,+3% and+1% . After applying them the field estimate was found to be 46.7±2.3 μT. The likelihood that the anisotropy corrections are justified is diminished when it is realised that they do not reduce the dispersion of the data. This is seen even more clearly in the directional analyses that will be considered next. An attempt to determine a cooling rate correction was made but there was no consistency between the fast cooled TRMs showing that alteration was taking place during the intervening slow cooling. As pointed out in chapter 6, cooling rate corrected results show systematic bias to low values and should be treated cautiously, despite the theoretical justification of the procedure, so their failure should not be regarded as indicative of an unreliable result.

14.4 Archaeodirection

Table 14.2 reported the MAD taken over the points used to determine archaeointensity but in the case of 5A , when this was unacceptably large there was still a clear direction of primary remanence that could be isolated. Also the samples form brick 13, showed reasonably straight-line demagnetisation plots although 13A exhibited something akin to a two component remanence and the resulting direction was not considered to be reliable. Table 14.5 gives the directions and MADs of the remaining 15 samples.

Table 14.5 Direction and maximum angle of deviation (M.A.D.) of samples with a single component of remanence.

Sample	Declination	Inclination	M.A.D.
1A	338.7	71.8	3.2
1B	321.8	71.7	2.1
2A	338.2	68.3	3.2
2B1	349.6	69.7	1.6
2B2	345.1	70.1	1.8
5A	336.0	71.1	1.4
6A	343.8	69.6	3.3
6B	337.0	70.2	2.8
7A	323.0	74.1	2.1
7B	331.7	71.1	2.3
10A	326.4	74.1	2.5
10B	335.2	72.8	2.4
12	334.5	77.4	3.6
13B	351.6	71.5	2.7
13C	344.9	69.4	3.7

The directions are plotted in figure 14.5.

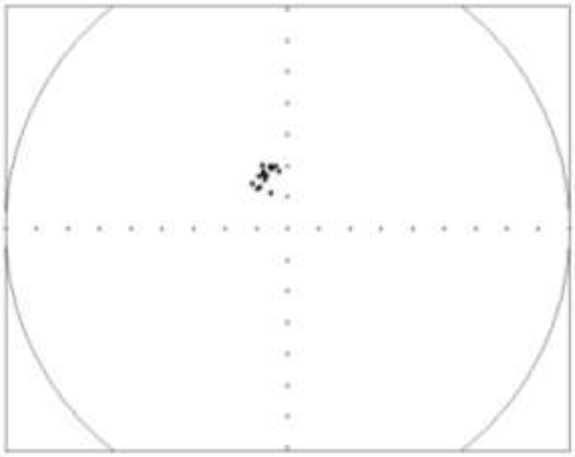

Figure 14.5 Circular plot of the directions in table 14.5

The mean direction is 22.3°W, with an inclination of 71.7° and an α_{95} of 1.7°. The mean direction with 95% confidence limits is compared with the prediction of the field model gufm (Jackson et al. 2000) for the site in figure 14.6.

Figure 14.6 Mean direction and 95% confidence limits from the kiln compared with the field model gufm.

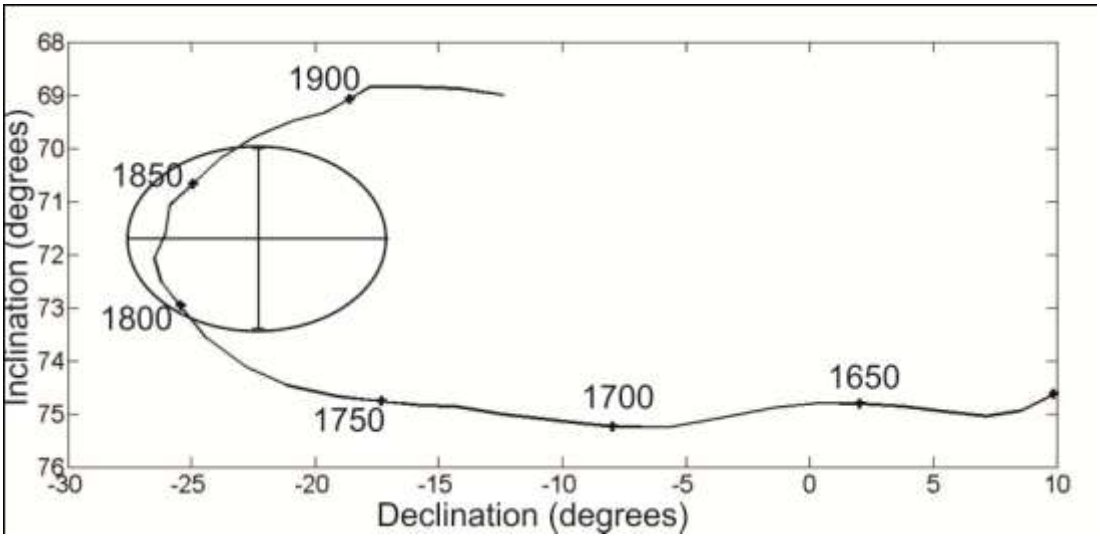

The inclination is rather too shallow to fit the direction expected from gufm with the 95% confidence limit excluding dates before around 1800. It is common practice however in archaeomagnetic dating to add 2.4° to the inclination of floors and flat structures to allow for "magnetic refraction" (Aitken and Hawley 1971). Such a correction would make the archaeodirection entirely congruent with the model in this case and yield an accurate date for the firing of the structure, but as the purpose of this study is neither to determine the direction of the field nor the date of the last use of the kiln, the question of refraction will be looked at closely. Little, if any , consideration has been given to the effect of "refraction" on archaeointensity and previous attempts to model the phenomenon (Lanos 1987, Abrahmsen 1992, Soffel and Schurr 1990) have been found wanting as they require unrealistically large susceptibilities to account for the observed distortion in the field.

Before considering refraction in detail, the effect of the anisotropy on the archaeodierection can be calculated. Assuming the matrices for the anisotropy of TRM determined experimentally are accurate, new directions for the field for each sample, can be found. The resulting mean direction is 30.6°W with an inclination of 71.2° and an α95 of 3°. The anisotropy correction increases the scatter in directions and migrates the mean direction away from the expected direction for 1785. This justifies the approach taken

earlier where it was argued that the anisotropy correction could not be considered precise enough to apply to the intensity results. It also suggests that the inclination shallowing is not due to anisotropy but is in fact a case of “magnetic refraction”, which is now considered.

14.5 Magnetic refraction

The shallowing of inclinations in flat structures was observed and quantified empirically by Aitken and Hawley (1971), who explained the phenomenon by refraction of the magnetic lines of force. Later attempts were made to model the effect but these were always done by appealing to the demagnetising field within a magnetised body. Confusingly, this was still termed “refraction” and indeed some authorities have gone as far to state that magnetic refraction is caused by demagnetising fields (Abrahamsen 1992). Even Soffel and Schurr (1990), who solved the potential equations for the boundary conditions imposed by a hemispherical model explicitly, stated that the effect was due to demagnetising fields, rather than refraction in the strict sense of the word. None of the models so far have been capable of producing any significant distortion in the direction of the field if the susceptibilty is less than 0.1, a very large susceptibilty to find in archaeological material. Nor, as far as can bedetermined, has anyone considered the effect on the intensity if the distortion of 2-3° was actually caused by demagnetising fields.

Figure 14.7 shows the geometry of the demagnetising field as considered by Abrahamsen(1992) and Soffel and Schurr (1990), when a slab of susceptibilty χ and demagnetising factors N_x and N_y is placed in a magnetic field H.

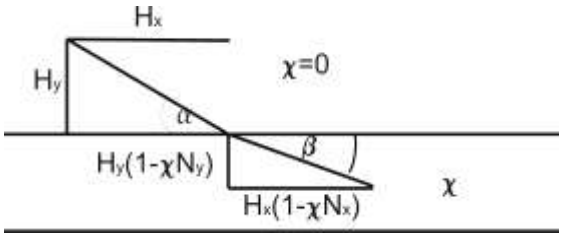

Figure 14.6 The geometry of demagnetising fields in a slab of susceptibilty χ , discussed in the text.

If the slab is infinitely thin N_x is 0 and N_y is 1 and it is easy to show by simple trigonmetry that $\tan\beta = (1-\chi)\tan\alpha$ (14.1). This is what is somewhat misleadingly referred to as the law of refraction. Even for a moderately large susceptibilty of , say, 1% this leads to a distortion of less than 0.2° for a magnetic field inclined at 70° to the slab and this is assuming that a kiln floor is realistically modelled by a homogenous infinitely thin slab.

Naturally occurring materials are not uniformly magnetised but are heterogeneous mixtures of magnetic and non-magnetic grains. Even if theory based on demagnetising field could account for a distortion of 2° in the inclination one would have to consider the corresponding change in the intensity which would be reduced by around 10%, for an incident field of inclination 70°. While in archaeomagnetic dating using directions it is perfectly normal to appeal to the demagnetising field to adjust the inclination, no such corrections are ever proposed for intensity. The demagnetising field theory for inclination shallowing is inconsistent, insufficient and something of a misnomer, yet shallow inclinations are observed in horizontal flat structures.

An alternative explanation based on true refraction is shown in figure 14.7.

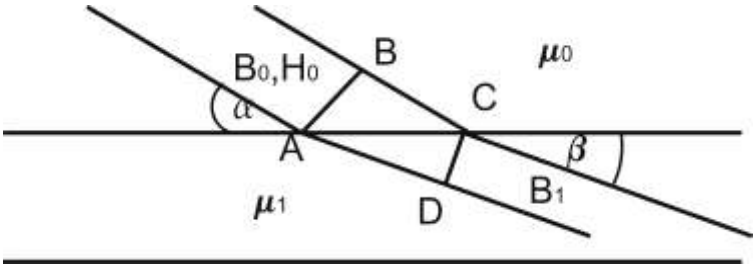

Figure 14.7 Schematic of a field line being refracted on entering a substance of magnetic permeability μ_1 as discussed in the text.

The magnetic flux passing through AB must be the same as that passing through CD, therefore $B_0 \sin\alpha = B_1 \sin\beta$ or $\sin\alpha = (\chi + 1)\sin\beta$ (14.2) Similarly the magnetomotive force between B and C must equal that between A and D, but this is a less useful condition because the H field is not continuous but will be the sum of the field H and the demagnetising fields within individual grains along AD. If H_1 was uniform along AD then we could write $H_0 \cos\alpha = H_1 \cos\beta$ (14.3). Dividing equation 14.2 by equation 14.3 gives equation 14.1 but this is not a solution to the two simultaneous equations; there is only one value of α and β that satisfies both equations. Equation 14.2 must undoubtedly be true because of the continuous nature of the field B, so as a first order approximation we assume the angle of incidence α to equal the inclination of the ambient field. The actual susceptibilty at the blocking temperature is not known but it is clear that the correction to the inclination is now of the proper order of magnitude. For instance a susceptibility of 1% would give an inclination of 73.5° instead of 71.7°, almost exactly congruent with the model gufm for the site in 1785. From these arguments it is possible to state that the direction of the magnetisation recorded in the kiln floor is consistent with the model gufm and there is no reason to suspect any large local field anomalies due to the presence of iron kiln furniture, for example. This is further supported by the low dispersion seen in the directions. It is reasonable to take the intensity derived from this structure and use it to

examine the evolution of the dipole during the late 18th century if it is accepted that the oft cited phenomenon of inclination shallowing is due to true refraction , rather than internal demagnetising fields.

14.6 A late 18th C dipole low?

The mean intensity is plotted along with the prediction of the model gufm (Jackson et al. 2000), with three different rates of dipole decay, according to the suggestions of Gubbins et al. (2006), Finlay (2008) and the rate proposed in chapter 6 (figure 14.8). The first thing to notice is that the intensity is surprisingly low, lower in fact than the model prediction for

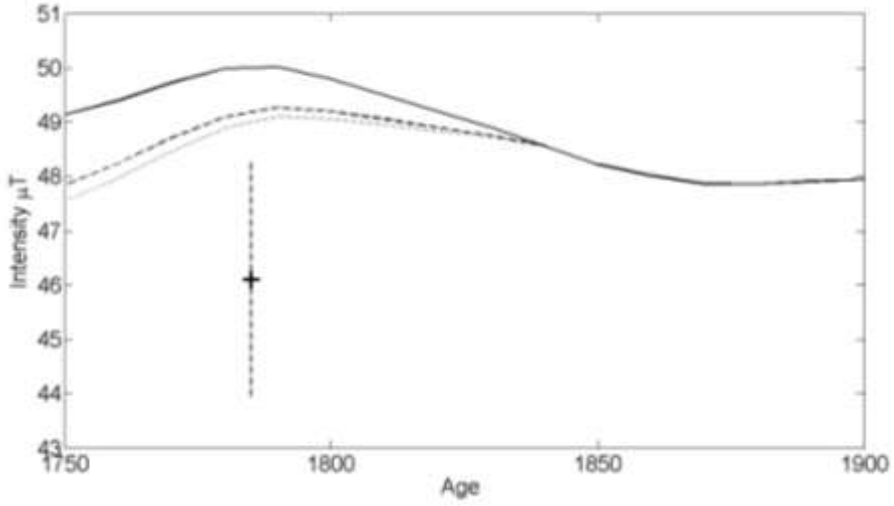

Figure 14.8 Mean intensity of the kiln plotted with gufm scaled by the suggestion of Gubbins et al. (2006) (dotted), Finlay (2008)(feint), and 12nT per year (bold).

In fact it is not possible to reject any of the models shown with any confidence on the strength of this one point. It is worth noting that the maximum in intensity predicted by the model does not coincide with a maximum in inclination and so is a result of non-dipole contributions to the modelled field. The best data set for comparison comes from France (Genevey et al. 2009), but this data may be too far away for a simple relocation assuming a dipole. Instead, the data from Genevey et al. (2009) and the datum from the Lancaster kiln are converted into the corresponding field coefficients of gufm, and the behaviour of the axial dipole g_1^0 is examined (see figure 14.9).

Figure 14.9 The intensity from the kiln (dotted bar) and the intensities for the period from Genevey et al. (2009) converted to the corresponding values of g_1^0 for the model gufm (see chapter 6). Also shown is g_1^0 from the model gufm (solid line) and the suggestion of Gubbins et al. (2006)(dotted line).

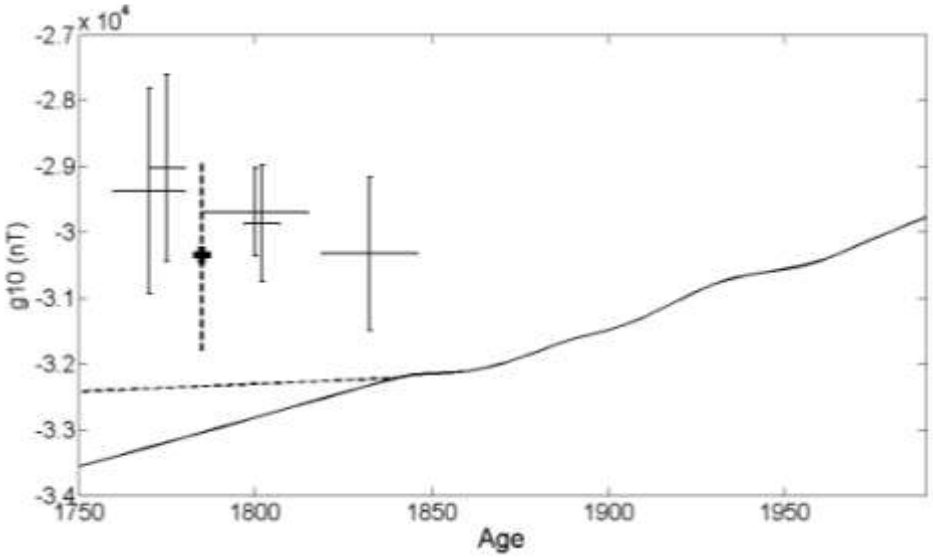

The result from Lancaster is seen to be more or less consistent with the series of archaeointensities from France and may help to confirm the hypothesis that the main field dropped to a low during the 18th Century before recovering and then beginning its present decay (Genevey et al. 2009). There is a danger in scaling global field models by small data sets , however precisely determined (e.g. chapter 6) and the offset between gufm in 1840, and the start of the series of archaeointensities is striking. The only measurements in intensity in from the 1830s came from Germany geographic separation of the sources of data is not great, yet should it be believed that the geomagnetic field increased in strength by around 10% in a few years at the very time people were first experimenting with its measurement? It seems more likely, that while the trend seen in the data in figure 14.9 may be real, the offset is due to inadequacies in the model or crustal contributions to the magnetic field. It is just these questions that require the sort of wider dialogue between modellers and experimentalists that was called for in chapter 6 where it was argued that that archaeointensities, however precisely determined will be subject to systematic effects and the optimal strategy for recovering information about the main global field may be through the analysis of less precise but more widely distributed and more numerous data.

14.7 Partially remagnetised brick

To conclude the analysis of this feature, we now consider the two samples taken from the partially remagnetised brick 9. It would be unwise to firmly assign a date to the event that produced the magnetisation unblocked above 300°C, although it looks consistent directionally with the brick being fired on its side. The kiln appears to have been built in the early 1750s so the brick, and its remanent magnetisation, may date from then or the brick could have been reused from a previous structure. The interest in looking at these samples in detail is to show that although the anisotropy corrections are poorly resolved, when the NRM is not sub-parallel to the applied laboratory field, the corrections become important. The two samples 9A and 9B gave low estimates of intensity: 41 and 38.8 μT respectively. In both cases the principal component of the anisotropy of TRM was close to the z-axis of the core, while the NRM was approximately perpendicular to it. This led to quite large estimates of anisotropy correction: 8% for 9A and 16% for 9B. The resulting intensities of 44.3 and 45.0 μT are much closer to the mean of the assemblage as a whole and we conclude that while the anisotropy determinations were quiet crude and lack precision, they seem to be of the right order when the effect is large.

Chapter 15

Valediction

15.1 Conspectus of results

The principal aim of this study was to produce an archaeointensity record for the UK. In this section all the results obtained are briefly reconsidered to see how well this aim has been achieved. The results are given in table 15.1 where date ranges are best estimates as described in the appropriate chapters. Where this archaeomagnetic data, this has still been given, but must clearly be treated cautiously if being used to constrain field models. Uncertainties are given as best estimates of the standard error of the mean, where possible. Otherwise a nominative uncertainty of 5 μT (e.g. Donadini et al.2009) has been given.

Table 15.1 Summary of archaeointensity results.

Chapter	Material	Age	Dating method /site name	Latitude	Longitude	Intensity (μT)	Error (μT)
7	Burnt clay	600-800	Archaeomagnetism Whitby	54.5	-0.6	49.5	1.0
8	Tobacco pipe	1667-1696	Makers mark T. Hunt, Marlborough	51.4	-1.7	61.3	5
8	Tobacco pipe	1700-1737	Makers mark J.Greenland, Marlborough	51.4	-1.7	50.7	5
9	Brick	1715-1735	Archaeomagnetism Hindhead	51.12	-0.74	64.2	2.4
10	Pottery	1640-1670	Archaeological/ Historical Brookhill	53.2	-3.1	59.8	5.0
11	Tile/kiln lining	1560-1640	Archaeomagnetism Tyler's Green	51.6	-0.7	73	2.1
12	Burnt clay	1070-1120	Archaeomagnetism Glastobury	51.1	-2.7	37.3	5
13	Burnt sandstone	1680-1730	Archaeomagnetism Bolsterstone	53.47	-1.59	51.7	1.3
13	Burnt sandstone	1800-1870	Archaeomagnetism Bolsterstone	53.47	-1.59	48.8	1.1
14	Brick	1785	Historical Luneside East	54.0	-2.5	46.1	2.2

The data come from a fairly small geographical region with a total range in latitude of less than 3.5°. For an axial dipole field, this would result in a variation of less than 3% in the strength of the field at the various locations so it is legitimate to plot the raw data without being too concerned about the need for relocation. The data is shown in figure 15.1 along with all previously obtained data for the UK, taken from the Archeoint database (Genevey et al. 2008).

Figure 15.1 Archaeointensities from this study plotted with all UK archaeointensities in the ArcheoInt database (Genevey et al. 2008)

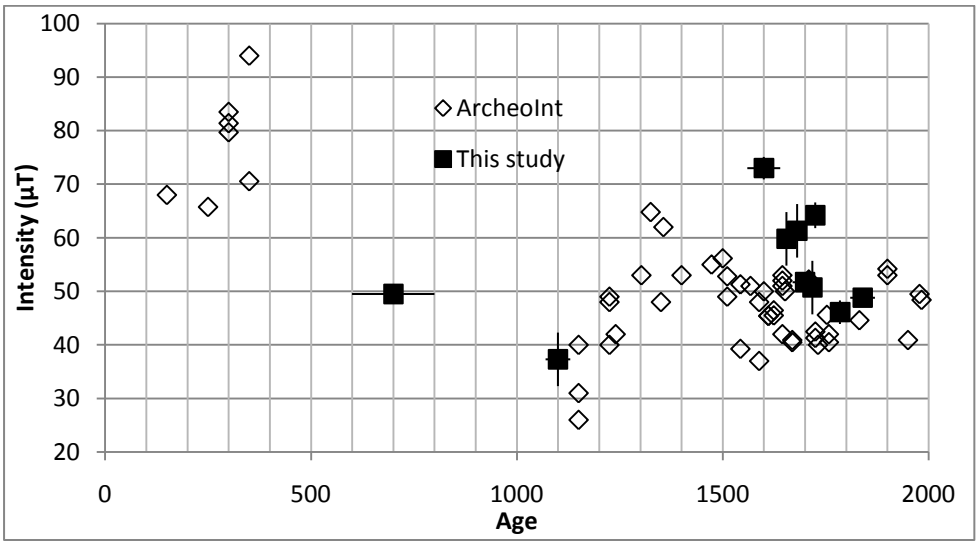

The data acquired here appears to reflect the overall trend of previous studies, but with higher values through the 17th century. In particular, four points can be identified as lying above the general trend in figure 15.1. There are a cluster of three points from the late 16thC: a pipe stem made by Thomas Hunt (1681), brick from the Hindhead kiln (c.1720) and Brookhill pottery (1640-1670) as well as a high datum of over 70µT at 1600 derived from tiles from the Tyler's Green kiln. Previously published data, shown as empty diamonds in figure 15.1, has been obtained by a variety of archaeointensity methods and has been shown without error bars. As discussed in chapter 6, published uncertainties are often unrealistic and it is doubtful whether there are any simple ways to assess the quality of data. It was further shown that archaeointensity data tended to be dispersed about the true field value, regardless of the experimental method and so, given the density of data

for the 17th C, the magnitude of the field in Britain at this time should be reasonably well constrained. This would in turn suggest that these four microwave archaeointensities are considerable overestimates of the historical field.

This possibility can be investigated further using field models. Figure 15.2 shows the post 1500 data compared with the intensity predicted by the field model gufm, and according to the suggestion of Gubbins et al. (2006). The model predictions are for a central location (53°N, 1°W). Here it can be argued that the result from Brookhill pottery (1665±15 years) is consistent with gufm, which it was argued in chapter 6, is a more probable model than the slowly decaying dipole model of Gubbins et al. (2006). Two points in particular are very much higher than either of the models shown: the Hindhead kiln bricks (chapter 9) at 1725 and the Tyler Green tile kiln (chapter 11) at 1600.

Figure 15.2 Post 1500 data compared with the field model gufm and the suggestion of Gubbins et al. (2006).

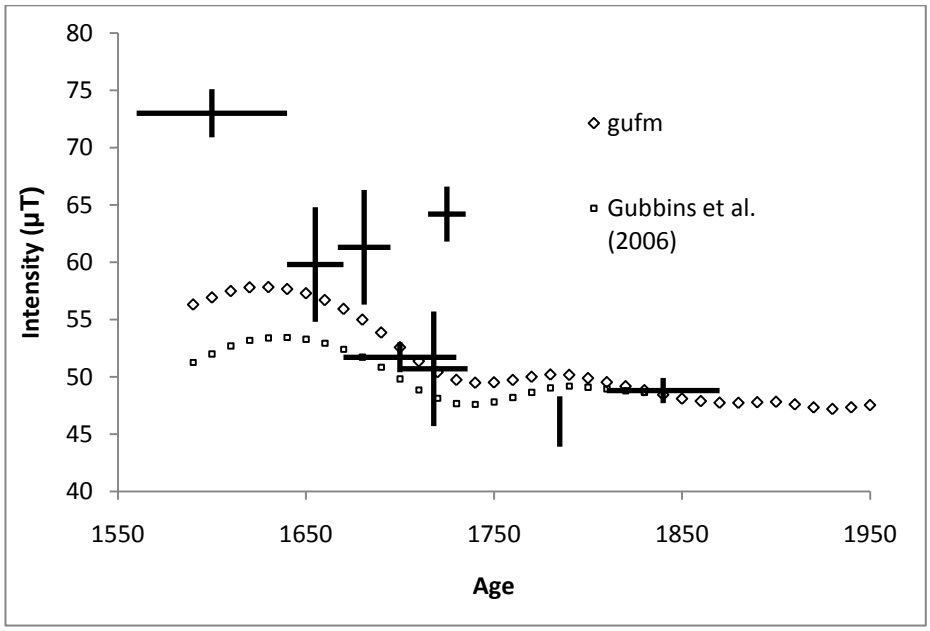

Experiments to assess the effect of cooling rate o the intensity derived from the Hindhead brick (chapter 9) were inconclusive but when a TRM was imparted in a conventional palaeomagnetic oven, cooling over 20 minutes, a microwave archaeointensity experiment successfully recovered the strength of the field. It would seem then, given the supposedly logarithmic nature of the cooling rate dependency of TRM (Dodson and McLelland-Brown 1980), that this effect is insufficient to account for the observed discrepancy. This conclusion is supported by a recent study of Lapita ceramics from the south-west Pacific,

which showed excellent agreement between microwave and conventional archaeointensities (Stark et al. 2010).

There is an important difference, in general, between recent British ceramics and the Melanesian ceramics studied by Stark et al. (2010), in terms of their microwave properties. The clay used to produce the Lapita ceramics of the south-west Pacific is tempered with volcanic dust; as shown in table 2.1 pyroxenes and plagioclase exhibit very high dielectric loss. Such minerals will usually not be present in ceramics from less volcanically active regions such as Britain. Similarly, the occurrence of magnetite in ceramics from different regions will be quite distinct. Ceramic tempered with volcanic dust will generally contain large grains of titano-magnetite before firing; in British ceramics much smaller grains of magnetite will be formed during the dehydroxylation of clay minerals (Wagner and Wagner 2004). A probable explanation for the anomalous results seen in figure 15.2 may be related to the low dielectric loss of the ceramics used. It was shown in chapter 3 that the dielectric properties of the sample are the principal factors damping the fields in the cavity. When the sample has low dielectric loss the fields will grow to very high levels and, correspondingly, large gradients will exist across the sample giving rise to sudden and intense local heating. Why this should results in what appear to be generally high archaeointensities is not clear, but a mechanism could be envisaged where, above a critical electric field, energy is rapidly dissipated over a very small area. If this results in a change in the structure at the focus of the heating, the sample's behaviour will change and subsequent steps will not reproduce the same effect. While such a mechanism may give anomalous archaeointensities, it would not appear to be capable of explaining the tendency toward high results.

15.2 Implications for archaeomagnetic dating

Not enough data has been produced to produce a reliable archaeointensity reference curve for the purpose of archaeomagnetic dating in the UK. The methods used here may not be capable of producing such a dataset, even if there was more material available and it has to be acknowledged that the dating of fired archaeological artefacts using archaeointensity is always going to be challenging. There are exceptions when the measurement of intensity may help to constrain an archaeomagnetic date. In chapter 14 it was shown that the intensity from an 18th century Delftware kiln fitted a data set from France very well and in

this case would actually have improved the precision of the date derived from archaeomagnetic directions. If the late 18th century dipole low can be confirmed by more data then it might add a useful additional constraint in a period when the direction of the field moves only about 2.5° in 50 years. It seems that the methods used in this study may be able to pick out general trends in archaeointensity, but lack the accuracy required to produce a valid reference curve. The analysis presented in chapter 6 suggests that uncertainties in all archaeointensity data make large amounts of data necessary, preferably from a range of different sites, to obtain a useful model. The spatio-temporal distribution of the artefacts studied here was not wide enough to achieve these aims and a great deal more data would be required to draw any firm conclusions regarding the evolution of the geomagnetic field over historic times.

The data derived from archaeointensity studies can still be used to constrain geomagnetic field models that may ultimately be used in archaeomagnetic dating (Lodge and Holme 2008). For such studies to be incorporated into these models the wider issue of error estimation must be addressed as discussed in chapter 6. Until there is a consistent and universal estimate of uncertainty, there is a danger that any model that maximises the likelihood of the data will be prone to hidden bias. Such a consistent estimate of uncertainty will only be achieved by the accumulation of more data from different sources. Increasing the precision of a few data by reducing the experimental error can only have a small effect on the fidelity of a global field model.

The microwave archaeointensity method, while appealing in terms of speed and minimal impact on culturally important assemblages, may not be the most effective way to obtain archaeointensity from British ceramics. Either because of the underlying geology and mineralogy of the clay, or because of the pyrotechnology, many of the ceramics studied exhibited low loss at microwave frequencies. As shown in chapter 3, in the absence of loss, the field in the microwave cavity can reach magnitudes that will cause catastrophic damage to archaeomagnetic samples. There may also be a large cooling rate dependency of the field estimates that is extremely difficult to quantify. It was shown, however, that under the right conditions, it was possible to demagnetise a sample of basalt using microwaves without significant heating, so future work may yet find a way for applying the technique successfully to ceramics and indeed recent studies suggest that this is already being achieved (Stark et al. 2010).

15.3 Geophysical implications

The most important finding of the study from geophysical viewpoint was the finding that the ad hoc estimation of uncertainty in archaeointensity and palaeointensity has the potential to introduce large biases into geomagnetic field models. It was shown in chapter 6 that recent suggestions that the present decay of the geomagnetic dipole started around 1840 (Gubbins et al. 2006, Finlay 2008) were in fact a consequence of inconsistent error estimation. The importance of this finding goes far beyond increasing our understanding of the geodynamo. The models based on the steady axial dipole hypothesis have been used to modulate proxy records for solar variability (Bard et al. 2007)and our findings are therefore important in the continuing debate regarding the contribution of solar variability to climate change (e.g. Solanki et al. 2004).

It was also shown that, when using archaeointensity to elucidate the evolution of the geodynamo, numerous widely distributed data is more informative than few data of arbitrarily high experimental precision. The speed of the microwave palaeointensity method means that it may, if applied to appropriate materials, play an important role in increasing the global data set. To constrain global field models, future palaeointensity and archaeointensity studies should focus on the rapid acquisition of data, even at the cost of some precision.

15.4 Conclusions and further work

It was not possible to produce the high quality archaeointensity record which the project set out to do, although certain aspects of this work were successful. In particular the result confirming low field strengths in the 18th century may well prove to be a useful starting point for such a record. It may be that the a high precision archaeointensity record is a flawed construct if, as argued in chapter 6, the principle source of variance in archaeointensity data is not experimental but systematic. Future work might better focus on the acquisition of large amounts of data with wide spatio-temporal coverage and it is suggested that this would be greatly informative even if it entailed the loss of precision. The theory of microwave demagnetisation has been thoroughly explored and the behaviour of the cavity and the fields therein fully elucidated. While limited success was achieved with the method in this study, now that a sound theoretical framework has been

established, it may be possible to improve the methodology. Future research might address the question of the optimum frequency to use for different materials. Whatever technique is used to obtain archaeointensity, realistic estimations of experimental error should be used in order that the different contributions to the total error budget can be better understood. To this end, a wider dialogue between experimentalists and geomagnetic field modellers is necessary so that resources can be targeted strategically to answer the important geophysical issues.

References

Abrahamsen, N., 1992. On farsidedness of palaeomagnetic poles: Magnetic refraction, sediment compaction and dipole off-set. Studia Geophysica Et Geodaetica. 36, 26-41.

Aitken, M. J. and Hawley, N. H., 1971. Archaeomagnetism: evidence for magnetic refraction in kiln structures. Archaeometry. 13, 83-85.

Aitken, M. J., 1964. Archaeomagnetic results: some geophysical implications. Archaeometry. 7, 43-46.

Aitken, M. J., Allsop, A. L., Bussell, G. D., Winter, M. B., 1988. Determination of the intensity of the Earth's magnetic field during archaeological times: reliability of the Thellier technique. Reviews of Geophysics. 26, 3-12.

Aitken, M. J. and Weaver, G. H., 1962. Magnetic dating: some archaeomagnetic measurements in Britain. Archaeometry. 5, 4-18.

Anscombe, F. J., 1973. Graphs in Statistical Analysis. American Stastician. 27, 17-21.

Baden Fuller, A.J., 1987. Ferrites at microwave frequencies. Peregrinus on behalf of the Institution of Electrical Engineers, London.

Barbetti , M., 1979 Determination of ancient geomagnetic strengths from specimens with multi-component magnetizations. Journal of Archaeological Science.6, 195-199.

Bard, E., Raisbeck, G. M., Yiou, F., Jouzel, J., 2007. Comment on "Solar activity during the last 1000 yr inferred from radionuclide records" by Muscheler et al. (2007). Quaternary Science Reviews. 26, 2301-2304.

Barlow, R.J., 1989. Statistics: a guide to the use of statistical methods in the physical sciences. John Wiley & Sons, Chichester,p151.

Barraclough, D. R., 1974. Spherical harmonic models of the geomagnetic field for eight epochs between 1600 and 1910. Geophys. J. R. Astron. Soc. 36, 497-513.

Biggin, A. J., Perrin, M., Dekkers, M. J., 2007. A reliable absolute palaeointensity determination obtained from a non-ideal recorder. Earth Plan. Sci. Lett. 257, 545-563.

Bohnel, H., Biggin, A. J., Walton, D., Shaw, J., Share, J. A., 2003. Microwave palaeointensities from a recent Mexican lava flow, baked sediments and reheated pottery. Earth and Planetary Science Letters. 214, 221-236.

Bohren, C.F.,Huffman D.R, 1983. Absorption and scattering of light by small particles. John Wiley & Sons, New York.

Brown, M. C., Gratton, M. N., Shaw, J., Holme, R., Soler, V., 2009. Microwave palaeointensity results from the Matuyama-Brunhes geomagnetic field reversal. Physics of the Earth and Planetary Interiors. 173, 75-102.

Calvo, M., Prévot, M., Perrin, M., Riisager, J., 2002. Investigating the reasons for the failure of palaeointensity experiments: A study on historical lava flows from Mt. Etna (Italy). Geophys. J.Int. 149, 44-63.

Carter, R. G., 2001. Accuracy of microwave cavity perturbation measurements. IEEE Transactions on Microwave Theory and Techniques. 49, 918-923.

Casas, L., Shaw, J., Gich, M., Share, J. A., 2005. High-quality microwave archaeointensity determinations from an early 18th century AD English brick kiln. Geophysical Journal International. 161, 653-661.

Chauvin, A., Garcia, Y., Lanos, P., Laubenheimer, F., 2000.
Paleointensity of the geomagnetic field recovered on archaeomagnetic sites from France. Physics of the Earth and Planetary Interiors. 120, 111-136.

Chen, L.F., Neo, C.P., Ong, C.K., 2004. Microwave electronics : measurement and materials characterisation. John Wiley, Chichester.

Clark, A. J., Tarling, D. H., Noël, M., 1988. Developments in archaeomagnetic dating in Britain. Journal of Archaeological Science. 15, 645-667.

Cochran, W. G., 1947. Some consequences when the assumption for the analysis of variance are not satisfied. Biometrics. 3, 22-38.

Coe, R. S., 1967. Paleo-Intensities of the Earth's magnetic field determined from Tertiary and Quaternary Rocks. J. Geophys. Res. , 72, 3247–3262. 72, 3247-3262.

Coe, R., Grommé, S., Mankinen,E., 1978. Geomagnetic Paleointensities From Radiocarbon-Dated Lava Flows on Hawaii and the Question of the Pacific Nondipole Low. J. Geophys. Res. 83(B4), 1740-1756.

Davies, C. J., 2009. Assessing the effect of mineral alteration on palaeointensities derived from Cretaceous material. Unpublished PhD thesis, University of Liverpool.

Day, R., Fuller, M., Schmidt, V. A., 1977. Hysteresis properties of titanomagnetites: Grain-size and compositional dependence. Physics of the Earth and Planetary Interiors. 13, 260-267.

Dekkers, M. J., Böhnel, H. N., 2006. Reliable absolute palaeointensities independent of magnetic domain state. Earth and Planetary Science Letters. 248, 507-516.

Dodson, M. H. and McLelland-Brown, E., 1980. Magnetic blocking temperatures of single-domain grains during slow cooling. Journal of Geophysical Research. 85, 2625-2637.

Domen, H., 1977. A single heating method of paleomagnetic field intensity determination applied to old roof tiles and rocks. Phys. Earth Planet. Inter. 13, 315-318.

Donadini, F., Korte, M., Constable, C. G., 2009. Geomagnetic field for 0-3 ka: 1. New data sets for global modeling. Geochemistry, Geophysics, Geosystems. 10, Q06007, doi:10.1029/2008GC002295.

Draine, B. T. and Lazarian, A., 1999. Magnetic dipole microwave emission from dust grains. Astrophysical Journal. 512, 740-754.

Dunlop, D.J., Özdemir, Ö., 1997. Rock magnetism. Fundamentals and frontiers. Cambridge University Press, Cambridge.

Dunlop, D. J., 2002. Theory and application of the Day plot (Mrs/Ms versus Hcr/Hc) 1. Theoretical curves and tests using titanomagnetite data. Journal of Geophysical Research B: Solid Earth. 107, 4-11.

Fabian, K. 2001. A theoretical treatment of paleointensity determination experiments on rocks containing pseudo-single or multi domain magnetic particles. Earth and Planetary Science Letters. 188, 45-58.

Fannin, P. C., Marin, C. N., Malaescu, I., Stefu, N., 2007. Microwave dielectric properties of magnetite colloidal particles in magnetic fluids. Journal of Physics: Condensed Matter. 19. 036104 doi:10.1088/0953-8984/19/3/036104

Finlay, C. C., 2008. Historical variation of the geomagnetic axial dipole. Physics of the Earth and Planetary Interiors. 170, 1-14.

Fox, J. M. W. and Aitken, M. J., 1980. Cooling-rate dependence of thermoremanent magnetisation . Nature. 283, 462-463.

Gallet, Y., Genevey, A., Courtillot, V., 2003. On the possible occurrence of 'archaeomagnetic jerks' in the geomagnetic field over the past three millennia. Earth and Planetary Science Letters. 214, 237-242.

Gallet, Y., Genevey, A., Fluteau, F., 2005. Does Earth's magnetic field secular variation control centennial climate change? Earth and Planetary Science Letters. 236, 339-347.

Games, K. P. and Davey, P. J., 1985. Archaeomagnitude determinations from Britain and south-west USA from 600 AD to 1700 AD and their implications for Medieval pottery studies. Medieval Ceramics. 9, 43-50.

Games, K. P. and Baker, M. E., 1981. Determination of geomagnetic archaeomagnitudes from clay pipes. Nature. 289, 478-479.

Genevey, A., Gallet, Y., 2002. Intensity of the geomagnetic field in western Europe over the past 2000 years: New data from ancient French pottery. J. Geophys. Res.107, 2285, doi:10.1029/2001JB000701

Genevey, A., Gallet, Y., Constable, C. G., Korte, M., Hulot, G., 2008. ArcheoInt: An upgraded compilation of geomagnetic field intensity data for the past ten millennia and its application to the recovery of the past dipole moment. Geochemistry, Geophysics, Geosystems. 9, Q04038, doi:10.1029/2007GC001881

Genevey, A., Gallet, Y., Rosen, J., Le Goff, M., 2009. Evidence for rapid geomagnetic field intensity variations in Western Europe over the past 800 years from new French archeointensity data. Earth and Planetary Science Letters. 284, 132-143.

Gómez-Paccard, M., Chauvin, A., Lanos, P., Thiriot, J. 2008. New archeointensity data from Spain and the geomagnetic dipole moment in western Europe over the past 2000 years. J. Geophys. Res. 113, B09103, doi:10.1029/2008JB005582.

Gubbins, D., Jones, A. L., Finlay, C. C., 2006. Fall in earth's magnetic field is erratic. Science. 312, 900-902.

Hale, C. J., Fuller, M., Bailey, R. C., 1978. On the application of microwave heating to lunar paleointensity determination. Proc. Ninth Lunar Sci. Conf. 3165-3179.

Hartmann, G. A., Genevey, A., Gallet, Y., Trindade, R. I. F., Etchevarne, C., Le Goff, M., Afonso, M. C., 2010. Archeointensity in Northeast Brazil over the past five centuries. Earth and Planetary Science Letters. 296, 340-352.

Hill, M. J., 2000. The microwave palaeointensity technique and its application to lava. Unpublished Ph.D thesis, University of Liverpool.

Hill, M. J., Gratton, M. N., Shaw, J., 2002. Palaeomagnetic investigation of Tertiary lava from Barrington Tops, NSW, Australia, using thermal and microwave techniques. Earth and Planetary Science Letters. 198, 245-256.

Hill, M. J., Shaw, J., 1999. Palaeointensity results for historic lavas from Mt Etna using microwave demagnetization/remagnetization in a modified Thellier-type experiment. Geophysical Journal International. 139, 583-590.

Hill, M. J., Shaw, J., Herrero-Bervera, E., 2005. Palaeointensity record through the Lower Mammoth reversal from the Waianae volcano, Hawaii. Earth and Planetary Science Letters. 230, 255-272.

Hulot, G., Khokhlov, A., Le Mouël, J. L., 1997. Uniqueness of mainly dipolar magnetic fields recovered from directional data. Geophys. J.Int. 129, 347-354.

Hulot, G., Finlay, C. C., Constable, C. G., Olsen, N., Mandea, M., 2010. The magnetic field of planet earth. Space Science Reviews. 152, 159-222.

Jackson, A., Jonkers, A. R. T., Walker, M. R., 2000. Four centuries of geomagnetic secular variation from historical records. Philosophical Transactions of the Royal Society A: Mathematical, Physical and Engineering Sciences. 358, 957-990.

Johnson, C. L. and Constable, C. G., 1997.
The time-averaged geomagnetic field: global and regional biases for 0–5 Ma. Geophysical Journal International. 131, 643-666.

Karloukovski, V. and Hounslow, M., 2006. Bolsterstone Glass House, Stocksbridge, Sheffield, South Yorkshire. Archaeomagnetic dating report. Unpublished report, Centre for Environmental Magnetism and Palaeomagnetism, Lancaster University.

Kirschvink, J. L., 1980. The least-squares line and plane and the analysis of palaeomagnetic data. Geophysical Journal, Royal Astronomical Society. 62, 699-718.

Kissel, C. and Laj, C., 2004. Improvements in procedure and paleointensity selection criteria (PICRIT-03) for Thellier and Thellier determinations: Application to Hawaiian basaltic long cores. Physics of the Earth and Planetary Interiors. 147, 155-169.

Korte, M. and Constable, C. G., 2005. Continuous geomagnetic field models for the past 7 millennia: 2. CALS7K. Geochem., Geophys., Geosyst. 6, Q02H16, doi:10.1029/2004GC000801.

Korte, M., Genevey, A., Constable, C. G., Frank, U., Schnepp, E., 2005. Continuous geomagnetic field models for the past 7 millennia: 1. A new global data compilation. Geochem., Geophys., Geosyst. 6, Q02H15, doi:10.1029/2004GC000800.

Kovacheva, M., Boyadziev, Y., Kostadinova-Avramova, M., Jordanova, N., Donadini, F., 2009. Updated archeomagnetic data set of the past 8 millennia from the Sofia laboratory, Bulgaria. Geochem. Geophys. Geosyst. 10, Q05002, doi:10.1029/2008GC002347.

Lanos, P., 1987. The effects of demagnetizing fields on thermoremanent magnetization acquired by parallel-sided baked clay blocks. Geophysical Journal of the Royal Astronomical Society. 91, 985-1012.

Le Goff, M. and Gallet, Y., 2004. A new three-axis vibrating sample magnetometer for continuous high-temperature magnetization measurements: Applications to paleo- and archeo-intensity determinations. Earth and Planetary Science Letters. 229, 31-43.

Lifshitz, E.M., Landau, L.D. 1984. Electrodynamics of continuous media, 2nd ed. Pergamon, Oxford.

Linford, P., 2004. Rose Cottage Tyler's Green ,Penn, Buckinghamshire:Archaeomagnetic dating report. CfA report no.24/2004. English Heritage.

Linford, P., 2003. St. John's School, Glastonbury, Somerset:Archaeomagnetic dating report. CfA report no. 99/2003. English Heritage.

Linford, P., 2002. Whitby Abbey Cliff, Whitby, North Yorkshire:Archaeomagnetic dating report. CfA report no.98/2002. English Heritage.

Lodge, A. and Holme, R., 2009. Towards a new approach to archaeomagnetic dating in Europe using geomagnetic field modelling. Archaeometry. 51, 309-322.

Longworth, C., 2006. Buckley Ceramics in the Seventeenth Century: Socio-Economic Status of the Potters and Possible Design Influences. Interpreting Ceramics. 6. http://www.uwic.ac.uk/icrc/issue006/articles/01.htm

Malin, S. R. C., Bullard, E., 1981. The Direction of the Earth's Magnetic Field at London, 1570-1975. Philos. Trans. R. Soc. Lond. A. 299, 357-423.

McClelland Brown, E., 1984. Experiments on TRM intensity dependence on cooling rate. Geophysical Research Letters. 11, 205-208.

McClelland Brown, E., 1984. Experiments on TRM intensity dependence on cooling rate. Geophys.Res.Lett. 11, 205-208.

Michalk, D. M., Muxworthy, A. R., Böhnel, H. N., Maclennan, J., Nowaczyk, N., 2008. Evaluation of the multispecimen parallel differential pTRM method: A test on historical lavas from Iceland and Mexico. Geophys. J.Int. 173, 409-420.

Mochizuki, N., Tsunakawa, H., Oishi, Y., Wakai, S., Wakabayashi, K.-I., Yamamoto, Y., 2004. Palaeointensity study of the Oshima 1986 lava in Japan: Implications for the reliability of the Thellier and LTD-DHT Shaw methods.. Phys. Earth Planet. Inter. 146, 395-416.

Morrish, A. H., 1965. The Physical Principles of Magnetism. Wiley, New York.

Nagata, T., Arai, Y., Momose, K., 1963. Secular variation of the geomagnetic total force during the last 5000 years. J. Geophys. Res. 68, 5277-5282.

Oishi, Y., Tsunakawa, H., Mochizuki, N., Yamamoto, Y., Wakabayashi, K.-I., Shibuya, H., 2005. Validity of the LTD-DHT Shaw and Thellier palaeointensity methods: A case study of the Kilauea 1970 lava. Phys. Earth Planet. Inter. 149, 243-257.

Olson, P., 2002. Geophysics: The disappearing dipole. Nature. 416, 591-594.

Peacey, A. A., 1996. The development of the clay tobacco pipe kiln in the British Isles. British Archaeological Reports. British series 246.

Pick, T. and Tauxe, L., 1993. Holocene paleointensities: Thellier experiments on submarine basaltic glass from the East Pacific Rise. Journal of Geophysical Research. 98, 17,949-17,964.

Pozar, D.M., 2004. Microwave engineering, 3rd ed. Wiley, New York.

Riisager, P. and Riisager, J., 2001. Detecting multidomain magnetic grains in Thellier palaeointensity experiments. Physics of the Earth and Planetary Interiors. 125, 111-117.

Rizzi, P.A., 1988. Microwave engineering : passive circuits. Prentice-Hall, Englewood Cliffs, N.J.

Roy, R., Peelamedu, R., Hurtt, L., Cheng, J., Agrawal, D., 2002. Definitive experimental evidence for Microwave Effects: radically new effects of separated E and H fields, such as decrystallization of oxides in seconds. Materials Research Innovations. 6, 128-140.

Rusakoff, G., 1970. A derivation of the microscopic Maxwell equations. American Journal of Physics. 38, 1185-1195.

Selkin, P. A. and Tauxe, L., 2000. Long-term variations in palaeointensity. Philosophical Transactions of the Royal Society A: Mathematical, Physical and Engineering Sciences. 358, 1065-1088.

Shaw, J., 1974. Rapid changes in the magnitude of the archaeomagnetic field. Geophys. J. R. Astron. Soc. 58, 107-116.

Shaw, J., Walton, D., Yang, S., Rolph, T. C., Share, J. A., 1996. Microwave archaeointensities from Peruvian ceramics. Geophys. J.Int. 124, 241-244.

Slater, J. C., 1946. Microwave Electronics. Reviews of Modern Physics. 18, 441-512.

Soffel, H. C. and Schurr, K., 1990. Magnetic refraction studied on two experimental kilns. Geophysical Journal International. 102, 551-562.

Solanki, S. K., Usoskin, I. G., Kromer, B., Schüssler, M., Beer, J., 2004. Unusual activity of the Sun during recent decades compared to the previous 11,000 years. Nature. 431, 1084-1087.

Sommerfeld, A., 1964. Electrodynamics – Lectures on Theoretical Physics Volume III. Academic Press, London.

Stacey, F.D., Banerjee, S.K., 1974. The Physical Principles of Rock Magnetism. Elsevier, Amsterdam.

Stark, F., Cassidy, J., Hill, M. J., Shaw, J., Sheppard, P., Establishing a first archaeointensity record for the SW Pacific. Earth and Planetary Science Letters. Article in press.

Sternberg, R. S., 1989. Archaeomagnetic paleointensity in the American Southwest during the past 2000 years . Phys. Earth Planet. Inter. 56, 1-17.

Sternberg, R.S., 2008. Archaeomagnetism in archaeometry: semi-centennial review. Archaeometry. 50, 983-998.

Suhl, H., 1958. Origin and use of instabilities in ferromagnetic resonance. Journal of Applied Physics. 29, 416-421.

Suttie, N., Shaw, J., Hill, M. J., 2010. Direct demonstration of microwave demagnetization of a whole rock sample with minimal heating. Earth and Planetary Science Letters. 292, 357-362.

Thellier, E., and O. Thellier, 1959. Sur l'intensité du champ magnétique terrestre dans le passé historique et géologique. Ann. Geophys. 15, 285-376.

Tulloch, A.M., 1992. A study of recent secular variation of the geomagnetic field as recorded by lavas from Mount Vesuvius and the Canary islands. Unpublihed PhD thesis, University of Liverpool.

Valstyn, E. P., Hanton, J. P., Morrish, A. H., 1962. Ferromagnetic Resonance of Single-Domain Particles. Physical Review. 128, 2078-2088.

Wagner, F.E. and Wagner, U. 2004 Mössbauer spectra of clays and ceramics. Hyperfine interactions. 154, 35-82.

Walton, D., 1984. Re-evaluation of Greek archaeomagnitudes. Nature. 310, 740-743.

Walton, D., 2004. Avoiding mineral alteration during microwave magnetization. Geophysical Research Letters. 31, L03606, doi:10.1029/2003GL019011

Walton, D., 2002. Conditions for ferromagnetic resonance in nanoparticles and microwave magnetization. Geophysical Research Letters. 29, 2165, doi:10.1029/2002GL016049

Walton, D. and Boehnel, H. N., 2008. The microwave frequency method. Physics of the Earth and Planetary Interiors. 167, 145-148.

Walton, D., Shaw, J., Share, J., Hakes, J., 1992. Microwave Demagnetization. Journal of Applied Physics. 71, 1549-1551.

Walton, D., Share, J., Rolph, T. C., Shaw, J., 1993. Microwave Magnetization. Geophysical Research Letters. 20, 109-111.

Walton, D., Snape, S., Rolph, T. C., Shaw, J., Share, J., 1996. Application of ferrimagnetic resonance heating to palaeointensity determinations. Physics of the Earth and Planetary Interiors. 94, 183-186.

Walton, D., Boehnel, H., Dunlop, D. J., 2004a. 2d order ferromagnetic resonance in nanoparticles. Physica Status Solidi (A) Applied Research. 201, 3257-3262.

Walton, D., Boehnel, H., Dunlop, D. J., 2004b. Response of magnetic nanoparticles to microwaves. Applied Physics Letters. 85, 5367-5369.

Whitworth, R. W. and Stopes-Roe, H. V., 1971. Experimental Demonstration that the Couple on a Bar Magnet depends on H, not B. Nature. 234, 31-33.

Williamson, J.H., 1968 Least-squares fitting of a straight line. Can. J. Phys. 46, 1845-1847.

Wilson, R. L., 1961. Wilson, R. L. 1961 Paleomagnetism in Northern Ireland. Part I, The thermal demagnetization of natural magnetic moments in Rocks. Geophys. J. R. Astron. Soc. 5, 45-58.

Yamamoto, Y., Tsunakawa, H., Shibuya, H., 2003. Palaeointensity study of the Hawaiian 1960 lava: Implications for possible causes of erroneously high intensities. Geophys. J.Int. 153, 263-276.

Yu, Y., Dunlop, D. J., Özdemir, Ö., 2003. On the resolution of multivectorial remanences. Earth and Planetary Science Letters. 208, 13-26.

Zheng, Y., Wang, S. J., Feng, J. M., Ouyang, Z., Li, X. Y., 2005. Measurement of the complex permittivity of dry rocks and minerals: application of polythene dilution method and Lichtenecker's mixture formulae. Geophysical Journal International. 163, 1195-1202.

Zhu, R., Lo, C.-H., Shi, R., Shi, G., Pan, Y., Shao, J., 2004. Palaeointensities determined from the middle Cretaceous basalt in Liaoning Province, northeastern China. Physics of the Earth and Planetary Interiors. 142, 49–59.